Distribution Agreement

In presenting this thesis or dissertation as a partial fulfillment of the requirements for an advanced degree from Emory University, I hereby grant to Emory University and its agents the non-exclusive license to archive, make accessible, and display my thesis or dissertation in whole or in part in all forms of media, now or hereafter known, including display on the world wide web. I understand that I may select some access restrictions as part of the online submission of this thesis or dissertation. I retain all ownership rights to the copyright of the thesis or dissertation. I also retain the right to use in future works (such as articles or books) all or part of this thesis or dissertation.

Signature:

_____ _____

Marc A. Schureck Date

Structural and functional studies of a toxin-antitoxin system involved in translational inhibition

By

Marc A. Schureck
Doctor of Philosophy

Graduate Division of Biological and Biomedical Science
Biochemistry, Cell and Developmental Biology

_____ [Advisor's signature]
Christine M. Dunham, Ph.D.
Advisor

_____ [Member's signature]
Anita H. Corbett, Ph.D.
Committee Member

_____ [Member's signature]
Eric A. Ortlund, Ph.D.
Committee Member

_____ [Member's signature]
Philip N. Rather, Ph.D.
Committee Member

_____ [Member's signature]
Daniel Reines, Ph.D.
Committee Member

Accepted:

_____
Lisa A. Tedesco, Ph.D.
Dean of the James T. Laney School of Graduate Studies

_____
Date

Structural and functional studies of a toxin-antitoxin system involved in translational inhibition

By

Marc A. Schureck
B.S., University of Florida, 2010

Advisor: Christine M. Dunham, Ph.D.

An abstract of
A dissertation submitted to the Faculty of the
James T. Laney School of Graduate Studies of Emory University
in partial fulfillment of the requirements for the degree of
Doctor of Philosophy
in Graduate Division of Biological and Biomedical Science
Biochemistry, Cell and Developmental Biology
2016

Abstract

Structural and functional studies of a toxin-antitoxin system involved in translational inhibition

By Marc A. Schureck

Bacteria regulate protein synthesis during environmental stress as a survival mechanism. One way translation is regulated is through cleavage of ribosome-bound mRNA by ribosome-dependent toxins. This mRNA cleavage stops the synthesis of the protein encoded by the cleaved-mRNA, conserves nutrients and likely plays an important, yet unknown, role in altering the spectrum of proteins translated during stress. A very unique feature of ribosome-dependent toxins is that they can recognize and cleave several mRNA sequences on the ribosome. In this dissertation, the molecular mechanism of recognition and cleavage of adenosine-rich mRNA codons by the *Proteus vulgaris* HigB toxin, which was originally identified on a drug-resistance plasmid from a *P. vulgaris* urinary tract infection, was investigated. Structural and biochemical studies reveal that the HigB toxin displays degenerate substrate specificity by creating two A-site nucleotide-binding pockets capable of interacting with numerous nucleotides. Surprisingly, the third nucleotide-binding pocket of HigB is adenosine-specific. Recognition of the third A-site nucleotide appears to be a distinct feature of ribosome-dependent toxins and likely influences which mRNAs are targeted for cleavage during environmental stress.

Ribosome-dependent toxins must be highly regulated. The HigA antitoxin binds to and inactivates the HigB toxin when cells are not in a stressed state. Structural investigation shows that HigA and HigB form a tetrameric complex consisting of two HigA proteins and two HigB proteins. This structure reveals that HigA does not inactivate HigB through direct interactions with the HigB active site, as observed in many other toxin-antitoxin complexes. Instead, HigA binding to HigB likely inhibits HigB by blocking association of HigB with the ribosome. The knowledge of how HigB activity is regulated and its unique specificity provides a molecular framework for scientists to uncover how ribosome-dependent toxins control translation during environmental stress.

Structural and functional studies of a toxin-antitoxin system involved in translational inhibition

By

Marc A. Schureck
B.S., University of Florida, 2010

Advisor: Christine M. Dunham, Ph.D.

A dissertation submitted to the Faculty of the
James T. Laney School of Graduate Studies of Emory University
in partial fulfillment of the requirements for the degree of
Doctor of Philosophy
in Graduate Division of Biological and Biomedical Science
Biochemistry, Cell and Developmental Biology
2016

Table of Contents

Table of figures

Table of tables

Abbreviations

A site: Aminoacyl site

APS: Advanced Photon Source

ATP: Adenosine triphosphate

BCDB: Biochemistry, Cellular and Molecular Biology

DOE: Department of Energy

E site: Exit site

EF-G: Elongation factor G

EF-Tu: Elongation factor Tu

fs: frameshift

GTP: Guanosine triphosphate

HigA: Host inhibition of growth A

HigB: Host inhibition of growth B

HigBA: HigB-HigA

HPF: Hibernation promoting factor

HipAB: HipA-HipB

Hr: hour

HTH: Helix-turn-helix

IDT: Integrated DNA Technologies

IF1: Initiation factor 1

IF2: Initiation factor 2

IF3: Initiation factor 3

IPTG: Isopropyl-1-thio-β-D-galactopyranoside

kDa: kilodalton

LSQ: Least-squares

Min: minute

MME: monomethylether

MqsRA: MqsR-MqsA

mRNA: Messenger RNA

NE-CAT: Northeastern-Collaborative Access Team

NIH: National Institute of Health

Nt: nucleotide

P site: Peptidyl site

PDB: Protein Data Bank

PEG: Polyethylene glycol

Pisa: Protein Interfaces, Surfaces, and Assemblies

PMSF: Phenylmethylsulfonyl fluoride

(p)ppGpp: Guanosine tetra/penta phosphate

pY: Protein Y

RelBE: RelE-RelB

RHH: Ribbon-helix-helix

RMF: Ribosome modulation factor

RMSD: Root-mean-square deviation

rRNA: ribosomal RNA

RMF: Ribosome modulation factor

SAD: Single anomalous dispersion

SDS-PAGE: Sodium dodecyl sulfate polyacrylamide gel electrophoresis

SEC: Size exclusion chromatography

SER-CAT: Southeast Regional Collaborative Access Team

SSM: Secondary-structure matching

TA: Toxin-antitoxin

tRNA: Transfer RNA

Tth: *Thermus thermophilus*

XDS: X-ray Detector Software

XRE-HTH: Xenobiotic response element-helix-turn-helix family

β-ME: β-mercaptoethanol

Chapter 1

Introduction: Toxin-antitoxin systems

1.1 Abstract

Bacteria encounter diverse environmental conditions and as a result contain multiple pathways that allow for survival in the challenging conditions they face. Toxin-antitoxin systems regulate replication and translation in response to environmental stress. Toxin-antitoxin genes are typically two-component systems that encode a toxin and antitoxin protein. During non-stress conditions, the antitoxin protein has two major functions: to bind to and inhibit the toxin's enzymatic activity and as a DNA binding protein, to repress transcription from its own operon. Proteotoxic stress results in antitoxin degradation releasing the toxin. The free toxin typically limits growth by inhibiting components of essential cellular processes including replication and translation. Therefore toxins are beneficial for bacteria and indeed, cells containing activated toxins are antibiotic tolerant. Intriguingly, bacterial genomes often encode multiple and redundant toxin-antitoxin genes suggesting functional distinctions that are important for bacterial survival.

1.2 Antibiotics

Effective clearance of pathogenic bacteria is essential for human health. The human immune system actively recognizes many bacterial species and can rid the body of these bacteria (1). However, infections in individuals with compromised immune systems or bacteria that evade immune detection are especially problematic and require chemical intervention in the form of antibiotics to eradicate pathogenic bacteria. Antibiotics are small molecules that disrupt essential bacterial processes and are classified as either bacteriostatic, which stop bacterial growth, or bactericidal, which kill bacteria (2). Antibiotics are an important defense against bacterial infections.

Bacteria evade antibiotics in a number of different ways. Acquisition of genes that inhibit an antibiotic from reaching its target or mutation of the antibiotic binding site allow bacteria to survive antibiotic exposure (3). Some of the ways bacteria have evolved to survive antibiotic exposure are export of the antibiotic through efflux pumps (4), modification of the antibiotic (5) or modification of the antibiotic binding site on its target (6). Treatment with an antibiotic that the pathogenic bacteria is resistant to allows the bacterial infection to increase in severity, requires identification of an antibiotic that bacteria are not resistant to, and increases the chances of patient mortality (7). A startling reality is that certain bacteria are becoming resistant to several antibiotics. For example, multidrug-resistant tuberculosis is resistant to two front-line antibiotics, isoniazid and rifampicin (8). Clearance of multidrug-resistant tuberculosis typically requires treatment for more than six months with several antibiotics (8). A few strains of methicillin-resistant *Staphylococcus aureus*, a drug-resistant form of *Staphylococcus aureus* that is especially problematic in hospital settings, have been identified as resistant to the best

antibiotic to clear this infections, vancomycin (9). Recently, a strain of *Neisseria gonorrhoeae* resistant to all known first-line antibiotics was discovered (10). The emergence of multidrug-resistant bacterial strains highlights the need to understand mechanisms of antibiotic failure.

1.3 Molecular mechanisms of antibiotic action

Most antibiotics target replication, transcription or translation of the central dogma. The central dogma describes the sequential flow of genetic material from DNA to RNA to protein and involves polymerases and associated proteins. Each mechanism involved in the central dogma is targeted by at least one class of antibiotics and bacteria have evolved mechanisms to evade these antibiotics.

The quinolone class of antibiotics targets DNA replication (3). Replication of DNA involves unwinding of duplex DNA and this places tension on the DNA strand. Topoisomerase proteins bind DNA next to the replication fork and create DNA breaks to relieve the tension in DNA before religation. The quinolone class of antibiotics binds topoisomerase II and IV after they create double-stranded DNA breaks and prevents ligation of the DNA (2). This inhibition causes DNA breaks throughout the genome and leads to cell death. Mutations in topoisomerase II and/or IV lead to quinolone resistance (11).

Rifampicin stops cell growth through RNA polymerase inhibition. As DNA is threaded through RNA polymerase, complementary RNA is synthesized and exits the active site (12). Rifampicin does not bind to the active site of RNA polymerase but instead binds outside the active site, preventing the elongation of RNA (12). Rifampicin

resistance arises from amino acid changes within the rifampicin-binding pocket of RNA polymerase.

1.4 Antibiotics and the ribosome

The ribosome is targeted by over half of the antibiotics used in clinic (13,14). The ribosome synthesizes all proteins in the cell. The bacterial ribosome consists of a large 50S subunit and a small 30S subunit (**Figure 1.1**) (15). The 50S subunit is where peptide bond formation occurs. The large ribosomal subunit consists of two ribosomal RNAs (rRNA) and 31 proteins. Protein is made of amino acids whose sequence is encoded by messenger RNA (mRNA). The 30S ribosomal subunit interacts with mRNA and consists of one ribosomal RNA and 21 proteins. The 50S and 30S subunits interact with each other to generate transfer RNA binding sites in which tRNAs bind both mRNA on the 30S and position their aminoacyl ends on the 50S to undergo peptide bond formation. The decoding of mRNA by tRNA on the ribosomes is crucial for all protein synthesis.

Three nucleotides of mRNA form one codon and each codon specifies one amino acid to be added to the growing polypeptide. The anticodon of tRNAs base pair with mRNA codons and the aminoacyl end of tRNA contains a covalently attached aminoacyl group that will be added to the growing polypeptide. The ribosome has three tRNA binding sites (aminoacyl (A), peptidyl (P) and exit (E)) and tRNAs initially bind the A site during tRNA selection and sequentially progress to the P and E sites during elongation to add amino acids to the growing polypeptide chain.

In bacteria, the initiation of protein synthesis starts by mRNA binding the 30S subunit to position the AUG start codon in the P site (**Figure 1.2**) (15,16). Next, fMet-$tRNA^{fMet}$ binds the AUG start codon and initiation factor 2 (IF2) in the P site and

subsequently initiation factors 1 (IF1) and 3 (IF3) join. Finally, IF2 promotes association of the 50S subunit and the initiation factors leave, creating a 70S ribosome capable of undergoing initiation.

The mRNA located in the A site of the ribosome codes for the second amino acid to be added to the growing polypeptide chain. A ternary complex of tRNA, guanosine triphosphate (GTP) and elongation factor Tu (EF-Tu) binds the A-site and upon cognate tRNA-mRNA pairing, GTP hydrolysis occurs and the tRNA is accommodated into the A site (**Figure 1.2**). Spontaneous peptide bond formation occurs when the amine of aminoacyl group attacks the ester carbonyl carbon of the formyl methionine group. This peptidyl-tRNA moves to the 50S P site through conformations known as hybrid states. Elongation factor G (EF-G) then translocates the A-site tRNA-mRNA pair to the P site. The A-site mRNA now codes for the third amino acid to be added. This iterative process of peptide bond formation followed by translocation of tRNAs continues until a stop codon is reached and the fully synthesized protein is hydrolyzed from the P-site tRNA by a release factor protein. Recycling of ribosomes after the termination process is achieved through the concerted efforts of ribosome recycling factor and EF-G. This process is performed to synthesize every protein in the cell.

Some ribosome-targeting antibiotics interfere with the process of tRNA selection during decoding by binding to the decoding center and causing miscoding, resulting in the synthesis of aberrant proteins (13). Other ribosome-targeting antibiotics inhibit the elongation of the nascent polypeptide by binding at the peptidyl transferase center or by blocking the ribosomal exit tunnel from which the growing polypeptide exits the ribosome. With the diverse modes of action of ribosome-targeting antibiotics, there are

several mechanisms by which bacteria evade these antibiotics. Like the antibiotics that inhibit replication and transcription, ribosome-targeting antibiotics can be exported from cells, modified or degraded. The antibiotic binding site can be disrupted by mutation of rRNA, mutation of ribosomal protein or even modification rRNA. Although the ribosome is targeted by many antibiotics, several mechanisms exist to allow bacteria to stop the action of these antibiotics.

1.5 Bacteria that are antibiotic tolerant - Persisters

Bacteria can also evade clearance by antibiotics through entering what is known as the persistent state (17). Unlike antibiotic-resistant bacteria, persister cells are genetically identical to the antibiotic-sensitive cells but these cells can survive antibiotic exposure. Within a pool of antibiotic-sensitive bacterial cells, a small fraction of cells will be persisters (**Figure 1.3**). Even with clearance of the vast majority of bacteria, the small pool of remaining bacteria can reinfect the host causing a relapse of infection. In contrast to resistant bacteria, once a persister cell population regrows, it creates a phenotypically similar population to that which it was derived, with the vast majority of cells being sensitive to antibiotics and a small fraction of persister cells.

An example of the importance that persister cells play in infection is found in the disease cystic fibrosis (17). Here, mutation of the chloride channel cystic fibrosis transmembrane conductance regulator causes lungs to have excess mucus and this supports growth of bacteria such as *Pseudomonas aeruginosa* and *Burkholderia cepacia* complex species (18). To combat these pathogens, cystic fibrosis patients must remain on a constant antibiotic regimen. Over time, bacterial cells can develop mutations that increase the fraction of lung-resident persister cells (19). These mutations do not cause

antibiotic resistance but exhibit a higher phenotypic switching into the persistent state (19). The selection for pro-persister cell mutations shows persistence is a viable way to escape antibiotics and highlights the need to understand mechanisms of persistence.

1.6 Mechanisms of persister cell formation

The study of persister cell formation is challenging because persister cells make up an extremely small fraction of the population (<~0.1%), are phenotypic variants therefore preventing genotypic identification and it appears that no single gene deletion can ablate persister cell formation (20). Because of the difficulties in studying persister cells, our understanding of persister cells is constantly evolving. For example, it was thought that persister cells were tolerant to antibiotics because they were non-dividing and metabolically dormant (17). However, a recent study of *Salmonella typhimurium* persister cells in a mouse model found that the persistent population is actually active in protein synthesis (21). The topic of persister cell formation is an area of active research with many principles that remain to be discovered.

Entrance into the persistent state appears to be a stochastic process (17). Certain proteins help drive cells into the persistent state. The bacterial cells with the highest levels of proteins contributing to persister cell formation are likely the cells that become persistent. The bacterial stringent response and toxin proteins appear to have roles in the stochastic induction of persistence (22-25). There are several proteins and mechanisms that are important for persister cell formation. Here, I will focus on the involvement of the stringent response and toxin-antitoxin systems in persister cell formation.

1.7 The bacterial stringent response

When limited for nutrients such as amino acids and fatty acids, bacteria halt processes that are non-essential during stress, such as transcription of genes encoding ribosomal proteins, and upregulate processes to survive in their absence, such as amino acid synthesis (23,26). This reallocation of cellular resources in response to nutrient shortage is called the stringent response. For the stringent response to be activated, bacteria must sense when nutrients are in short supply, signal the lack of nutrients and redirect cellular processes to enable survival. Although lack of several nutrients can activate the stringent response (27), I will focus on activation of the stringent response by lack of amino acids as this process has been shown to be important for activation of toxin-antitoxin systems (28,29).

1.8 Activation of the stringent response through the lack of amino acids

The stringent response is activated by a shortage of amino acids that causes deacylated tRNA to bind the A site and stall on the ribosome (**Figure 1.4**). An A-site tRNA lacking an amino acid cannot undergo peptide bond formation, hence causing stalling. The RelA protein senses the lack of an amino acid attached to A-site tRNA and synthesizes guanosine tetra/penta phosphate ((p)ppGpp) from adenosine triphosphate (ATP) and GTP molecules (30,31).

(p)ppGpp is a global signaling molecule that interacts with several proteins to alter their function. (p)ppGpp binds RNA polymerase to inhibit transcription of genes not needed under nutritional stress, such as genes encoding ribosomal proteins. In contrast, (p)ppGpp increases transcription of genes important for survival, such as those found in biosynthetic operons (26,27,32). (p)ppGpp can also bind polyphosphate kinase and

stimulate the synthesis of long polyphosphate polymers that interact with AAA^+ ATPase proteases and stimulate degradation of select proteins. This proteotoxic degradation replenishes the amino acid pool and also activates bacterial proteins known as toxins by degrading their cognate antitoxin (32). The activity of toxin proteins appears to be important for entrance into the persistent state as well as other processes that change bacterial physiology (21,22,24).

1.9 Toxin-Antitoxin Systems

There are five classes of toxin-antitoxin systems which differ in the way the antitoxin inhibits toxin function (23). Type I antitoxins are small RNAs that prevent expression of their cognate toxins while type II and III antitoxins are proteins and RNA, respectively, that inhibit toxin function through direct interactions. Type IV antitoxins bind the substrate to protect it from toxin activity and type V antitoxins are RNases that degrade the mRNA of their toxin. In this thesis, I focus on type II toxin-antitoxin systems. Type II toxin-antitoxin systems are found chromosomally or on associated plasmids in several hundred bacterial species (33). The name “toxin” is derived from experiments in which overexpression of the toxin halts cell growth. However, when the antitoxin or antidote protein is co-expressed with its cognate toxin, the toxin-mediated growth inhibition is prevented. Toxin proteins from toxin-antitoxin systems are usually not toxic to bacterial cells (or humans) but merely suppress growth. In fact, toxins are beneficial to the host because they regulate key cellular processes to facilitate survival during stress (23).

The antitoxin protein of type II toxin-antitoxin systems directly interacts with the toxin protein to inhibit toxin protein activity and this interaction is regulated through

proteolysis (32). During non-stress conditions, as when amino acids are plentiful, the antitoxin protein interacts with the toxin protein to inhibit its activity (**Figure 1.5a**). The antitoxin protein, alone or in complex with its cognate toxin, also binds its promoter to autoregulate transcription from its operon. Most antitoxin proteins have an N-terminal DNA-binding domain and C-terminal domain that neutralizes toxin (34-37) (**Figure 1.6**). Toxin-antitoxin complexes contain two antitoxin subunits and can typically bind between two to four toxin proteins at a maximum (34,37,38). The antitoxin-mediated transcriptional autoregulation keeps toxin-antitoxin system transcript levels low during non-stress conditions.

Stress can activate all or a subset of toxins. Toxin-antitoxin system transcript levels increase during toxin activation and this increase in toxin-antitoxin system mRNA levels can be used as a proxy for toxin activation. Engulfment of *Salmonella typhimurium* by macrophages was recently shown to increase the fraction of persister cells in the population (21). Analysis of the toxin transcript levels showed that this engulfment causes a 5-30 fold increase in the mRNA levels of type II toxin-antitoxin systems. In a different experiment, the *E. coli* YafO-YafN (YafON) and HigB-HigA (HigBA) toxin-antitoxin transcript levels were measured in response to several stresses (39). Remarkably, chloramphenicol and serine hydroxamate, both translation inhibitors, caused elevated levels of both toxin-antitoxin system transcripts while isoleucine and glucose starvation only elevated transcript levels of YafON. Analysis of *M. tuberculosis* RelE-1, RelE-2 and YoeB transcript levels showed that these toxins are differentially activated in response to a variety of environmental stresses and antituberculosis drugs (40). Lastly, The *E. coli* YefM and *P. vulgaris* HigA antitoxins appear to be degraded in response to heat shock

(41-43). These investigations highlight that certain stresses only activate a subset of toxins.

The antitoxin protein presumably has to be replenished before unperturbed cellular function resume. Upon stress, proteases selectively degrade antitoxin proteins to activate toxins (23). There are dozens of toxin proteins that each target a different biological process but a majority of toxins inhibit DNA replication or protein synthesis (**Figure 1.5b**). After stress has passed, but before growth can be restored, the toxin protein would have to be inactivated by interaction with newly synthesized antitoxin protein. The exact mechanism by which antitoxin levels are restored is unknown.

1.10 Transcriptional regulation of toxin-antitoxin systems

Besides direct inhibition of toxin function, the antitoxin, alone or in complex with its cognate toxin, is also a transcription factor that represses transcription by binding to operator regions of DNA that overlap with the -35 and -10 sites of its toxin-antitoxin operon (23). Therefore, antitoxin-mediated repression keeps toxin activity and expression low during exponential growth. Transcription from toxin-antitoxin loci is de-repressed during certain environmental stresses (21,28,39). Antitoxin proteins are degraded during stress, which results in an increase in transcription from the toxin-antitoxin operon.

Several toxin-antitoxin systems are transcriptionally regulated by the ratio of toxin to antitoxin. For the RelE-RelB (RelEB), CcdA-CcdB, and Phd-Doc toxin-antitoxin systems, at low molar ratios of toxin to antitoxin, the toxin-antitoxin complex binds to its operator DNA with high affinity and efficiently represses transcription from its toxin-antitoxin operon (44-46). At high ratios of toxin binding to antitoxin, the antitoxin affinity for DNA is decreased, the toxin-antitoxin complex dissociates from DNA and

transcription occurs from the operon. It is hypothesized that under low ratios of toxins to antitoxins, two toxin-antitoxin complexes will bind cooperatively to DNA, while at high ratios of toxin to antitoxin, the toxin-antitoxin complexes have decreased affinity for DNA. This mechanism is referred to as conditional cooperativity (46).

Current models for conditional cooperativity suggest that antitoxins fully occupied by toxins bind DNA with low affinity (**Figure 1.7**) (34). The antitoxin is an obligate homodimer and can exist free of toxin, bound to one toxin or bound to two toxins. Typical DNA operators are about twenty nucleotides in length and can bind two antitoxin dimers. The current model for conditional cooperativity suggests that two antitoxin dimers, each bound to one toxin, can bind DNA with high-affinity, but, if each antitoxin dimer is bound to two toxins, the toxin-antitoxin complexes have low affinity for DNA. The authors suggest that additional toxins create a steric clash between the two toxin-antitoxin complexes bound to DNA causing the reduced affinities of heterotetrameric complexes for DNA. Therefore, antitoxin dimers sub-occupied by toxin proteins may have the highest affinity for DNA.

The YafQ-DinJ toxin-antitoxin system is structurally similar to the RelEB toxin-antitoxin system but does not appear to be regulated by conditional cooperativity (37). The DinJ antitoxin is a member of the RelB antitoxin family but binds DNA efficiently in the absence of YafQ toxin. A high ratio of YafQ to DinJ does not destabilize interactions between DinJ and DNA. Lastly, a single DinJ dimer is sufficient to repress transcription from the DinJ-YafQ operon. Thus, the fact that two toxin-antitoxin complexes resemble one another does not indicate whether both are transcriptionally regulated in the same manner.

1.11 Molecular targets of toxin proteins

Similar to antibiotics, toxin proteins interact with and affect many different cellular processes (23). Much like the quinolone class of antibiotics, the toxin protein CcdB binds and traps topoisomerase II bound to DNA causing double-strand DNA breaks (47). A large number of toxins affect translation by modification of almost every macromolecule involved in the translation process. Toxins MazF and MqsR cleave free mRNA (48,49); toxins Doc and HipA modify translation factors such as EF-Tu and tRNA glutamyl synthetase (50-52). *E. coli* MazF and *M. tuberculosis* VapC cleave rRNA at important functional sites (53,54). A final category of toxins does not cleave free mRNA, but only cleave mRNA bound to the ribosome during translation (55-59). The family of toxins that cleaves ribosome-bound mRNA is the subject of this thesis.

1.12 Toxin-antitoxin systems and persister cell formation

One toxin that promotes persister cell formation is HipA (25,60). HipA phosphorylates the active site of glutamyl-tRNA synthetase inhibiting aminoacylation of $tRNA^{Glu}$ and stalling translation (52). Conditions that select for increased persister cells, both experimentally and clinically, cause mutations in the HipA-HipB (HipAB) toxin-antitoxin system (17,61). These mutations decrease the affinity of the toxin-antitoxin complex for its DNA operator (61). As the toxin-antitoxin complex autoregulates its own transcription, a decrease in affinity for its operator leads to higher levels of HipA toxin, an increase in the levels of deacylated $tRNA^{Glu}$ and decreased translation. This translational inhibition triggers the stringent response by recruitment of RelA to the stalled-ribosome, causing RelA to synthesize (p)ppGpp. The cumulative effect of decreased translation and increased stringent response signaling causes an increase in

persister cells to ~1% of the bacterial population (60). With its ability to directly contribute to the stringent response, HipA may also activate other toxin-antitoxin systems especially, ribosome-dependent toxins (29).

The exact role of other toxin-antitoxin systems in persister cell formation is still unclear. Toxins may simply downregulate common targets of antibiotics (replication and translation machinery) and thereby diminish antibiotic effectiveness. Another possibility is that toxin activity may have a more sophisticated mechanism of contributing to persistence such as promoting the expression of proteins required for persistence. In *E. coli*, deletion of individual toxin-antitoxin systems has little to no effect on persister cell formation in liquid cell culture while deletion of multiple toxin-antitoxin systems (five or more) has a large effect on persister cell formation (24). The necessity for deleting multiple toxin-antitoxin systems in *E. coli* to decrease persister cell formation suggests that some of the toxin-antitoxin systems may have redundant functions. However, a recent *in vivo* study suggests that individual toxin-antitoxin systems are important for persister cell formation in *Salmonella typhimurium*. *S. typhimurium* live within the lysosomes of macrophages and entrance into this habitat increases the fraction of *S. typhimurium* persister cells (21). Deletion of individual toxin-antitoxin systems in *S. typhimurium* decreases the fraction of macrophage-induced persister cells suggesting individual toxins have important roles in *S. typhimurium* persister cell formation (21). Therefore, toxin-antitoxin systems may play different roles in persister cell formation in various organisms and environments.

The mRNA levels of toxin-antitoxin genes appear to be elevated in persister cells (21,22,25). Analysis of transcript levels of *E. coli* persister cells after ampicillin exposure

found several toxin-antitoxin mRNAs increased (25). Single-cell analysis of *E. coli* found that stochastically, a fraction of a percent of cells had high levels of toxin-antitoxin system expression (22). When tested for persistence, the cells with high levels of toxin-antitoxin system expression showed tolerance to antibiotic treatment while cells with low levels of toxin-antitoxin system transcripts were not persistent (22). Toxin-antitoxin transcript levels rapidly increased after incubation of *Salmonella* with macrophages, a condition that increases the fraction of persister cells. This increase was dependent on stringent response signaling (21). Thus, higher levels of toxin-antitoxin systems appear to be important for persister cell formation.

1.13 Other roles of toxin-antitoxin systems

Toxin-antitoxin systems have many additional roles outside persister cell formation. For example, the presence of a toxin-antitoxin system on a plasmid effectively stabilizes the inheritance of this plasmid (32). Antitoxin proteins have shorter half-lives than toxins and if the plasmid encoding a toxin-antitoxin system is lost, the antitoxin cannot be replaced leading to uncontrolled toxin activation and cell death. Toxin-antitoxin systems may contribute to survival during stress by inhibiting energetically expensive cellular processes to conserve critical resources. Another possibility is that toxin-antitoxin systems may be involved in programmed cell death, although the latter role does not seem to be universal among all bacteria (62-64). Some toxins, such as YafQ and MqsR appear to be important for biofilm formation (65) while other toxins even help protect bacteria against phage infection (66). Our understanding of the biological role of toxin proteins is constantly evolving.

1.14 Translational inhibition during stress

Bacteria contain several factors that regulate protein synthesis in response to changing metabolic requirements such as nutrient limitation (67). One common mechanism of translation inhibition is by direct binding of factors to important functional sites on the ribosome that restrict normal activity. For example, the energy-dependent translational throttle A protein binds the ribosomal exit (E) site to stall translation in response to low ATP/ADP ratios, such as during stationary phase (68,69). Protein Y (pY), ribosome modulation factor (RMF) and hibernation promoting factor (HPF) also inhibit protein synthesis during stationary phase by directly competing for mRNA and tRNA binding sites (**Figure 1.8a**) (67,70). In all these cases, each inhibitory protein binds to a single ribosome, thus requiring high levels to successfully inhibit large numbers of ribosomes.

In contrast to this saturating mode of inhibition is the manner in which type II toxin-antitoxin systems inhibit translation (23). Toxin proteins are enzymes that modify translation factors, cleave tRNA, rRNA, free mRNA and even mRNA bound to a translating ribosome in response to diminishing nutrients (**Figure 1.8b**). These inhibitory proteins are present at low levels during stationary and exponential phase growth, likely because as multi-turnover enzymes, toxins can target multiple molecules in direct contrast to translational inhibitors pY, RMF and HPF.

1.15 Ribosome-dependent toxins

Ribosome-dependent toxins only cleave mRNA bound to a ribosome. Incubation of ribosome-dependent toxins with free mRNA results in no mRNA degradation while

ribosome-dependent toxins rapidly cleave ribosome-bound mRNA (55,59,71). Thus, specific features of mRNA bound to the ribosome facilitate toxin-mediated cleavage.

In general, there are five ribosome-dependent toxins. The YafQ, RelE, HigB and YoeB ribosome-dependent toxins cleave mRNA in the A site of the ribosome (32). Each toxin has a particular preference for the codon(s) it cleaves: *E. coli* YafQ toxin cleaves AAA lysine codons (57); *E. coli* RelE most efficiently cleaves the CAG glutamine and UAG stop codons (55); *Proteus vulgaris* HigB cleaves several adenosine-rich codons (56); *E. coli* YoeB toxin cleaves codons following the start codon and the UAA stop codon (58,59,72). Like YafQ, RelE, HigB and YoeB, the *E. coli* YafO toxin requires the ribosome for activity (73). However, the site of YafO-mediated mRNA cleavage is roughly 8 nucleotides downstream of the A-site, which is likely near where mRNA enters the ribosome (73). Therefore, YafO is distinct from the other four ribosome-dependent toxins. It is unclear why ribosome-dependent toxins have different mRNA cleavage specificities. If the goal of ribosome-dependent toxins is to globally halt translation in response to stress then it appears that one ribosome-dependent toxin should be sufficient.

Ribosome-dependent toxins recognize A-site mRNA in a unique fashion. The majority of translation factors that interact with ribosomal A-site codons are tRNAs and release factors. tRNAs use Watson-Crick base pairing to read or decode the three nucleotide codon sequence (15). Each tRNA recognizes one or a few A-site codons and any degeneracy in base pairing between the third A-site nucleotide and tRNA, which is referred to as the “wobble”. Release factor 1 recognizes the UAA and UAG stop codons and release factor 2 recognizes the UGA and UAA stop codons (15). In contrast, some ribosome-dependent toxins can recognize several different codons on the ribosome.

Exactly how toxins display degeneracy in A-site codon recognition, while many translation factors are so stringent in decoding A-site codons, is unknown.

Limited studies of how ribosome-dependent toxin overexpression affects transcript levels show that specific transcripts are degraded. *M. tuberculosis* RelE-1, RelE-2 and YoeB (formally RelE-3) were overexpressed and the levels of mRNA were analyzed by microarray (40). The effect on the mRNA profile for RelE-1 and RelE-2 was similar, but did not resemble known metabolic pathways. YoeB overexpression resulted in a different mRNA profile compared to RelE-1 and RelE-2 and this mRNA profile resembled treatment with ribosome-targeting antibiotics. RNA sequencing after *M. tuberculosis* HigB overexpression revealed that the steady-state levels of 34 transcripts were decreased while those of two transcripts were increased (74). Many of the transcripts that decreased upon HigB overexpression are downregulated by IdeR and Zur, metal-dependent transcriptional regulators of zinc and iron levels, respectively, while one of the transcripts increased is transcriptionally upregulated by IdeR. Some of the changes observed upon HigB overexpression may be a direct result of HigB cleavage but many changes likely occurred due to downstream consequences of the alterations HigB caused in the proteome. These studies show that ribosome-dependent toxins can elicit specific changes in the mRNA pool and that these changes can have downstream consequences.

1.16 The HigB-HigA toxin-antitoxin system

The *higB-higA* (*higBA*) toxin-antitoxin locus encodes the HigB toxin and HigA antitoxin. This toxin-antitoxin system was originally identified on the rts1 plasmid in a post-operative *P. vulgaris* urinary tract infection (43). The rts1 plasmid is 217 kilobases and encodes approximately 300 genes (75). In addition to carrying a kanamycin-

resistance gene, the rts1 plasmid also encodes a temperature-sensitive phenotype, cell growth is limited at 42 °C, and the *higBA* locus appears to be responsible for this phenotype (43,76). Additionally, this phenotype is dependent on Lon protease (42). These data suggest that at normal temperatures, the antitoxin HigA is stable and inhibits HigB activity however, at elevated temperatures, HigA is unstable and degraded by Lon, therefore freeing HigB toxin to suppress growth. These, and other studies (56,77), determined that the function of HigB is to inhibit protein synthesis by cleaving adenosine-rich A-site codon sequences but only in the presence of the ribosome.

Although the *higBA* locus was originally discovered associated with *P. vulgaris*, it is present in many bacteria. For example, a HigB orthologue with over 90% sequence identity to *P. vulgaris* rts1 HigB has been identified in *Salmonella enterica* and *Providencia alcalifaciens*, both human pathogens, and *Photorhabdus luminescens,* a luminescent insect pathogen (78). Interestingly, hundreds of other species of bacteria contain putative HigB orthologues. Several residues are highly conserved throughout HigB proteins suggesting these play important, yet unknown, roles in HigB-mediated mRNA cleavage. My studies are the first to demonstrate the molecular basis of action of the HigBA complex.

1.17 Questions addressed

The HigBA toxin-antitoxin system has several unique molecular features that are not understood. In **Chapter 2**, I address the molecular basis for how the HigA antitoxin inhibits HigB toxin activity by solving the HigBA X-ray crystal structure and further, testing the functional basis for the heterotetrameric complex's function (79). In **Chapter 3**, I investigated how HigB interacts with the ribosome to cleave mRNA. I found that the

large subunit is not essential for HigB-mediated mRNA cleavage as mRNA bound to the 30S subunit is a HigB substrate. I further solved the X-ray crystal structure of HigB bound to the small subunit and used functional assays to determine which interactions between HigB and the ribosome were essential for function (Schureck et al., submitted). In **Chapter 4**, I determined the molecular basis for mRNA recognition by HigB. Using biochemical assays and structural approaches, I found that HigB has three nucleotide binding sites. Each binding site confers a unique specificity ranging from almost no specificity to an adenosine-specificity (80). In **Chapter 5**, I address the mechanistic basis of HigB cleavage of mRNA using single turnover kinetics. Through mutational analysis of proposed active site residues, I found that individual mutation of four residues drastically reduced HigB-mediated mRNA cleavage and I propose a mechanism by which HigB catalyzes mRNA cleavage (Schureck et al., submitted). My studies allowed us to identify several unique features of the HigBA toxin-antitoxin system and propose several previously unappreciated commonalities among toxin-antitoxin systems that aid our understanding of their biological functions. Finally in **Chapter 6**, I argue that each ribosome-dependent toxin likely plays a unique, but unknown role, in translational regulation during stress. I discuss future experiments to address key questions of ribosome-dependent toxins. I additionally describe some common features and differences between ribosome-dependent toxin members that are often conserved among homologs of individual family members.

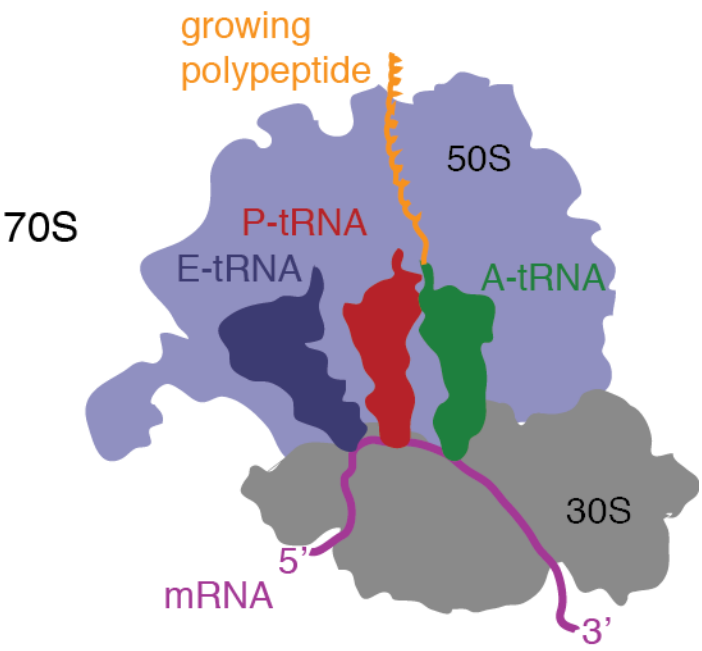

Figure 1.1: Overview of the bacterial ribosome.

The bacterial ribosome is made of a large 50S subunit (light purple) and a small 30S subunit (gray). mRNA (purple) interacts with the 30S subunit and is decoded by tRNA located in the aminoacyl (A) site. All three tRNAs are shown (A-tRNA, green; peptidyl, P-tRNA, red; exit tRNA, E-tRNA, blue) and the nascent polypeptide chain is shown in orange).

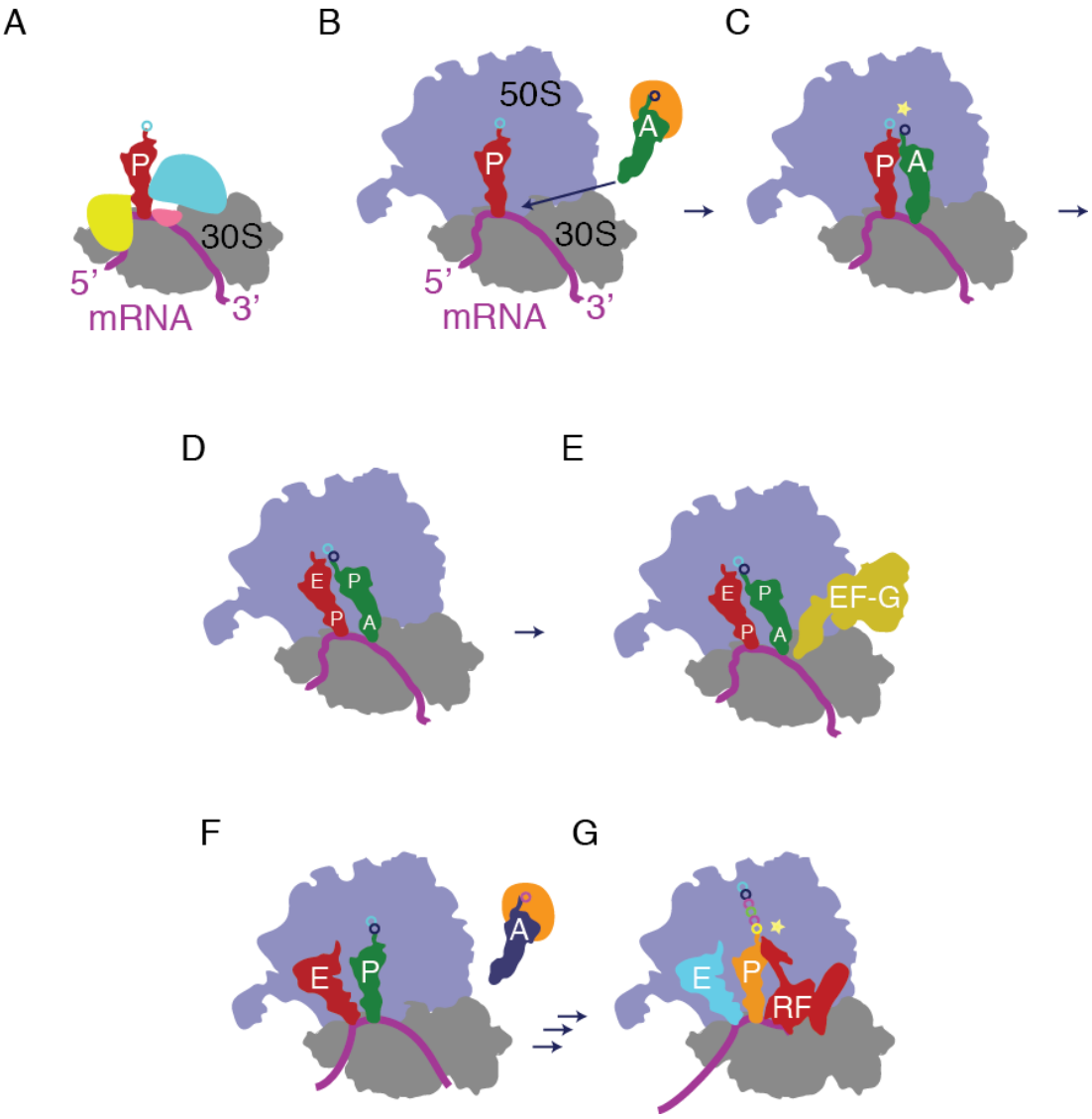

Figure 1.2: Overview of the translation process.

In all panels, the tRNAs are labeled A, P or E corresponding to the tRNA-binding site they are located within. (A) An initiator fMet-tRNA^{fMet} (red) located is in the P site carries a formylmethionine amino acid (light blue circle). Initiation factors 1 (pink), 2 (yellow) and 3 (blue) are bound to prevent A-site mRNA binding, facilitate P-site fMet-tRNA^{fMet} binding and prevent 50S association, respectively. (B) The initiation factors are no longer bound to the 30S ribosomal subunit and the 50S subunit is bound to the 30S. A tRNA (green) cognate to the A-site mRNA bound to GTP-bound EF-Tu (orange) enters

the ribosome. (C) The P-site fMet-tRNA^{fMet} and A-site tRNA are both bound and poised for peptide bond formation. (D) Peptide bond formation occurs. The nitrogen of the A-site tRNA amino acid attacks the carbonyl group of the P-site tRNA amino acid. The formylmethionine is now separated from P-site tRNA and is attached to the A-site tRNA amino acid (dark blue circle). The CCA ends of A and P-site tRNA move to the P and E sites of the 50S, respectively, while the anticodon stem loops stay in the A and P sites, respectively. (E) The mRNA, A and P-site tRNA anticodon step loops now move three nucleotides in the 5' direction, to the E and P sites of the ribosome, respectively. This movement is facilitated by EF-G. (F) tRNA cognate to the new A-site codon (dark blue) bound to GTP-bound EF-Tu (orange) binds to the A site and the translation cycle repeats until a stop codon is reached. (G) A release factor (red) binds an A-site stop codon and releases the growing polypeptide from the P-site tRNA by a hydrolysis event (yellow star).

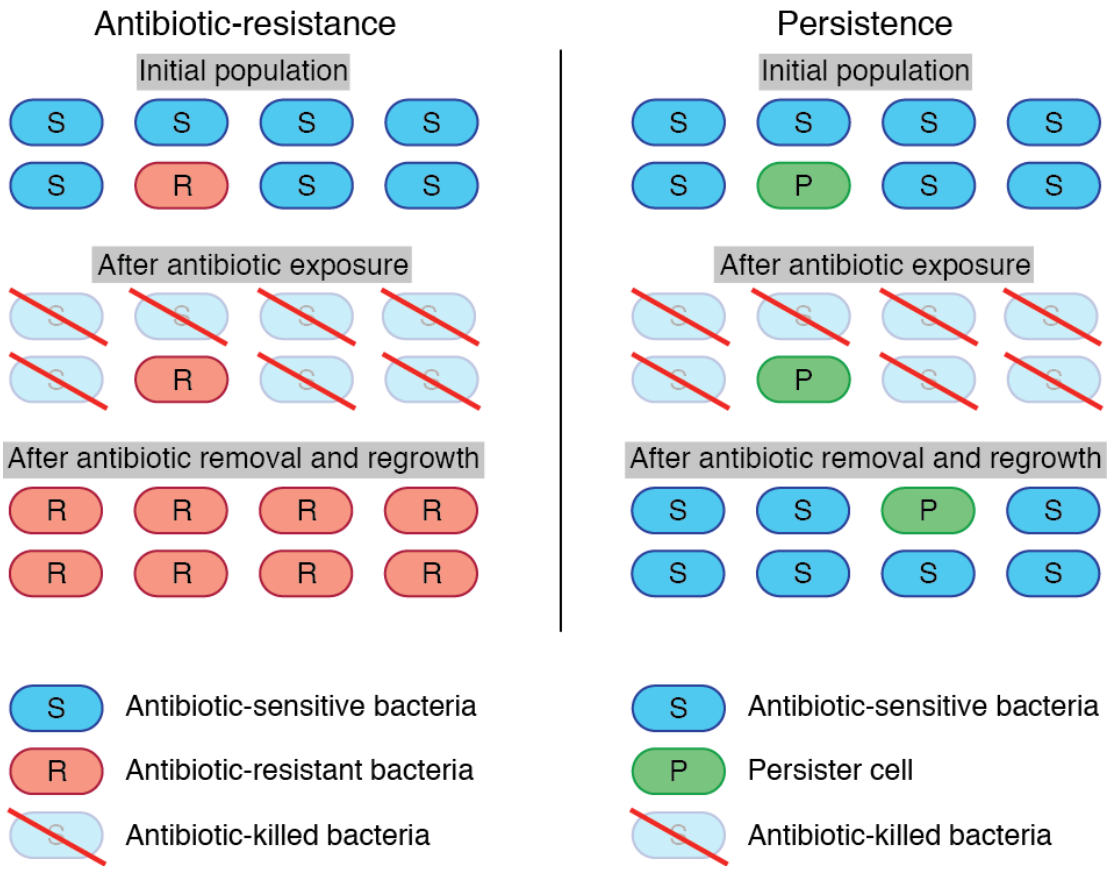

Figure 1.3: Schematic of difference between antibiotic-resistance and persistence. Left, the initial bacterial population consists of antibiotic-sensitive bacteria and bacteria with an antibiotic-resistance mechanism encoded in their genome. Antibiotic exposure kills all antibiotic-sensitive bacteria but not antibiotic-resistant bacteria. After removal and regrowth of antibiotic, antibiotic-resistant bacteria divide to create an entirely antibiotic-resistant population that is now genetically distinct from the starting population. Right, the initial bacterial population consists of antibiotic-sensitive bacteria and antibiotic-tolerant cells or what we call persister-primed cells. Antibiotic treatment kills antibiotic-sensitive cells but not persister cells. After removal of the antibiotic and regrowth of bacteria in liquid culture, a mixed population containing largely antibiotic-sensitive and a few persister cells is formed, identical to the starting population.

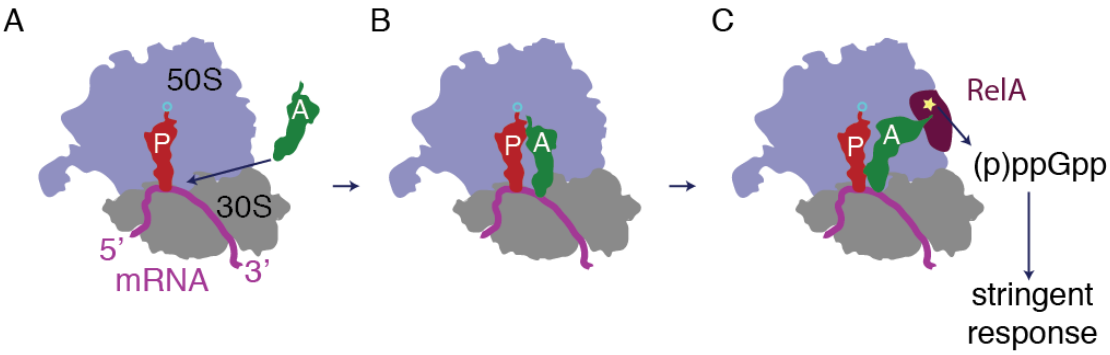

Figure 1.4: Schematic of stringent response activation by uncharged tRNA entering the ribosome.

The stringent response is activated in several ways (27), but here, I focus on amino acid deprivation that activates RelA. (A) tRNA charged with an amino acid (light blue circle) is bound to the P site. During shortage of amino acids, uncharged tRNA cognate to the A-site mRNA codon can bind the ribosomal A-site. (B) A and P-site tRNAs are bound to the ribosome but no peptide bond formation can occur. (C) The RelA protein interacts with uncharged A-site tRNA and synthesizes guanosine tetra/penta phosphate ((p)ppGpp), which activates the stringent response. The enzymatic reaction to create (p)ppGpp is denoted by a yellow star.

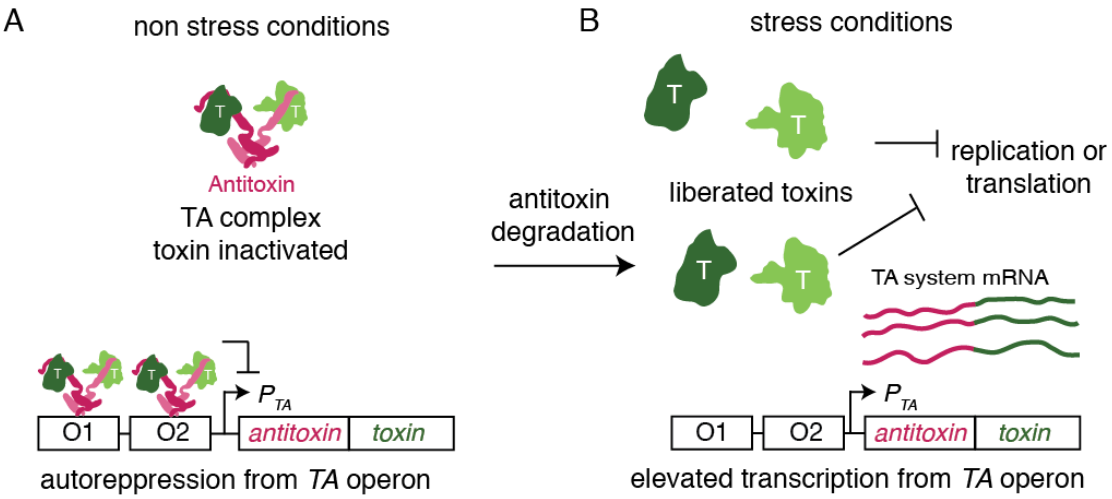

Figure 1.5: Schematic of toxin and antitoxin degradation.

The toxin proteins are colored green and labeled T and the antitoxin proteins are colored pink. (A) During non-stressed cell growth, the antitoxin binds and inhibits toxin activity and binds the operator DNA repressing toxin-antitoxin (TA) transcription. (B) Environmental stress activates toxin proteins by selectively degrading antitoxins. In the absence of antitoxin, toxins target cellular processes such as replication or translation and transcription from the toxin-antitoxin operon is de-repressed.

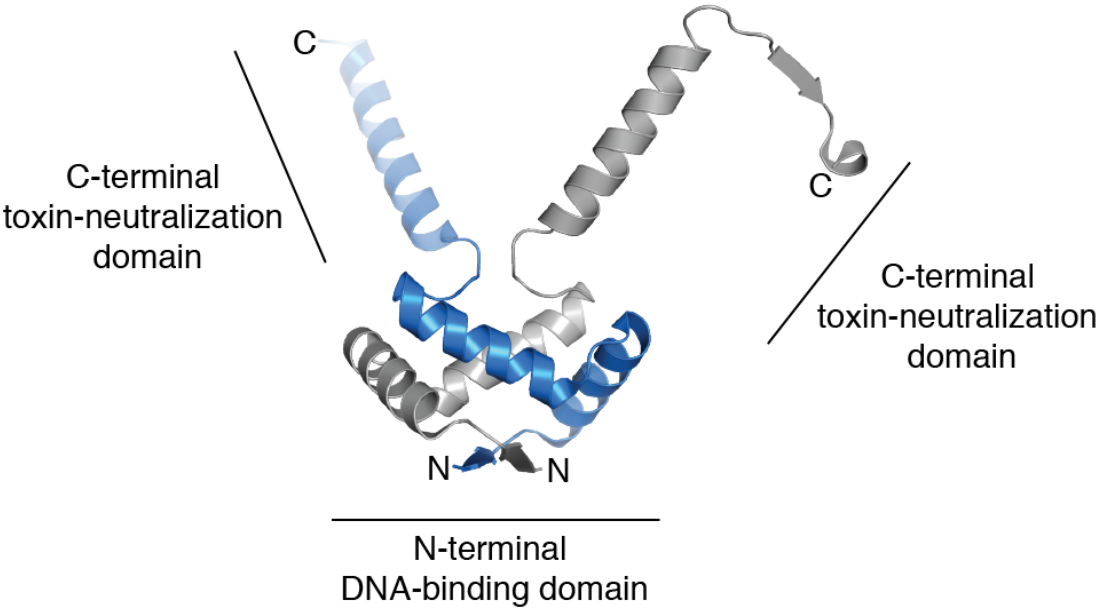

Figure 1.6: Antitoxins typically contain an N-terminal DNA-binding domain and a C-terminal toxin-neutralization domain.

Structure of the RelB antitoxin (PDB ID 4fxe) with its DNA-binding and toxin-neutralization domains labeled. The organization of the RelB antitoxin is typical of most antitoxins with its N-terminus forming the DNA-binding domain and its C-terminus forming the toxin-neutralization domain.

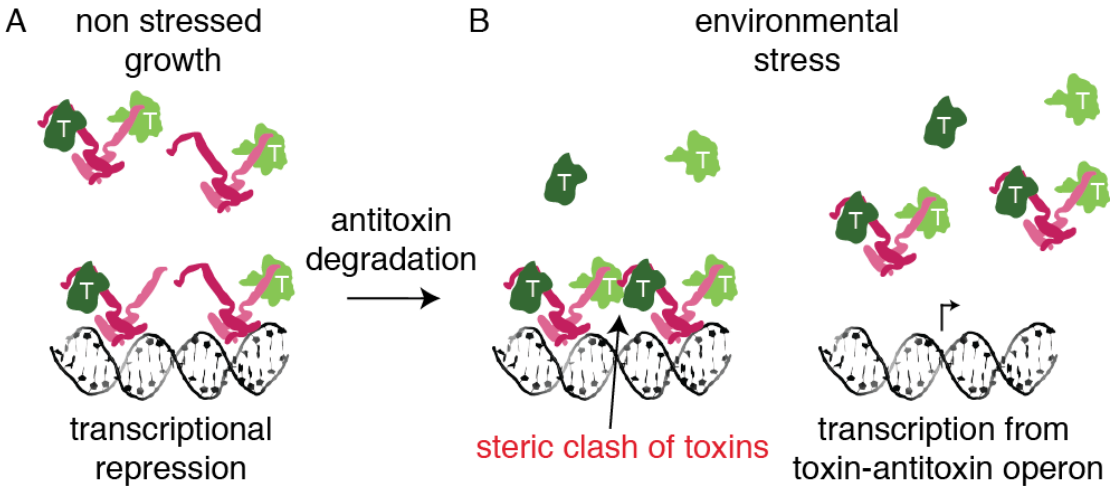

Figure 1.7: Current model for conditional cooperativity.

Toxin proteins are shown in green and labeled as "T" and antitoxins are colored dark and light pink. For simplicity, only the DNA representing one operator is shown. (A) It is proposed that during non-stressed growth, two antitoxin dimers that are each bound to one toxin bind DNA with high affinity and repress transcription from the toxin-antitoxin operon. (B) During environmental stress, the antitoxin protein is degraded causing higher toxin than antitoxin levels to be present. It is proposed that when an antitoxin dimer binds two toxins (a tetramer), the additional toxins create a steric clash and the toxin-antitoxin complexes have low affinity for DNA allowing for transcription from the toxin-antitoxin operon.

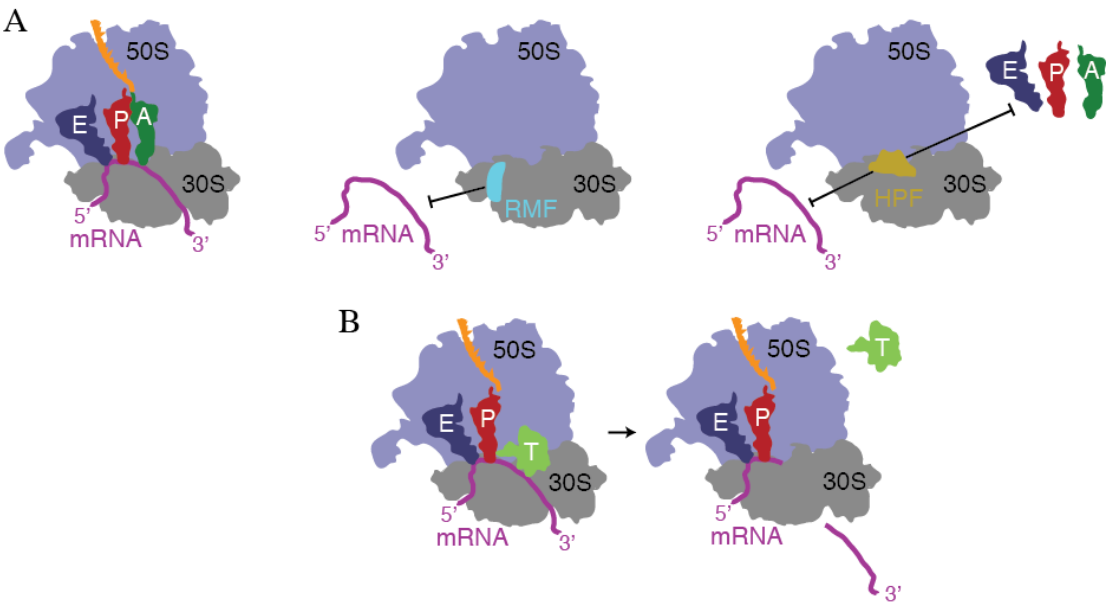

Figure 1.8: Translational inhibition by stoichiometric and enzymatic factors.

(A) Schematic of how ribosomal modulation factor (RMF) (middle) and hibernation promoting factor (HPF) (right) occupy mRNA and mRNA and tRNA binding sites (left), respectively, to inhibit translation. (B) Schematic of how ribosome-dependent toxins inhibit translation by cleavage of mRNA on the ribosome. mRNA is colored magenta, A-site tRNA forest green, P-site tRNA red, E-site tRNA blue, the 50S subunit light purple, the 30S subunit gray and the growing polypeptide chain yellow/orange.

1.18 References

1. Monack, D. M., Mueller, A., and Falkow, S. (2004) Persistent bacterial infections: the interface of the pathogen and the host immune system. *Nature reviews. Microbiology* **2**, 747-765
2. Kohanski, M. A., Dwyer, D. J., and Collins, J. J. (2010) How antibiotics kill bacteria: from targets to networks. *Nature reviews. Microbiology* **8**, 423-435
3. Blair, J. M., Webber, M. A., Baylay, A. J., Ogbolu, D. O., and Piddock, L. J. (2015) Molecular mechanisms of antibiotic resistance. *Nature reviews. Microbiology* **13**, 42-51
4. Sun, J., Deng, Z., and Yan, A. (2014) Bacterial multidrug efflux pumps: mechanisms, physiology and pharmacological exploitations. *Biochemical and biophysical research communications* **453**, 254-267
5. Wright, G. D. (2005) Bacterial resistance to antibiotics: enzymatic degradation and modification. *Advanced drug delivery reviews* **57**, 1451-1470
6. Lambert, P. A. (2005) Bacterial resistance to antibiotics: modified target sites. *Advanced drug delivery reviews* **57**, 1471-1485
7. Finch, R. G. (2004) Antibiotic resistance: a view from the prescriber. *Nature reviews. Microbiology* **2**, 989-994
8. Gandhi, N. R., Nunn, P., Dheda, K., Schaaf, H. S., Zignol, M., van Soolingen, D., Jensen, P., and Bayona, J. (2010) Multidrug-resistant and extensively drug-resistant tuberculosis: a threat to global control of tuberculosis. *Lancet* **375**, 1830-1843

9. Arias, C. A., and Murray, B. E. (2009) Antibiotic-resistant bugs in the 21st century--a clinical super-challenge. *The New England journal of medicine* **360**, 439-443

10. Ohnishi, M., Saika, T., Hoshina, S., Iwasaku, K., Nakayama, S., Watanabe, H., and Kitawaki, J. (2011) Ceftriaxone-resistant Neisseria gonorrhoeae, Japan. *Emerging infectious diseases* **17**, 148-149

11. Redgrave, L. S., Sutton, S. B., Webber, M. A., and Piddock, L. J. (2014) Fluoroquinolone resistance: mechanisms, impact on bacteria, and role in evolutionary success. *Trends in microbiology* **22**, 438-445

12. Campbell, E. A., Korzheva, N., Mustaev, A., Murakami, K., Nair, S., Goldfarb, A., and Darst, S. A. (2001) Structural mechanism for rifampicin inhibition of bacterial rna polymerase. *Cell* **104**, 901-912

13. Wilson, D. N. (2014) Ribosome-targeting antibiotics and mechanisms of bacterial resistance. *Nature reviews. Microbiology* **12**, 35-48

14. Franceschi, F. (2007) Back to the future: the ribosome as an antibiotic target. *Future microbiology* **2**, 571-574

15. Schmeing, T. M., and Ramakrishnan, V. (2009) What recent ribosome structures have revealed about the mechanism of translation. *Nature* **461**, 1234-1242

16. Voorhees, R. M., and Ramakrishnan, V. (2013) Structural basis of the translational elongation cycle. *Annual review of biochemistry* **82**, 203-236

17. Lewis, K. (2010) Persister cells. *Annual review of microbiology* **64**, 357-372

18. Mahenthiralingam, E., Urban, T. A., and Goldberg, J. B. (2005) The multifarious, multireplicon Burkholderia cepacia complex. *Nature reviews. Microbiology* **3**, 144-156

19. Mulcahy, L. R., Burns, J. L., Lory, S., and Lewis, K. (2010) Emergence of Pseudomonas aeruginosa strains producing high levels of persister cells in patients with cystic fibrosis. *Journal of bacteriology* **192**, 6191-6199

20. Rowe, S. E., Conlon, B. P., Keren, I., and Lewis, K. (2016) Persisters: Methods for Isolation and Identifying Contributing Factors--A Review. *Methods in molecular biology* **1333**, 17-28

21. Helaine, S., Cheverton, A. M., Watson, K. G., Faure, L. M., Matthews, S. A., and Holden, D. W. (2014) Internalization of Salmonella by macrophages induces formation of nonreplicating persisters. *Science* **343**, 204-208

22. Maisonneuve, E., Castro-Camargo, M., and Gerdes, K. (2013) (p)ppGpp controls bacterial persistence by stochastic induction of toxin-antitoxin activity. *Cell* **154**, 1140-1150

23. Maisonneuve, E., and Gerdes, K. (2014) Molecular mechanisms underlying bacterial persisters. *Cell* **157**, 539-548

24. Maisonneuve, E., Shakespeare, L. J., Jorgensen, M. G., and Gerdes, K. (2011) Bacterial persistence by RNA endonucleases. *Proceedings of the National Academy of Sciences of the United States of America* **108**, 13206-13211

25. Keren, I., Shah, D., Spoering, A., Kaldalu, N., and Lewis, K. (2004) Specialized persister cells and the mechanism of multidrug tolerance in Escherichia coli. *Journal of bacteriology* **186**, 8172-8180

26. Potrykus, K., and Cashel, M. (2008) (p)ppGpp: still magical? *Annual review of microbiology* **62**, 35-51

27. Boutte, C. C., and Crosson, S. (2013) Bacterial lifestyle shapes stringent response activation. *Trends in microbiology* **21**, 174-180

28. Christensen, S. K., Mikkelsen, M., Pedersen, K., and Gerdes, K. (2001) RelE, a global inhibitor of translation, is activated during nutritional stress. *Proceedings of the National Academy of Sciences of the United States of America* **98**, 14328-14333

29. Germain, E., Roghanian, M., Gerdes, K., and Maisonneuve, E. (2015) Stochastic induction of persister cells by HipA through (p)ppGpp-mediated activation of mRNA endonucleases. *Proceedings of the National Academy of Sciences of the United States of America* **112**, 5171-5176

30. Haseltine, W. A., and Block, R. (1973) Synthesis of guanosine tetra- and pentaphosphate requires the presence of a codon-specific, uncharged transfer ribonucleic acid in the acceptor site of ribosomes. *Proceedings of the National Academy of Sciences of the United States of America* **70**, 1564-1568

31. Haseltine, W. A., Block, R., Gilbert, W., and Weber, K. (1972) MSI and MSII made on ribosome in idling step of protein synthesis. *Nature* **238**, 381-384

32. Gerdes, K., Christensen, S. K., and Lobner-Olesen, A. (2005) Prokaryotic toxin-antitoxin stress response loci. *Nature reviews. Microbiology* **3**, 371-382

33. Pandey, D. P., and Gerdes, K. (2005) Toxin-antitoxin loci are highly abundant in free-living but lost from host-associated prokaryotes. *Nucleic acids research* **33**, 966-976

34. Boggild, A., Sofos, N., Andersen, K. R., Feddersen, A., Easter, A. D., Passmore, L. A., and Brodersen, D. E. (2012) The crystal structure of the intact E. coli RelBE toxin-antitoxin complex provides the structural basis for conditional cooperativity. *Structure* **20**, 1641-1648

35. Kamada, K., and Hanaoka, F. (2005) Conformational change in the catalytic site of the ribonuclease YoeB toxin by YefM antitoxin. *Molecular cell* **19**, 497-509

36. Liang, Y., Gao, Z., Wang, F., Zhang, Y., Dong, Y., and Liu, Q. (2014) Structural and functional characterization of Escherichia coli toxin-antitoxin complex DinJ-YafQ. *The Journal of biological chemistry* **289**, 21191-21202

37. Ruangprasert, A., Maehigashi, T., Miles, S. J., Giridharan, N., Liu, J. X., and Dunham, C. M. (2014) Mechanisms of toxin inhibition and transcriptional repression by Escherichia coli DinJ-YafQ. *The Journal of biological chemistry* **289**, 20559-20569

38. Simanshu, D. K., Yamaguchi, Y., Park, J. H., Inouye, M., and Patel, D. J. (2013) Structural basis of mRNA recognition and cleavage by toxin MazF and its regulation by antitoxin MazE in Bacillus subtilis. *Molecular cell* **52**, 447-458

39. Christensen-Dalsgaard, M., Jorgensen, M. G., and Gerdes, K. (2010) Three new RelE-homologous mRNA interferases of Escherichia coli differentially induced by environmental stresses. *Molecular microbiology* **75**, 333-348

40. Singh, R., Barry, C. E., 3rd, and Boshoff, H. I. (2010) The three RelE homologs of Mycobacterium tuberculosis have individual, drug-specific effects on bacterial antibiotic tolerance. *Journal of bacteriology* **192**, 1279-1291

41. Janssen, B. D., Garza-Sanchez, F., and Hayes, C. S. (2015) YoeB toxin is activated during thermal stress. *MicrobiologyOpen* **4**, 682-697

42. Tian, Q. B., Ohnishi, M., Murata, T., Nakayama, K., Terawaki, Y., and Hayashi, T. (2001) Specific protein-DNA and protein-protein interaction in the hig gene system, a plasmid-borne proteic killer gene system of plasmid Rts1. *Plasmid* **45**, 63-74

43. Tian, Q. B., Ohnishi, M., Tabuchi, A., and Terawaki, Y. (1996) A new plasmid-encoded proteic killer gene system: cloning, sequencing, and analyzing hig locus of plasmid Rts1. *Biochemical and biophysical research communications* **220**, 280-284

44. Afif, H., Allali, N., Couturier, M., and Van Melderen, L. (2001) The ratio between CcdA and CcdB modulates the transcriptional repression of the ccd poison-antidote system. *Molecular microbiology* **41**, 73-82

45. Garcia-Pino, A., Balasubramanian, S., Wyns, L., Gazit, E., De Greve, H., Magnuson, R. D., Charlier, D., van Nuland, N. A., and Loris, R. (2010) Allostery and intrinsic disorder mediate transcription regulation by conditional cooperativity. *Cell* **142**, 101-111

46. Overgaard, M., Borch, J., Jorgensen, M. G., and Gerdes, K. (2008) Messenger RNA interferase RelE controls relBE transcription by conditional cooperativity. *Molecular microbiology* **69**, 841-857

47. Bernard, P., and Couturier, M. (1992) Cell killing by the F plasmid CcdB protein involves poisoning of DNA-topoisomerase II complexes. *Journal of molecular biology* **226**, 735-745

48. Zhang, Y., Zhang, J., Hoeflich, K. P., Ikura, M., Qing, G., and Inouye, M. (2003) MazF cleaves cellular mRNAs specifically at ACA to block protein synthesis in Escherichia coli. *Molecular cell* **12**, 913-923

49. Yamaguchi, Y., Park, J. H., and Inouye, M. (2009) MqsR, a crucial regulator for quorum sensing and biofilm formation, is a GCU-specific mRNA interferase in Escherichia coli. *The Journal of biological chemistry* **284**, 28746-28753

50. Castro-Roa, D., Garcia-Pino, A., De Gieter, S., van Nuland, N. A., Loris, R., and Zenkin, N. (2013) The Fic protein Doc uses an inverted substrate to phosphorylate and inactivate EF-Tu. *Nature chemical biology* **9**, 811-817

51. Kaspy, I., Rotem, E., Weiss, N., Ronin, I., Balaban, N. Q., and Glaser, G. (2013) HipA-mediated antibiotic persistence via phosphorylation of the glutamyl-tRNA-synthetase. *Nature communications* **4**, 3001

52. Germain, E., Castro-Roa, D., Zenkin, N., and Gerdes, K. (2013) Molecular mechanism of bacterial persistence by HipA. *Molecular cell* **52**, 248-254

53. Winther, K. S., Brodersen, D. E., Brown, A. K., and Gerdes, K. (2013) VapC20 of Mycobacterium tuberculosis cleaves the sarcin-ricin loop of 23S rRNA. *Nature communications* **4**, 2796

54. Schifano, J. M., Edifor, R., Sharp, J. D., Ouyang, M., Konkimalla, A., Husson, R. N., and Woychik, N. A. (2013) Mycobacterial toxin MazF-mt6 inhibits translation through cleavage of 23S rRNA at the ribosomal A site. *Proceedings of the National Academy of Sciences of the United States of America* **110**, 8501-8506

55. Pedersen, K., Zavialov, A. V., Pavlov, M. Y., Elf, J., Gerdes, K., and Ehrenberg, M. (2003) The bacterial toxin RelE displays codon-specific cleavage of mRNAs in the ribosomal A site. *Cell* **112**, 131-140

56. Hurley, J. M., and Woychik, N. A. (2009) Bacterial toxin HigB associates with ribosomes and mediates translation-dependent mRNA cleavage at A-rich sites. *The Journal of biological chemistry* **284**, 18605-18613

57. Prysak, M. H., Mozdzierz, C. J., Cook, A. M., Zhu, L., Zhang, Y., Inouye, M., and Woychik, N. A. (2009) Bacterial toxin YafQ is an endoribonuclease that associates with the ribosome and blocks translation elongation through sequence-specific and frame-dependent mRNA cleavage. *Molecular microbiology* **71**, 1071-1087

58. Christensen-Dalsgaard, M., and Gerdes, K. (2008) Translation affects YoeB and MazF messenger RNA interferase activities by different mechanisms. *Nucleic acids research* **36**, 6472-6481

59. Zhang, Y., and Inouye, M. (2009) The inhibitory mechanism of protein synthesis by YoeB, an Escherichia coli toxin. *The Journal of biological chemistry* **284**, 6627-6638

60. Moyed, H. S., and Bertrand, K. P. (1983) hipA, a newly recognized gene of Escherichia coli K-12 that affects frequency of persistence after inhibition of murein synthesis. *Journal of bacteriology* **155**, 768-775

61. Schumacher, M. A., Balani, P., Min, J., Chinnam, N. B., Hansen, S., Vulic, M., Lewis, K., and Brennan, R. G. (2015) HipBA-promoter structures reveal the basis of heritable multidrug tolerance. *Nature* **524**, 59-64

62. Nariya, H., and Inouye, M. (2008) MazF, an mRNA interferase, mediates programmed cell death during multicellular Myxococcus development. *Cell* **132**, 55-66

63. Kolodkin-Gal, I., Hazan, R., Gaathon, A., Carmeli, S., and Engelberg-Kulka, H. (2007) A linear pentapeptide is a quorum-sensing factor required for mazEF-mediated cell death in Escherichia coli. *Science* **318**, 652-655

64. Engelberg-Kulka, H., Amitai, S., Kolodkin-Gal, I., and Hazan, R. (2006) Bacterial programmed cell death and multicellular behavior in bacteria. *PLoS genetics* **2**, e135

65. Harrison, J. J., Wade, W. D., Akierman, S., Vacchi-Suzzi, C., Stremick, C. A., Turner, R. J., and Ceri, H. (2009) The chromosomal toxin gene yafQ is a determinant of multidrug tolerance for Escherichia coli growing in a biofilm. *Antimicrobial agents and chemotherapy* **53**, 2253-2258

66. Sberro, H., Leavitt, A., Kiro, R., Koh, E., Peleg, Y., Qimron, U., and Sorek, R. (2013) Discovery of functional toxin/antitoxin systems in bacteria by shotgun cloning. *Molecular cell* **50**, 136-148

67. Starosta, A. L., Lassak, J., Jung, K., and Wilson, D. N. (2014) The bacterial translation stress response. *FEMS microbiology reviews* **38**, 1172-1201

68. Boel, G., Smith, P. C., Ning, W., Englander, M. T., Chen, B., Hashem, Y., Testa, A. J., Fischer, J. J., Wieden, H. J., Frank, J., Gonzalez, R. L., Jr., and Hunt, J. F. (2014) The ABC-F protein EttA gates ribosome entry into the translation elongation cycle. *Nature structural & molecular biology* **21**, 143-151

69. Chen, B., Boel, G., Hashem, Y., Ning, W., Fei, J., Wang, C., Gonzalez, R. L., Jr., Hunt, J. F., and Frank, J. (2014) EttA regulates translation by binding the ribosomal E site and restricting ribosome-tRNA dynamics. *Nature structural & molecular biology* **21**, 152-159

70. Polikanov, Y. S., Blaha, G. M., and Steitz, T. A. (2012) How hibernation factors RMF, HPF, and YfiA turn off protein synthesis. *Science* **336**, 915-918

71. Maehigashi, T., Ruangprasert, A., Miles, S. J., and Dunham, C. M. (2015) Molecular basis of ribosome recognition and mRNA hydrolysis by the E. coli YafQ toxin. *Nucleic acids research* **43**, 8002-8012

72. Christensen, S. K., Maenhaut-Michel, G., Mine, N., Gottesman, S., Gerdes, K., and Van Melderen, L. (2004) Overproduction of the Lon protease triggers inhibition of translation in Escherichia coli: involvement of the yefM-yoeB toxin-antitoxin system. *Molecular microbiology* **51**, 1705-1717

73. Zhang, Y., Yamaguchi, Y., and Inouye, M. (2009) Characterization of YafO, an Escherichia coli toxin. *The Journal of biological chemistry* **284**, 25522-25531

74. Schuessler, D. L., Cortes, T., Fivian-Hughes, A. S., Lougheed, K. E., Harvey, E., Buxton, R. S., Davis, E. O., and Young, D. B. (2013) Induced ectopic expression of HigB toxin in Mycobacterium tuberculosis results in growth inhibition, reduced abundance of a subset of mRNAs and cleavage of tmRNA. *Molecular microbiology* **90**, 195-207

75. Murata, T., Ohnishi, M., Ara, T., Kaneko, J., Han, C. G., Li, Y. F., Takashima, K., Nojima, H., Nakayama, K., Kaji, A., Kamio, Y., Miki, T., Mori, H., Ohtsubo, E., Terawaki, Y., and Hayashi, T. (2002) Complete nucleotide sequence of plasmid

Rts1: implications for evolution of large plasmid genomes. *Journal of bacteriology* **184**, 3194-3202

76. Terawaki, Y., Kakizawa, Y., Takayasu, H., and Yoshikawa, M. (1968) Temperature sensitivity of cell growth in Escherichia coli associated with the temperature sensitive R(KM) factor. *Nature* **219**, 284-285

77. Christensen-Dalsgaard, M., and Gerdes, K. (2006) Two higBA loci in the Vibrio cholerae superintegron encode mRNA cleaving enzymes and can stabilize plasmids. *Molecular microbiology* **62**, 397-411

78. Altschul, S. F., Madden, T. L., Schaffer, A. A., Zhang, J., Zhang, Z., Miller, W., and Lipman, D. J. (1997) Gapped BLAST and PSI-BLAST: a new generation of protein database search programs. *Nucleic acids research* **25**, 3389-3402

79. Schureck, M. A., Maehigashi, T., Miles, S. J., Marquez, J., Cho, S. E., Erdman, R., and Dunham, C. M. (2014) Structure of the Proteus vulgaris HigB-(HigA)2-HigB toxin-antitoxin complex. *The Journal of biological chemistry* **289**, 1060-1070

80. Schureck, M. A., Dunkle, J. A., Maehigashi, T., Miles, S. J., and Dunham, C. M. (2015) Defining the mRNA recognition signature of a bacterial toxin protein. *Proceedings of the National Academy of Sciences of the United States of America* **112**, 13862-13867

Chapter 2

Structure of the *P. vulgaris* HigB-$(HigA)_2$-HigB toxin-antitoxin complex

Marc A. Schureck, Tatsuya Maehigashi, Stacey J. Miles, Jhomar Marquez, Shein Ei Cho, Rachel Erdman, and Christine M. Dunham

During non-stressed growth, the HigA antitoxin inhibits HigB-mediated cleavage of ribosome-bound mRNA and represses transcription from the *hig* operon. To gain structural insights into how HigA performs these two functions, I solved the X-ray crystal structure of the HigA in complex with HigB. I found that HigA is an obligate dimer and each HigA binds one HigB to form a heterotetramer. In this complex, HigB is likely prevented from binding the ribosome. On the opposite surface that HigA binds HigB with, HigA forms a helix-turn-helix DNA-binding motif. Thus, HigA is able to inhibit HigB and transcription from the *hig* operon because of the use of two distinct binding sites.

This research was originally published in the Journal of Biological Chemistry. Schureck MA, Maehigashi T, Miles SJ, Marquez J, Ei Cho S, Erdman R, and Dunham CM. Structure of the *Proteus vulgaris* HigB-$(HigA)_2$-HigB Toxin-Antitoxin Complex. *Journal of Biological Chemistry*. 2014 289(2):1060-70.

Author contributions: M.A.S. and C.M.D. designed research; M.A.S., T.M., S.J.M., J.M., S.E.C., and R.E. performed research; M.A.S., T.M., and C.M.D. analyzed data; and M.A.S., T.M., and C.M.D. wrote the paper.

2.1 Abstract

Bacterial toxin-antitoxin (TA) systems regulate key cellular processes to promote cell survival during periods of stress. During steady-state cell growth, antitoxins typically interact with their cognate toxins to inhibit activity presumably by preventing substrate recognition. We solved two X-ray crystal structures of the *Proteus vulgaris* tetrameric HigB-$(HigA)_2$-HigB TA complex and find that, unlike most other TA systems, the antitoxin HigA makes minimal interactions with the toxin HigB. HigB adopts a RelE-family tertiary fold containing a highly conserved, concave surface where we predict its active site is located. HigA does not cover the solvent exposed HigB active site, suggesting that in general, toxin inhibition is not solely mediated by active site hindrance by its antitoxin. Each HigA monomer contains a helix-turn-helix (HTH) motif that binds to its own DNA operator to repress transcription during normal cellular growth. This is distinct from antitoxins belonging to other super families that typically only form DNA-binding motifs upon dimerization. We further show that disruption of the HigB-$(HigA)_2$-HigB tetramer to a HigBA heterodimer ablates operator binding. Taken together, our biochemical and structural studies elucidate the novel molecular details of the HigBA TA system.

2.2 Introduction

Toxin-antitoxin (TA) systems are chromosomally- or plasmid-encoded gene pairs found in free-living bacteria that aid in survival during environmental and chemical stresses (1). TA systems have been implicated in diverse functions such as programmed cell death, growth and gene regulation, biofilm formation and persistence during increased antibiotic exposure, but their precise physiological functions are controversial

(2-8). Their roles in persistence, adaptation and survival mechanisms underscores their great potential as novel antimicrobial targets (9).

Type II TA operons encode both a small antitoxin and toxin protein (8-12 kDa each) that under normal growth conditions, form a tight, non-toxic complex. These complexes transcriptionally autorepress by binding at operator sequences in their promoter region (1). Upon stress, the antitoxin is degraded by proteases, allowing the toxin to target key cellular processes including replication (DNA gyrase) and translation (free mRNA, ribosome-bound mRNA or the ribosome itself) (10-17). Tightly regulating and/or reducing these energetically expensive processes leads to an overall decrease in metabolite consumption and halts cell growth. This bacteriostatic state continues until the stress passes (1).

RelE is one of the best-studied ribosome-dependent toxins and functions by degrading mRNAs preferentially at stop codons in the ribosomal A site (11). Recent evidence suggests RelE may recognize additional codons but the molecular details of this specificity remain unclear (18,19). RelE family member YafQ cleaves at lysine codons while YoeB cleaves at both sense and stop codons (14,20,21). The *host inhibition of growth* (HigB) protein from *Proteus spp* is a RelE family member with a relaxed codon specificity (13,22). HigB preferentially degrades 5'-AAA-3' codons (lysine) but codons containing only one adenosine are sufficient for degradation by HigB (13).

The *Proteus vulgaris* HigBA TA system was first discovered on an exogenous plasmid that conferred kanamycin resistance and post-segregational killing at elevated temperatures (23). This plasmid was isolated from a post-operative pyelonephitis, an ascending urinary tract infection (23,24). The *higBA* gene pair is not found in *E. coli* K12

but is found chromosomally in pathogens such as *Vibrio cholerae*, *Streptococcus pneumoniae, E. coli* CFT073 and *E. coli* O157:H7 (25).

The HigB toxin gene and protein are distinguished from those of other RelE family toxins in three ways. First, the *higBA* operon has an inverted gene structure with the HigB toxin gene preceding its cognate antitoxin (**Fig. 2.1A**) (23). This gene arrangement is only seen in the MqsRA and hicAB TA systems (15,25). Second, sequence alignments with other RelE family members indicate that HigB appears to lack conserved catalytic residues required for mRNA recognition and degradation (**Fig. 2.4A**). Lastly, a single adenosine in the context of a codon is sufficient for degradation by HigB (13). This contrasts with previously proposed strict mRNA sequence requirements for other toxins (11,14).

We report the structural and biochemical characterization of the novel TA pair HigBA. Remarkably, unlike most antitoxins, HigA makes relatively few contacts with its toxin partner and does not cover the solvent accessible, HigB active site. This structural arrangement implies a possible novel model of inhibition. We also present biochemical data that demonstrates that tetrameric HigBA (henceforth denoted as HigB-$(HigA)_2$-HigB to reflect its spatial organization) is required for productive binding to its own DNA operator sequences, validating the functional relevance of our structural data.

2.3 Experimental procedures

Plasmids pET21c-HigBA and pET28a-his_6HigBA were generous gifts from Dr. Nancy A. Woychik (Rutgers- Robert Wood Johnson Medical School). A C-terminal hexahistidine (His_6) tag encoded on the pET21c construct was added to HigA of the pET21c-HigBA construct by removal of the natural HigA stop codon using site-directed

mutagenesis to create pET21c-HigBAhis$_6$. The pET28a-his$_6$HigBA (Δ84-104) plasmid was created by placing a premature stop codon in HigA after the codon 83. All sequences were verified by DNA sequencing (GeneWiz).

2.3a HigBA expression and purification

E. coli BL21(DE3) cells harboring pET21c-HigBAhis$_6$ and pET28a-his$_6$HigBA were grown at 37 °C with shaking in Lysogeny Broth medium with either 100 μg/ml ampicillin or 10 μg/ml kanamycin respectively. Protein expression was induced with 0.05 mM isopropyl-1-thio-β-D-galactopyranoside (IPTG) and cultures were grown for an additional three hours except for pET28a-his$_6$HigBA (Δ84-104) which was grown at 18 °C for 12 hours after induction. All cells were pelleted at 4,000 x *g* for 15 minutes, washed with size exclusion column buffer (40 mM Tris-HCl pH 7.5, 250 mM KCl, 5 mM $MgCl_2$, and 5 mM β-mercaptoethanol (β-ME)), pelleted again at 7,000 x *g* for 10 minutes and stored at -20 °C.

Cell pellets were thawed on ice, resuspended in lysis buffer (20 mM Tris-HCl pH 7.5, 10% (w/v) glycerol, 250 mM KCl, 5 mM β-ME, 0.2 mM phenylmethylsulfonyl fluoride (PMSF) and 0.1% (w/v) Triton X-100) and lysed by sonication. Each supernatant was collected by centrifugation at 39,000 x *g* for 45 minutes and filtered through a 0.45 μm filter (Millipore), prior to loading onto a 5 ml Ni^{2+}-NTA column using an ÄKTApurifier10 (GE Healthcare) at 10 °C. The column was washed with buffer A (40 mM Tris-HCl pH 7.5, 10% (w/v) glycerol, 250 mM KCl, 5 mM $MgCl_2$, 5 mM β-ME and 50 mM imidazole) and eluted with a linear gradient of the same buffer supplemented with 500 mM imidazole. Elution fractions containing the target proteins were concentrated with a 3 kDa molecular weight cutoff concentrator (Millipore), filtered and loaded onto a

Superdex 200 16/60 column (GE Healthcare). Protein fractions determined to be >95% pure by SDS-PAGE were pooled and used for crystallization or biochemical analyses. Selenomethionine-incorporated HigBA-His_6 protein was expressed in *E. coli* BL21(DE3) cells as described (26) and purified as described above.

2.3b Crystallization, X-ray data collection and structural determination of HigBA complexes.

HigBA-His_6 (Crystal Form 1) - Crystals of trypsinized selenomethionine-derivitized HigBA-His_6 were grown by sitting drop vapor diffusion in 3-10% PEG 3350, 0.2 M L-proline, and 0.1 M HEPES pH 7.5 over approximately two days at 10 ˚C. Ethylene glycol was used as a cryoprotectant and added in two increments to a final concentration of 30%. Crystals were flash frozen in liquid nitrogen and a Single Anomalous Dispersion (SAD) dataset was collected at the Northeastern-Collaborative Access Team (NE-CAT) 24-IDC beamline at the Advanced Photon Source (APS) using 0.979 Å radiation (Table 1). A total of 113,311 reflections were collected, indexed and reduced to 16,748 unique reflections (unmerged) to a resolution of 2.8 Å with the program HKL2000 (27). Phase determination was carried out using the intrinsic anomalous signals from selenium. A total of 11 heavy atom sites were identified and used for initial phases with the program Autosol of the PHENIX Suite (28). The starting model was initially built by PHENIX Autobuild (28), followed by manual building in Coot (29). During refinement, XYZ coordinates, real-space and B-factors (isotropic) were refined to a final R_{work}/R_{free} of 19.7/23.8. The final model contained two HigB and two HigA molecules per asymmetric unit (**Figs. 2.1 & 2.2A**).

His_6HigBA (Crystal Form 2) - Crystals of His_6HigBA were grown by sitting drop vapor diffusion in 90 mM sodium acetate pH 4.6, 180 mM ammonium acetate, 25% PEG 4000 and 4% acetone at 20 °C in 1 week. For cryoprotection, dextrose was dissolved in the reservoir solution and added to the crystallization drop in 15% increments up to 30% (w/v) by exchanging the mother liquor. This was followed by 1-2 minutes of equilibration, flash frozen in liquid nitrogen and a native dataset was collected NE-CAT 24-IDE beamline. A total of 172,519 reflections were collected, indexed and reduced to 31,287 unique reflections with the program XDS (30). The structure was solved to 2.2 Å by molecular replacement using the AutoMR PHENIX program (28) with one HigB and one HigA molecule from the previously solved HigBA complex as a search model (Form 1). Three HigB and three HigA molecules were found in the asymmetric unit (**Fig. 2.2B**). A similar PHENIX refinement scheme was used as with Form 1, but with the addition of TLS refinement. Manual model building in Coot was performed to a final R_{work}/R_{free} of 17.5/21.3% (29).

Protein Interfaces, Surfaces, and Assemblies (PISA) program was used to calculate molecular interfaces and oligomeric states (31) while ConSurf was used to map HigB sequence conservation onto the crystal structure (32). Sequence alignments were performed with ClustalW (33) and all figures were generated using PyMOL(34).

2.3c Size exclusion chromatography (SEC) assays

One hundred microliters of 75 μM protein in SEC buffer were loaded onto a Superdex 75 10/300 column (GE Healthcare). Estimated molecular weights were calculated by comparison to molecular weight standards (Bio-Rad) (**Fig. 2.7D**). Peaks

from the SEC chromatogram corresponding to different protein-protein complexes were run on a 15% SDS-PAGE gel for analysis (**Fig. 2.7E**).

2.3d Electrophoretic mobility shift assay (EMSA)

Assays were performed as described previously (35) but with slight modifications. Double-stranded DNA representing the *Phig* region was generated by mixing chemically synthesized DNA (IDT), heating to 90 °C for 2 minutes and slowly cooling to room temperature (**Fig. 2.7A**). Protein at a final concentration of 0, 0.25, 0.5, 1, and 2 μM was incubated with 10 ng DNA for 20 minutes on ice along with 0.5 mg/ml BSA. Free and protein-bound DNA were resolved on a native 8% PAGE gel prepared with Tris-Borate pH 8-EDTA buffer (**Fig. 2.7C**). The gel was run at 10 °C for 1 hour and DNA was stained with SYBR Green dye (Invitrogen) and visualized using a Typhoon Trio (GE Healthcare).

2.3e Molecular modeling HigB on the 70S ribosome

HigB was modeled on *E. coli* RelE bound to the *Thermus thermophilus* 70S ribosome (36) (**Figs. 2.8 & 2.9**) (PDB ID 3K1Q). The HigB coordinates were optimally superimposed onto RelE using secondary-structure matching (SSM) in Coot (37). Conserved secondary structural motifs of the RNase fold of RelE and HigB aligned with a root mean square deviation (r.m.s.d.) of 2.4 Å (for 63 equivalent α carbons pairs) (**Fig. 2.9**).

2.4 Results

2.4a Structural determination of the HigB-$(HigA)_2$-HigB complex.

By placing the hexahistidine tag at either the N terminus of HigB or the C terminus of HigA, we were able to solve two different X-ray crystal structures of the HigBA complex (**Figs. 2.1 & 2.2**). Given how small each protein is (the antitoxin is 11.5 kDa while the toxin is 10.7 kDa), we were concerned that the affinity tag may influence potential crystal packing interactions and the overall oligomeric states. However, both crystal structures are entirely consistent, with an overall r.m.s.d of 0.9 Å for 366 equivalent α carbon pairs with only a single minor difference within loop 5 of HigB (**Fig. 2.2C**) (38).

The HigBA-His_6 complex (Form 1) crystallized in the hexagonal spacegroup $P3_221$ with two HigBA heterodimers per asymmetric unit (**Fig. 2.2A**). The initial phases to 2.8 Å were obtained by the single wavelength anomalous dispersion method (SAD) using selenomethionine derivatized protein (**Table 2.1**). This model was used as an initial search model for the His_6-HigBA structure (Form 2), solved using molecular replacement to 2.2 Å (Table 1). The Form 2 complex grew in the hexagonal spacegroup $P6_2$ with three HigB and three HigA molecules per asymmetric unit (**Table 2.1 & Fig. 2.2B**). Both Form 1 and 2 contain a HigB-$(HigA)_2$-HigB tetramer while Form 2 contains an additional HigBA dimer in the asymmetric unit. A full tetramer is formed by applying a two-fold crystallographic symmetry (**Fig. 2.2B**). Thus, the overall subunit compositions of HigB and HigA are identical.

In Form 1, residues 1-90 (92 total) were built for one HigB molecule while unambiguous density allowed building of all HigB residues of the second molecule. The

C terminus of the fully built HigB is involved in crystal contacts with a neighboring crystallographic symmetry related molecule, which presumably stabilized this region. The side chain and backbone of HigB residues Lys57, Asp59, and Glu61 have poor electron density in both crystal forms and two out of the three HigB molecules from Form 2 showed little to no Cα electron density for Lys57 and Asp59. Therefore, the backbone was built using neighboring residues as guides for α carbon positions. In Form 2, residues 1-90 were built for all three HigB molecules. In both crystal forms, HigA (104 amino acids total) was modeled to either residue 92 or 93 as no interpretable electron density was seen beyond these positions.

Both HigBA structures adopt nearly identical tertiary and quaternary structures (**Fig. 2.2C**). Two HigA molecules form a dimer similar to that observed in previous HigA crystal structures without the toxin (39) (**Fig. 2.3A)**. Each HigA interacts with one HigB molecule to form a heterodimer that with additional HigA-HigA interactions completes a dimer of heterodimers (**Figs. 2.1B & 2.1C**). Consistent with our structural results, PISA predicts the HigBA complex to exist as a tetramer (31). The structure of the *P. vulgaris* HigA dimer in the context of the TA complex is very similar to that of HigA alone from *E. coli* CFT073 (PDB IDs 2ICT and 2ICP) (39) and *C. burnetti* (PDB ID 3TRB3) with r.m.s.ds of 2.5 Å, 1.6 Å and 1.6 Å, respectively. This indicates HigA does not undergo large conformational changes upon toxin binding (**Fig. 2.3A**).

2.4b HigB adopts a microbial RNase fold.

HigB is a member of the RelE toxin family, which includes ribosome-dependent toxins RelE, YafQ and YoeB (22,25,40). Despite low sequence identity with these toxins (14-18%), HigB shows an overall tertiary fold consistent with the RelE/YoeB family

(**Fig. 2.4A**). This family shares a microbial RNase fold characterized by a single α helix that packs against an antiparallel β sheet (**Fig. 2.1B**). HigB is a small globular protein consisting of two N-terminal α helices (α1-2) flanked by three twisted, antiparallel β strands (β1-3) and six loops (**Fig. 2.1B**). A Dali search reveals HigB is most similar to *Mycobacterium tuberculosis* RelK (PDB ID 3OEI), *E. coli* YoeB (PDB ID 2A6S), *Pyrococcus horikoshii* RelE (PDB ID 1WMI) and *M. tuberculosis* RelE-2 (PDB ID 3G5O), with Z-scores of 8.3, 8.4, 7.7 and 6.4, and r.m.s.ds. of 2.7 Å, 2.8 Å, 2.7 Å and 2.7 Å, respectively (using 79, 80, 73 and 73 aligned α carbon backbone atoms, respectively) (38,41-43). The two N-terminal HigB α helices (α1 and α2) and loops 1 and 3 are in proximity to the HigA N terminus, α1, α5, and loop 5. HigB α2 and loop 3 form the majority of the interactions with HigA (**Fig. 2.1B**). Opposite to the HigA-HigB interface, HigB forms a distinctive concave surface comprised of three β strands (β1-3), loops 3 and 4, and the C terminus of HigB (**Fig. 2.1B**). This concave surface consists of highly conserved residues among HigB homologues, indicating its potential functional importance (**Figs. 2.4A & 2.4B**). HigB also has an extensive hydrophobic core consistent with other known ribosome-dependent RNase toxins (41,43)

2.4c The interface between HigA and HigB is novel.

Previous TA complex structures of the RelE toxin family demonstrate that antitoxins interact with their cognate toxin by wrapping one, two or three α helices around the toxin, presumably to block access to its active site (**Fig. 2.6E**) (41,43-48). HigA does not utilize any of its five α helices to conceal or wrap around HigB, demonstrating a novel mode of antitoxin interaction with HigB (**Fig. 2.1B**). HigA primarily contacts HigB at two positions via largely hydrogen bonding and electrostatic

interactions (**Fig. 2.5**). The N terminus, α1, α5 and loop 5 of HigA pack directly against the HigB N terminus, α1, α2 and loop 3 (**Fig. 2.1B**). The HigA N terminus interacts with HigB α1 via hydrogen bonding of the backbone carbonyls of Phe14 and Asn31 to the backbone of HigA Phe4 and the side chain of Gln3, respectively (**Fig. 2.5A**). Two water-mediated interactions occur between HigA residues Lys5 and Ser7 and HigB residues Leu13, Asn31, Gln35, and Asp32, forming a hydrogen-bonding network (**Fig. 2.5A**). Four HigA residues, Arg15, Asp16, and Asp19 (α1) and Arg69 (α5), make ionic interactions with HigB residues Asp32 (α2), Arg48 (loop 3), Arg29 (α2) and Glu45 (loop 3), respectively (**Figs. 2.5A & 2.5B**). These ionic interactions surround a hydrophobic core mediated by HigA residues Met12, Phe66, and Leu70 and HigB residues Ala36, Thr39, Leu46, and Tyr51 (**Fig. 2.5C**). Both HigB and HigA residues involved in the HigA-HigA and HigA-HigB interfaces are not highly conserved amongst HigB and HigA homologues (**Fig. 2.4A & 2.6A, circles and triangles**).

2.4d HigA monomer contains an intact DNA binding domain.

The *P. vulgaris* HigA protein contains a compact five α-helical bundle and a disordered C terminus (residues 93/94-104) (**Fig. 2.1B**). All α helices are juxtaposed and their relative orientation is very similar to members of the Xenobiotic response element-Helix-Turn-Helix family (XRE-HTH) of DNA-binding proteins (49). Family members include the P22 C2 and phage 434 proteins, which transcriptionally repress specific genes by binding to their operator regions in the major groove in a sequence specific manner (50,51).

HigA has a number of unique structural characteristics in addition to the presence of the HTH motif. For example, each HigA monomer contains a defined hydrophobic

core unlike other antitoxins that recognize RelE family members. Normally antitoxins only form a hydrophobic core upon self dimerization and have typically been classified as partially unstructured (41,43,44,52,53). Additionally, most antitoxins that recognize RelE family members form one DNA binding motif upon dimerization (41,43,44,52,53). In sharp contrast, each HigA monomer contains a complete DNA binding motif. Therefore, the HigA dimer contains two DNA- binding motifs that fully extends over the two 9-nucleotide inverted repeats of the *hig* operator shown to interact with HigA through DNase protection assays (35) (**Figs. 2.1A, 2.7A & 2.3B**) These results imply that a single HigB-$(HigA)_2$-HigB tetramer can repress an operator site consisting of two inverted repeat sequences (**Figs. 2.1A & 2.7A**).

2.4e HigA mediates the formation of the HigB-$(HigA)_2$-HigB complex.

HigA dimerizes to form a dimer of heterodimers (**Figs. 2.1B & 2.1C**). These HigA dimers interact in a two-fold symmetrical manner mainly stabilized by hydrophobic interactions (**Figs. 2.6B & 2.6C**). HigA α5 packs against α5' of the partner HigA molecule in an antiparallel fashion (**Fig. 2.6C**). Loop 6' packs against α4 of its partner Hig and caps the junction formed by α1, α2 and α4 of the adjacent HigA molecule (**Figs. 2.6C & 2.6D**). This 1240 $Å^2$ interface is mediated primarily via hydrophobic amino acids (Ile54, Leu68, Leu76, Leu79, Ile83, Ile88, and Tyr91) from both molecules (**Fig. 2.6C**). For comparison, the HigB-HigB interface is 280 $Å^2$ (**Fig. 2.1B**). Thus, the HigA-HigA interaction plays a major role in driving the formation of the tetrameric HigB-$(HigA)_2$-HigB complex.

2.4f HigA does not mask the HigB active site.

The HigB active site is likely located at a concave surface where a high density of conserved residues reside, including the proposed catalytic HigB amino acid His92 (13) (**Figs. 2.4A & 2.4B**). RelE amino acids that contact and cleave mRNA, cluster in a similar concave surface (36) (**Fig. 2.4C**). This surface is located ~20 Å distal opposite to the HigA-HigB interface (**Fig. 2.1B**). Additionally, the active site is solvent accessible and this suggests that simple active site steric occlusion by HigA is not the mechanism of HigB inactivation.

2.4g A HigB-$(HigA)_2$-HigB tetramer is required to interact with its DNA operator.

Antitoxins generally require dimerization to form one DNA binding domain. These include members of the Ribbon-Helix-Helix (RHH) (RelB, VapB-3 and FitA), AbrB (MazE) and PhD/YefM super families (22,39,41,43,44,47,53-56). There are two DNA binding motifs in the context of the HigB-$(HigA)_2$-HigB structure. This implies that one tetramer could bind two inverted repeats of a single operator site (**Figs. 2.7A & 2.3B**). This is in contrast to canonical TA systems which appear to require two TA oligomeric complexes, or four antitoxins in total, to interact with a single operator site (55-57). To test whether a single HigA HTH can interact with DNA, we attempted to disrupt the HigB-$(HigA)_2$-HigB tetrameric state and test whether this complex could productively interact with the *higBA* operator. We truncated HigA at loop 6 (HigA Δ84-104) to disrupt the HigA-HigA interface (**Fig. 2.7A)**.

The *higBA* operator sequence used in the EMSAs include two endogenous operator sites which in turn, both contain two inverted repeats (**Fig. 2.7A**). Wild-type HigB-$(HigA)_2$-HigB binds to its own operator DNA with increasingly higher oligomeric

states (**Fig. 2.7C, lanes 3-5**). This indicates more than one HigB-$(HigA)_2$-HigB complex interacts with its promoter. However, we found that HigBA (Δ84-104) is unable to bind to this same DNA promoter (**Fig. 2.7C, lanes 6-10**). Considering that each HTH motif of HigA is left intact in this mutant, it is surprising that HigBA (Δ84-104) is unable to bind DNA. Two possibilities for this result exist: the first is that the HigA mutation caused destabilization of the protein and little to no soluble HigA is produced; the second possibility is that removal of the C terminus of HigA disrupts the HigA-HigA dimerization interface resulting in a HigBA heterodimer.

The SEC results show wild-type HigB-$(HigA)_2$-HigB elutes as the expected tetrameric complex of 56 kDa while purified HigBA (Δ84-104) elutes with an apparent molecular weight of 23 kDa (**Fig. 2.7D**). This is approximately the molecular weight of a dimer of HigA or HigB, or HigBA heterodimer. To differentiate between these options, we analyzed the fractions of each peak with SDS-PAGE (**Fig. 2.7E**). The 56 kDa peak of the wild-type HigB-$(HigA)_2$-HigB complex shows a large band at ~10 kDa which is most likely both His_6HigB (13.0 kDa) and HigA (11.5 kDa) (**Fig 2.7E, lane 1**). These bands could be separated by treatment with thrombin to release the N-terminal His_6 tag and the linker region of HigB; this allows the identification of both HigB and HigA (**Fig. 2.7E, lane 2**). The HigBA (Δ84-104) complex that runs at ~23 kDa shows two distinct bands on the SDS-PAGE gel (**Fig. 2.7E, lane 3**). Upon thrombin treatment to release the N-terminal His_6 tag and the linker region of HigB, we again see the appearance of tag-free HigB (**Fig. 2.7E, lane 4**). Therefore, HigBA (Δ84-104) is indeed a heterodimer of HigB and truncated HigA (Δ84-104). Taken together, these results demonstrate that the oligomeric state of the HigBA complex, specifically a HigB-$(HigA)_2$-HigB tetrameric

state, is required for productive DNA interaction. This is despite each HigA monomer containing a full HTH motif.

2.5 Discussion

TA systems commonly contain at least two operator regions with two imperfect inverted repeats comprising a single operator site (**Fig. 2.7A**). Antitoxin proteins belonging to the RHH, AbrB and PhD/YefM super families require dimerization to form a single DNA binding domain that recognize an inverted repeat (**Figs. 2.1A & 2.7A**). Direct binding of either an antitoxin dimer or a toxin-antitoxin complex confers transcriptional autorepression with differences in binding affinities attributed to the strength of the repression.

The crystal structures of the HigB-$(HigA)_2$-HigB complex presented here reveal the TA complex is a tetramer containing two, rather than one, DNA binding motifs (**Figs. 2.1B & 2.1C**). Our biochemical results indicate that a HigB-$(HigA)_2$-HigB tetrameric complex is essential for DNA binding (**Fig. 2.7C**). The loss of DNA binding upon disruption of HigA dimerization (thus forming a HigBA heterodimer) may result from a diminished interaction surface, culminating in reduced binding. Both the HigA dimer and HigB-$(HigA)_2$-HigB tetramer provide the same surface area for the inverted repeats to interact with, that is halved in the context of the HigBA dimer. Moreover, another possible reason for the HigBA dimer ablating DNA binding is that the HTH motifs, in the context of the HigB-$(HigA)_2$-HigB tetramer, are tethered or rigidly held in place because they are part of the HigA globular domain formed from HigA dimerization (**Figs. 2.1B & 2.1C**). In this manner, the precise structural arrangement may be functioning as a molecular ruler for specific recognition of both inverted repeats as seen in other HTH-

containing proteins, such as Fis (58). In summary, both the DNA-interaction area formed by the HigA dimer and the spatial organization of the HTH motifs coordinate to recognize DNA and render the area impenetrable to RNA polymerase.

Transcriptional autorepression by TA complexes has been proposed to occur by regulation of the overall molar ratio of toxins and antitoxins as shown *in vivo* for RelEB (57). By varying the molar ratio, different stoichiometric complexes form, which may function to repress transcription to different magnitudes or cause complete derepression. *In vitro* biochemical experiments for the RelEB, PhD-Doc and CcdAB TA systems demonstrate that once a saturated TA-DNA complex is formed, increasing the amount of free toxin protein destabilizes the DNA-TA interaction and probably allows for derepression of transcription (56,57,59,60). These studies led to a model referred to as conditional cooperativity (56,57). This model can help explain why toxins function as either anti or corepressors depending upon environmental changes that require bacteria to respond and regulate metabolic processes quickly.

Despite these studies, the mechanism by which different TA complexes repress transcription is still not entirely clear. Structural and modeling studies of the RelEB and the PhD-Doc TA complexes suggest two tetrameric TA complexes sterically clash at single operator sites while in the case of RelEB, modeling studies indicated that trimeric complexes can coexist (44,56). However, the proposed trimeric complexes of RelEB and PhD-Doc have not been observed structurally. Therefore, it is not obvious how the diverse oligomeric states from structural studies fit with these models (43,44,56).

In contrast, structures of TA complexes such as *Neisseria gonorrhoeae* FitAB and *Rickettsia felis* VapBC bound to two inverted repeats suggest that higher oligomeric

states can simultaneously bind to two inverted repeats without steric clashes (55,61). Since the spacing between inverted repeats may play a role in which oligomeric complexes fit, it is interesting that the *fitAB* promoter contains twelve basepairs between inverted repeats while the *vapBC* promoter has only two repeats. So in this context, both short and long spacings between inverted repeats give rise to higher oligomeric state binding to DNA. Modeling of our HigB-$(HigA)_2$-HigB structure on the structure of phage 434 bound to a double stranded 20 nucleotide DNA (PDB ID 1RPE), indicates it is possible for both HTH motifs of the HigB-$(HigA)_2$-HigB tetramer to interact with one complete operator site (two inverted repeats) without steric clashes (**Fig. 2.3B**).

HigA is not the only antitoxin that contains a HTH motif. MqsA and HipB antitoxins also possess HTH motifs but there are key structural and functional differences amongst the three (62,63). The first is the location of the HTH motif relative to the toxin (**Fig. 2.3C**). The HipA toxin binds to HipB at a location orthogonal to its HTH motif while MqsAR has a separate N-terminal toxin neutralization domain and a C-terminal DNA-binding domain (**Fig. 2.3C**). The HipA toxin is also a much larger protein and is not homologous to either MqsR or HigB (63). Secondly, HipA contacts two HipB antitoxins while HigB and MqsR only contact one. Lastly, an important difference is that the MqsA antitoxin alone, and not the MqsRA TA complex, binds DNA (64). Thus in this example, the toxin does not appear to act as a co-repressor. In summary, while all three have a HTH motif in common, they show substantial functional and structural differences underscoring antitoxin plasticity.

HigB is a ribosome-dependent RNase that cleaves codons containing at least a single adenosine located most likely, in the A site of the ribosome (13). Our HigB

structure reveals a solvent exposed, concave surface containing highly conserved residues (**Fig. 2.4B**). Several lines of evidence suggest this HigB concave surface is its active site. Microbial RNases such as RNase T1 or RNase Sa contain similar concave surfaces and ribosome-dependent toxins have been proposed to degrade mRNA in an analogous manner (36,65,66). An X-ray crystal structure of RelE bound to the 70S ribosome shows the same concave surface interacts with mRNA (36). Additionally, mutagenesis experiments of other toxins also implicate the same concave surface residues as important for function (36,41,43,62). In summary, HigB appears to use the same tertiary fold and surface to recognize ribosome-bound mRNA.

A hallmark of toxin inactivation is a direct interaction in which the antitoxin wraps around the toxin much like a pincer (**Fig. 2.6E**) (43,44,52,56,61,62,67-69). This toxin-antitoxin interaction ablates activity of the toxin and although the precise mechanism is unknown, it has been proposed to occur via antitoxin masking of the toxin active site. Our structure reveals that the antitoxin HigA does not wrap around and mask the active site of HigB. Instead only two regions of contact are made distant from the active site (**Figs. 2.1 & 2.5**). The MqsRA and the HipBA TA pairs also do not wrap around their cognate toxins but interact in a manner and location distinct from HigB-$(HigA)_2$-HigB (**Figs. 2.6F & 2.3C**)(62,63).

Comparison of toxin active sites in toxin alone, toxin-antitoxin and toxins bound to the ribosome structures reveal there are only minor structural rearrangements of the toxin (36,41,53). To further explore the inhibitory mechanism of HigB by HigA, we superimposed the HigB-$(HigA)_2$-HigB complex on the structure of RelE bound to mRNA on the 70S and found that HigB-$(HigA)_2$-HigB can not be accommodated (36) (**Fig. 2.8**).

A steric clash exists between HigB-$(HigA)_2$-HigB and ribosomal protein S12 and 16S rRNA helix 18 (h18). The position of a large portion of the N terminus of HigA (α1-4) overlaps with the entire h18 (**Fig. 2.8, clash 1**). The second clash site is with the C terminus of HigA' that overlays with S12 residues 108-113 and the tetraloop of h18 (**Fig. 2.8, clash 2**). Thus we propose binding of HigA sterically inhibits HigB from interacting with mRNA in the A site of the 30S ribosome.

Taken together, our results expand the molecular understanding of how diverse antitoxins counteract the activity of toxin proteins. As Blower *et al*. described, the tertiary structure of toxins are a static scaffold that may contain myriad possible active site residues to determine substrate specificity (70). This appears to be consistent with what is known about ribosome-dependent toxins. However, the antitoxin structure and interaction with its cognate toxin varies and can be structurally divergent depending upon its DNA-binding domain and the structural features of the antitoxin and toxin interface. This antitoxin structural plasticity underscores the expansive nature of TA-mediated bacterial survival mechanisms.

2.6 Acknowledgments-

We thank I. Kourinov and F. V. Murphy at the NE-CAT beamline for assistance during data collection; G. L. Conn and A. Ruangprasert for helpful discussions throughout the project and critical reading of the manuscript; and J. A. Dunkle, C. E. Fagan and A. Ruangprasert for assistance in data collection, processing and refinement.

2.7 Footnotes

***** This work was supported by a NSF CAREER award number MCB 0953714 (CMD) and pre-doctoral BCMB graduate training grant (5T32GM8367) and NIH NRSA

fellowship (GM108351)(MAS). CMD is a Pew Scholar in the Biomedical Sciences. This work is based on research conducted at the Advanced Photon Source on the NE-CAT beamlines, which is supported by National Center for Research Resources (National Institutes of Health) Award RR-15301, and at the SER-CAT beamline. Use of the Advanced Photon Source, an Office of Science User Facility operated for the US Department of Energy (DOE) Office of Science by Argonne National Laboratory, was supported by the US DOE under Contract DE-AC02-06CH11357.

The atomic coordinates and structure factors (codes 4MCT and 4MCX) have been deposited in the Protein Data Bank (http://wwpdb.org/).

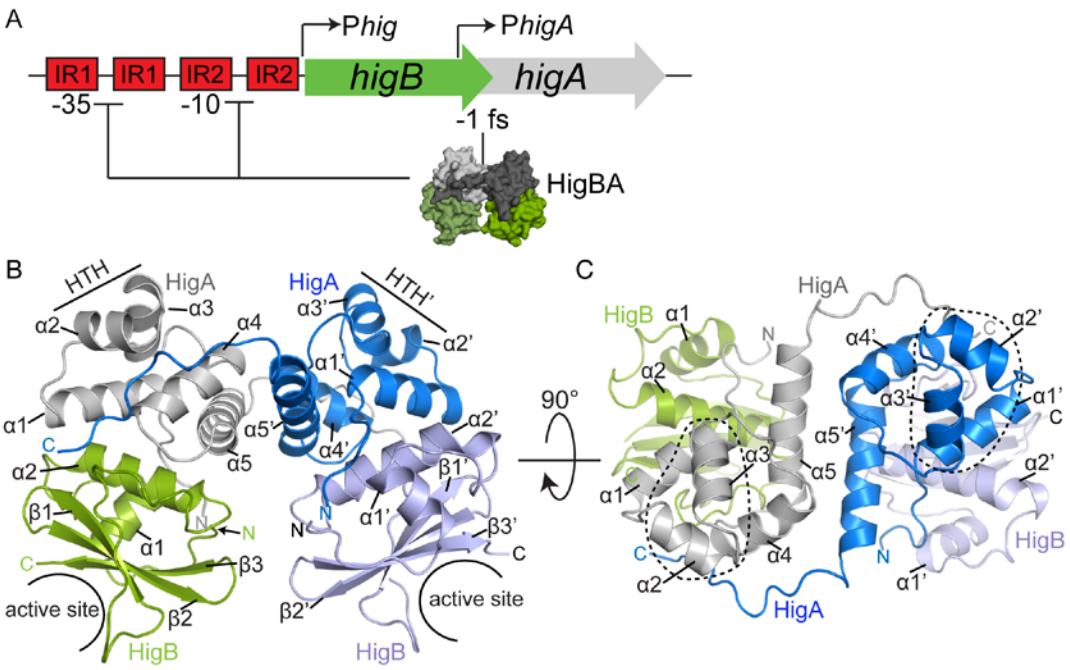

Figure 2.1. X-ray crystal structure of the HigB-(HigA)$_2$-HigB complex.

A. Organization of the *hig* operon. The *higB* gene overlaps *higA* by one base pair, indicated by -1 frameshift (fs). The HigBA complex binds two inverted repeats (IR) that

span the -35 and -10 promoter boxes. B. The tetrameric HigB-$(HigA)_2$-HigB structure with the indicated active site and helix-turn-helix (HTH) DNA-binding motifs are located at opposite ends of the complex. C. A 90° rotated view of *panel* B highlighting the HigA-HigA interface and HTH motifs (circled).

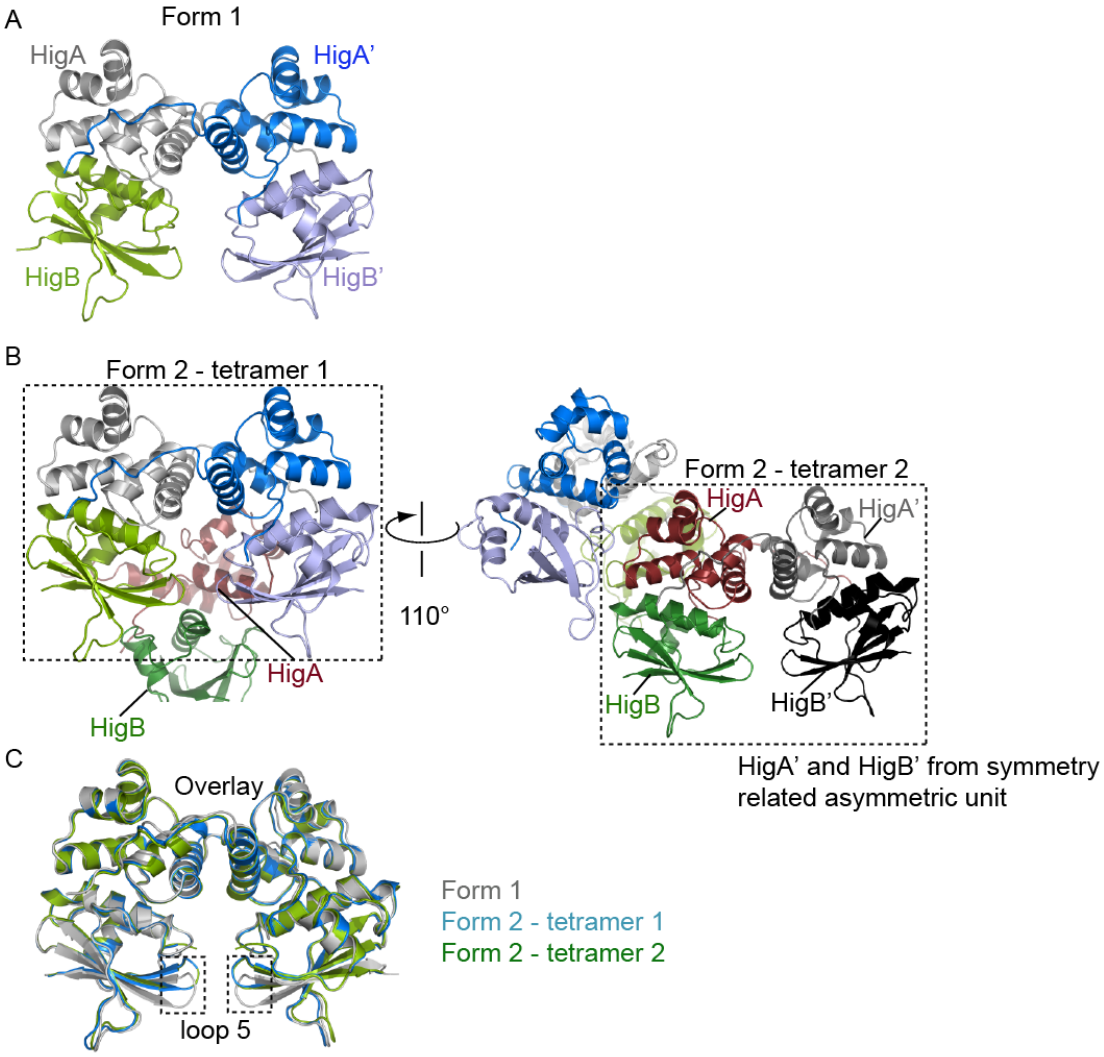

Figure 2.2. HigBA forms a heterotetramer in both crystal forms.

A. View of the asymmetric hexagonal unit of Form 1 with the color scheme the same as in Fig. 2.1. B. Two views of the asymmetric unit of Form 2 (left) with HigBA tetramer 1 colored as in panel A (boxed). The heterodimer HigBA of tetramer 2 is shown behind in green (HigB) and red (HigA). A ~110° rotation about the vertical axis emphasizes the second tetramer 2 (boxed) with HigA (red) and green HigB (green) from the same unit cell as the tetramer 1 on the left. HigA' (gray) and HigB' (black) comprise tetramer 2 but are from an adjacent asymmetric unit. C. Overlay of the three HigBA tetrameric

complexes from Form 1 and Form 2. Loop 5 of HigB is boxed to emphasize the slight differences between the complexes.

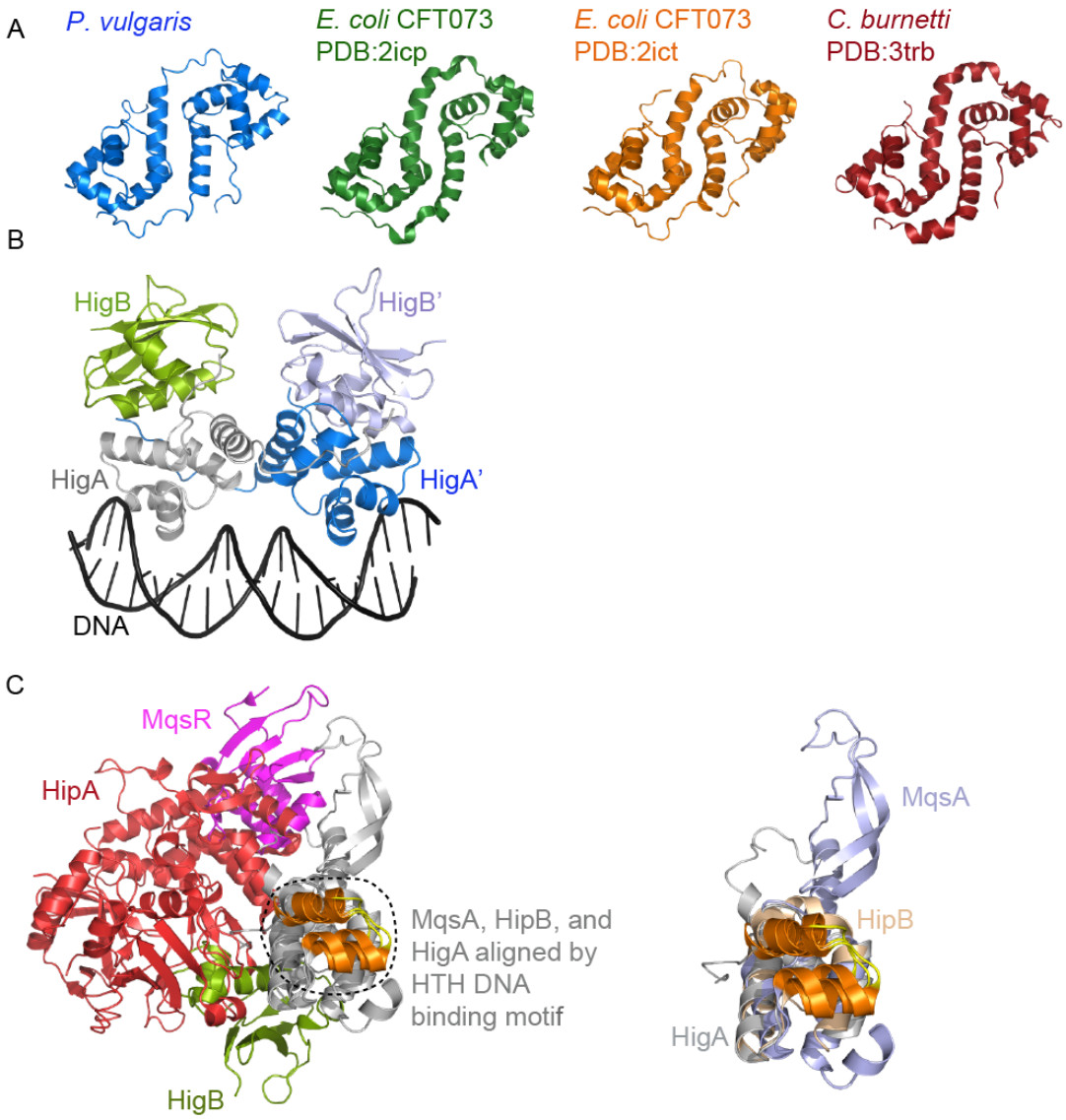

Figure 2.3. Structural comparisons of HigA antitoxin.

A. Comparison of the P. vulgaris HigA dimer (our structure) to E. coli CFT073 (PDB IDs 2ICT and 2ICP) and C. burnetti HigA dimers (PDB ID 3TRB). For E. coli CFT073 HigA dimers, one HigA molecule is present in each asymmetric unit and the dimer is formed between two asymmetric units related by 2-fold symmetry. B. Model of the tetrameric HigBA complex bound to DNA using the X-ray crystal structure of phage 434 bound to a 20mer DNA (PDB ID 1RPE) as an alignment guide. Alignments were performed in Coot using secondary-structure matching (SSM) (37). A HigBA tetramer can easily span an

entire palindromic site. C. Alignment of the HigBA, MqsRA (gray), and HipAB (red; PDB ID 3DNV) TA complexes displays the different binding surfaces of antitoxins relative to their cognate toxin domain despite all three containing a HTH motif (circled). Alignments were based on the position of the HTH motif (orange for the helices and yellow for the loop). Only one toxin and antitoxin pair is shown for each complex. The MqsRA full length model is derived from the full-length antitoxin structure (gray; PDB ID 3GN5) and the MqsA N-terminus bound to MqsR structure (gray; PDB ID 3HI2).

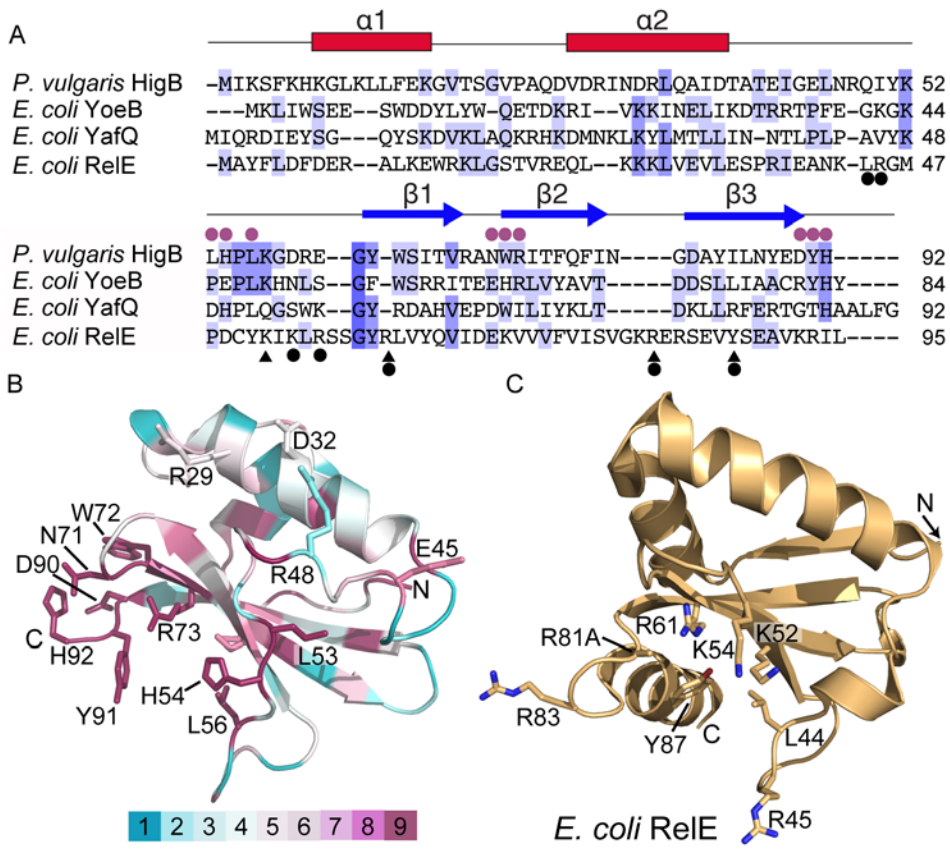

Figure 2.4. Highly conserved amino acids of HigB cluster in a concave, solvent accessible surface.

A. Sequence alignments using ClustalW (33) of *P. vulgaris* HigB with other ribosome-dependent toxins showing residues with 50, 75, or 100% sequence identity as light, medium, or deep purple, respectively. Residues located within the HigB concave surface (purple circles) and *E. coli* RelE amino acids that recognize and/or degrade mRNA (black circles and triangles, respectively) are indicated. B. HigB toxin structure colored by amino acid conservation among HigB homologs according to the scale shown (1 is least conserved while 9 is the most). Residues located on the concave surface proposed to contain active site residues are shown as sticks. HigB residues that make ionic interactions with HigA are also shown as sticks and colored by conservation. C. *E. coli*

RelE R81A toxin structure (PDB ID 4FXI) with residues identified as important for mRNA recognition or cleavage shown as sticks.

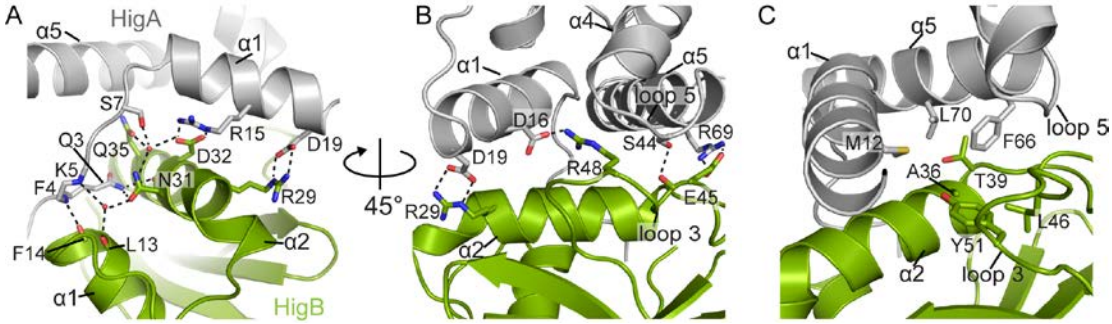

Figure 2.5. Minimal interface between HigB and HigA.

A. Zoomed in view of HigB-HigA salt bridge and hydrogen bonding interactions (dashed lines). Water molecules are shown as red spheres and color scheme is the same as in Figure 2.1. B. A ~45° rotated view of *panel* A highlighting additional salt bridge and hydrogen bonding interactions. C. Hydrophobic interactions formed between HigA and HigB.

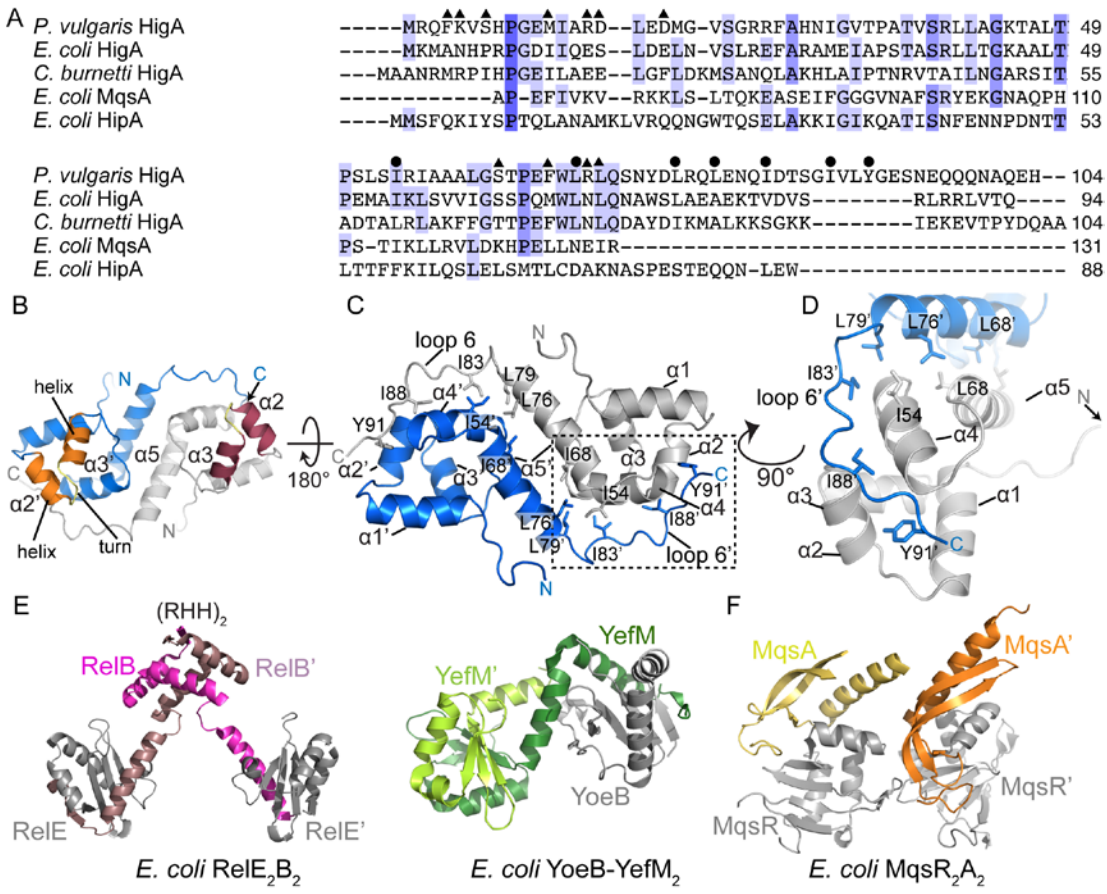

Figure 2.6. *P. vulgaris* HigA-HigA interface is mediated mainly via hydrophobic interactions and each monomer contains a HTH motif.

A. Sequence alignments using ClustalW (33) of *P. vulgaris* HigA with similar antitoxin proteins, with 60, 80, or 100% sequence identity colored as light, medium, or deep purple, respectively. HigA residues that contact HigB (triangles) or the symmetry-related HigA molecule (circles) are indicated. B. Schematic of the HigA-HigA interface shows the HTH motifs of both HigA monomers (helices shown in red and orange with connecting loops in yellow) are distal from the interface. C. A 180° rotated view of *panel* B emphasizing the extensive hydrophobic interface between HigA dimers with residues involved shown as sticks. D. A 90° rotation around the vertical axis of the view shown in *panel* C. E. X-ray crystal structures of RelEB (PDB ID 4FXE), YoeB-YefM (PDB ID 2A6Q)

and MqsRA (PDB ID 3HI2) TA complexes emphasizing that the antitoxins (shown in pink, green and orange, respectively) interact with their cognate toxins (grey) in a manner distinct from the HigBA complex. RelB and YefM antitoxins wrap or engulf the toxin F. while MqsR does not. The ribbon-helix-helix (RHH) motif of RelB forms one DNA binding motif, in contrast to the two DNA binding motifs present in a HigA dimer (*panel* B). The DNA binding motif of MqsA was not solved in this TA complex.

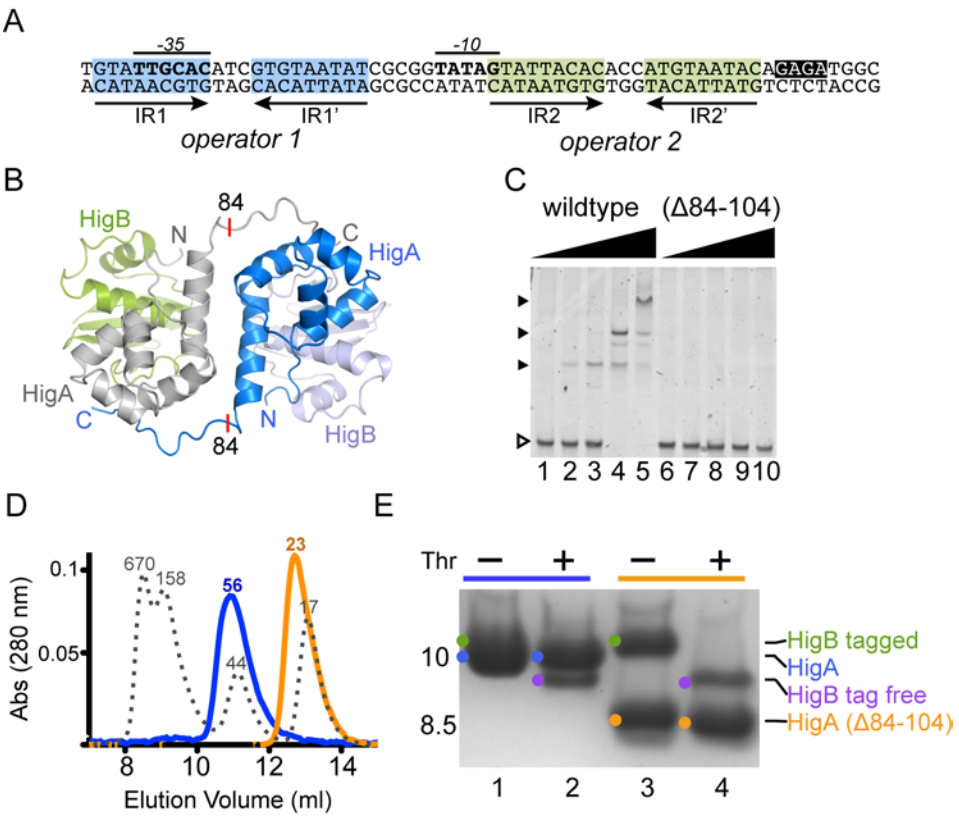

Figure 2.7. The tetrameric HigB-$(HigA)_2$-HigB complex containing two DNA binding motifs is required for interactions with DNA.

A. The *hig* promoter region emphasizing the two operator sites, transcriptional start sites (-35 and -10) and Shine-Dalgarno (black box). B. Structure of the HigBA complex with HigA truncated at residue 84 as indicated with a red line. C. EMSAs of *hig* DNA promoter region with increasing concentrations (0, 0.25, 0.5, 1, and 2 μM) of HigBA and HigBA (Δ84-104). Free probe (empty triangle) and protein bound-DNA (solid triangles) are indicated. D. Size exclusion chromatographic (SEC) analysis of wild-type HigBA (blue) and HigBA (Δ84-104) (orange) complexes with the estimated molecular weight calculated by comparison to protein standards (shown as a dotted line). E. SDS-PAGE gel of samples from the SEC analysis in *panel* D. Lanes 1-2 were pooled from the wild-type HigBA (blue) SEC experiment in *panel* D while lanes 3-4 were pooled from the

HigBA (Δ84-104) (orange) SEC experiment in *panel* D. Lane 1 contains wild-type HigBA where HigB (13.0 kDa; green dot) overlaps with HigA (11.5 kDa; blue dot). Upon HigB treatment with thrombin to release its N-terminal His_6 tag along with a linker region, results in tag free HigB (11.1 kDa; magenta dot) that can be distinguished from HigA (blue dot; lane 2). Lane 3 shows HigB (13.0 kDa; green dot) and HigA (Δ84-104) (9.2 Da; orange dot). Upon HigB treatment with thrombin to release its N-terminal His_6 tag along with a linker region, results in tag free HigB (11.1 Da; magenta dot) that can be distinguished from HigA (Δ84-104) (orange dot).

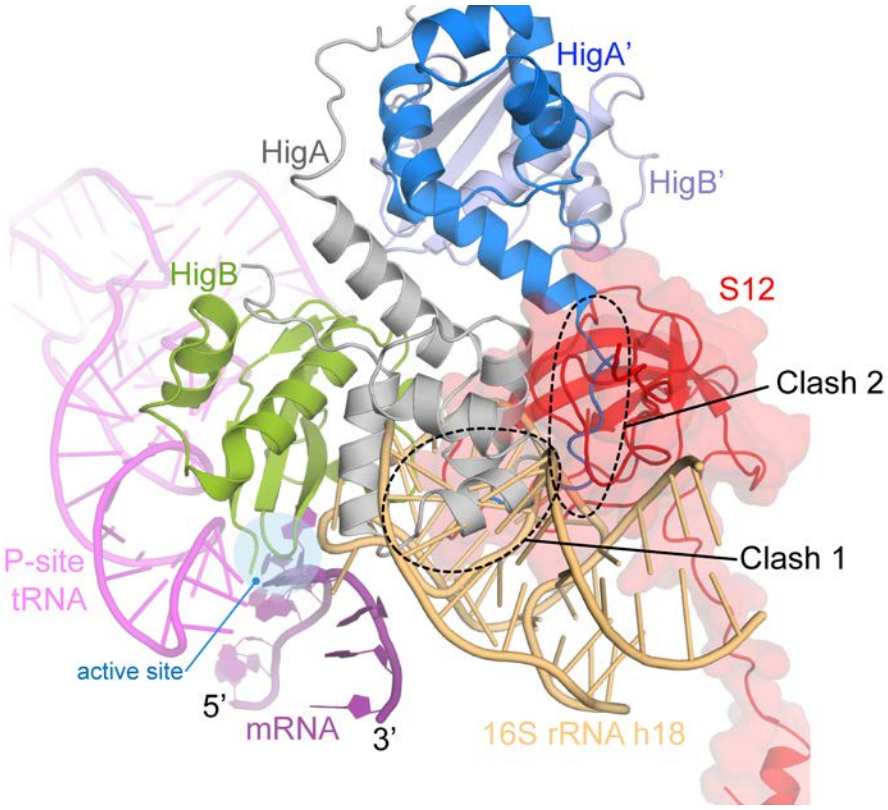

Figure 2.8. HigB-$(HigA)_2$-HigB complex clashes with S12 and 16S rRNA in the A site of the ribosome.

HigBA was modeled on the RelE-70S complex (36) (PDB ID 3K1Q). HigA (grey) bound to HigB (green) directly clashes with 16S rRNA h18 (tan) (Clash 1) while HigA' (blue) of the other HigBA' dimer, clashes with h18 and S12 (red) (Clash 2). The active site of HigB (green) is located at the light blue circle. P-site tRNA and mRNA are shown in magenta and purple, respectively.

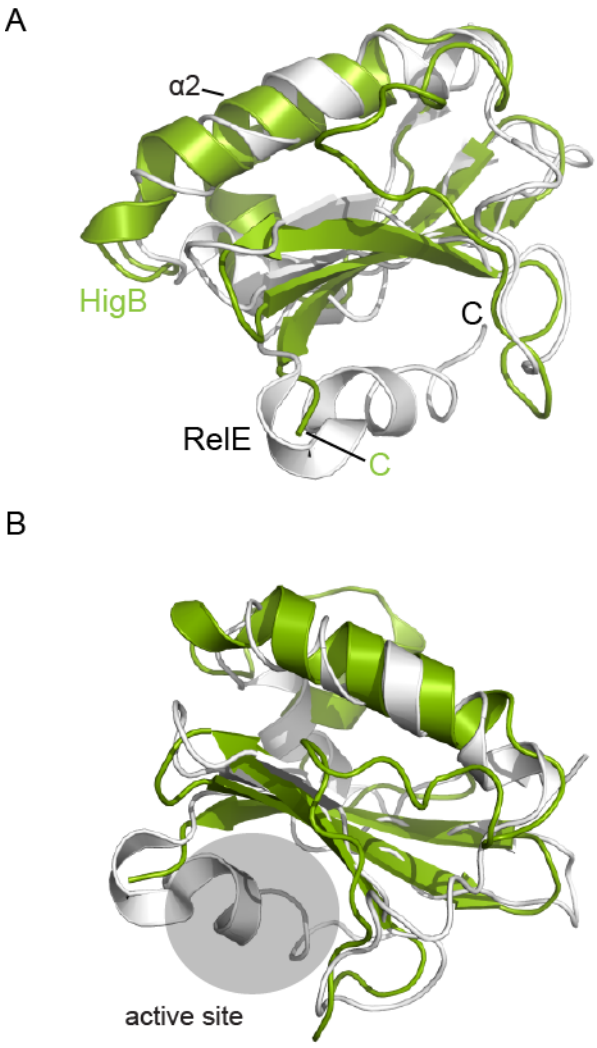

Figure 2.9. HigB (green) alignment with RelE (white; PDB ID 3K1Q).

A. Alignment of HigB and RelE was performed using secondary-structure matching in Coot in the context of the 70SRelE complex (37). B. Rotation of panel A to emphasize the active sites. RelE has a C terminal α helix that is not present in HigB.

Table 2.1.
Crystallographic data and refinement statistics

	Form 1 HigBA-His_6 (SeMet)	Form 2 His_6-HigBA (Native)
Data collection		
Space group	*$P3_221$*	*$P6_2$*
Cell dimensions		
a, b, c (Å)	94.9, 94.9, 126.8	120.5, 120.5, 64.5
α, β, γ (°)	90, 90, 120	90, 90, 120
Wavelength (Å)	0.98	0.98
Resolution range (Å)	41.1 – 2.8 (2.9-2.8)	30.8– 2.1 (2.17 – 2.1)
Total observations	113,311	172,519
Unique reflections	16,748	31,287
Redundancy[a]	6.8 (6.2)	5.5 (5.5)
$I / \sigma(I)$	13.8 (2.1)	17.3 (1.7)
R_{merge}[a]	0.155 (0.752)	0.079 (.957)
R_{pim}[a]	0.064 (0.320)	0.037 (0.448)
Completeness (%)[a]	100.0 (100.0)	99.9 (99.9)
Refinement[b]		
Resolution (Å)	47.4 – 2.8	30.8 – 2.2
No. atoms	2983	4606
Protein	2943	4403
Water	40	203
R_{work}[c] / R_{free}	0.197/0.238	0.173/0.211
Mean *B*-factors	62.8	36.2
Protein	62.9	36.2
Main chain	61.9	33.7
Side chain	63.9	38.5
Water	55.2	37.2
R.m.s.d.		
Bond lengths (Å)	0.010	0.011
Bond angles (°)	1.32	1.18
R.m.s.d. ΔB ($Å^2$)[d]		
All atoms	3.91	3.75
Main-main	1.81	2.63
Side-side	5.82	4.88
Main-side	1.81	3.39
Nonbonded	4.53	6.90

* Values in parentheses are for the highest resolution shell.

[a]Both R_{merge} as well as R_{pim} values (redundancy independent factor) are provided for direct comparisons. R_{pim} is defined as:

$$R_{p.i.m.} = \frac{\sum_{hkl}\sqrt{\frac{1}{n-1}\sum_{i=1}^{n}|I_{hkl,i}-\langle I_{hkl}\rangle|}}{\sum_{hkl}\sum_{i} I_{hkl,i}}.$$

Given the high redundancy of the datasets, R_{pim} is a more appropriate measure of data quality than R_{merge}.

[b]Values calculated by PHENIX

[c]R factors calculated for all data (working + test set) are 20.1% and 17.5% for the Form 1 and 2, respectively.

[d]Values calculated by MOLEMAN2 (71).

2.8 References

1. Gerdes, K., Christensen, S. K., and Lobner-Olesen, A. (2005) Prokaryotic toxin-antitoxin stress response loci. *Nature reviews. Microbiology* **3**, 371-382
2. Black, D. S., Kelly, A. J., Mardis, M. J., and Moyed, H. S. (1991) Structure and organization of hip, an operon that affects lethality due to inhibition of peptidoglycan or DNA synthesis. *Journal of bacteriology* **173**, 5732-5739
3. Gonzalez Barrios, A. F., Zuo, R., Hashimoto, Y., Yang, L., Bentley, W. E., and Wood, T. K. (2006) Autoinducer 2 controls biofilm formation in Escherichia coli through a novel motility quorum-sensing regulator (MqsR, B3022). *Journal of bacteriology* **188**, 305-316
4. Harrison, J. J., Wade, W. D., Akierman, S., Vacchi-Suzzi, C., Stremick, C. A., Turner, R. J., and Ceri, H. (2009) The chromosomal toxin gene yafQ is a determinant of multidrug tolerance for Escherichia coli growing in a biofilm. *Antimicrobial agents and chemotherapy* **53**, 2253-2258
5. Kim, Y., and Wood, T. K. (2010) Toxins Hha and CspD and small RNA regulator Hfq are involved in persister cell formation through MqsR in Escherichia coli. *Biochemical and biophysical research communications* **391**, 209-213
6. Kolodkin-Gal, I., Verdiger, R., Shlosberg-Fedida, A., and Engelberg-Kulka, H. (2009) A differential effect of E. coli toxin-antitoxin systems on cell death in liquid media and biofilm formation. *PloS one* **4**, e6785

7. Ren, D., Bedzyk, L. A., Thomas, S. M., Ye, R. W., and Wood, T. K. (2004) Gene expression in Escherichia coli biofilms. *Applied microbiology and biotechnology* **64**, 515-524

8. Wang, X., and Wood, T. K. (2011) Toxin-antitoxin systems influence biofilm and persister cell formation and the general stress response. *Applied and environmental microbiology* **77**, 5577-5583

9. Williams, J. J., and Hergenrother, P. J. (2012) Artificial activation of toxin-antitoxin systems as an antibacterial strategy. *Trends in microbiology* **20**, 291-298

10. Bernard, P., and Couturier, M. (1992) Cell killing by the F plasmid CcdB protein involves poisoning of DNA-topoisomerase II complexes. *Journal of molecular biology* **226**, 735-745

11. Pedersen, K., Zavialov, A. V., Pavlov, M. Y., Elf, J., Gerdes, K., and Ehrenberg, M. (2003) The bacterial toxin RelE displays codon-specific cleavage of mRNAs in the ribosomal A site. *Cell* **112**, 131-140

12. Zhang, Y., Zhang, J., Hoeflich, K. P., Ikura, M., Qing, G., and Inouye, M. (2003) MazF cleaves cellular mRNAs specifically at ACA to block protein synthesis in Escherichia coli. *Molecular cell* **12**, 913-923

13. Hurley, J. M., and Woychik, N. A. (2009) Bacterial toxin HigB associates with ribosomes and mediates translation-dependent mRNA cleavage at A-rich sites. *The Journal of biological chemistry* **284**, 18605-18613

14. Prysak, M. H., Mozdzierz, C. J., Cook, A. M., Zhu, L., Zhang, Y., Inouye, M., and Woychik, N. A. (2009) Bacterial toxin YafQ is an endoribonuclease that associates with the ribosome and blocks translation elongation through sequence-

specific and frame-dependent mRNA cleavage. *Molecular microbiology* **71**, 1071-1087

15. Jorgensen, M. G., Pandey, D. P., Jaskolska, M., and Gerdes, K. (2009) HicA of Escherichia coli defines a novel family of translation-independent mRNA interferases in bacteria and archaea. *Journal of bacteriology* **191**, 1191-1199
16. Schifano, J. M., Edifor, R., Sharp, J. D., Ouyang, M., Konkimalla, A., Husson, R. N., and Woychik, N. A. (2013) Mycobacterial toxin MazF-mt6 inhibits translation through cleavage of 23S rRNA at the ribosomal A site. *Proceedings of the National Academy of Sciences of the United States of America* **110**, 8501-8506
17. Yamaguchi, Y., Park, J. H., and Inouye, M. (2009) MqsR, a crucial regulator for quorum sensing and biofilm formation, is a GCU-specific mRNA interferase in Escherichia coli. *The Journal of biological chemistry* **284**, 28746-28753
18. Goeders, N., Dreze, P. L., and Van Melderen, L. (2013) Relaxed cleavage specificity within the RelE toxin family. *Journal of bacteriology* **195**, 2541-2549
19. Hurley, J. M., Cruz, J. W., Ouyang, M., and Woychik, N. A. (2011) Bacterial toxin RelE mediates frequent codon-independent mRNA cleavage from the 5' end of coding regions in vivo. *The Journal of biological chemistry* **286**, 14770-14778
20. Christensen, S. K., Maenhaut-Michel, G., Mine, N., Gottesman, S., Gerdes, K., and Van Melderen, L. (2004) Overproduction of the Lon protease triggers inhibition of translation in Escherichia coli: involvement of the yefM-yoeB toxin-antitoxin system. *Molecular microbiology* **51**, 1705-1717

21. Zhang, Y., and Inouye, M. (2009) The inhibitory mechanism of protein synthesis by YoeB, an Escherichia coli toxin. *The Journal of biological chemistry* **284**, 6627-6638

22. Anantharaman, V., and Aravind, L. (2003) New connections in the prokaryotic toxin-antitoxin network: relationship with the eukaryotic nonsense-mediated RNA decay system. *Genome Biol* **4**, R81

23. Tian, Q. B., Ohnishi, M., Tabuchi, A., and Terawaki, Y. (1996) A new plasmid-encoded proteic killer gene system: cloning, sequencing, and analyzing hig locus of plasmid Rts1. *Biochemical and biophysical research communications* **220**, 280-284

24. Terawaki, Y., Takayasu, H., and Akiba, T. (1967) Thermosensitive replication of a kanamycin resistance factor. *Journal of bacteriology* **94**, 687-690

25. Pandey, D. P., and Gerdes, K. (2005) Toxin-antitoxin loci are highly abundant in free-living but lost from host-associated prokaryotes. *Nucleic acids research* **33**, 966-976

26. Van Duyne, G. D., Standaert, R. F., Karplus, P. A., Schreiber, S. L., and Clardy, J. (1993) Atomic structures of the human immunophilin FKBP-12 complexes with FK506 and rapamycin. *Journal of molecular biology* **229**, 105-124

27. Otwinowski, Z., and Minor, W. (1997) Processing of X-ray Diffraction Data Colleceted in Oscillation Mode. in *Methods in Enzymology* (Carter, J., C. C, and Sweet, R. M. eds.), Academic Press, New York. pp 307-326

28. Adams, P. D., Afonine, P. V., Bunkoczi, G., Chen, V. B., Davis, I. W., Echols, N., Headd, J. J., Hung, L. W., Kapral, G. J., Grosse-Kunstleve, R. W., McCoy, A. J.,

Moriarty, N. W., Oeffner, R., Read, R. J., Richardson, D. C., Richardson, J. S., Terwilliger, T. C., and Zwart, P. H. (2010) PHENIX: a comprehensive Python-based system for macromolecular structure solution. *Acta crystallographica. Section D, Biological crystallography* **66**, 213-221

29. Emsley, P., Lohkamp, B., Scott, W. G., and Cowtan, K. (2010) Features and development of Coot. *Acta crystallographica. Section D, Biological crystallography* **66**, 486-501

30. Kabsch, W. (2010) Xds. *Acta crystallographica. Section D, Biological crystallography* **66**, 125-132

31. Krissinel, E., and Henrick, K. (2007) Inference of macromolecular assemblies from crystalline state. *Journal of molecular biology* **372**, 774-797

32. Landau, M., Mayrose, I., Rosenberg, Y., Glaser, F., Martz, E., Pupko, T., and Ben-Tal, N. (2005) ConSurf 2005: the projection of evolutionary conservation scores of residues on protein structures. *Nucleic acids research* **33**, W299-302

33. Larkin, M. A., Blackshields, G., Brown, N. P., Chenna, R., McGettigan, P. A., McWilliam, H., Valentin, F., Wallace, I. M., Wilm, A., Lopez, R., Thompson, J. D., Gibson, T. J., and Higgins, D. G. (2007) Clustal W and Clustal X version 2.0. *Bioinformatics* **23**, 2947-2948

34. The PyMOL Molecular Graphics System. 1.2r3pre Ed., Schrödinger, LLC.

35. Tian, Q. B., Ohnishi, M., Murata, T., Nakayama, K., Terawaki, Y., and Hayashi, T. (2001) Specific protein-DNA and protein-protein interaction in the hig gene system, a plasmid-borne proteic killer gene system of plasmid Rts1. *Plasmid* **45**, 63-74

36. Neubauer, C., Gao, Y. G., Andersen, K. R., Dunham, C. M., Kelley, A. C., Hentschel, J., Gerdes, K., Ramakrishnan, V., and Brodersen, D. E. (2009) The structural basis for mRNA recognition and cleavage by the ribosome-dependent endonuclease RelE. *Cell* **139**, 1084-1095

37. Krissinel, E., and Henrick, K. (2004) Secondary-structure matching (SSM), a new tool for fast protein structure alignment in three dimensions. *Acta crystallographica. Section D, Biological crystallography* **60**, 2256-2268

38. Holm, L., and Rosenstrom, P. (2010) Dali server: conservation mapping in 3D. *Nucleic acids research* **38**, W545-549

39. Arbing, M. A., Handelman, S. K., Kuzin, A. P., Verdon, G., Wang, C., Su, M., Rothenbacher, F. P., Abashidze, M., Liu, M., Hurley, J. M., Xiao, R., Acton, T., Inouye, M., Montelione, G. T., Woychik, N. A., and Hunt, J. F. Crystal structures of Phd-Doc, HigA, and YeeU establish multiple evolutionary links between microbial growth-regulating toxin-antitoxin systems. *Structure* **18**, 996-1010

40. Christensen-Dalsgaard, M., and Gerdes, K. (2006) Two higBA loci in the Vibrio cholerae superintegron encode mRNA cleaving enzymes and can stabilize plasmids. *Molecular microbiology* **62**, 397-411

41. Kamada, K., and Hanaoka, F. (2005) Conformational change in the catalytic site of the ribonuclease YoeB toxin by YefM antitoxin. *Molecular cell* **19**, 497-509

42. Miallau, L., Jain, P., Arbing, M. A., Cascio, D., Phan, T., Ahn, C. J., Chan, S., Chernishof, I., Maxson, M., Chiang, J., Jacobs, W. R., Jr., and Eisenberg, D. S. (2013) Comparative proteomics identifies the cell-associated lethality of M. tuberculosis RelBE-like toxin-antitoxin complexes. *Structure* **21**, 627-637

43. Takagi, H., Kakuta, Y., Okada, T., Yao, M., Tanaka, I., and Kimura, M. (2005) Crystal structure of archaeal toxin-antitoxin RelE-RelB complex with implications for toxin activity and antitoxin effects. *Nature structural & molecular biology* **12**, 327-331

44. Boggild, A., Sofos, N., Andersen, K. R., Feddersen, A., Easter, A. D., Passmore, L. A., and Brodersen, D. E. (2012) The crystal structure of the intact E. coli RelBE toxin-antitoxin complex provides the structural basis for conditional cooperativity. *Structure* **20**, 1641-1648

45. Francuski, M., Reutzel-Selke, A., Weiss, S., Pascher, A., Jurisch, A., Ulrich, F., Schumacher, G., Faber, W., Kohler, S., Volk, H. D., Neuhaus, P., Tullius, S. G., and Pratschke, J. (2009) Donor brain death significantly interferes with tolerance induction protocols. *Transplant international : official journal of the European Society for Organ Transplantation* **22**, 482-493

46. Heaton, B. E., Herrou, J., Blackwell, A. E., Wysocki, V. H., and Crosson, S. (2012) Molecular structure and function of the novel BrnT/BrnA toxin-antitoxin system of Brucella abortus. *The Journal of biological chemistry* **287**, 12098-12110

47. Kamada, K., Hanaoka, F., and Burley, S. K. (2003) Crystal structure of the MazE/MazF complex: molecular bases of antidote-toxin recognition. *Molecular cell* **11**, 875-884

48. Li, G. Y., Zhang, Y., Inouye, M., and Ikura, M. (2009) Inhibitory mechanism of Escherichia coli RelE-RelB toxin-antitoxin module involves a helix displacement

near an mRNA interferase active site. *The Journal of biological chemistry* **284**, 14628-14636

49. Luscombe, N. M., Austin, S. E., Berman, H. M., and Thornton, J. M. (2000) An overview of the structures of protein-DNA complexes. *Genome Biol* **1**, REVIEWS001

50. Shimon, L. J., and Harrison, S. C. (1993) The phage 434 OR2/R1-69 complex at 2.5 A resolution. *Journal of molecular biology* **232**, 826-838

51. Watkins, D., Hsiao, C., Woods, K. K., Koudelka, G. B., and Williams, L. D. (2008) P22 c2 repressor-operator complex: mechanisms of direct and indirect readout. *Biochemistry* **47**, 2325-2338

52. Francuski, D., and Saenger, W. (2009) Crystal structure of the antitoxin-toxin protein complex RelB-RelE from Methanococcus jannaschii. *Journal of molecular biology* **393**, 898-908

53. Li, G. Y., Zhang, Y., Inouye, M., and Ikura, M. (2008) Structural mechanism of transcriptional autorepression of the Escherichia coli RelB/RelE antitoxin/toxin module. *Journal of molecular biology* **380**, 107-119

54. Miallau, L., Faller, M., Chiang, J., Arbing, M., Guo, F., Cascio, D., and Eisenberg, D. (2009) Structure and proposed activity of a member of the VapBC family of toxin-antitoxin systems. VapBC-5 from Mycobacterium tuberculosis. *The Journal of biological chemistry* **284**, 276-283

55. Mattison, K., Wilbur, J. S., So, M., and Brennan, R. G. (2006) Structure of FitAB from Neisseria gonorrhoeae bound to DNA reveals a tetramer of toxin-antitoxin

heterodimers containing pin domains and ribbon-helix-helix motifs. *The Journal of biological chemistry* **281**, 37942-37951

56. Garcia-Pino, A., Balasubramanian, S., Wyns, L., Gazit, E., De Greve, H., Magnuson, R. D., Charlier, D., van Nuland, N. A., and Loris, R. (2010) Allostery and intrinsic disorder mediate transcription regulation by conditional cooperativity. *Cell* **142**, 101-111

57. Overgaard, M., Borch, J., Jorgensen, M. G., and Gerdes, K. (2008) Messenger RNA interferase RelE controls relBE transcription by conditional cooperativity. *Molecular microbiology* **69**, 841-857

58. Stella, S., Cascio, D., and Johnson, R. C. (2010) The shape of the DNA minor groove directs binding by the DNA-bending protein Fis. *Genes & development* **24**, 814-826

59. Van Melderen, L., Thi, M. H., Lecchi, P., Gottesman, S., Couturier, M., and Maurizi, M. R. (1996) ATP-dependent degradation of CcdA by Lon protease. Effects of secondary structure and heterologous subunit interactions. *The Journal of biological chemistry* **271**, 27730-27738

60. Afif, H., Allali, N., Couturier, M., and Van Melderen, L. (2001) The ratio between CcdA and CcdB modulates the transcriptional repression of the ccd poison-antidote system. *Molecular microbiology* **41**, 73-82

61. Mate, M. J., Vincentelli, R., Foos, N., Raoult, D., Cambillau, C., and Ortiz-Lombardia, M. (2012) Crystal structure of the DNA-bound VapBC2 antitoxin/toxin pair from Rickettsia felis. *Nucleic acids research* **40**, 3245-3258

62. Brown, B. L., Grigoriu, S., Kim, Y., Arruda, J. M., Davenport, A., Wood, T. K., Peti, W., and Page, R. (2009) Three dimensional structure of the MqsR:MqsA complex: a novel TA pair comprised of a toxin homologous to RelE and an antitoxin with unique properties. *PLoS pathogens* **5**, e1000706

63. Schumacher, M. A., Piro, K. M., Xu, W., Hansen, S., Lewis, K., and Brennan, R. G. (2009) Molecular mechanisms of HipA-mediated multidrug tolerance and its neutralization by HipB. *Science* **323**, 396-401

64. Brown, B. L., Lord, D. M., Grigoriu, S., Peti, W., and Page, R. (2013) The Escherichia coli toxin MqsR destabilizes the transcriptional repression complex formed between the antitoxin MqsA and the mqsRA operon promoter. *The Journal of biological chemistry* **288**, 1286-1294

65. Bauerova-Hlinkova, V., Dvorsky, R., Perecko, D., Povazanec, F., and Sevcik, J. (2009) Structure of RNase Sa2 complexes with mononucleotides--new aspects of catalytic reaction and substrate recognition. *The FEBS journal* **276**, 4156-4168

66. Heinemann, U., and Saenger, W. (1983) Crystallographic study of mechanism of ribonuclease T1-catalysed specific RNA hydrolysis. *J Biomol Struct Dyn* **1**, 523-538

67. Dalton, K. M., and Crosson, S. (2010) A conserved mode of protein recognition and binding in a ParD-ParE toxin-antitoxin complex. *Biochemistry* **49**, 2205-2215

68. Dienemann, C., Boggild, A., Winther, K. S., Gerdes, K., and Brodersen, D. E. (2011) Crystal structure of the VapBC toxin-antitoxin complex from Shigella flexneri reveals a hetero-octameric DNA-binding assembly. *Journal of molecular biology* **414**, 713-722

69. Gazit, E., and Sauer, R. T. (1999) Stability and DNA binding of the phd protein of the phage P1 plasmid addiction system. *The Journal of biological chemistry* **274**, 2652-2657

70. Blower, T. R., Salmond, G. P., and Luisi, B. F. (2011) Balancing at survival's edge: the structure and adaptive benefits of prokaryotic toxin-antitoxin partners. *Current opinion in structural biology* **21**, 109-118

71. Kleywegt, G. J. (1997) Validation of protein models from Calpha coordinates alone. *Journal of molecular biology* **273**, 371-376

Chapter 3

mRNA bound to the 30S subunit is a HigB endonuclease substrate

Marc A. Schureck, Tatsuya Maehigashi, Stacey J. Miles, Jhomar Marquez and Christine M. Dunham

HigB requires mRNA to be bound to the ribosome for cleavage to occur. mRNA contacts the small 30S subunit while not contacting the large 50S subunit. Therefore, we tested whether 30S-bound tRNA with the P site tRNA was sufficient for mRNA cleavage and found that HigB could cleave mRNA bound in this state. To understand how HigB interacts with 30S subunit, we solved the X-ray crystal structure of HigB bound to the 30S ribosome and used site-directed mutagenesis to identify HigB residues necessary for HigB function. Our studies identify how HigB interacts with the ribosome and suggest that mRNA bound the 30S ribosome, as in the case of translation initiation, may be a HigB substrate. This manuscript is under review at RNA.

Author contributions: M.A.S. and C.M.D. designed research; M.A.S., T.M., S.J.M. and J.M. performed research; M.A.S. and C.M.D. analyzed data; M.A.S. and C.M.D. created figures; and M.A.S. and C.M.D. wrote the paper.

3.1 Abstract

Activation of bacterial toxins during stress results in cleavage of mRNAs in the context of the ribosome. These toxins are thought to function as global translational inhibitors yet recent studies suggest each may have distinct mRNA specificities that result in selective translation for bacterial survival. Here we demonstrate that mRNA in the context of a bacterial 30S subunit is sufficient for ribosome-dependent toxin HigB endonucleolytic activity. We determined the X-ray crystal structure of HigB bound to the 30S revealing two solvent-exposed clusters of HigB basic residues directly interact with 30S 16S rRNA helices 18, 30 and 31. We further show that these HigB residues are essential for ribosome recognition and function. Comparison with other ribosome-dependent toxins RelE and YoeB reveals each interacts with similar features of the 30S aminoacyl (A) site yet do so through presentation of diverse structural motifs.

3.2 Introduction

Restriction of energy-consuming processes during stress is required to conserve metabolites and maintain basal levels of growth. The bacterial stress or stringent response detects diminishing nutrients and promotes a cascade of events to limit growth and activate specific gene expression to survive new environmental conditions (1). Toxin-antitoxin genes are part of the stringent response whereby antitoxin degradation releases toxin proteins to aid in growth limitation (2). Many bacteria contain multiple toxin-antitoxin genes and in some, specific toxin-antitoxin families are greatly expanded (3,4). These observations suggest that certain toxin-antitoxin families acquired additional functions in addition to their established roles in biofilm formation, persister state formation and growth regulation (2,3).

There are five types of toxin-antitoxin systems with the type II protein-protein family being the most abundant (2,5). During non-stress growth, the toxin-antitoxin complex binds to upstream DNA operator regions to inhibit transcription and limit their expression. Stress triggers antitoxin degradation by AAA+ ATPase proteases Lon, ClpAP and ClpXP resulting in transcriptional de-repression at the toxin-antitoxin operon and inhibition of replication and translation by the free toxin (2,5). A majority of type II toxins are RNases that cleave tRNAs, rRNAs, and mRNAs, either free or specifically bound to the ribosome. Why certain toxin RNases require mRNAs bound to the ribosome for activity is unclear but this specificity suggests a more specialized mechanism of selective translation that may be signaled upon toxin activation to facilitate a defined response to a specific stress.

E. coli contains at least 36 proposed toxin-antitoxin genes with at least five that require the ribosome to cleave mRNA (3). The RelE, YoeB, YafQ and HigB ribosome-dependent toxin cleaves at a preferred mRNA sequence at positions along the entire transcript in the ribosomal aminoacyl (A) site on the 30S subunit. Since the mRNA is bound to the ribosome, cleavage along the entire mRNA suggests that the three stages of the protein synthesis cycle, initiation, elongation, termination, can be targeted by ribosome-dependent toxins. *E. coli* RelE and YoeB cleave both sense and stop codons (6-9) while *E. coli* YafQ and *Proteus vulgaris* HigB cleave at a single AAA lysine codon and adenosine-rich codons, respectively (10,11). Interestingly, the AAA lysine codon, preferentially targeted by YafQ and HigB toxins, is the most common codon to directly follow the AUG start codon in *Proteus mirabilis* and *E. coli* K12 (11,12). This observation suggests that some ribosome-dependent toxins may target an initiation-competent ribosomal complex, that is, the small 30 subunit containing mRNA and initiator $tRNA^{fMet}$, expanding the number of ribosomal states that are potential toxin targets.

During translation, ribosome-dependent toxins compete with EF-Tu•tRNA•GTP ternary complexes and translation factors including initiation factor 1 (IF1) and release factors 1 and 2 (RF1 and RF2) for the empty, or non-tRNA bound, A site. Recently it was shown that the YafQ toxin has a comparable affinity for the ribosomal A site as tRNAs and translation factors (13). However, since toxin-antitoxin complexes are expressed at extremely low levels under both non-stress and stress conditions (14,15), one important question is, how do these toxins gain access to the A site to cleave mRNAs when they are low abundant and have comparable A-site affinities as translation factors and tRNAs?

Here we address one aspect of this question with the *P. vulgaris* host inhibitor of growth B (HigB) toxin, a ribosome-dependent endonuclease initially discovered on a kanamycin-resistance plasmid associated with *Proteus vulgaris* (16). HigB cleaves adenosine-rich codon sequences and the AAA lysine codon is a primary mRNA target sequence (11). Our results show that HigB cleaves mRNA programmed on the 30S-initiation competent complex. Moreover, we report a 3.6-Å X-ray crystal structure of HigB bound to the 30S, identify two clusters of basic residues that interact with 16S rRNA helices, and confirm their importance using mutagenesis and bacterial growth assays. Our results demonstrate that HigB, like RelE (6), is active on the 30S subunit and suggest that initiation, in addition to elongation and termination, can be targeted by ribosome-dependent toxins.

3.3 Results

3.3a HigB toxin can target the initiation step of translation.

HigB cleaves multiple codon sequences with the AAA lysine codon being a major HigB target as shown by primer extension analysis (11). Moreover in *Proteus mirabilis* and *E. coli* K12, the AAA lysine codon is the most common codon at the second position after the AUG start codon (11,12). These observations suggest that the HigB endonuclease may target ribosomes during both initiation and elongation. We previously demonstrated that HigB recognizes a 70S elongation complex with the ribosome being essential for HigB-mediated mRNA cleavage (17). However, whether HigB is active in cleaving mRNA on a 30S subunit is unknown.

To test whether HigB cleaves mRNAs bound to a 30S initiation-competent complex, we first programmed *E. coli* 30S subunits with a 25 nucleotide mRNA

containing a strong Shine-Dalgarno sequence (AGGAGG) optimally spaced preceding an AUG start codon in the P site, and an AAA lysine codon in the A site (**Figure 3.1A**). Next we added 2.5-fold molar excess of *E. coli* $tRNA^{fMet}$ to bind in the P site. In the absence of the 30S, HigB is unable to cleave mRNA demonstrating that HigB requires the ribosome for activity (**Figure 3.1B; lane 4**). Additionally, incubation of 30S subunits with mRNA and $tRNA^{fMet}$ in the absence of HigB confirms the lack of contaminating RNase activity in these components (**Figure 3.1B; lane 5**). Incubation of the 30S initiation-competent complex with HigB results in mRNA cleavage over a 60 min time course (**Figure 3.1B; lanes 6-11**). HigB likely cleaves the mRNA transcript between the second and third A-site nucleotides yielding a 20 nucleotide product containing a 2'-3' or 3'-phosphate (**Figure 3.1B; open arrow**). The presence of a 3'-end phosphate results in faster migration in the gel as observed for RelE, YoeB and YafQ toxins (13,18,19) and the appearance of an apparent ~19 nucleotide fragment. Although HigB was proposed to interact with the 50S subunit (11), these results demonstrate that the 50S is not required for HigB-mediated mRNA cleavage.

3.3b Structural basis of HigB toxin recognition of the 30S subunit.

To reveal the structural basis for HigB recognition of the ribosomal A site in the context of the 30S, we solved the 3.6-Å X-ray crystal structure of HigB bound to the *Thermus thermophilus (Tth)* 30S (**Figures 3.1C-F; Table 4.1**). Crystals of the *Tth* 30S subunit only grow in the *apo* form (20). In this crystal form, the tip of 16S rRNA helix 6 (known as the 30S subunit spur) from one 30S docks in the ribosomal P site of a second subunit, resembling a tRNA anticodon stem loop (**Figure 3.2A**). Additionally, the 3' end of the 16S rRNA in this crystal form folds back into the mRNA tunnel and interacts with

the spur to mimic an anticodon-codon interaction. As a result, it is impossible to bind any P-site ligands including mRNA in this crystal. We attempted to soak into pre-formed 30S crystals HigB and a noncleavable six nucleotide mRNA (5'-AAA UAG-3') which should program a AAA lysine codon in the A site and a UAG codon residing 3' outside the A site. In this mRNA fragment, the AAA lysine codon contained a 2'-methoxy modification that our laboratory showed prevents cleavage (17). This approach is similar to that previously used to observe 30S-bound ligands including IF1, 16S rRNA methyltransferase NpmA, and anticodon stem loops of tRNAs bound to cognate and near-cognate codons of mRNAs (21-24). Unbiased F_o-F_o electron difference density maps clearly reveal HigB bound in the A site (**Figure 3.1C)** but, no interpretable electron density was observed for the mRNA. Thus, although this crystal structure does not provide any direct insights into how HigB interacts with the mRNA when bound to a 30S complex, it demonstrates that HigB can bind the ribosome in the absence of the mRNA, informs on key A-site interactions with HigB, and lastly, allows us to compare the 30S-HigB orientation with that of a 70S-HigB elongation complex (17).

A-site bound HigB makes extensive interactions with 16S rRNA helices h18, h30/31, h32, h34 and h44 and ribosomal protein S12 (**Figures 3.1D and 3.1E**). HigB is a small, compact protein (10.7 kDa) containing a single β-sheet surrounded by two flanking α-helices with a number of solvent-exposed, basic residues that likely play an important role in the recognition of the A-site environment. Like other ribosome-dependent toxins RelE and YoeB (18,19), HigB fits snugly in the A site positioning a distinctive concave active site towards the mRNA path. Unlike interactions between tRNA and the A site, HigB makes a number of other interactions with five 16S rRNA

helices likely to stabilize binding. Similar interactions of tRNAs with 16S rRNA may not be required for efficient binding because tRNAs bind to both the 30S and 50S subunits, with the chemical group attached to the tRNA 3'-end (*e.g.* deacylated, aminoacylated or peptidyl) defining the ribosomal binding site preference (25,26). In contrast, HigB interacts exclusively with the small subunit and forms a network of hydrogen bonds and electrostatic interactions with the backbone of 16S rRNA helices that may aid in HigB recognizing the A site.

The absence of mRNA in our structure is in contrast to all previous structures of the RelE, YoeB and HigB toxins bound to the 70S ribosome (17-19), in which the mRNA is pulled ~9 Å from its normal path in the A site into the active site of the toxin (**Figure 3.2B**). The lack of P-site tethering in the 30S crystal form, due to the 30S spur occupying the P site, may not allow for the extreme rearrangement of the mRNA observed in 70S-toxin structures and explain why mRNA was not observed in our structure.

We next compared the 30S-HigB structure with that of 70S-HigB structures caught in precleavage and postcleavage states (17) (PDB codes 4YPB and 4W4G). HigB adopts an overall similar fold when bound to a 30S or 70S complex and binds in a nearly identical location in the A site (**Figure 3.1F**). Interestingly, the relative location of the 30S head domain differs slightly between the 30S- and 70S-bound forms of HigB. The 30S head domain is known to be flexible most prominently during the movement of mRNA and tRNA during translocation (27-29). In the 30S-HigB structure, the 30S subunit adopts a more open head domain conformation (3 Å) compared to the 70S-HigB complex (17). One reason for these differences in domain closure may be the absence of P-site tRNA and the 50S. However, the fact that HigB can bind to two different

conformations of the 30S head domain indicates there is flexibility in HigB-ribosome interactions which allow for recognition of the different ribosome conformational states.

The A-site 16S rRNA nucleotides A1492, A1493 and G530 adopt different positions depending on the identity of the ligand bound at the A site. In the context of the 30S-HigB structure, A1492 and A1493 appear to be conformationally dynamic but are located within h44 while G530 adopts a *syn* conformation, similar to the *apo* 30S structure (20). A 70S structure containing mRNA but no tRNA in the A site reveals that A1492 is partially extruded from h44 and A1493 is flipped from h44 (30). In these two contexts, G530 also adopts the *syn* conformation. During decoding when tRNA engages the mRNA codon in the A site, 16S rRNA nucleotide C1054 packs beneath the third A-site nucleotide of the codon (24). The A-site mRNA reorganization when HigB binds to the 70S positions the Hoogsteen edge of the third A-site adenosine to base pair with the Watson-Crick face of C1054 (17) (PDB code 4YPB). Comparison of these structures with the 30S-HigB bound structures reveals no significant changes in the position of C1054. In summary, the binding of HigB to the ribosome, in the presence or absence of mRNA, causes no remodeling of the A site in contrast to when tRNA recognizes mRNA codons.

3.3c Two surface-exposed clusters of basic residues are required for HigB function. The HigB toxin has four surfaces that contact the ribosomal A-site 16S rRNA helices and S12 ribosomal protein. The first surface is closest to the ribosomal P site and includes three HigB lysine residues, K6, K8 and K11 (from α1) that form hydrogen bonds with the backbone of 16S rRNA head domain residues G954 (h30), U960-C962 and A959 (h31), respectively (**Figure 3.3A**). Adjacent to the first surface are the side chains of

HigB loop 2 residues T19 and Q25 and the carbonyl of S20 that interact with C1214, U531 and G1050 (h18), respectively. And on the opposite side of the first HigB surface are residues R29 (from α2) and R69 (from β1) that likely form electrostatic interactions with G517 and U531 (h18), respectively. Lastly HigB residues Q49 interacts with ribosomal protein S12 residues T44 and S50. The structures of RelE and YoeB bound to the 70S all contact several regions of the A site but two patches of basic residues that contact h30/h31 and h18 of the head domain are common features among all three (**Figure 3.4**).

To examine the role these basic residues play in HigB function, we monitored bacterial growth upon overexpression of HigB proteins altered in these regions. One possibility in these assays is that the introduction of HigB point variants alters the overall tertiary fold thus making HigB insoluble. This outcome would lead to the restoration of normal bacterial growth suggesting erroneously that the residues play a key role in HigB function. Therefore, to confirm that each HigB variant was expressed and soluble, we examined the expression of HigB variants after 4 hrs by Western blot analysis using polyclonal antibodies against the HigBA complex (**Figure 3.3B**). We first show that *E. coli* harboring WT HigB does not result in a detectable signal in the immunoblot indicative of the toxin causing an overall inhibition of protein synthesis as seen with other toxins such as MqsR (31) (**Figure 3.3B, lane 3**). Similarly, the single point variants K6A and K11A show no signal for HigB (**Figure 3.3B, lanes 4 and 6**), HigB K8A, R29A, R69A, K6A/K8A and R29A/R69A shows a robust signal for HigB expression (**Figure 3.3B, lanes 5, 7-19, 11**) with the HigB double variant K8A/K11A exhibiting slightly less expression (**Figure 3.3B, lane 10**).

Overexpression of wild-type (WT) HigB in *E. coli* causes growth inhibition and mutation of residues essential for HigB toxicity relieves the growth suppression (11,16). Single alanine substitutions of HigB residues K6 and K11 result in HigB variants that retain the ability to suppress bacterial growth while the mutation of K8 shows a slight alleviation of the growth defect (**Figure 3.3C**). Thus, each of these three lysine residue are not individually critical for HigB function. The HigB K6A/K8A variant also slightly relieved growth suppression, similarly to the K8A single variant, while the K8A/K11A double variant allowed for normal growth (**Figure 3.3D**). This latter result suggests HigB activity is ablated upon substitution of both K8 and K11. These results indicate that the combined interactions of HigB residues K8 and K11 with 16S rRNA h31 nucleotides A959-C962 are likely critical for HigB recognition of the ribosomal A site.

The importance of the other two solvent-exposed HigB residues R29 and R69 was similarly tested. HigB proteins carrying single point variants R29A and R69A display an intermediate growth suppression phenotype, while a double R29A/R69A variant inactivated HigB, allowing for normal growth (**Figure 3.3E**). Together, these data demonstrate that HigB uses both patches of basic residues to probe the contours of the A-site rRNA, and these interactions are necessary for HigB activity.

3.4 Discussion

Our biochemical and structural analyses demonstrate that the ribosome-dependent HigB toxin productively recognizes the 30S subunit suggesting an initiation complex may be an *in vivo* target. HigB is positioned in the ribosomal A site and uses two solvent exposed basic patches of lysine and arginine residues to recognize the 16S rRNA backbone. We further show that mutating these clusters of residues in combination

(K8A/K11A or R29A/R69A) impacts HigB activity and therefore toxicity, allowing for bacterial growth (**Figure 3.4A)**. Comparison with another ribosome-dependent toxin RelE reveals two equivalent clusters of solvent-exposed residues that interact with the ribosome albeit derived from distinct secondary structural elements (18) (**Figure 3.4B**). Although RelE and HigB are structural homologs (rmsd 2.2 Å; PDB codes 4FXE and 4MCT) containing a core β-sheet flanked by 2 or 3 α-helices, RelE residues R10, K13 and K17 emanate from α1 to contact h31 similar to HigB α1 although the helices differ in their orientation by ~90 ° (**Figures 3.4A** and **3.4B**). In contrast, RelE residues K28 and K29 from α2 interact with h18 while HigB residues R29 and R69 from the tips of α2 and β1, respectively protrude to recognize h18. Despite the differences in the modes of 16S rRNA recognition, common features of the RelE and HigB remain intact and suggest a conserved binding mechanism for ribosome-dependent mRNA endonucleases.

Ribosome-dependent toxin YoeB also adopts a similar microbial RNase core fold of RelE and HigB, but differs considerably in its interactions with the ribosomal A site (19) (**Figure 3.4C)**. First, YoeB forms a dimer off and on the ribosome, a state that alters how it interacts with 16S rRNA (19,32). The YoeB protomer that interacts with mRNA (called YoeB-a) has a similar α-helix (α2) positioned to form interactions with 16S rRNA h18. However, the interaction with YoeBa α1 and 16S rRNA h31, which is present in HigB and RelE, is nonexistent likely because of the dimer interface. Instead, the second protomer of YoeB (YoeB-b) interacts more distantly on h31 with nucleotides U956, A958 and A959. Recent studies demonstrate that YoeB is activated during thermal stress (33); this temperature-dependence may be an underlying reason for YoeB adopting

a dimeric form presumably to provide thermal stability but this is not currently understood.

Toxin abundance and accessibility of the A site likely both play important roles in determining optimal mRNA substrate selection and activity by ribosome-dependent toxins. Since toxins are expressed at low levels during both non-stress and stress environmental conditions (14,15), and bind within the same range of affinities as tRNAs (13), an argument could be made that the most important determinant for their activity is the accessibility of the A-site mRNA. A preference for cleaving mRNAs during initiation or termination of translation would allow toxins greater access to the A-site mRNA given that each of these steps in translation is slow and, in the case of initiation, is the rate-limiting step of protein synthesis. Indeed, a number of toxins appear to target these two ribosomal states. Although RelE cleaves sense codons (34), it appears to have a preference for stop codons (6). Moreover, YoeB cleaves at codons following the AUG start codon in addition to at the UAA stop codon (7-9). YafQ is thought to only cleave the AAA lysine codon while AAA is a preferred HigB target, a codon that is the most abundant after the start codon in certain bacteria (10,11). Exploitation of the slowest steps in translation by ribosome-dependent toxins may have evolved to limit competition with highly abundant molecules like tRNAs or translation factors. Our results show that the 30S initiation-competent complex is a substrate for HigB similar to previously observed for the RelE toxin (6). Additionally, since ribosome profiling experiments show that ribosomes spend a large amount of time at the beginning of transcripts, this may provide toxins like YafQ, YoeB or HigB an advantage in accessing their substrates (35).

If the bacterial initiation step of translation is a target for HigB, one question is, when during initiation? Initiation is a multistep, kinetically-controlled process whereby initiation factors IF1, IF2 and IF3 along with mRNA and fMet-tRNA^{fMet} form a 30S initiation complex (36). Hydrolysis of GTP by IF2 signals the dissociation of factors before subunit association with the 50S. Comparison of IF1 bound to the 30S to the 30S-HigB structure indicates significant steric clash between HigB α2, loop 3, β1, loop 4 and β2 and IF1 (**Figure 3.5A**). This clashing suggests HigB would have access to the 30S A site only after IF1 dissociation. Since both the 30S initiation-competent and the 70S initiation complexes are targeted by HigB (this study and (17)) and ribosomes spend a large amount of time at the initiation stage (35), both states present equally good opportunities to cleave ribosome-bound mRNA to alter the translational landscape during stress.

Translation initiation is rate-limiting and the slowest step of protein synthesis presenting an ideal situation for a toxin to target mRNA for cleavage. However, ribosome-dependent toxins RelE, HigB, YoeB and YafQ have overlapping binding sites indicating they can not bind in the A site while IF1 is present (**Figure 3.5B**). The YafO toxin requires the ribosome for mRNA cleavage similar to the HigB, RelE, YoeB and YafQ toxins (37,38), yet does not cleave mRNAs in the A site of the ribosome and instead cleaves ~8 nucleotides downstream of the A-site codon near the mRNA entrance tunnel (37). Thus, in contrast to other ribosome-dependent toxins, YafO-mediated mRNA cleavage would not be inhibited by the presence of IF1 likely allowing YafO to cleave mRNA during the initiation process even in the presence of IF1 but also at any point along the entire translation cycle (**Figure 3.5C**). Therefore, it appears bacteria may have

multiple mechanisms to inhibit translation initiation and the biological importance of each should highlight key aspects of bacterial survival during stress.

3.5 Methods and materials

3.5a Strains and plasmids.

E. coli BW25113 (Δ(*araD-araB*)567 Δ(*rhaD-rhaB*)568 Δ*lacZ*4787(::rrnB-3) *lacI*p-400(*lacI*Q)λ- *rpoS*396(Am) *rph*-1 *rrnB*-4 *hsdR*514) cells were used for all bacterial growth assays and to express WT HigB$(His)_6$ (39). Plasmids pBAD24-HigB and pBAD-Myc-HisA-HigB$(His)_6$ were kind gifts from Prof. Nancy A. Woychik (Rutgers University). All single amino acid changes were introduced by site-directed mutagenesis and sequences were verified by DNA sequencing (Genewiz).

3.5b Purification of *E. coli* 30S ribosomes.

E. coli 30S ribosomes were similarly purified as described previously (40). *E. coli* MRE600 cells were grown in LB to an optical density (OD) of 0.7 at 37 °C followed by incubation on ice for 20 mins. Cells were pelleted (all centrifugation steps carried out at 4 °C), washed in buffer 1 (10 mM HEPES/KOH pH 7.6, 10 mM $MgCl_2$, 1 M NH_4Cl, and 6 mM β-mercaptoethanol (β-Me)), and resuspended in buffer 2 (same as buffer 1 except with NH_4Cl reduced to 100 mM). Cells were lysed using a high-pressure homogenizer (Emulsiflex), cell debris was pelleted for 10 min at 17,000 *x g* and the supernatant containing ribosomes was further centrifuged for 3 hrs at 274,000 *x g*. The pelleted ribosomes were resuspended in 4 mL buffer 2 and dialyzed against 10 mM HEPES/KOH pH 7.6, 0.3 mM $MgCl_2$, 100 mM NH_4Cl and 6 mM β-Me to separate the subunits. This solution was applied to a 10-30% linear sucrose gradient, centrifuged overnight at 23,000

rpm in a Beckman SW28 rotor, and the 30S and 50S subunits fractionated. The 30S fractions were pooled, buffer adjusted to 10 mM $MgCl_2$, concentrated by pelleting through a 1.2 M sucrose cushion at 274,000 *x g*, resuspended in buffer 2, flash-frozen in liquid nitrogen and stored at -80 °C.

3.5c HigB expression and purification.

HigB was purified similarly to a previously published purification scheme for the toxin-antitoxin HigBA with a few differences (41). Overnight cultures of *E. coli* BW25113 cells harboring pBAD-Myc-HisA-HigB$(His)_6$ were grown in M9 minimal medium supplemented with 0.2% w/v casamino acids, 100 μg/ml ampicillin, 0.2% (w/v) glucose overnight at 37 °C. A 1:100 dilution was used to inoculate 1 L of fresh M9 medium supplemented with 0.21% (w/v) glycerol, and the culture was grown until an OD at 600 nm of 0.7 was reached. Protein expression was induced with 0.04% w/v arabinose and cultures were grown for an additional 3 hrs before harvesting by centrifugation at 3,500 *x g* and stored at -20 °C. Thawed cell pellets from 1 L cultures were resuspended in 35 mL lysis buffer (20 mM Tris-HCl, pH 7.5, 10% (w/v) glycerol, 250 mM KCl, 5 mM $MgCl_2$, 5 mM β-Me, 0.2 mM phenylmethylsulfonyl fluoride and 0.1% (w/v) triton X-100) and lysed by sonication. Cell debris was removed by centrifugation for 45 min at 39,000 *x g*. The supernatant was passed through a 0.45 μM filter before loading onto a 1 ml Ni^{2+}-nitrilotriacetic acid column attached to an ÄKTApurifier10 (GE Healthcare) at 10 °C. The column was washed with 25 column volumes of loading buffer (40 mM Tris-HCl, pH 7.5, 10% (w/v) glycerol, 250 mM KCl, 5 mM $MgCl_2$, 5 mM β-Me and 20 mM imidazole) and protein was eluted with a linear 25 CV gradient of loading buffer containing 500 mM imidazole. Fractions containing HigB protein were concentrated in a

3,000 MWCO concentrator (Millipore), filtered through a 0.45 μM Spin-X filter (Corning) and loaded onto a Superdex S75 10/300 column (GE Healthcare) preequilibrated in sizing buffer (40 mM Tris-HCl, pH 7.5, 250 mM KCl, 5 mM $MgCl_2$ and 5 mM β-Me). Fractions containing HigB judged to be over 95% pure by SDS-PAGE were pooled, concentrated to 10 μM, flash frozen in liquid nitrogen and stored at -80 °C.

3.5d mRNA cleavage assays.

A final concentration of 1.2 μM *E. coli* 30S was incubated with 0.6 μM 5'-^{32}P mRNA (5'-GGCAAGGAGGUAAAAAUGAAAUAGU-3'; Thermofisher) at 37 °C for 6 min followed by incubation with 3 μM *E. coli* $tRNA^{fMet}$ (Chemical Block) for 30 min at 37 °C. Reactions were initiated by the addition of 0.9 μM HigB and aliquots were removed at 1, 3, 10, 30 and 60 min, and quenched by the addition of 2X formamide dye (98% formamide, 10 mM EDTA, pH 8.0 and 0.2 mg ml^{-1} bromophenol blue) followed by heating at 70 °C for 2 min. The reactions were run on a denaturing 8M urea, 18% polyacrylamide gel where the mRNA substrate was separated from cleavage products. The gel was fixed, dried and visualized by exposure to a phosphor screen followed by imaging on a Typhoon FLA 7000 gel imager (GE Healthcare).

3.5e Structural determination of the 30S-HigB complex.

Thermus thermophilus 30S ribosomes were purified and crystallized and cryoprotected as described previously (42). Before soaking into the 30S crystals, HigB was equilibrated into the ribosome buffer (5 mM HEPES pH 7.5, 50 mM KCl, 10 mM NH_4Cl and 10 mM MgOAc) via dilution followed by concentration in a 3,000 MWCO concentrator. A solution containing a final concentration of 175 μM HigB and 700 μM mRNA (5'-AmAmAm UAG-3' where "m" indicates a 2'-OCH_3 modification to prevent

cleavage) was incubated with the apo 30S crystals for 24 hrs. Crystals were flash frozen in liquid nitrogen and data collection performed at the Northeast Regional Access Team (NE-CAT) 24-IDE beamline. X-ray diffraction images were collected at a wavelength of 0.979 Å using 0.2° oscillations for 36°. Diffraction images were processed using XDS (43) and the test set of reflections was inherited from a previously solved structure of the 30S (PDB code 1J5E). The initial structure was determined by molecular replacement using this same 30S structure as a starting model (20). The initial refinement of the 30S coordinates lacking HigB or mRNA produced unbiased F_o-F_c difference electron density with a clear signal for HigB. Model building was performed in Coot (44) and iterative refinement rounds with grouped B-factors were performed in Phenix (45). After remodeling of A-site rRNA in Coot, rRNA flanking the remodeled regions were individually refined while all other rRNA and ribosomal proteins were refined as a single rigid body group. The structure of HigB was derived from the structure of HigB bound in the precleavage state to the AAA lysine codon on the 70S ribosome (PDB code 4ZSN). Residues 1-89 of HigB were placed into unbiased F_o-F_o difference electron density and refined as a rigid body group. The C-terminus of HigB was modeled and refined individually. The 30S-HigB complex was refined to a final R_{work}/R_{free} of 21.4/23.9%.

3.5f Bacterial growth assays.

Monitoring of bacterial growth upon overexpression of wild-type and HigB variants were performed as previously described (11). *E. coli* BW251113 cells carrying pBAD24 vectors encoding either wild-type or HigB variants were grown in M9 minimal medium supplemented with 0.2% w/v casamino acids, 100 μg/ml ampicillin and either glucose (0.2% w/v) for overnight cultures, or glycerol (0.21% w/v) for protein

overexpression assays. Cultures were inoculated with a 1:100 dilution of an overnight culture, shaken at 250 rpm at 37 °C and induced with 0.2% (w/v) arabinose at an OD_{600} of 0.2. Growth was monitored every hour for six hrs after induction, and the average OD_{600} values along with the standard error of the mean (SEM) were plotted in GraphPad Prism 5. The supernatants (from the 4 hr time point) were assayed for soluble HigB protein expression using Western blot analysis with primary polyclonal antibodies against the HigBA complex (kind gift from Prof. Nancy A. Woychik, Rutgers University). The soluble fraction from equal numbers of cells was separated on a 4-20% denaturing SDS-PAGE gel (Bio-Rad) and anti-rabbit IgG (Sigma) and the ECL-prime kit (GE Healthcare) was used for chemiluminescent detection.

3.6 Acknowledgements

Research reported in this publication was partially supported by a National Science Foundation CAREER award MCB 0953714 (CMD), National Institutes of Health (NIH) GM093278 (CMD), a NIH Biochemistry, Cellular and Molecular Biology (BCMB) Graduate Training Grant 5T32GM8367 (MAS), and NIH NRSA F31 Fellowship GM108351 (MAS). CMD is a Pew Scholar in the Biomedical Sciences. We thank Dunham lab members CE Fagan and JA Dunkle for help in data collection and analysis. We also thank Dr. GL Conn for critical reading of the manuscript. This work is based on research conducted at the APS on the NE-CAT ID24-E beamline, which is supported by National Institute of General Medical Sciences from the National Institutes of Health (P41 GM103403), and at the SER-CAT beamline. Use of the APS, an Office of Science User Facility operated for the US DOE Office of Science by ANL was supported under Contract DE-AC02-06CH11357.

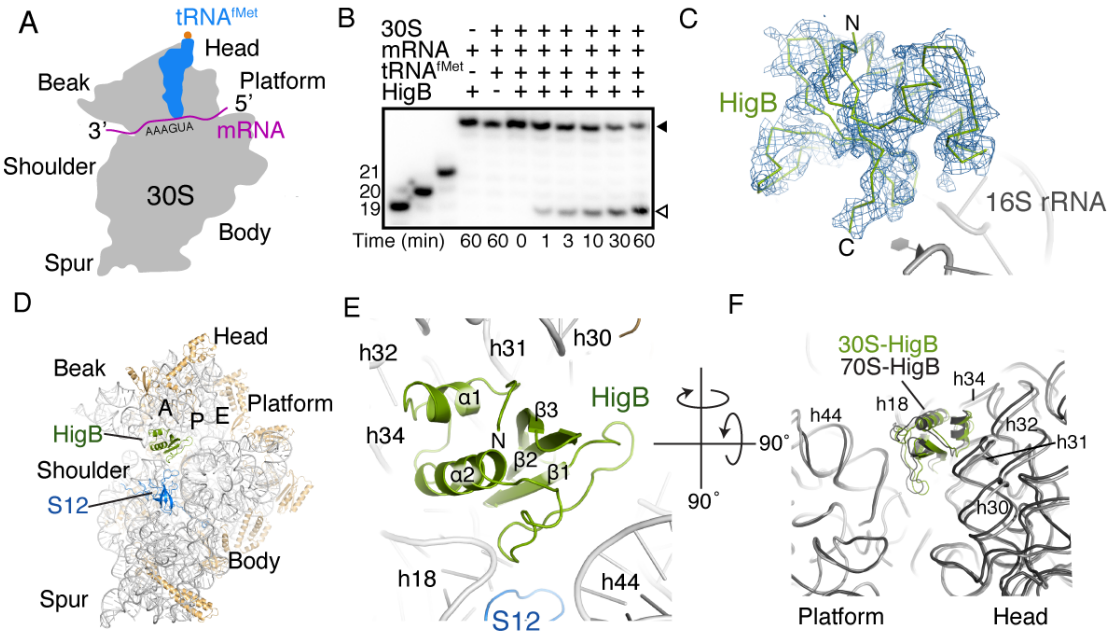

Figure 3.1: HigB recognizes the 30S subunit.

A. Schematic of *in vitro* cleavage assays performed on the *E. coli* 30S ribosomal subunit with 30S domains labeled. B. *E. coli* 30S was programmed with ^{32}P 25-mer mRNA containing an A-site 5'-AAA-3' lysine codon, P-site tRNA^{fMet} and HigB toxin, and mRNA cleavage was monitored over 60 min. Solid arrow indicates uncleaved mRNA, open arrow indicates the cleaved mRNA product and 19-mer, 20-mer, and 21-mer standards are shown to the left. C. Unbiased F_o-F_o difference electron density map of the 3.6 Å X-ray crystal structure of HigB bound to the *Thermus thermophilus* 30S subunit contoured to 2σ. F_o-F_o difference electron density map was calculated using the structure factors of the apo 30S structure (PDB code 1J5E). D. The X-ray crystal structure of HigB (green) bound to the A site of the 30S subunit. 16S rRNA and ribosomal proteins are shown in grey and tan, respectively and the aminoacyl (A), peptidyl (P), exit (E) sites and 30S domains are labeled. E. Zoomed in view in the same orientation as in (D) emphasizing how HigB interacts with multiple 16S rRNA helices and ribosomal protein

S12. F. Comparison of how HigB interacts with the 30S small subunit in the context of the 30S-HigB structure (green; this study) and 70S-HigB ΔH92 precleavage state structure (dark grey; PDB code 4YPB). The 16S rRNA body domain (nucleotides 560-912) of each structure were aligned by least-squares fit in the program Coot (44). 16S rRNA nucleotides from the 30S-HigB and 70S-HigB structures are depicted in light grey and dark grey, respectively.

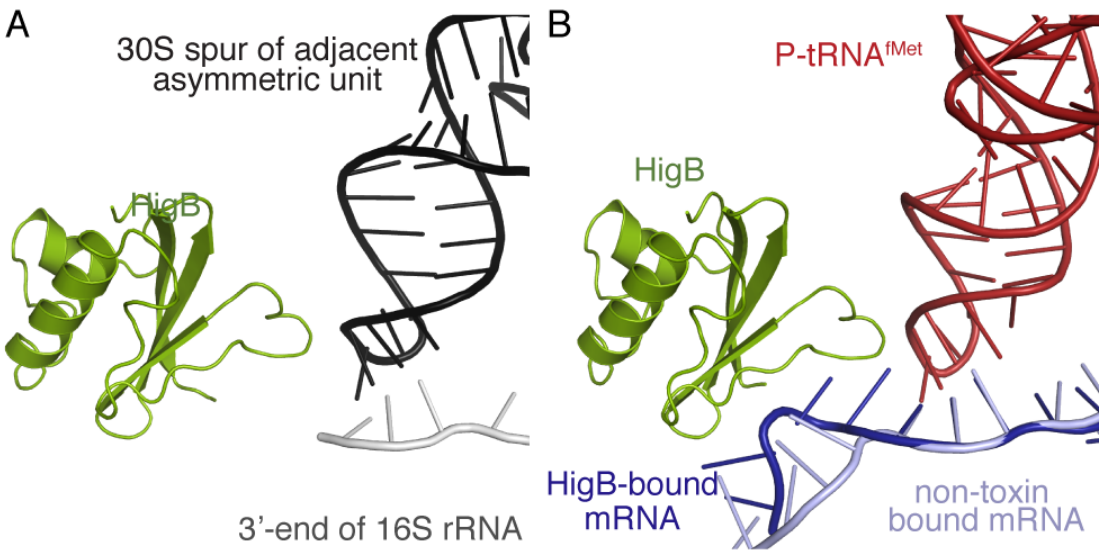

Figure 3.2: 30S crystal form likely prevents toxin-engaged mRNA in the A site.

A. In the context of the 30S crystal form, the 30S spur from a crystallographic symmetry mate packs in the P site and interacts with the 3'- end of the 16S rRNA, mimicking a P-site tRNA-mRNA pair. This arrangement only allows mRNA to be programmed starting at the A site in the 30S crystal form. B. HigB binding to the ribosomal A site facilitates the mRNA being pulled into its active site in the context of a 70S-HigB ΔH92 complex in a precleavage state (PDB code 4YPB). The orientation that the mRNA adopts in the absence of toxin or tRNA is shown for comparison as light purple (PDB code 4V6G).

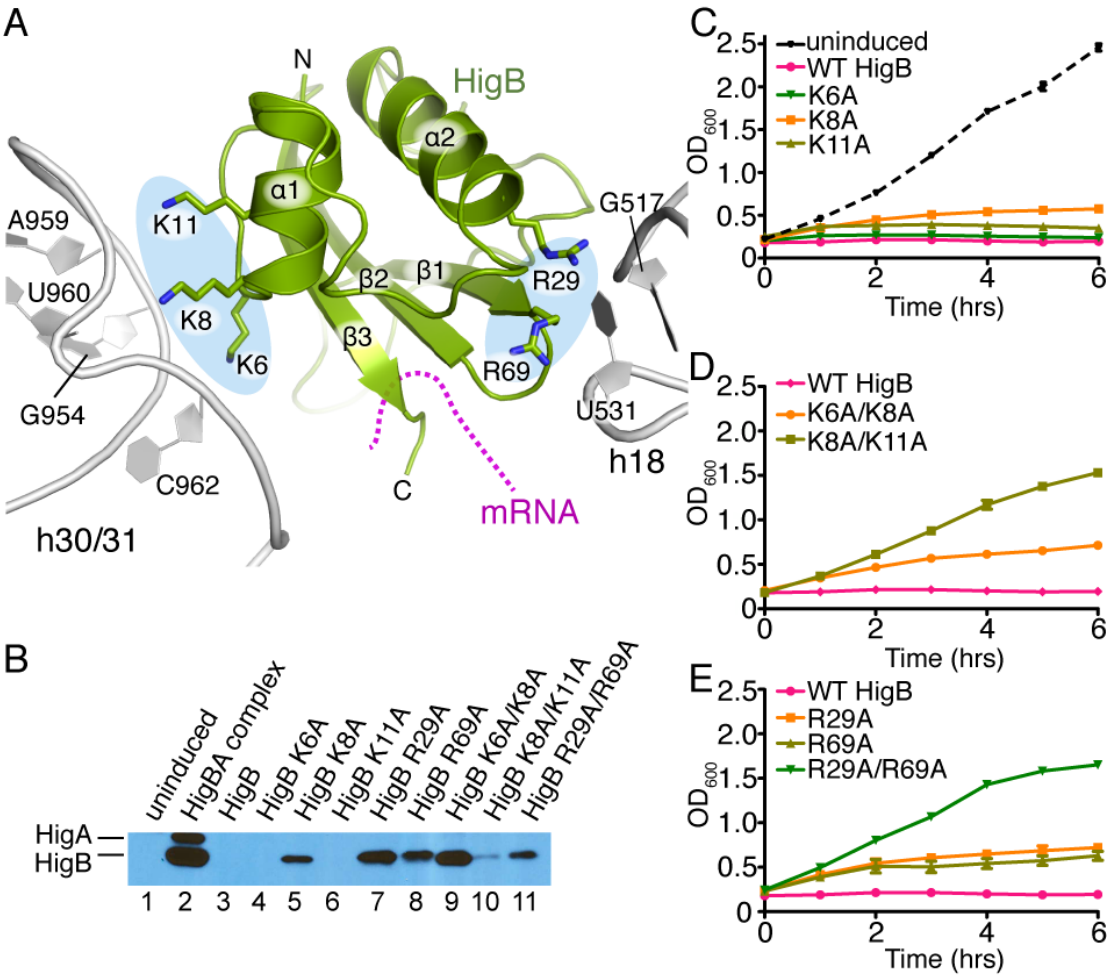

Figure 3.3: Two basic patches on the surface of HigB mediate recognition of 16S rRNA helices 18, 30 and 31.

A. HigB basic residues that interact with 16S rRNA cluster along two exposed surfaces (blue ovals) and are depicted as sticks. The mRNA path is shown as a dotted line as modeled from the 70S-HigB ΔH92 precleavage state (PDB code 4YPB). B. Western blot analysis of the soluble fraction from *E. coli* growth assays (panels C-F) at 4 hrs postinduction using polyclonal antibodies against the HigBA toxin-antitoxin complex. Overexpression of WT HigB halts cell growth and no soluble HigB protein is detected (lane 3) likely due to the effect of HigB-mediated translational repression similar to

overexpression of the MqsR toxin (31). Recombinant HigBA complex is shown as a standard in lane 2 where HigA(His)6 and HigB are 13.5 and 10.7 kDa, respectively. C. *E. coli* growth assays show that overexpression of wild-type (WT) HigB halts cell growth (pink line) while uninduced HigB allows growth (black dash). HigB basic residues that directly interact with 16S rRNA were mutated to alanine and their effect on *E. coli* growth was monitored by optical density (OD) at 600 nm over 6 hrs. HigB patch one residues (K6, K8, and K11) were singly mutated and then doubly mutated in the sensitized K8A background (D). E. HigB patch two residues (R29 and R69) were singly and in combination mutated to alanine and their effect on *E. coli* growth was monitored at an OD at 600 nm over 6 hrs. For panels B-D, error bars display standard error of the mean from at least three experiments.

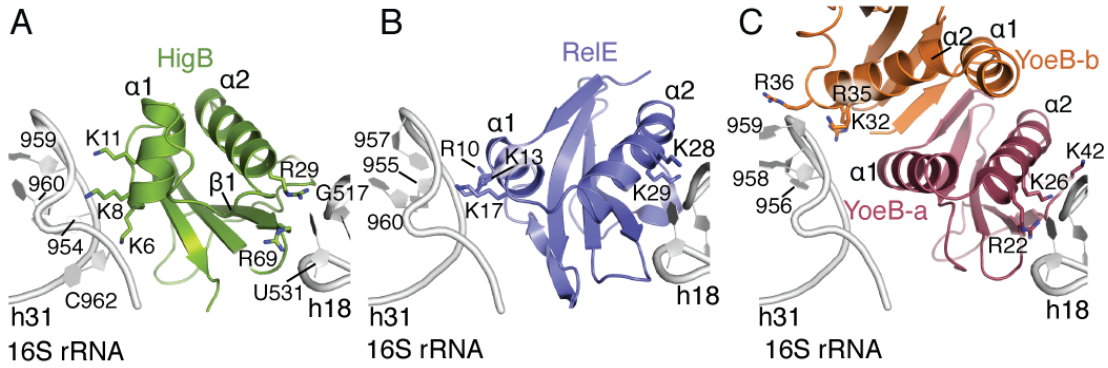

Figure 3.4: Ribosome-dependent toxins recognize the head domain of the 30S subunit.

Views of HigB (A; this study), RelE (B; PDB code 4V7J) and YoeB (C; PDB code 4V8X) interacting with h18 and h31 rRNA via basic residues. The RelE and YoeB structures were captured in the precleavage state and basic residues within hydrogen bonding distance of h18 and h31 are shown as sticks.

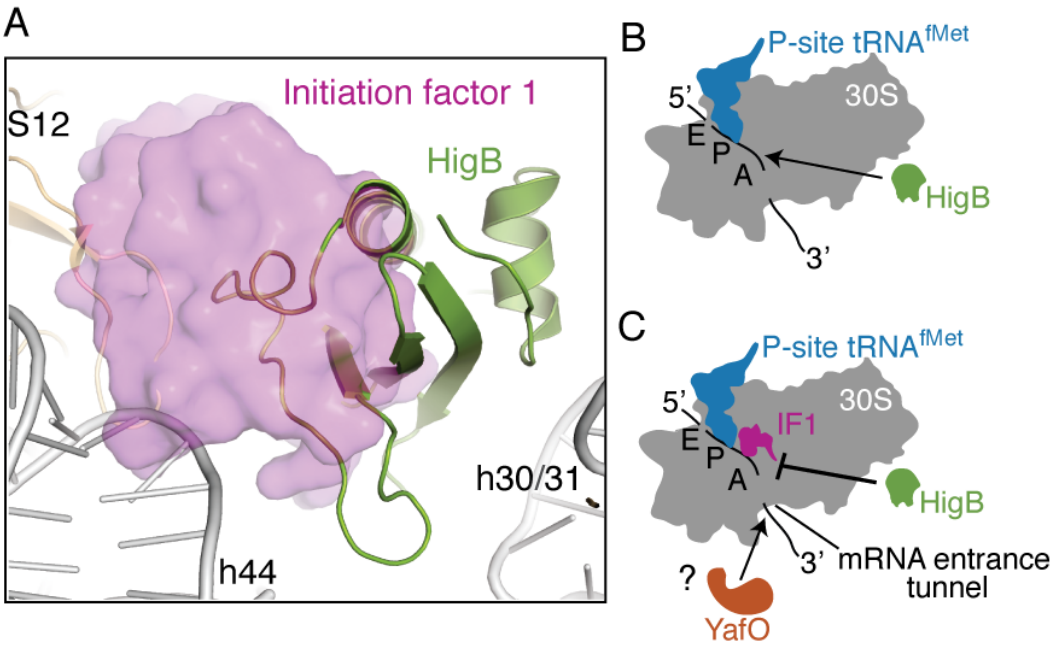

Figure 3.5: Model for toxin recognition of the ribosome.

A. Overlay of Initiation factor 1 (IF1, pink) and HigB (green) bound to 30S subunit. The IF1 protein is shown as a surface representation to highlight the extensive overlap between HigB and IF1. The 30S-IF1 structure (PDB code 1HR0) was aligned to the 30-HigB structure by least-squares fitting of 16S rRNA. B. HigB can targets a 30S-initiation competent complex but not in the presence of IF1. C. The YafO toxin likely cleaves mRNA at the downstream mRNA entrance tunnel and not in the A site as other ribosome-dependent toxins in contrast to HigB, YafQ, YoeB and RelE and during the entire translation cycle.

Table 3.1. Crystallography statistics for the 30S-HigB structure.

Data collection	
Space group	P 4_1 2_1 2
Cell dimensions	
a, *b*, *c* (Å)	402.6, 402.6, 176.0
α,β,γ (°)	90, 90, 90
Resolution (Å)	50 – 3.60 (3.73 – 3.60)[a]
R_{meas} (%)	11.9 (72.2)
R_{pim} (%)[b]	6.7 (40.8)
I/σ	9.8 (1.8)
Completeness (%)	98.6 (99.6)
Redundancy	3.0 (3.0)
Refinement	
Resolution (Å)	50 – 3.60
Total reflections	491,888
Unique reflections	163,739
R_{work} / R_{free}	0.214/0.239
No. atoms	52,640
Protein/RNA	52,444
Ligand/ion	196
Water	0
B-factors	102.4
Protein/RNA	102.5
Ligand/ion	59.3
Water	0
R.m.s. deviations	
Bond lengths (Å)	0.007
Bond angles (°)	1.23
PDB ID	4YY3

One crystal was used for dataset collection.
[a]Values in parentheses are for the highest resolution shell.
[b]Values were calculated by PHENIX

3.7 References

1. Boutte, C. C., and Crosson, S. (2013) Bacterial lifestyle shapes stringent response activation. *Trends in microbiology* **21**, 174-180
2. Maisonneuve, E., and Gerdes, K. (2014) Molecular mechanisms underlying bacterial persisters. *Cell* **157**, 539-548
3. Yamaguchi, Y., and Inouye, M. (2011) Regulation of growth and death in Escherichia coli by toxin-antitoxin systems. *Nature reviews. Microbiology* **9**, 779-790
4. Pandey, D. P., and Gerdes, K. (2005) Toxin-antitoxin loci are highly abundant in free-living but lost from host-associated prokaryotes. *Nucleic acids research* **33**, 966-976
5. Gerdes, K., Christensen, S. K., and Lobner-Olesen, A. (2005) Prokaryotic toxin-antitoxin stress response loci. *Nature reviews. Microbiology* **3**, 371-382
6. Pedersen, K., Zavialov, A. V., Pavlov, M. Y., Elf, J., Gerdes, K., and Ehrenberg, M. (2003) The bacterial toxin RelE displays codon-specific cleavage of mRNAs in the ribosomal A site. *Cell* **112**, 131-140
7. Christensen, S. K., Maenhaut-Michel, G., Mine, N., Gottesman, S., Gerdes, K., and Van Melderen, L. (2004) Overproduction of the Lon protease triggers inhibition of translation in Escherichia coli: involvement of the yefM-yoeB toxin-antitoxin system. *Molecular microbiology* **51**, 1705-1717
8. Christensen-Dalsgaard, M., and Gerdes, K. (2008) Translation affects YoeB and MazF messenger RNA interferase activities by different mechanisms. *Nucleic acids research* **36**, 6472-6481

9. Zhang, Y., and Inouye, M. (2009) The inhibitory mechanism of protein synthesis by YoeB, an Escherichia coli toxin. *The Journal of biological chemistry* **284**, 6627-6638

10. Prysak, M. H., Mozdzierz, C. J., Cook, A. M., Zhu, L., Zhang, Y., Inouye, M., and Woychik, N. A. (2009) Bacterial toxin YafQ is an endoribonuclease that associates with the ribosome and blocks translation elongation through sequence-specific and frame-dependent mRNA cleavage. *Molecular microbiology* **71**, 1071-1087

11. Hurley, J. M., and Woychik, N. A. (2009) Bacterial toxin HigB associates with ribosomes and mediates translation-dependent mRNA cleavage at A-rich sites. *The Journal of biological chemistry* **284**, 18605-18613

12. Sato, T., Terabe, M., Watanabe, H., Gojobori, T., Hori-Takemoto, C., and Miura, K. (2001) Codon and base biases after the initiation codon of the open reading frames in the Escherichia coli genome and their influence on the translation efficiency. *Journal of biochemistry* **129**, 851-860

13. Maehigashi, T., Ruangprasert, A., Miles, S. J., and Dunham, C. M. (2015) Molecular basis of ribosome recognition and mRNA hydrolysis by the E. coli YafQ toxin. *Nucleic acids research* **43**, 8002-8012

14. Overgaard, M., Borch, J., Jorgensen, M. G., and Gerdes, K. (2008) Messenger RNA interferase RelE controls relBE transcription by conditional cooperativity. *Molecular microbiology* **69**, 841-857

15. Li, G. W., Burkhardt, D., Gross, C., and Weissman, J. S. (2014) Quantifying absolute protein synthesis rates reveals principles underlying allocation of cellular resources. *Cell* **157**, 624-635

16. Tian, Q. B., Ohnishi, M., Tabuchi, A., and Terawaki, Y. (1996) A new plasmid-encoded proteic killer gene system: cloning, sequencing, and analyzing hig locus of plasmid Rts1. *Biochemical and biophysical research communications* **220**, 280-284

17. Schureck, M. A., Dunkle, J. A., Maehigashi, T., Miles, S. J., and Dunham, C. M. (2015) Defining the mRNA recognition signature of a bacterial toxin protein. *Proceedings of the National Academy of Sciences of the United States of America* **112**, 13862-13867

18. Neubauer, C., Gao, Y. G., Andersen, K. R., Dunham, C. M., Kelley, A. C., Hentschel, J., Gerdes, K., Ramakrishnan, V., and Brodersen, D. E. (2009) The structural basis for mRNA recognition and cleavage by the ribosome-dependent endonuclease RelE. *Cell* **139**, 1084-1095

19. Feng, S., Chen, Y., Kamada, K., Wang, H., Tang, K., Wang, M., and Gao, Y. G. (2013) YoeB-ribosome structure: a canonical RNase that requires the ribosome for its specific activity. *Nucleic acids research* **41**, 9549-9556

20. Wimberly, B. T., Brodersen, D. E., Clemons, W. M., Jr., Morgan-Warren, R. J., Carter, A. P., Vonrhein, C., Hartsch, T., and Ramakrishnan, V. (2000) Structure of the 30S ribosomal subunit. *Nature* **407**, 327-339

21. Carter, A. P., Clemons, W. M., Jr., Brodersen, D. E., Morgan-Warren, R. J., Hartsch, T., Wimberly, B. T., and Ramakrishnan, V. (2001) Crystal structure of an initiation factor bound to the 30S ribosomal subunit. *Science* **291**, 498-501

22. Dunkle, J. A., Vinal, K., Desai, P. M., Zelinskaya, N., Savic, M., West, D. M., Conn, G. L., and Dunham, C. M. (2014) Molecular recognition and modification of the 30S ribosome by the aminoglycoside-resistance methyltransferase NpmA. *Proceedings of the National Academy of Sciences of the United States of America* **111**, 6275-6280

23. Ogle, J. M., Brodersen, D. E., Clemons, W. M., Jr., Tarry, M. J., Carter, A. P., and Ramakrishnan, V. (2001) Recognition of cognate transfer RNA by the 30S ribosomal subunit. *Science* **292**, 897-902

24. Ogle, J. M., Murphy, F. V., Tarry, M. J., and Ramakrishnan, V. (2002) Selection of tRNA by the ribosome requires a transition from an open to a closed form. *Cell* **111**, 721-732

25. Lill, R., Robertson, J. M., and Wintermeyer, W. (1986) Affinities of tRNA binding sites of ribosomes from Escherichia coli. *Biochemistry* **25**, 3245-3255

26. Schilling-Bartetzko, S., Franceschi, F., Sternbach, H., and Nierhaus, K. H. (1992) Apparent association constants of tRNAs for the ribosomal A, P, and E sites. *The Journal of biological chemistry* **267**, 4693-4702

27. Guo, Z., and Noller, H. F. (2012) Rotation of the head of the 30S ribosomal subunit during mRNA translocation. *Proceedings of the National Academy of Sciences of the United States of America* **109**, 20391-20394

28. Zhou, J., Lancaster, L., Donohue, J. P., and Noller, H. F. (2013) Crystal structures of EF-G-ribosome complexes trapped in intermediate states of translocation. *Science* **340**, 1236086

29. Ratje, A. H., Loerke, J., Mikolajka, A., Brunner, M., Hildebrand, P. W., Starosta, A. L., Donhofer, A., Connell, S. R., Fucini, P., Mielke, T., Whitford, P. C., Onuchic, J. N., Yu, Y., Sanbonmatsu, K. Y., Hartmann, R. K., Penczek, P. A., Wilson, D. N., and Spahn, C. M. (2010) Head swivel on the ribosome facilitates translocation by means of intra-subunit tRNA hybrid sites. *Nature* **468**, 713-716

30. Jenner, L., Demeshkina, N., Yusupova, G., and Yusupov, M. Structural rearrangements of the ribosome at the tRNA proofreading step. *Nature structural & molecular biology* **17**, 1072-1078

31. Brown, B. L., Grigoriu, S., Kim, Y., Arruda, J. M., Davenport, A., Wood, T. K., Peti, W., and Page, R. (2009) Three dimensional structure of the MqsR:MqsA complex: a novel TA pair comprised of a toxin homologous to RelE and an antitoxin with unique properties. *PLoS pathogens* **5**, e1000706

32. Kamada, K., and Hanaoka, F. (2005) Conformational change in the catalytic site of the ribonuclease YoeB toxin by YefM antitoxin. *Molecular cell* **19**, 497-509

33. Janssen, B. D., Garza-Sanchez, F., and Hayes, C. S. (2015) YoeB toxin is activated during thermal stress. *MicrobiologyOpen* **4**, 682-697

34. Hurley, J. M., Cruz, J. W., Ouyang, M., and Woychik, N. A. (2011) Bacterial toxin RelE mediates frequent codon-independent mRNA cleavage from the 5' end of coding regions in vivo. *The Journal of biological chemistry* **286**, 14770-14778

35. Oh, E., Becker, A. H., Sandikci, A., Huber, D., Chaba, R., Gloge, F., Nichols, R. J., Typas, A., Gross, C. A., Kramer, G., Weissman, J. S., and Bukau, B. (2011) Selective ribosome profiling reveals the cotranslational chaperone action of trigger factor in vivo. *Cell* **147**, 1295-1308

36. Schmeing, T. M., and Ramakrishnan, V. (2009) What recent ribosome structures have revealed about the mechanism of translation. *Nature* **461**, 1234-1242

37. Zhang, Y., Yamaguchi, Y., and Inouye, M. (2009) Characterization of YafO, an Escherichia coli toxin. *The Journal of biological chemistry* **284**, 25522-25531

38. Christensen-Dalsgaard, M., Jorgensen, M. G., and Gerdes, K. (2010) Three new RelE-homologous mRNA interferases of Escherichia coli differentially induced by environmental stresses. *Molecular microbiology* **75**, 333-348

39. Datsenko, K. A., and Wanner, B. L. (2000) One-step inactivation of chromosomal genes in Escherichia coli K-12 using PCR products. *Proceedings of the National Academy of Sciences of the United States of America* **97**, 6640-6645

40. Powers, T., and Noller, H. F. (1991) A functional pseudoknot in 16S ribosomal RNA. *Embo J* **10**, 2203-2214

41. Schureck, M. A., Maehigashi, T., Miles, S. J., Marquez, J., Cho, S. E., Erdman, R., and Dunham, C. M. (2014) Structure of the Proteus vulgaris HigB-(HigA)2-HigB toxin-antitoxin complex. *The Journal of biological chemistry* **289**, 1060-1070

42. Clemons, W. M., Jr., Brodersen, D. E., McCutcheon, J. P., May, J. L., Carter, A. P., Morgan-Warren, R. J., Wimberly, B. T., and Ramakrishnan, V. (2001) Crystal structure of the 30 S ribosomal subunit from Thermus thermophilus: purification,

crystallization and structure determination. *Journal of molecular biology* **310**, 827-843

43. Kabsch, W. (2010) Xds. *Acta crystallographica. Section D, Biological crystallography* **66**, 125-132

44. Emsley, P., Lohkamp, B., Scott, W. G., and Cowtan, K. (2010) Features and development of Coot. *Acta crystallographica. Section D, Biological crystallography* **66**, 486-501

45. Adams, P. D., Afonine, P. V., Bunkoczi, G., Chen, V. B., Davis, I. W., Echols, N., Headd, J. J., Hung, L. W., Kapral, G. J., Grosse-Kunstleve, R. W., McCoy, A. J., Moriarty, N. W., Oeffner, R., Read, R. J., Richardson, D. C., Richardson, J. S., Terwilliger, T. C., and Zwart, P. H. (2010) PHENIX: a comprehensive Python-based system for macromolecular structure solution. *Acta crystallographica. Section D, Biological crystallography* **66**, 213-221

Chapter 4

Defining the mRNA recognition signature of a bacterial toxin protein

Marc A. Schureck, Jack A. Dunkle, Tatsuya Maehigashi, Stacey J. Miles, and Christine M. Dunham

The HigB toxin recognizes A-site mRNA in a unique fashion. tRNA and release factors usually recognize one or just a few A-site codons. The HigB toxin is able to recognize and cleave several A-site codons. To understand how the HigB toxin cleaves multiple codons, I solved the X-ray crystal structure of HigB bound to two adenosine-rich codons and characterized HigB cleavage specificity *in vitro*. HigB recognizes several different codons with the use of binding sites that can accept more than one nucleotide. Surprisingly, although HigB can recognize more than one nucleotide at the first two A-site nucleotide positions, HigB is highly selective for an adenosine at the third A-site position. This study defines the unique mRNA recognition properties of HigB and suggests cleavage of codons containing a third position adenosine is an important feature of HigB function.

This research was originally published in the Proceedings of the National Academy of Sciences of the United States of America. Schureck MA, Dunkle JA, Maehigashi T, Miles SJ, Marquez J, and Dunham CM. Defining the mRNA recognition signature of a bacterial toxin protein. *Proceedings of the National Academy of Sciences of the United States of America*. 2015 112(45):13862-7.

Author contributions: M.A.S. and C.M.D. designed research; M.A.S. and S.J.M. performed research; M.A.S., J.A.D., T.M., and C.M.D. analyzed data; and M.A.S., J.A.D., and C.M.D. wrote the paper.

4.1 Abstract

Bacteria contain multiple type II toxins that selectively degrade mRNAs bound to the ribosome to regulate translation, growth and facilitate survival during the stringent response. Ribosome-dependent toxins recognize a variety of three-nucleotide codons within the Aminoacyl (A) site, but how these endonucleases achieve substrate specificity remains poorly understood. Here, we identify the critical features for how the HigB toxin recognizes each of the three A-site nucleotides for cleavage. X-ray crystal structures of HigB bound to two different codons on the ribosome illustrate how HigB utilizes a microbial RNase-like nucleotide recognition loop to recognize either cytosine or adenosine at the second A-site position. Strikingly, a single HigB residue and 16S rRNA residue C1054 form an adenosine-specific pocket at the third A-site nucleotide, in contrast with how tRNAs decode mRNA. Our results demonstrate that the most important determinant for mRNA cleavage by ribosome-dependent toxins is interaction with the third A-site nucleotide.

4.2 Significance

Bacteria have a tremendous capacity to rapidly adapt their gene expression profiles and metabolic rates through global regulatory responses. Toxin-antitoxin complexes act as metabolic regulators that limit their own expression under exponential growth but inhibit energy-demanding processes like protein synthesis during stress. A majority of toxins display exquisite endonucleolytic specificity for mRNAs but only in the context of the ribosome. The molecular basis for this selectivity is unclear given their simple microbial RNase architecture. Here we demonstrate the mechanistic determinants for HigB toxin selection of mRNA substrates. Moreover we propose that ribosome-dependent toxins

recognize their mRNA substrates primarily through identification of the third nucleotide of the codon, contrary to how tRNAs and other translation factors also recognize the A site.

4.3 Introduction

Bacteria live in dynamic environments and as a consequence have developed robust stress responses to survive harsh conditions including temperature fluctuations, nutrient deprivation, and oxidative stress (1,2). Lack of nutrients activates the stringent response and the synthesis of the 'magic spot' alarmone, guanosine penta/tetraphosphate ((p)ppGpp). (p)ppGpp serves as a global signaling molecule and facilitates transcription of prosurvival genes and activation of downstream proteolysis of select substrates that inhibit replication and translation (1,3,4). This rapid inhibitory switch suppresses metabolite consumption and temporarily halts cell growth to promote bacterial survival until nutrients are readily available. Among the prosurvival genes regulated by (p)ppGpp production are toxin-antitoxin modules which have additional roles in antibiotic resistance and tolerance, biofilm and persister cell formation, and niche-specific colonization (5-11). The critical roles toxin-antitoxin pairs play in bacterial physiology underscore the importance of understanding their molecular targets and modes of action.

There are five different classes (I-V) of toxin-antitoxin systems defined by how the antitoxin represses toxin function (1). Type II toxin-antitoxin pairs form protein-protein complexes during exponential growth that serve two purposes: inhibition of toxin activity by antitoxin binding, and transcriptional autorepression to limit toxin expression (12). Antitoxins are proteolytically degraded after (p)ppGpp accumulation leading to derepression at the toxin-antitoxin promoter (8,12). Liberated toxin proteins inhibit the

replication or translation machinery by targeting DNA gyrase, initiator $tRNA^{fMet}$, glutamyl-tRNA synthetase, EF-Tu, free mRNA, ribosome-bound mRNA and the ribosome itself (13-20).

Ribosome-dependent toxins cleave mRNAs on the ribosome between the second and third nucleotides of the aminoacyl-site (A-site) codon (21-23). While collectively *E. coli* ribosome-dependent toxins target a diverse range of codons, each individual toxin appears to have a strong codon preference and cleaves at defined positions along the mRNA (24-26). RelE cleaves at UAG stop codons and the CAG sense codon (all codons denoted in the 5'-3' direction); YoeB cleaves at codons following a translational AUG start site and at the UAA stop codon; and YafQ cleaves a single AAA sense codon (16,24,27-29). In contrast, *Proteus vulgaris* HigB toxin degrades multiple codons encoding for different amino acids with the defining codon signature being a single adenosine (30). Further, recent studies have suggested that a number of toxins cleave a spectrum of codons irrespective of codon family (*i.e.* codons coding for the same amino acid) (16,25,27). This loose specificity exhibited by HigB and other toxins strongly suggests that canonical codon identity may play little to no role in defining a toxin mRNA substrate and, as an extension of this, that toxins recognize A-site codons in a manner distinct from tRNAs and release factors. However, as all ribosome-dependent toxins adopt a conserved microbial RNase fold (31-34) and cleave the mRNA using the same mechanism of in-line attack on the scissile phosphate (16,21-23), the structural features of each toxin that define different nucleotide preferences in the context of the ribosome remain elusive.

Here we elucidate the molecular basis for translation inhibition and nucleotide selectivity by the HigB toxin. We demonstrate that HigB recognizes each A-site nucleotide position distinctly. Since ribosome-dependent toxins contain a conserved protein architecture, these results provide a molecular framework for rationalizing the specificity of this enzyme family. Our structures reveal that HigB recognizes mRNA using hydrogen bonding capability to select for the second A-site nucleotide while an adenosine-specific binding pocket is formed by both HigB and 16S rRNA residues to confer specificity at the third A-site position. Lastly a single HigB residue modulates adenosine selectively at this third A-site position by a mode that is distinct from other ribosome-dependent toxins (21,22). As toxin proteins play prominent roles in persister cell formation and represent novel antimicrobial targets (8,11,35,36), determining the molecular basis of mRNA substrate specificity may provide insights to subvert toxin activity.

4.4 Results & Discussion

4.4a Structural determination of HigB-ribosome complexes.

To determine the molecular basis for substrate recognition by HigB, we solved three x-ray crystal structures of HigB bound to the *Thermus thermophilus (Tth)* 70S containing either an AAA or ACA codon in the A site in pre or postcleavage states, and a high resolution structure of HigB (**Tables 4.1-4.2**). The first precleavage state 70S structure was trapped by using a catalytically inactive HigB variant (ΔH92)(30) and mRNA containing a 2'-OCH_3 modification at all three A-site nucleotides (AmAmAm Lys codon). This structure was determined to 3.4-Å (I/σ = 1.8) (**Figs. 4.1*A* & 4.1*B*; Fig. 4.2*A*; Table 4.1**). The second structure is a postcleavage state that contains wild-type

HigB bound to unmodified mRNA and was solved to 3.3-Å resolution (I/σ = 1.8) (**Fig. 4.1*C*; Fig. 4.2*B* & Table 4.1**). Additionally, a 70S-HigB ΔH92 precleavage state bound to an AmCmAm codon was solved to 3.1-Å resolution (I/σ = 1.9) (**Fig. 4.2*C* & Table 4.1**). In all three structures, F_o-F_c difference electron density maps allowed unambiguous placement of P-site $tRNA^{fMet}$, mRNA and A-site bound HigB (**Figs. 4.2*A*-*C***). Lastly, a 1.25-Å x-ray structure of HigB was used as a starting model to confidently build HigB into lower resolution (3.1-3.4-Å) 70S electron density maps (**Table 4.2**).

The 1.25-Å structure of free HigB reveals that it adopts a microbial RNase fold consisting of a three-stranded, β-sheet appended by two N-terminal, α-helices (**Fig. 4.3A**). Comparison of this structure, HigB from the HigBA complex (33), and HigB in the 70S bound structures (discussed later), shows a similar overall HigB fold and concave cleft, the likely location of the active site (rmsd of 0.4-1.0 Å for residues 1-92) (**Fig. 4.3**). While other toxins are proposed to undergo allosteric regulation after release from the antitoxin (32,37,38), our data suggests that HigB has a preformed tertiary structure primed for interaction with the ribosome.

4.4b Recognition of the A site by HigB involves distortion of the mRNA.

HigB binds the A site between the head and body of the small subunit, similar to where tRNA interacts with mRNA (**Fig. 4.1*A***) (39). The selection of correct tRNAs results from the ribosome monitoring the Watson-Crick base pairing between the tRNA anticodon stem loop and the A-site codon. 16S rRNA nucleotides A1492/A1493 flip from an internal loop of helix 44 (h44) while G530 changes from a *syn* to an *anti* conformation to inspect the minor groove of the codon-anticodon interaction (39). In the two 70S-HigB precleavage state structures, A1492 remains within h44 while A1493

adopts an intermediate state between its fully extended flipped position, seen when a cognate mRNA-tRNA pair is present in the A site, and its position inside of h44 (Fig. S3*A*). In the postcleavage state structure, both A1492 and A1493 occupy an intermediate state, with A1493 in proximity to 23S rRNA nucleotide A1913 (Helix 69) and HigB residues L53 and H54 (**Fig. 4.4*A* & 4.4*B***). In all structures, G530 adopts a *syn* conformation, resembling an empty A-site 70S complex (40) (**Fig. 4.4*C***).

In both the pre and postcleavage state 70S structures, HigB binding causes a distortion of the mRNA backbone with the position of the A6 nucleotide changing the most dramatically (5 and 9 Å movement of the C1' and phosphate atoms, respectively) (**Fig. 4.1*D***). The structures of HigB bound to the 70S reveal that HigB interacts with each of the three A-site nucleotides in distinct ways. While a potential hydrogen bond between the nucleobase of A4 with the 2'-OH of the adjacent P-site tRNA nucleotide 35 may be present, no other direct interactions between HigB and the A4 nucleotide are observed, indicating any nucleotide would be recognized by HigB at this position (**Fig. 4.5*A***). In contrast, HigB residues H54, K57, A70, N71, R73, Y91 and H92 flank the +5 and +6 mRNA positions (**Figs. 4.1*B* & 4.1*C***). HigB loop residues between α2 and β1 (H54 and K57) directly interact with the +5 position; the Hoogsteen face of the A5 nucleotide forming two hydrogen bonds with the backbone of HigB lysine residue (K57) (**Fig. 4.5*B***). The only other nucleotide that can fulfill this same hydrogen bonding pattern is cytosine in an *anti* conformation (**Fig. 4.6**). Additional contacts include the nitrogen ε2 atom of the imidazole side chain of H54 with the 2'-OH of A5 (a 2'-OCH_3 in the precleavage structure) (**Fig. 4.5*B***).

Surprisingly, C-terminal HigB residues A70, N71, R73 and Y91 and 16S rRNA residues surround the nucleobase of A6 forming a nucleotide-specific pocket (**Fig. 4.5*C***). HigB R73 interacts with the A6 phosphate (the scissile phosphate) while HigB residues A70 and N71 flank one face of the nucleobase of A6, and 16S rRNA residues G530 and C1054 frame the opposite side. HigB residue N71 stacks with 16S rRNA nucleotide C1054, orienting the Watson-Crick face of C1054 for interaction with the Hoogsteen edge of A6. The interaction of A6 with the conserved C1054 provides one mechanism by which HigB selects for adenosines at the +6 position. HigB recognition of the +6 nucleotide is most similar to how release factors 1 or 2 (RF1/2) recognize stop codons, with one significant difference being the +6 nucleotide base stacks with decoding center nucleotide G530 upon RF binding, an interaction absent in HigB-mRNA recognition (41,42).

4.4c A-site nucleotide requirements for HigB cleavage.

Primer extension analysis of five transcripts cleaved upon HigB overexpression identified a preference for adenosine-rich codons (codons cleaved in the preference of AAA>GAA>CAA>AAC), but also codons containing a single adenosine (*e.g.* GCA>CCA>CAU) (30). We confirmed *in vitro* that HigB efficiently cleaves an AAA codon in a ribosome-dependent manner (**Fig. 4.7*A***). As our structures reveal that HigB interacts with each of the three A-site nucleotides in distinct ways, this provided initial evidence for why toxins may not have a strict three-nucleotide codon requirement. To further test this, we performed *in vitro* cleavage assays in which each A-site nucleotide position was varied in the context of the preferred AAA codon. Similar results were seen when an adenosine, guanosine or cytosine was located at the +4 position (observed rate

constants (k_{obs}) of 0.57, 0.25 and 0.69 min^{-1}, respectively) while an uridine substitution was cleaved less efficiently (0.088 min^{-1}) (**Fig. 4.7*B* & Fig. 4.8*A***). Together these data strongly suggest that there is no strong nucleotide preference at the +4 position.

Our structures of HigB bound to the ribosome reveal A5 makes specific interactions with the HigB backbone with cytosine being the only other nucleotide capable of forming similar interactions (**Fig. 4.6**). We tested the nucleotide preference at the +5 position and our results demonstrate similar observed cleavage rates for AAA and ACA codons (k_{obs} = 0.57 and 0.89 min^{-1}, respectively), whereas AGA and AUA codons were cleaved 7 and 27-fold less efficiently (0.077 and 0.021 min^{-1}, respectively; **Fig. 4.7*C* & Fig. 4.8*B***), further supporting our predictions based upon our structural work.

To directly test the possibility that an ACA codon forms a similar hydrogen-bonding network as the AAA codon, we solved a 3.1-Å x-ray crystal structure of 70S-HigB ΔH92 bound to the AmCmAm codon in a precleavage state (**Table 4.1**). The first and third A-site nucleotides (A4 and A6) are in identical positions as previously seen in our 70S-HigB bound to the AAA A-site codon structure (**Figs. 4.9*A* & 4.9*B*, Fig. 4.2**). Although C5 occupies a similar local position as A5, it adopts an *anti* conformation to form an analogous hydrogen-bonding pattern between A5 and the HigB backbone (**Figs. 4.9*A* & 4.9*B***). Specifically, the N3 amine and the N4 amino groups of C5 form hydrogen bonds with the backbone amino and carbonyl groups of K57, respectively. Additionally, the nitrogen ε2 atom of the imidazole side chain of H54 is within ~3 Å from the 2'-OH of C5 (**Fig. 4.9*B***). The requirement of A5 or C5 by HigB suggests that selection is driven by hydrogen bonding complementarity to properly orient the 2'-OH of the A5/C5 nucleotides for proton abstraction and in-line attack on the scissile phosphate.

Next we tested the nucleotide requirements of HigB at the +6 position. Our results show AAG/C/U codons were cleaved 9-10 fold less efficiently than the optimal AAA codon (0.051, 0.051 and 0.047 min^{-1} respectively; **Fig. 4.7*D* & Fig. 4.8*C***), demonstrating a clear preference for an adenosine. Taken together, these data support a model where HigB nucleotide specificity increases 5' to 3' of the A-site codon with the identity of the +4 nucleotide playing little to no role in HigB specificity. Conversely, tRNAs and RFs have vastly different recognition requirements. During tRNA selection, nucleotide identity and specifically a Watson-Crick interaction between the anticodon and codon is essential at the +4 and +5 positions while variation at the +6 or wobble position allows for degeneracy in the genetic code, while all three A-site nucleotides are important during RF-mediated termination. The differential recognition patterns of the three A-site nucleotides by HigB is surprising given what is known about tRNA and RF A-site recognition of mRNA.

Microbial endonucleases RNases T1 and U2 contain a recognition loop that interacts with the purine nucleobase 5' of the scissile phosphate in a similar manner as toxins probe the identity of the +5 nucleotide (this is also the nucleotide 5' of the scissile phosphate) (**Figs. 4.9*C* & 4.9*D*)** (43,44). Moreover, RNase T1 and U2 binding forces the preceding purine to adopt a *syn* conformation similar to what we observe with A5 in the 70S-HigB structures. This *syn* purine conformation allows for recognition of the Hoogsteen face of the nucleobase by the peptide backbone and recognition of the Watson-Crick face by a conserved glutamate residue. Lastly, a conserved histidine in both RNase T1 and U2 is within hydrogen bonding distance to the 2'-OH and has been proposed to function as a general base to initiate the in-line attack reaction, similar to a

possible role of HigB residue H54 adjacent to the scissile phosphate. One key difference is the absence of interactions between HigB and the Watson-Crick face of A5 (**Figs. 4.9*A* & 4.9*B***), likely because the HigB recognition loop is truncated by 8 or 11 residues, as compared to RNases T1 and U2, respectively. One consequence of this is that HigB, and likely other ribosome-dependent toxins, discriminates irrespective of base size but rather, by complementary surfaces between the mRNA and toxin.

4.4d Cross talk between A-site nucleotides drives efficient HigB recognition of mRNA.

To more completely define HigB sequence recognition requirements, we next varied more than one nucleotide position in the preferred AAA codon to test the combinatorial effects of adding together two single substitutions that are either cleaved efficiently or inefficiently. A CCA codon should, in theory, be efficiently cleaved by HigB because of C5 and A6. Compared to the CAA and ACA codons, a CCA codon is less efficiently cleaved (six- to seven-fold reduction, respectively; 0.12 min^{-1}) (**Fig. 4.7*E* & Fig. 4.8*D***). Consistent with the importance of a codon containing an adenosine at the +6 position, a CCC codon is cleaved by HigB with extremely low efficiency (**Fig. 4.7*E***). To define the effects of combining two substitutions that are cleaved inefficiently (AUA and AAU, which each results in a ~27 and 10-fold reduction of mRNA cleavage as compared to AAA, respectively), we tested HigB cleavage of the AUU codon (**Fig. 4.7*E***). Uridines at the +5 and +6 positions (AUU) completely ablated HigB activity. These data point to HigB cleavage as context-dependent, suggesting communication between the +5 and +6 sites in mRNA recognition.

The cleavage assays define the codon signatures recognized by HigB and demonstrate that HigB selects for a spectrum of A-site codons containing specific nucleotides at the +5 and +6 nucleotide positions. Based on these studies, we propose that upon entering the A site, HigB probes the nucleotide sequence at the +5 and +6 positions via hydrogen-bonding with the +5 nucleobase while also confirming an adenosine at the +6 position. If both requirements are met, the mRNA is optimally positioned for efficient HigB cleavage. Moreover, although we found the identity at the +4 position plays little role in HigB recognition when adenosines are present at the +5 and +6 A-site positions, we determined that the +4 and +5 nucleotides have a combinatorial effect on HigB activity (**Fig. 4.7*E***). While the codon specificities of only RelE and HigB have been quantitated with defined *in vitro* assays, we predict YafQ and YoeB are also likely to cleave a spectrum of codons as observed for HigB and RelE (24,27,28).

4.4e A single HigB residue modulates codon selectivity.

HigB selects for an adenosine at the +6 position through a *trans* Watson-Crick-Hoogsteen interaction with 16S rRNA C1054 and N71 stacking with C1054 (**Fig. 4.11*A***). Asparagine 71 is highly conserved in HigB homologs (>87% sequence identity) and to test the effect of N71 substitution, we assayed the HigB N71A variant for its ability to cleave +6 nucleotide substitutions in the context of the AAA lysine codon. Our results show that HigB N71A cleaves the AAA codon ~10-fold less efficiently than wild-type HigB but, surprisingly, HigB N71A cleaves AAG/C/U codons only ~2-fold less efficiently than wild-type HigB (**Fig. 4.11*D* & Fig. 4.8*E***). These results strongly suggest that the N71A variant corrupts the A6 binding pocket allowing for nucleotide promiscuity. The productive interaction between HigB N71 and C1054 likely drives efficient cleavage

of adenosines at the +6 positions, rather than discriminating against other nucleotides. In support of this, all codons tested for HigB N71A cleavage show similar low levels of mRNA degradation demonstrating that HigB specificity is conferred by a single amino acid.

4.5 Conclusions

We report a comprehensive molecular analysis of the bacterial toxin HigB, a type II ribosome-dependent mRNA endonuclease. The x-ray structures of HigB and HigB bound in a pre and postcleavage states reveal insights into mRNA specificity by toxins. Recent studies demonstrate that type II toxins play important roles in bacteria, such as in persister cell formation (8,11,36). Therefore determining the molecular basis for mRNA degradation provides significant insights into toxin function. Because many bacterial genomes encode for multiple ribosome-dependent toxins that upon overexpression inhibit translation and cell growth, whether all ribosome-dependent toxins function similarly during stress to simply impair translation, or whether each has a defined role in response to stress, is an unresolved, fundamental question.

Comparison of ribosome-dependent toxins reveals similarities in how each defines a spectrum of codons for degradation, but also reveals a number of striking distinctions. HigB, YoeB and YafQ all contain a four amino acid motif (H/E-P-L-X) in the recognition loop that directly contacts the +5 position of the A-site mRNA (**Figs. 4.9*A*, *4.9E* & 4.9*F***). The HigB recognition loop specifies an A or a C at the +5 nucleotide position with YoeB similarly recognizing an A5 in a *syn* conformation (22). Based on our biochemical assays of HigB and the structural analyses (21,22), we predict that YafQ and YoeB toxins may efficiently cleave codons containing +5 cytosines, along

with their well-characterized ability to cleave +5 adenosines (24,27-29). In contrast, RelE preferentially recognizes an A5 nucleotide that adopts an *anti* conformation. This unique mode of binding suggests RelE utilizes a different mechanism for recognition of a purine at the +5 position (16,21).

The most striking difference in the mechanism of mRNA selection by ribosome-dependent toxins is in how the +6 nucleotide is engaged by the toxin. Our results clearly show a strict HigB requirement for an adenosine at the +6 position where A6 forms a *trans* Watson-Crick-Hoogsteen interaction with C1054 (**Fig. 4.11*A*)**. However in the 70S-RelE structure, the nucleobase edge of G6 does not interact with C1054 to enforce specificity, but rather, G6 and C1054 stack with one another consistent with RelE preferring a purine at this position (**Fig. 4.11*B*)**(16,21). In the 70S-YoeB structure, the only contact with A6 is by YoeB itself (**Fig. 4.11*C*)**(22). These molecular differences for how ribosome-dependent toxins engage the +6 nucleotide appear to be what defines the spectrum of different codons selected.

In a complementary set of experiments, we identified HigB residue N71 as an important determinant of mRNA selection suggesting a mechanism by which specificity for an adenosine is enforced at the +6 position. Our characterization of the HigB N71A variant reveals that the mutant protein is functional in our cleavage assays but surprisingly, has an altered nucleotide selectivity and instead exhibits enzyme promiscuity. The identification of a single HigB residue that controls mRNA specificity implies that sequence-specific targeting has an adaptive advantage for HigB, and other ribosome-dependent toxins may be similarly manipulated. Although N71 is highly conserved among HigB homologs (87%), in some cases a glutamine or proline substitutes

(4% and 5%, respectively) but we predict that either residue could similarly form a +6 adenosine-specific pocket by maintaining stacking interactions with C1054. In the other diverse HigB homologs that don't contain an asparagine, glutamine or proline amino acid at position 71 (~4%), we predict altered mRNA selectivity. Future experiments to determine the codon specificity of YafQ and YoeB will be important to identify the degree of functional overlap among toxin family members.

What is the biological consequence of multiple ribosome-dependent toxins that degrade a spectrum of codons? One possibility is that the codon substrate and catalytic rate may be used to tune the global cellular rate of translation where mRNA cleavage is dependent on enzyme rate and codon frequencies that vary among different bacteria. An interesting additional aspect of this mechanism is that ribosome-dependent toxins active during translation elongation will have a higher probability of cleaving the most highly translated mRNA, that is mRNA with the highest ribosome occupancy. Therefore it remains unclear why some toxins target the translation initiation and translation termination steps. These steps are the slowest during protein synthesis perhaps allowing more time for toxins to efficiently recognize their preferred codons. Alternatively, differential targeting of mRNA for cleavage could lead to a selective translational program as seen for the ribosome-independent toxin MazF (14). Lastly, toxins may have a role in halting translation via ribosomal stalling to protect the translational machinery during the stringent response that would allow for rapid resumption of translation upon removal of the stress. We hypothesize that functional distinctions among ribosome-dependent toxins impact bacterial physiology by fine-tuning translation to modulate key cellular pathways.

4.6 Materials & Methods

4.6a Strains and plasmids.

E. coli BW25113 (Δ(*araD-araB*)567 Δ*lacZ*4787(::*rrnB*-4) *lacI*p-400(*lacI*Q)λ-*rpoS*396(Am) *rph*-1 Δ(*rhaD-rhaB*)568 *rrnB*-4 *hsdR*514) cells were used for all bacterial growth assays and wild-type Host inhibition of growth B (HigB)$(His)_6$, HigBΔH92$(His)_6$ and HigBN71A$(His)_6$ protein expression (45). Plasmids pBAD/Myc-HisA-HigB$(His)_6$ and pBAD/Myc-HigA-HigB ΔH92$(His)_6$ were generous gifts from Prof. Nancy A. Woychik (Rutgers University). All point mutations were introduced by site-directed mutagenesis and sequences were verified by DNA sequencing (Genewiz).

4.6b Sequence and structural alignments.

HigB homolog sequences were identified using the *P. vulgaris* HigB sequence as a search model in the NCBI protein Basic Local Alignment Search Tool using an E-value cutoff of 10^{-4} (46). All structural comparisons were aligned using the LSQ function in Coot (47). For comparisons of the mRNA paths, 70S structures with A, P, and E site-bound tRNA (PDB code 4V51) or 70S structures containing P and E-site tRNAs but with an empty A site (PDB code 4V6G), were each aligned to the P-site mRNA of the 70S-HigB precleavage state structure (AmAmAm codon). Residues 1-90 of HigB in the 70S-HigB precleavage state structure were aligned to HigB free residues 1-90. For comparison of the +6 interactions, the 30S head domains of the 70S-RelE and 70S-YoeB structures were aligned to that of the 70S-HigB structure.

4.6c Wild-type HigB, HigB ΔH92 and HigB N71A expression and purification.

E. coli BW25113 cells transformed with either pBAD/Myc-HisA-HigB$(His)_{6,}$ pBAD/Myc-HisA-HigBΔH92$(His)_6$ or pBAD/Myc-HisA-HigBN71A$(His)_6$ were grown at 37 °C in M9 glycerol minimal medium. Protein expression was induced at 0.7 OD_{600} with 0.04% w/v arabinose. After 3 hrs of protein expression, cells were harvested and frozen at -20 °C and protein purification was carried out as described for the *P. vulgaris* HigBA complex except that a S75 10/300 column (GE Healthcare) was used (33).

4.6d Structural determination of HigB.

Trypsinized wild-type HigB crystals (20 mg ml^{-1}) were grown in 30-40% (w/v) polyethylene glycol (PEG) monomethylether (MME) 2000 and 0.15 M KBr to dimensions of 50 x 400 x 400 μM in 1 day. Crystals were cryoprotected in the crystallization mother liquor supplemented with 10%-30% ethylene glycol and decreasing PEG MME 2000 from 30% - 10% in stepwise additions. Diffraction data was collected at the Southeast Regional Collaborative Access Team (SER-CAT) 22BM beamline at the Advanced Photon Source (APS) (Argonne, Illinois) and processed to 1.25 Å with the X-ray Detector Software (XDS) package (48). The structure was solved by molecular replacement using Phenix AutoMR (49) with the *P. vulgaris* HigB-HigA coordinates (PDB code 4MCT) (33). Iterative refinement using the XYZ coordinates, occupancies and B-factors (anisotropically for proteins and isotropically for waters) and model building was performed in Phenix and Coot, respectively (47), to final R/R_{free} values of 15.4/18.9%.

4.6e Structure Determination of 70S-HigB complexes.

Tth 70S ribosomes were purified as previously described (50). Purified *E. coli* $tRNA^{fMet}$ was purchased from Chemical Block (Russia), unmodified RNA was purchased from IDT and modified RNA was purchased from ThermoFisher Dharmacon (mRNAs are listed in **Table S3)**. The 70S-HigB ΔH92 precleavage state (AmAmAm codon) and 70S-HigB postcleavage state structures (AAA codon) were obtained by co-complexing the *Tth* 70S with unmodified or modified mRNA, $tRNA^{fMet}$, and HigB ΔH92 protein or wild-type HigB, respectively. Crystal growth was performed as previously described (50). 70S ribosomes at a final concentration of 4.4 μM were first incubated with a two-fold molar excess of either modified or unmodified mRNA for 6 min at 55 °C, then a four-fold molar excess of $tRNA^{fMet}$ for 30 min at 55 °C, and a five-fold molar excess of wild-type HigB or HigB ΔH92 at 37 °C for 1 hr. A final concentration of 2.4 mM detergent Deoxy Big Chap was added last before crystallization. Crystals grew to 70 x 70 x 400 μM in 1-2 weeks and were serially cryo-protected by increasing the concentration of PEG 550MME along with the addition of 25 μM HigB or HigB ΔH92 in the final cryo before flash freezing in liquid nitrogen.

For the 70S-HigB ΔH92 precleavage state structure containing the A-site codon AmCmAm, HigB was soaked into preformed *Tth* 70S empty A-site crystals. Formation of the complex was performed as previously described except a five-fold molar excess of CC-puromycin (Dharmacon) was first incubated with ribosomes for 30 min at 55 °C. Prior to cryoprotecting, 100 μM of HigBΔH92 was incubated with crystals for 17 hrs. Crystals were cryoprotected and frozen as described above.

Data was collected by either continuous vector scanning at the Northeast Collaborative Access Team (NE-CAT) ID-24C and ID-24E beamlines or through 4° wedges at the SER-CAT 22ID beamline. For all 70S data collections, at least 90° of data was collected using between 0.1 and 0.2° oscillations. Data was processed by XDS (48) and solved by molecular replacement using two copies of the 70S initiation model (51) (PDB code 4V6G) using 30S and 50S and their corresponding Mg^{2+} ions as rigid body groups in Phenix (49). Initial F_o-F_c difference electron density indicated that mRNA, $tRNA^{fMet}$ and HigB were bound. $tRNA^{fMet}$ and mRNA 5'- of the A site were modeled in Coot and individual site refinement was performed in Phenix using base-pair restraints and TLS. Modeling of HigB was next performed. The best HigB density was in the 70S-HigB ΔH92 precleavage state structure (AmCmAm codon; 3.1 Å) and this model was used as a starting model for all other 70S structures. Residues 1-90 of the 1.25 Å $HigB(His)_6$ model was placed into F_o-F_c electron density, built in Coot and refined in Phenix. In all 70S-HigB precleavage state structures, the electron density allowed for the placement of three nucleotides in the A site and one nucleotide 3' towards the mRNA entry tunnel while in the 70S postcleavage state structure, only density for two A-site nucleotides and a 3' phosphate was visible indicating HigB cleavage of the mRNA.

4.6f mRNA cleavage assays.

E. coli 70S ribosomes were purified as previously described (52). A final concentration of 1.2 μM ribosomes were programmed at 37 °C with 0.6 μM 5'-[^{32}P] mRNA for 6 min and 3 μM *E. coli* $tRNA^{fMet}$ for 30 min (**Table S3**). HigB protein at a final concentration of 0.9 μM was added to programmed ribosomes and aliquots were taken at 1, 3, 10, 30, and 60 min after HigB addition, the reaction was quenched with an equal volume of 2x

formamide dye (98% formamide, 10 mM EDTA (pH 8.0) and 0.2 mg ml^{-1} bromophenol blue), heated at 70 °C for two mins, and stored on ice or at -20 °C. Cleaved mRNA product was separated from full length on an 8M urea, 1X TBE, 18% polyacrylamide sequencing gel for 1.5 hrs. Quantitation of the cleaved product was performed by exposure of the dried gel to a GE phosphor screen imaging on a Typhoon FLA 7000 gel imager (GE Healthcare) with band density counted by ImageQuant software. Plots of the amount of product versus time were fit by GraphPad Prism 5 (GraphPad, Inc) using the single exponential equation:

$$\text{Product} = P_{max}(1\text{-}e^{-kt})$$

where P_{max} is the mRNA cleavage product plateau (pmol mRNA cleaved), k is the observed rate constant (min^{-1}) and t is the time the reaction progressed (min).

4.6g Remodeling of the 70S-YoeB mRNA A-site mRNA.

Electron density maps for the 70S-YoeB precleavage state structure were generated in Phenix (49) from the downloaded structure factors and coordinates (PDB code 4V8X). A-site mRNA nucleotides +4 to +8 were removed from the model and this new model was refined against structure factors. The mRNA path was modeled in Coot (47) and individual site refinement (mRNA only) and grouped B factor refinement were performed in Phenix using base-pair restraints.

4.7 Acknowledgements

Research reported in this publication was supported by a National Science Foundation CAREER award (MCB 0953714 to CMD), a National Institute of Health (NIH) Biochemistry, Cellular and Molecular Biology (BCMB) Graduate Training Grant (5T32GM8367), and NIH NRSA F31 Fellowship (GM108351 to MAS). CMD is a Pew

Scholar in the Biomedical Sciences. We thank F. M. Murphy IV and staff members of the NE-CAT beamlines for assistance during data collection and Dunham lab members C. Fagan, E. Hoffer, S. Subramanian, A. Ruangprasert and D. West, Profs. G. Conn and A. Corbett for critical reading of the manuscript. This work is based on research conducted at the APS on the NE-CAT beamlines, which is supported by NCRR NIH Award RR-15301, and at the SER-CAT beamline. Use of the APS, an Office of Science User Facility operated for the US DOE Office of Science by ANL was supported under Contract DE-AC02-06CH11357.

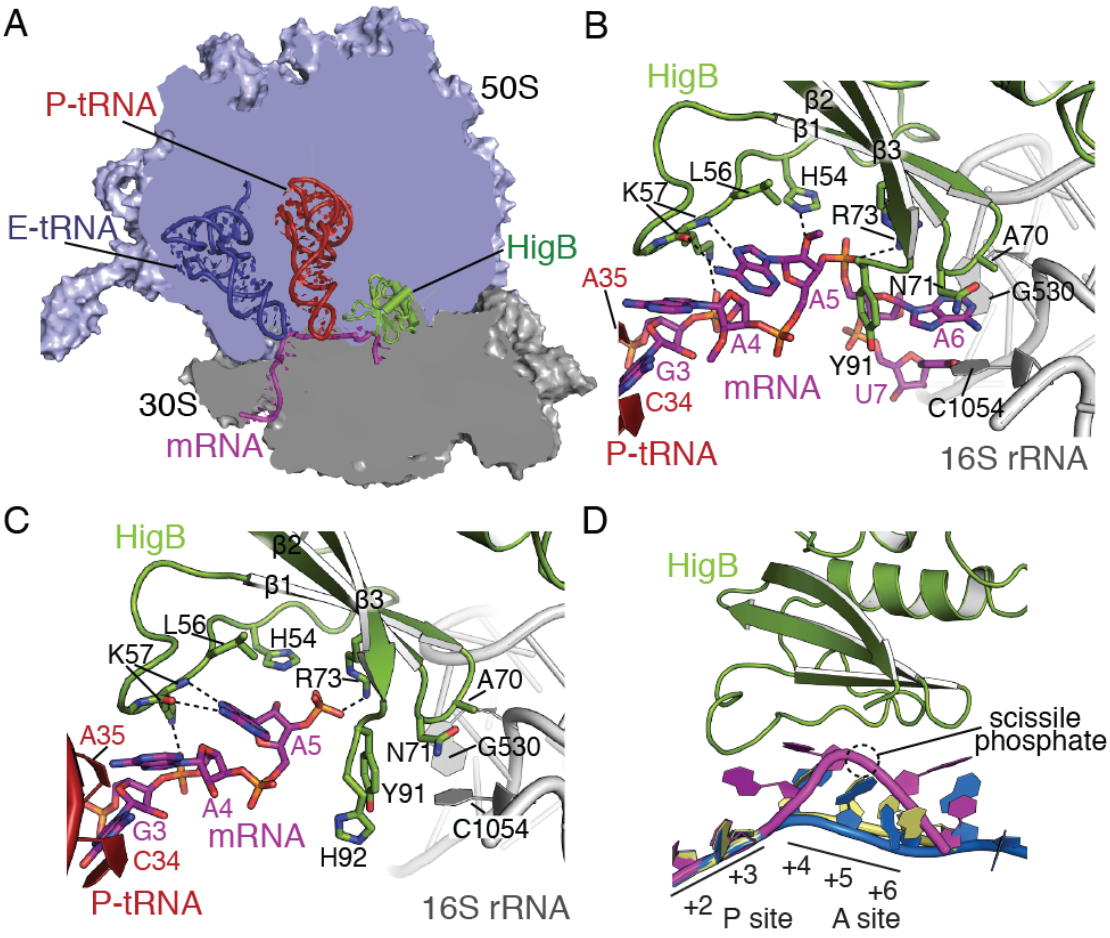

Figure 4.1. Structural basis for HigB recognition of mRNA on the 70S ribosome. (A) Overview of the structure of the 70S-HigB toxin complex containing A-site HigB showing the 30S and 50S subunits, P-site $tRNA^{fMet}$, E-site $tRNA^{fMet}$ and an A-site AAA lysine codon. (B) The x-ray crystal structures of the pre and postcleavage states (C) reveal how HigB recognizes an AAA A-site lysine codon (precleavage state A-site codon contains 2'-OCH_3 modifications to prevent mRNA cleavage). (D) Comparison of the mRNA path in the A-site when bound to HigB (mRNA is in magenta), tRNA (PDB code 4V51; yellow) or an empty A site (PDB code 4V6G; blue) emphasizing the large mRNA movement once HigB binds. P-site mRNA nucleotides (+2 and +3), A-site mRNA

nucleotides (+4, +5 and +6) and the location of the scissile phosphate during HigB cleavage are shown.

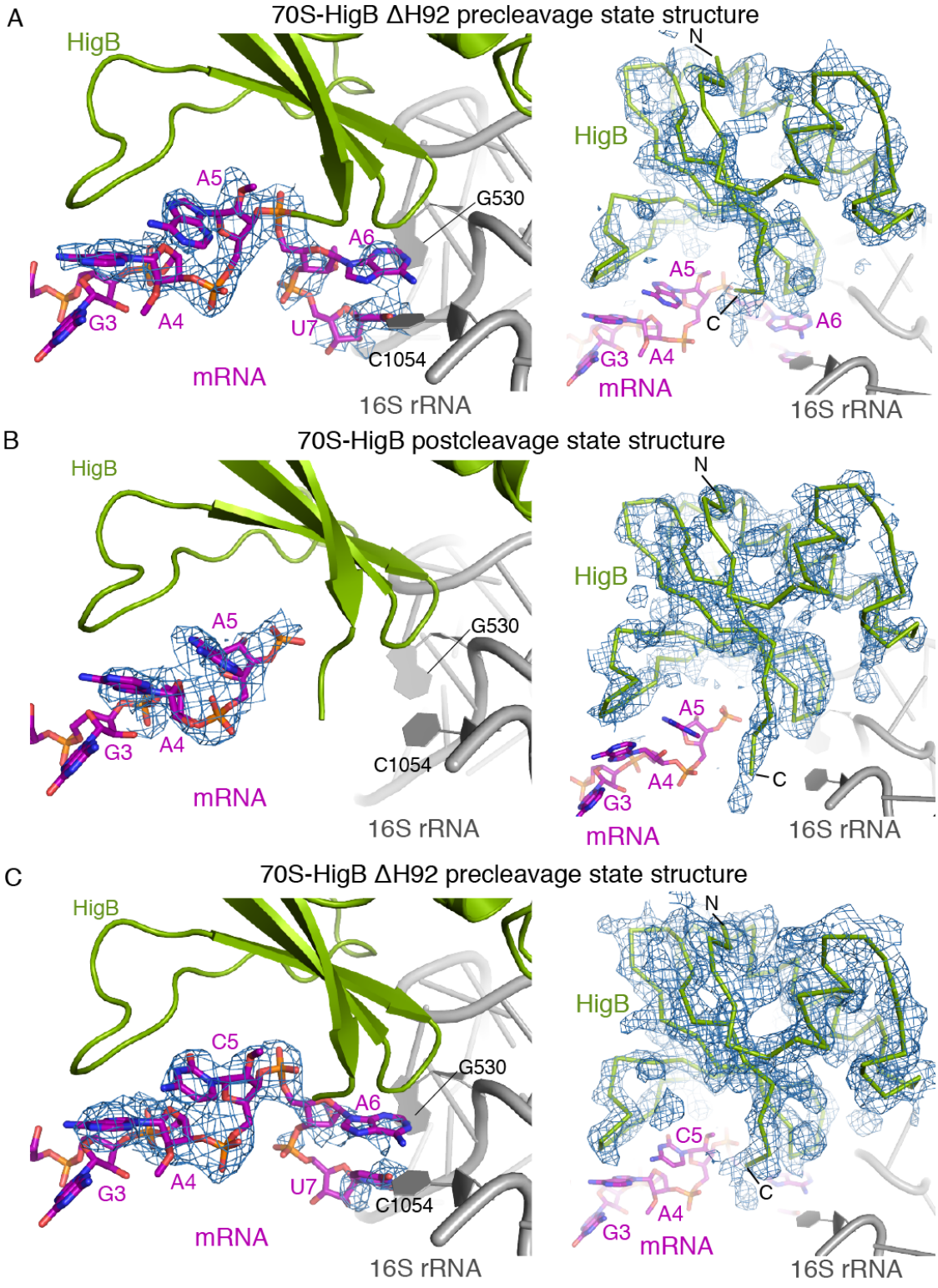

Figure 4.2. Quality of 70S-HigB bound maps and models.

Unbiased F_o-F_c difference electron density (contoured to 2σ unless noted otherwise) for both the mRNA (left) and HigB (right) for 70S ribosome structures bound to HigB. (A) A 3.4-Å x-ray crystal structure of the 70S-HigB ΔH92 precleavage state containing an A-site AmAmAm lysine codon. (B) A 3.3-Å x-ray crystal structure of the 70S-HigB postcleavage state containing an A-site AAA lysine codon. (C) A 3.1-Å x-ray crystal structure of the 70S-HigB ΔH92 precleavage state containing an A-site AmCmAm lysine codon. Here, unbiased F_o-F_c difference electron density is contoured to 1.5σ and 2σ the mRNA (left) and HigB (right), respectively.

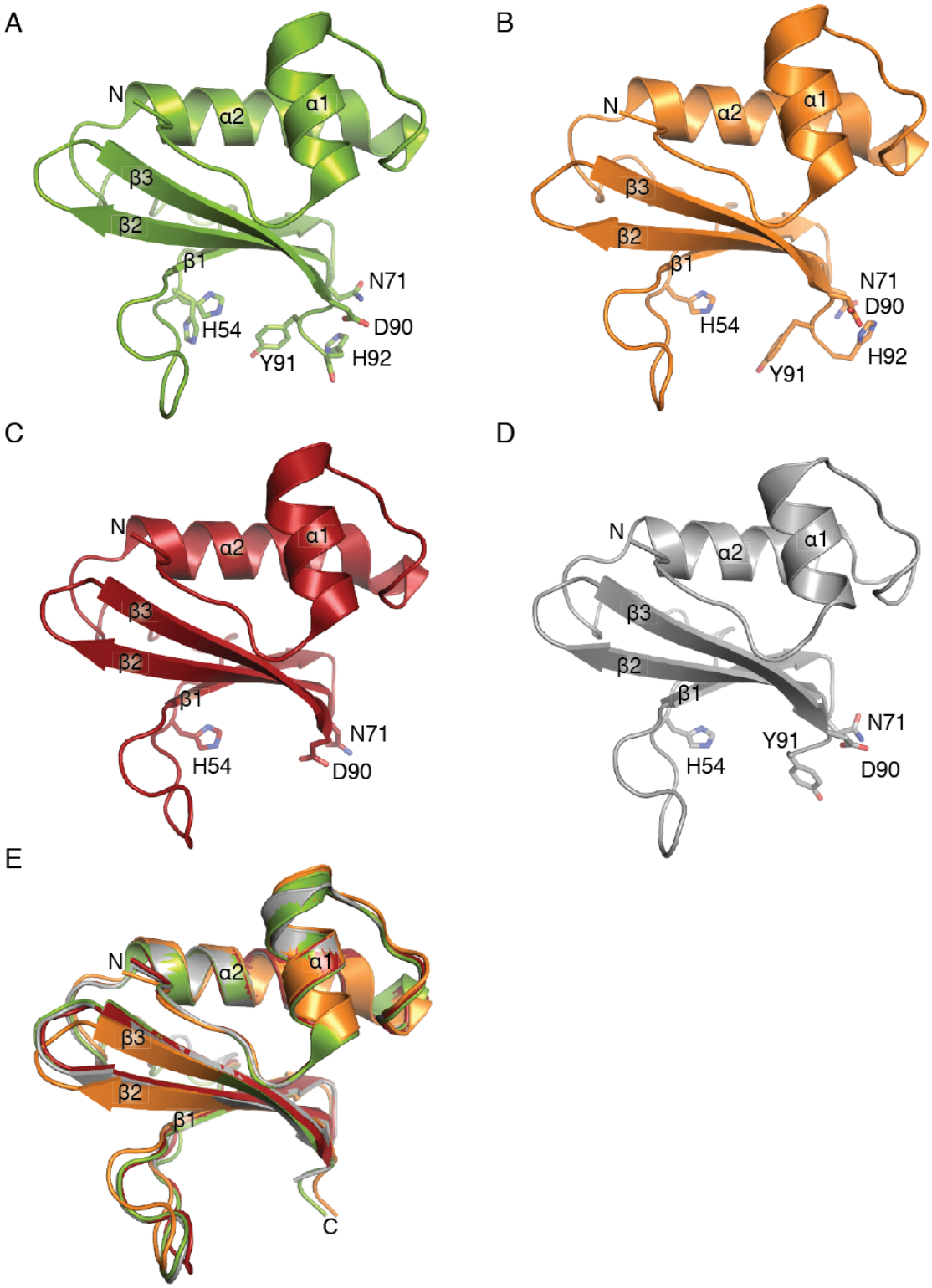

Figure 4.3. Comparison of HigB in different states.

(A) A 1.25-Å x-ray crystal structure of free HigB with active site residues shown as sticks. (B) A 2.8-Å x-ray crystal structure of the HigBA complex was solved but only HigB is depicted (PDB code 4MCT). (C) Structure of HigB from the 2.1-Å x-ray crystal structure of the HigBA complex (PDB code 4MCX). (D**)** A 3.4-Å x-ray crystal structure of HigB ΔH92 bound to the 70S ribosome in the precleavage state. **(**E**)** Overlay of all four HigB structures demonstrating their overall similar fold (rmsd 0.4-1.0 Å for residues 1-92).

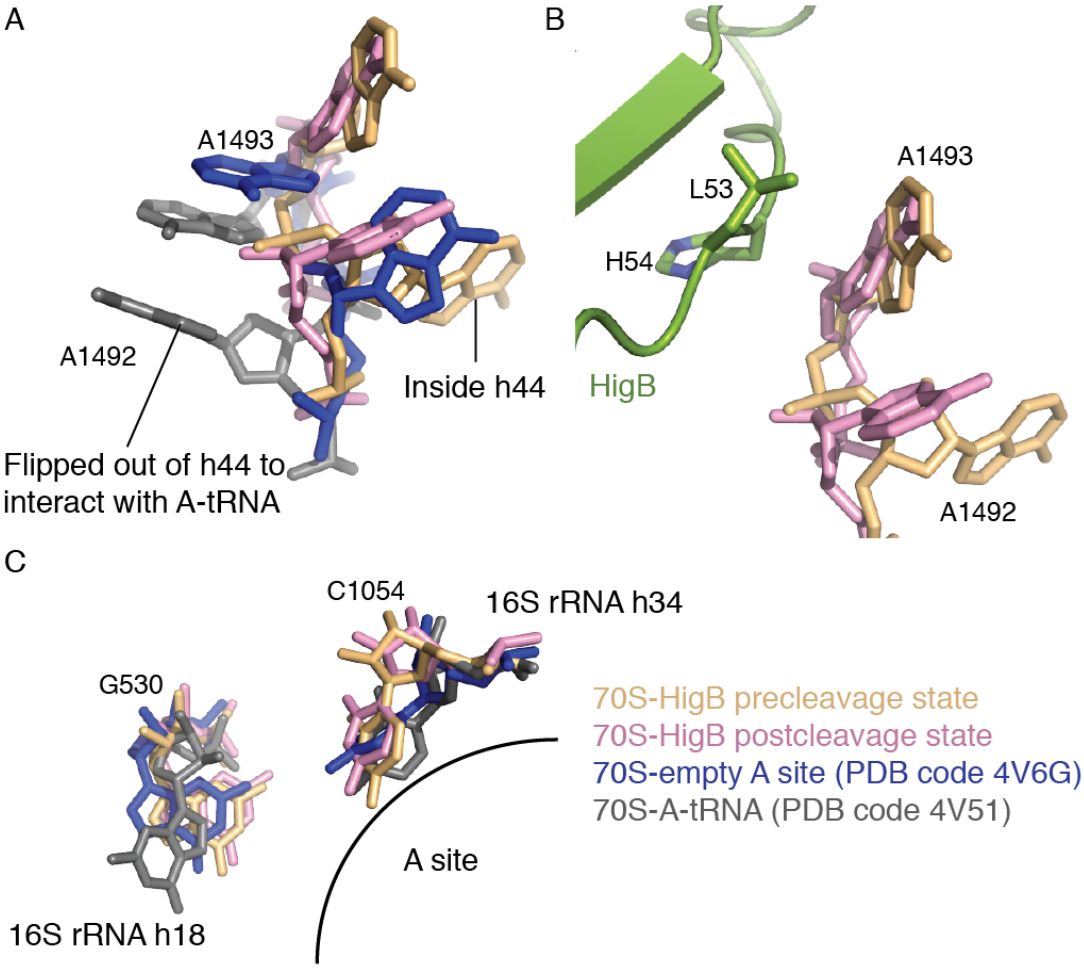

Figure 4.4. Orientation of A-site decoding center nucleotides upon HigB binding to the 70S.

(A) Comparison of 16S rRNA residues A1492 and A1493 when HigB binds to the 70S trapped in a precleavage state (tan), in a postcleavage state (pink), when no A-site ligand is bound (PDB code 4V6G; blue) and when cognate A-site tRNA is bound (PDB code 4V51; gray). (B) The location of A1492 and A1493 with respect to HigB in a precleavage state and in a postcleavage state and their proximity to loop 3 of HigB. (C) The orientation of 16S rRNA residues G530 and C1054 in precleavage and postcleavage state

structures of 70S-HigB compared to when the ribosomal A site contains cognate tRNA (gray) or is empty (blue).

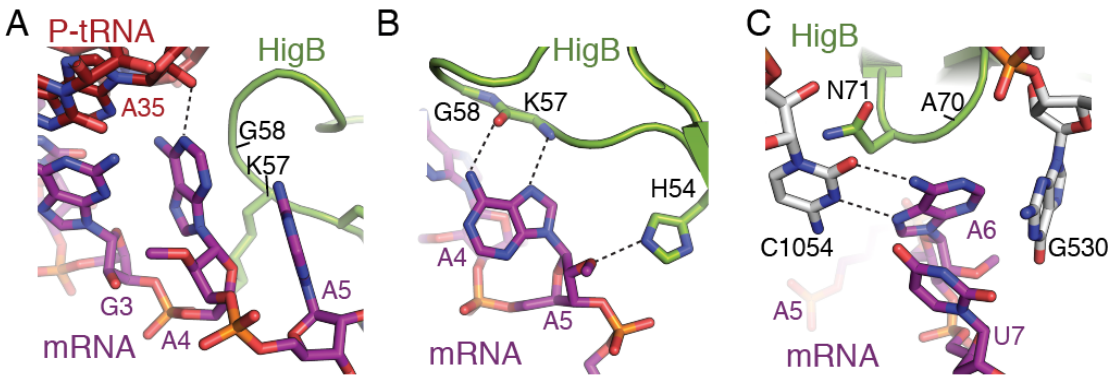

Figure 4.5: HigB recognition of A-site mRNA nucleotides.

(A) HigB forms no interactions with the A4 mRNA nucleobase or ribose to specify nucleotide identity. (B) Hydrogen bonds between the nucleobase of A5 with the backbone of HigB drive nucleotide specificity. (C) 16S rRNA residue C1054 and HigB residue N71 form an adenosine-specific binding pocket at the +6 mRNA position.

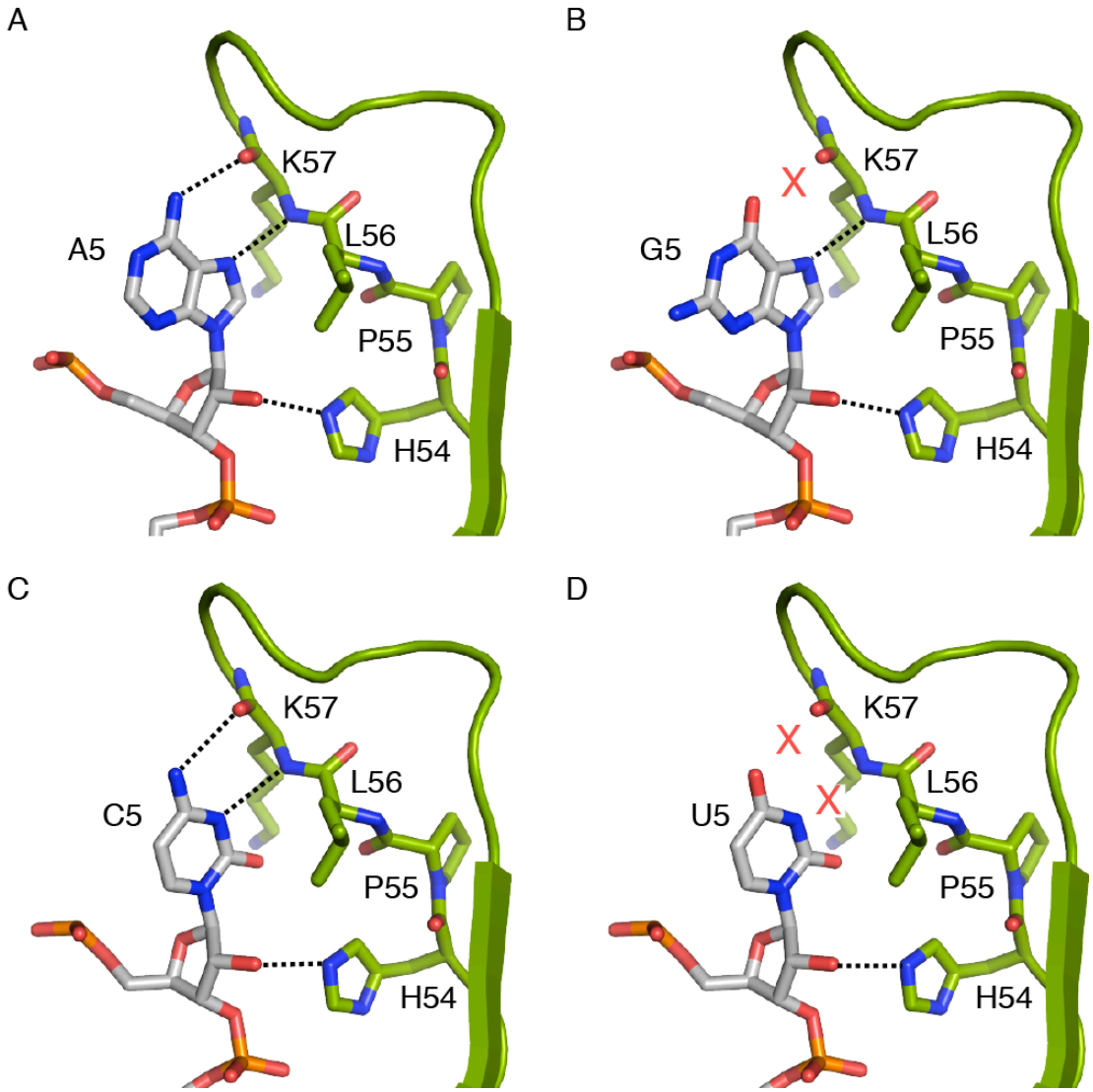

Figure 4.6. Model for the +5 nucleotide recognition by HigB that predicts G5 and U5 are incompatible.

(A) A5 forms hydrogen bonds with the backbone of HigB as seen in our 70S-HigB precleavage state structure. (B) Model for how G5 interacts with the HigB backbone. Note the guanosine O6 atom and the backbone carbonyl of K57 are unable to form a hydrogen bond (red X). (C) C5 forms hydrogen bonds with the backbone of HigB as seen in our 70S-HigB precleavage state structure. (D) Model for how U5 interacts with the

HigB backbone. Note the uracil O4 and N3 atoms and the backbone carbonyl of K57 are unable to form hydrogen bonds (red Xs).

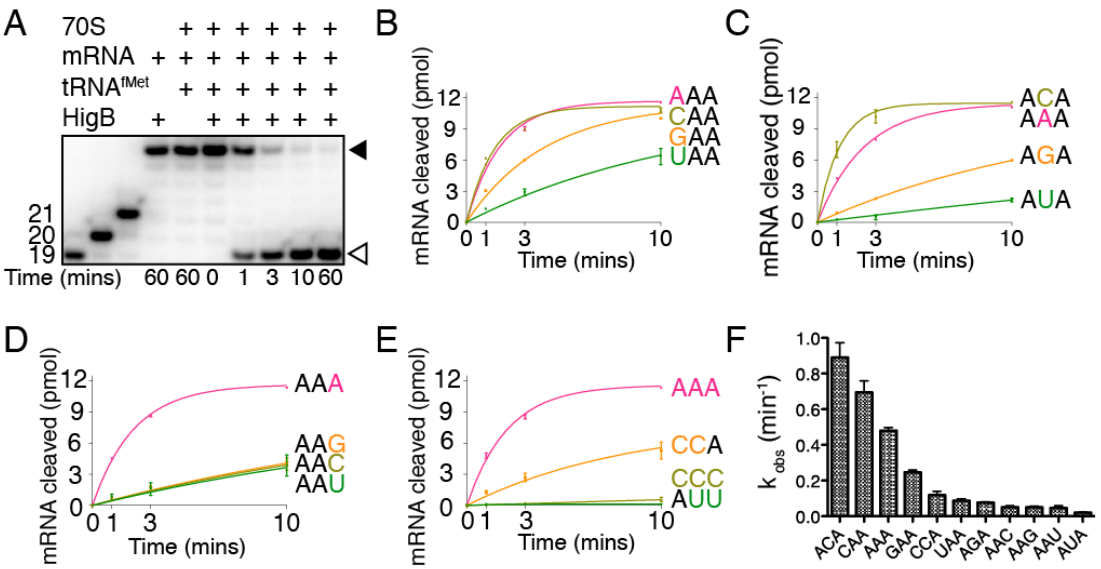

Figure 4.7. HigB demonstrates a clear preference at the third A-site nucleotide.

(A) *E. coli* 70S ribosomes were programmed with 5'-[^{32}P] mRNA containing an A-site AAA lysine codon, P-site tRNA^{fMet} and HigB. The reaction was followed for 60 min and the amount of mRNA cleaved (open arrow) compared to uncleaved (closed arrow) was determined by denaturing RNA gels (Fig. S5). A-site mRNA was varied at the +4 nucleotide position (B), the +5 nucleotide position (C), the +6 nucleotide position (D) and +4, +5 and +6 combinations (E). Each assay was performed for two technical replicates with the mean value ± SEM. (F) k_{obs} values (min^{-1}) as calculated from assays in panels B-E.

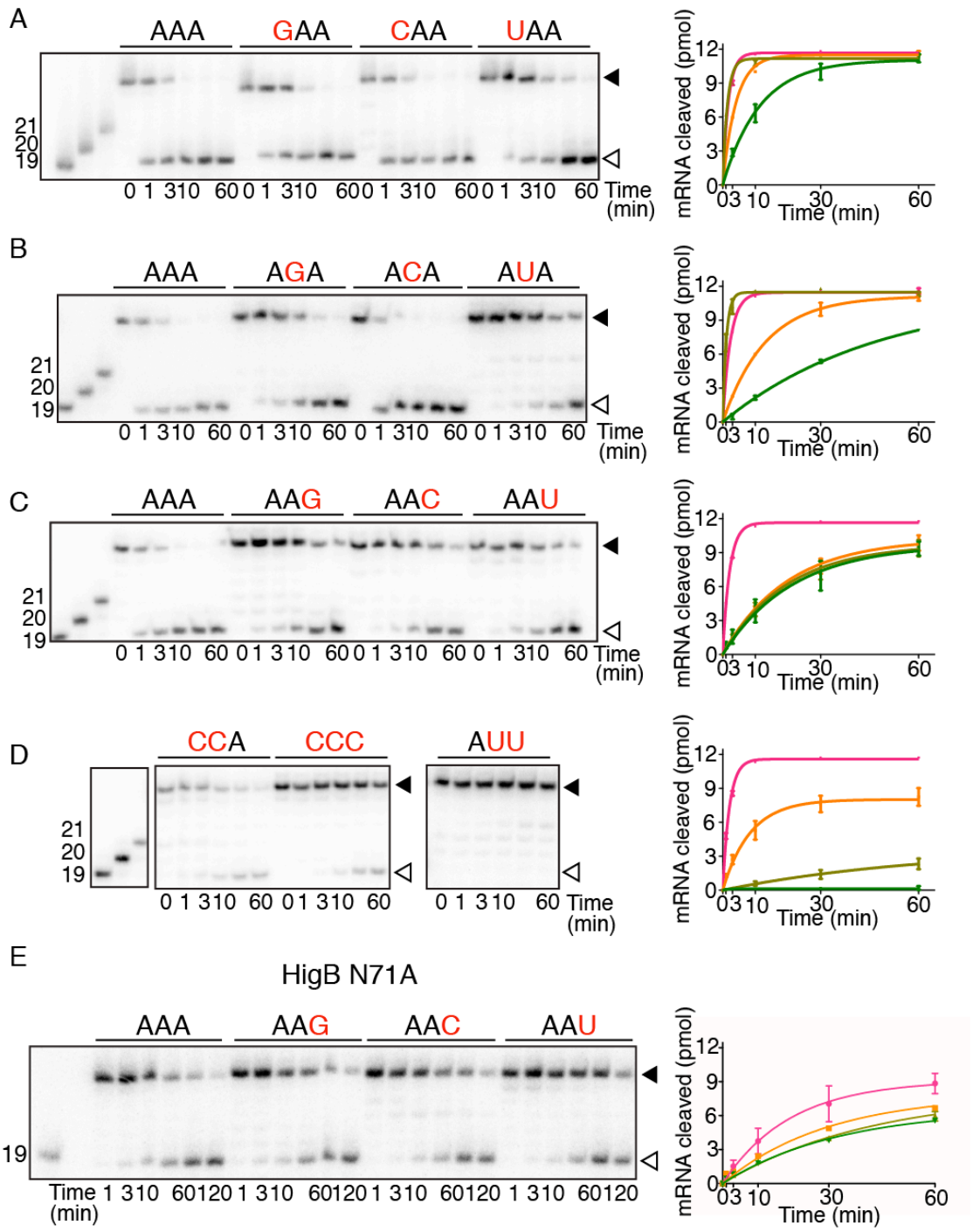

Figure 4.8. ***In vitro*** **analyses of ribosome-dependent mRNA cleavage by HigB.**

E. coli 70S ribosomes were programmed with 5'-[^{32}P]-mRNA containing an A-site AAA lysine codon, P-site tRNA^{fMet} and HigB. The reaction was followed for 60 min and the amount of mRNA cleaved (open arrow) compared to uncleaved (closed arrow) was

determined by denaturing RNA gels (left). 19, 20, and 21 mer standards are shown at the left of each gel. For wild-type HigB experiments, A-site mRNA was varied at the +4 nucleotide A-site position (A), the +5 nucleotide A-site position (B), the +6 nucleotide A-site position (C) and +4, +5 and +6 combinations (D). Lanes 1-6 represent 0, 1, 3, 10, 30 and 60 minute time points for each codon tested in panels A-D. (E) For the HigB N71A variant, the +6 nucleotide A-site position was varied. Lanes 1-6 represent 1, 3, 10, 30, 60 and 120 minute time points. The results were quantified using Image Quant and product progression curves of the RNA gels are plotted on the right (mean value ± SEM are displayed from at least two replicates).

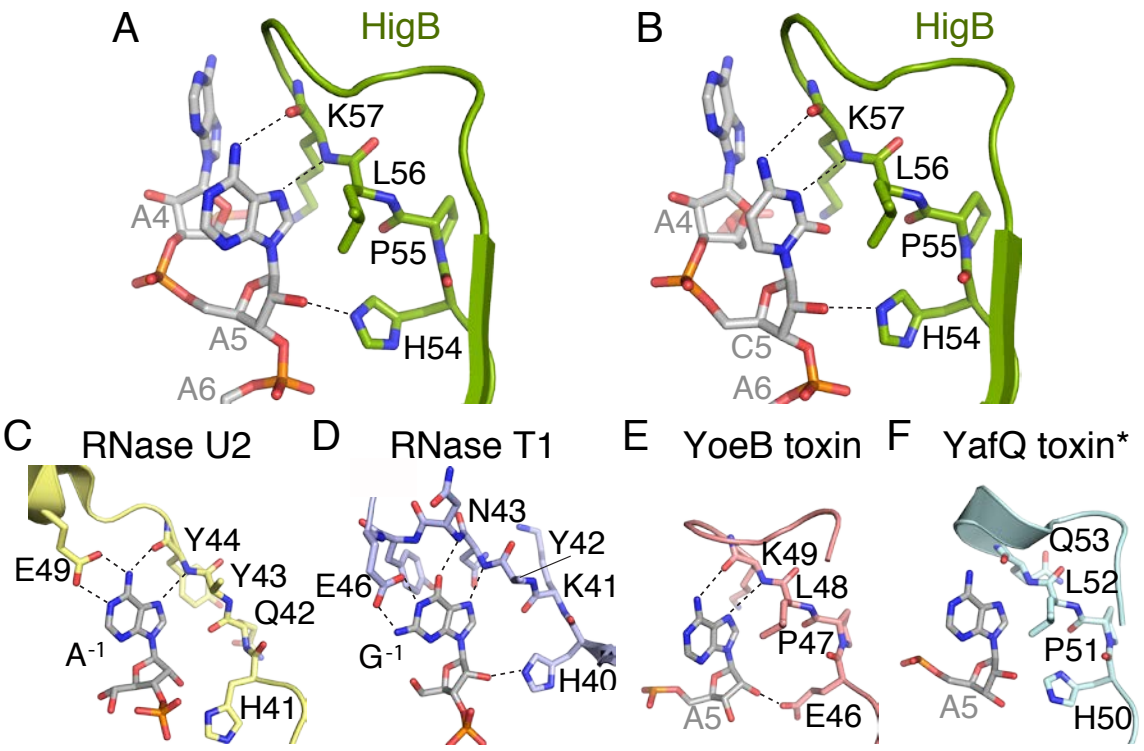

Figure 4.9. Structural basis for toxin specificity at the +5 nucleotide position and similarities to general RNases.

(A) & (B) The 3.4-Å x-ray crystal structure of the 70S-HigB ΔH92 precleavage state (AmAmAm A-site codon) as compared to the 3.1-Å x-ray crystal structure of the 70S-HigB ΔH92 precleavage state (AmCmAm A-site codon). Despite the differences at the +5 positions, similar hydrogen bonds are formed between A5 and the HigB backbone and C5 and the HigB backbone. Structures of the nucleotide recognition loop of RNase U2 (PDB code 3AGN) (C), RNase T1 (PDB code 1RGA) (D), and ribosome-dependent toxins YoeB (PDB code 4V8X) (E) and YafQ (PDB code 4ML2) (F), highlight the similarities for recognition of the nucleobase preceding the scissile phosphate. The side chains of RNase U2 and T1 residues Y43 and Y42, respectively stack with the -1 position but were removed for clarity. The 70S-YoeB mRNA was rebuilt using structure factors from the PDB databank (Fig. 4.10). The backbone carbonyl and amino groups of YoeB

K49 and YafQ Q53 are proposed to interact with A5 similar to HigB K57. The YafQ toxin structure was solved in the absence of the 70S ribosome and its interactions with A5 are based upon modeling in the ribosomal A site (denoted by a star).

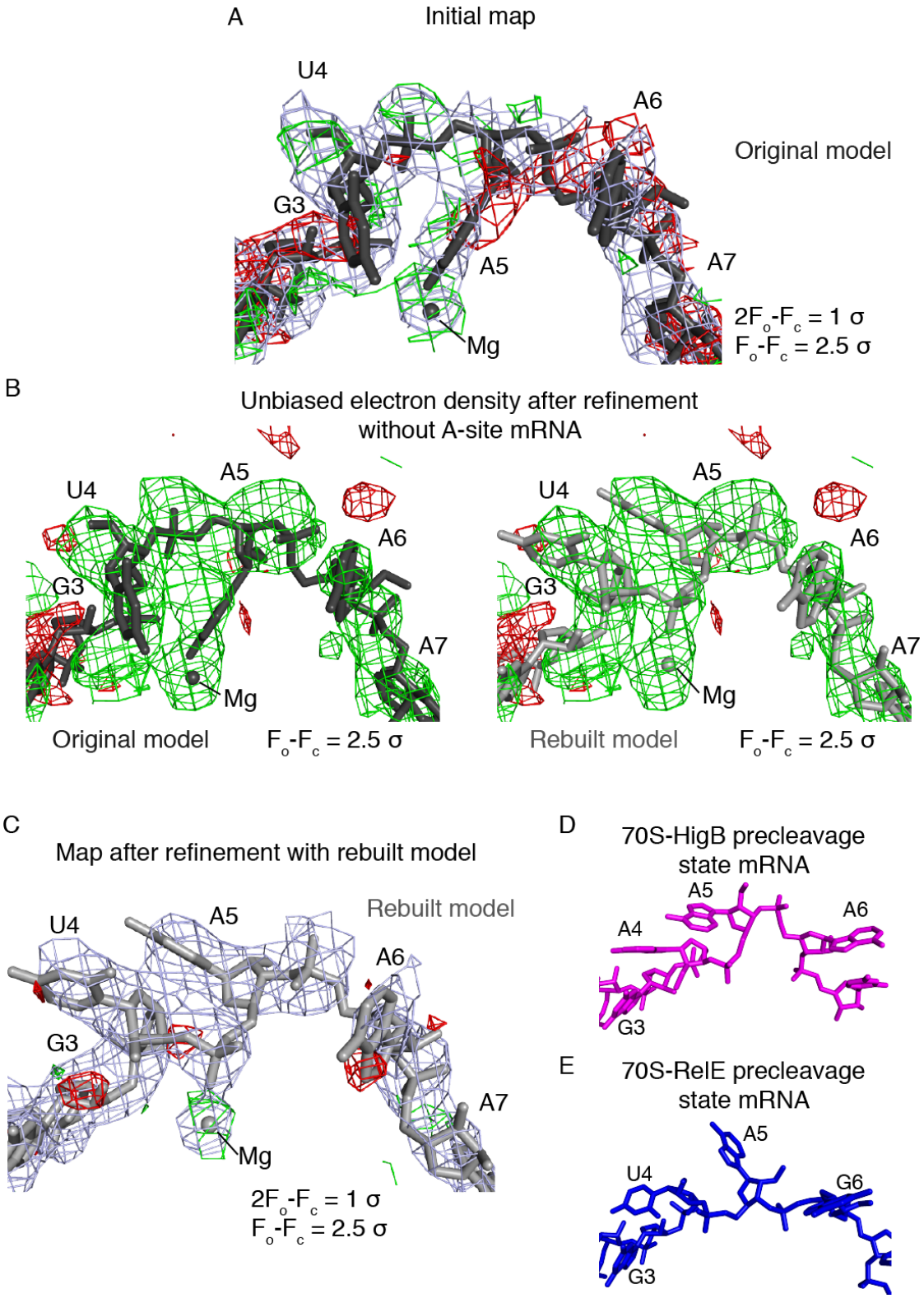

Figure 4.10. Rebuild of the 70S-YoeB structure.

(A) Examination of the electron density of the 70S-YoeB precleavage state structure (PDB code 4V8X) suggests an alternative modeling of the first two A-site nucleotides. Original mRNA model (dark gray) with electron density shown. (B) Original model (dark gray; left), rebuilt model (light gray; right) and difference electron density from refinement of 4V8X without mRNA nucleotides +4 to +8. (C) Rebuilt mRNA model and electron density map resulting from refinement. (D) mRNA paths when HigB binds to the A site (this study) and when RelE (E) binds the A site (PDB code 4V7J) revealing similar paths when ribosome-dependent toxins YoeB, RelE and HigB bind the 70S.

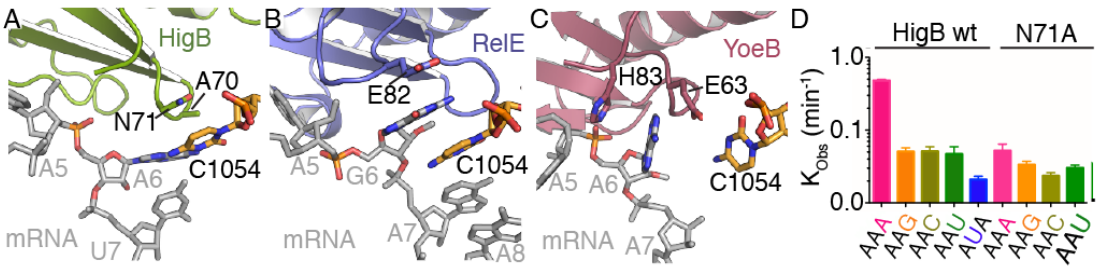

Figure 4.11. A single conserved HigB residue drives sequence specificity at the +6 position.

Structural comparison of how ribosome-dependent toxins and 16S rRNA residues select for nucleotides at the +6 mRNA position by the formation of stacking and electrostatic interactions. (A) 16S rRNA C1054 forms a *trans* Watson-Crick-Hoogsteen interaction with A6, while HigB residue N71 stacks with C1054. (B) In contrast, a continuous stack between RelE residue E82, G6 and C1054 (PDB code 4V7J) forms. (C) YoeB residues H83 and E63 stack around A6 with C1054 playing little to no role in nucleotide selection (PDB code 4V8X). All precleavage state structure of 70S bound to ribosome-dependent toxins were solved using uncleavable mRNA. (D) HigB N71A mRNA k_{obs} values were determined upon substitution at the +6 nucleotide position. Wild-type HigB cleavage assays were previously described in Fig. 3 & Fig. S5. HigB N71A cleavage assays were performed with two biological replicates with the mean value ± SEM reported.

Table 4.1. 70S-HigB structures

A-site codon state (HigB/A-site codon)	Precleavage (ΔH92/AmAmAm)	Postcleavage (WT/AAA)	Precleavage (ΔH92/AmCmAm)
Data collection			
Space group	P 2_1 2_1 2_1	P 2_1 2_1 2_1	P 2_1 2_1 2_1
Cell dimensions			
a,*b*,*c* (Å)	214.1, 453.9, 607.6	214.1, 453.9, 607.6	214.2, 453.3, 609.9
α,β,γ (°)	90, 90, 90	90, 90, 90	90, 90, 90
Resolution (Å)	35 - 3.4 (3.52 - 3.4)	35 - 3.3 (3.42 -3.3)	35 - 3.1 (3.21 - 3.10)
R_{meas} [a] (%)	24 (113)	19 (88)	23 (82)
R_{pim} (%)	9.6 (45)	8.9 (41)	11 (39)
I / σ	8.2 (1.8)	8.9 (1.8)	5.6 (1.9)
Completeness (%)	98.9 (99.6)	94.3 (94.4)	99.4 (95.9)
Redundancy	6.0 (6.0)	4.1 (3.9)	4.4 (4.0)
Refinement			
Resolution (Å)	35 - 3.4	35 - 3.3	35 - 3.1
Total reflections	4,743,702	3,393,142	4,584,941
Unique reflections	793,673	827,408	1,053,398
R_{work} / R_{free} (%)	21.5/24.8	21.0/23.8	20.3/23.8
No. atoms	297,549	297,400	294,445
Protein/RNA	296,237	296,156	293,095
Ligand/ion	1,312	1,244	1,350
Water	0	0	0
B-factors	91.4	94.7	75.3
Protein/RNA	91.7	95.0	75.5
Ligand/ion	35.2	45.2	41.3
R.m.s. deviations			
Bond lengths (Å)	0.005	0.004	0.004
Bond angles (°)	0.84	0.83	0.86
PDB ID	4YPB	4W4G	4YZV

[a]Values in parentheses are for the highest resolution shell.

Table 4.2. HigB structure

Data collection	
Space group	C2
Cell dimensions	
a,*b*,*c* (Å)	57.3, 31.3, 50.9
α,β,γ (°)	90, 112.2, 90
Resolution (Å)	15.7 - 1.25 (1.29 - 1.25)[a]
R_{meas} (%)	5.4 (65)
R_{pim} (%)	2.0 (24)
I / σ	19.3 (3.2)
Completeness (%)	99.9 (99.9)
Redundancy	7.2 (7.0)
Refinement	
Resolution (Å)	15.7 - 1.25
Total reflections	168,822
Unique reflections	23,296
R_{work} / R_{free} (%)	15.4/18.9
No. atoms	1033
Protein	907
Ion	4
Water	122
Mean B-factors (Å^2)	17.7
Protein (Å^2)	16.1
Ion (Å^2)	29.7
Water (Å^2)	29.7
R.m.s. deviations	
Bond lengths (Å)	0.013
Bond angles (°)	1.49
PDB ID	4PX8

[a]Values in parentheses are for the highest resolution shell.

Table 4.3. mRNAs used for structural and biochemical analysis.

mRNAs (5' - 3')	A-site codon	Assay(s) used in
GGCAAGGAGGUAAAAAU GAAAUAGU	AAA	mRNA cleavage assay WT HigB postcleavage structure
GGCAAGGAGGUAAAAAU GAmAmAmUAGU	AmAmAm	70S-HigB ΔH92 precleavage sate structure
GGCAAGGAGGUAAAAAU GGAAUAG	GAA	mRNA cleavage assay
GGCAAGGAGGUAAAAAU GCAAUAGU	CAA	mRNA cleavage assay
GGCAAGGAGGUAAAAAU GUAACAGA	UAA	mRNA cleavage assay
GGCAAGGAGGUAAAAAU GAGAUAGU	AGA	mRNA cleavage assay
GGCAAGGAGGUAAAAAU GACAUAGU	ACA	mRNA cleavage assay
GGCAAGGAGGUAAAAAU GAUAUAGU	AUA	mRNA cleavage assay
GGCAAGGAGGUAAAAAU GAAGUAGU	AAG	mRNA cleavage assay
GGCAAGGAGGUAAAAAU GAACUAGU	AAC	mRNA cleavage assay
GGCAAGGAGGUAAAAAU GAAUCAGA	AAU	mRNA cleavage assay
GGCAAGGAGGUAAAAAU GCCAGAAA	CCA	mRNA cleavage assay
GGCAAGGAGGUAAAAAU GCCCGAAA	CCC	mRNA cleavage assay
GGCAAGGAGGUAAAAAU GAUUUAGU	AUU	mRNA cleavage assay
GGCAAGGAGGUAAAAAU GAmCmAmUUU	AmCmAm	HigB ΔH92 precleavage state structure

Nucleotides followed by "m" contain a 2'-OCH_3 group used to prevent mRNA cleavage during crystallization.

4.8 References

1. Maisonneuve, E., and Gerdes, K. (2014) Molecular mechanisms underlying bacterial persisters. *Cell* **157**, 539-548
2. Boutte, C. C., and Crosson, S. (2013) Bacterial lifestyle shapes stringent response activation. *Trends in microbiology* **21**, 174-180
3. Potrykus, K., and Cashel, M. (2008) (p)ppGpp: still magical? *Annual review of microbiology* **62**, 35-51
4. Magnusson, L. U., Farewell, A., and Nystrom, T. (2005) ppGpp: a global regulator in Escherichia coli. *Trends in microbiology* **13**, 236-242
5. Harrison, J. J., Wade, W. D., Akierman, S., Vacchi-Suzzi, C., Stremick, C. A., Turner, R. J., and Ceri, H. (2009) The chromosomal toxin gene yafQ is a determinant of multidrug tolerance for Escherichia coli growing in a biofilm. *Antimicrobial agents and chemotherapy* **53**, 2253-2258
6. Kim, Y., and Wood, T. K. (2010) Toxins Hha and CspD and small RNA regulator Hfq are involved in persister cell formation through MqsR in Escherichia coli. *Biochemical and biophysical research communications* **391**, 209-213
7. Ren, D., Bedzyk, L. A., Thomas, S. M., Ye, R. W., and Wood, T. K. (2004) Gene expression in Escherichia coli biofilms. *Applied microbiology and biotechnology* **64**, 515-524
8. Maisonneuve, E., Castro-Camargo, M., and Gerdes, K. (2013) (p)ppGpp controls bacterial persistence by stochastic induction of toxin-antitoxin activity. *Cell* **154**, 1140-1150

9. Norton, J. P., and Mulvey, M. A. (2012) Toxin-antitoxin systems are important for niche-specific colonization and stress resistance of uropathogenic Escherichia coli. *PLoS pathogens* **8**, e1002954

10. Wang, X., and Wood, T. K. (2011) Toxin-antitoxin systems influence biofilm and persister cell formation and the general stress response. *Applied and environmental microbiology* **77**, 5577-5583

11. Helaine, S., Cheverton, A. M., Watson, K. G., Faure, L. M., Matthews, S. A., and Holden, D. W. (2014) Internalization of Salmonella by macrophages induces formation of nonreplicating persisters. *Science* **343**, 204-208

12. Gerdes, K., Christensen, S. K., and Lobner-Olesen, A. (2005) Prokaryotic toxin-antitoxin stress response loci. *Nature reviews. Microbiology* **3**, 371-382

13. Bernard, P., and Couturier, M. (1992) Cell killing by the F plasmid CcdB protein involves poisoning of DNA-topoisomerase II complexes. *Journal of molecular biology* **226**, 735-745

14. Vesper, O., Amitai, S., Belitsky, M., Byrgazov, K., Kaberdina, A. C., Engelberg-Kulka, H., and Moll, I. (2011) Selective translation of leaderless mRNAs by specialized ribosomes generated by MazF in Escherichia coli. *Cell* **147**, 147-157

15. Winther, K. S., and Gerdes, K. (2011) Enteric virulence associated protein VapC inhibits translation by cleavage of initiator tRNA. *Proceedings of the National Academy of Sciences of the United States of America* **108**, 7403-7407

16. Pedersen, K., Zavialov, A. V., Pavlov, M. Y., Elf, J., Gerdes, K., and Ehrenberg, M. (2003) The bacterial toxin RelE displays codon-specific cleavage of mRNAs in the ribosomal A site. *Cell* **112**, 131-140

17. Zhang, Y., Zhang, J., Hoeflich, K. P., Ikura, M., Qing, G., and Inouye, M. (2003) MazF cleaves cellular mRNAs specifically at ACA to block protein synthesis in Escherichia coli. *Molecular cell* **12**, 913-923

18. Castro-Roa, D., Garcia-Pino, A., De Gieter, S., van Nuland, N. A., Loris, R., and Zenkin, N. (2013) The Fic protein Doc uses an inverted substrate to phosphorylate and inactivate EF-Tu. *Nature chemical biology* **9**, 811-817

19. Kaspy, I., Rotem, E., Weiss, N., Ronin, I., Balaban, N. Q., and Glaser, G. (2013) HipA-mediated antibiotic persistence via phosphorylation of the glutamyl-tRNA-synthetase. *Nature communications* **4**, 3001

20. Schifano, J. M., Edifor, R., Sharp, J. D., Ouyang, M., Konkimalla, A., Husson, R. N., and Woychik, N. A. (2013) Mycobacterial toxin MazF-mt6 inhibits translation through cleavage of 23S rRNA at the ribosomal A site. *Proceedings of the National Academy of Sciences of the United States of America* **110**, 8501-8506

21. Neubauer, C., Gao, Y. G., Andersen, K. R., Dunham, C. M., Kelley, A. C., Hentschel, J., Gerdes, K., Ramakrishnan, V., and Brodersen, D. E. (2009) The structural basis for mRNA recognition and cleavage by the ribosome-dependent endonuclease RelE. *Cell* **139**, 1084-1095

22. Feng, S., Chen, Y., Kamada, K., Wang, H., Tang, K., Wang, M., and Gao, Y. G. (2013) YoeB-ribosome structure: a canonical RNase that requires the ribosome for its specific activity. *Nucleic acids research* **41**, 9549-9556

23. Maehigashi, T., Ruangprasert, A., Miles, S. J., and Dunham, C. M. (2015) Molecular basis of ribosome recognition and mRNA hydrolysis by the E. coli YafQ toxin. *Nucleic acids research* **43**, 8002-8012

24. Zhang, Y., and Inouye, M. (2009) The inhibitory mechanism of protein synthesis by YoeB, an Escherichia coli toxin. *The Journal of biological chemistry* **284**, 6627-6638

25. Hurley, J. M., Cruz, J. W., Ouyang, M., and Woychik, N. A. (2011) Bacterial toxin RelE mediates frequent codon-independent mRNA cleavage from the 5' end of coding regions in vivo. *The Journal of biological chemistry* **286**, 14770-14778

26. Yoshizumi, S., Zhang, Y., Yamaguchi, Y., Chen, L., Kreiswirth, B. N., and Inouye, M. (2009) Staphylococcus aureus YoeB homologues inhibit translation initiation. *Journal of bacteriology*

27. Christensen, S. K., Maenhaut-Michel, G., Mine, N., Gottesman, S., Gerdes, K., and Van Melderen, L. (2004) Overproduction of the Lon protease triggers inhibition of translation in Escherichia coli: involvement of the yefM-yoeB toxin-antitoxin system. *Molecular microbiology* **51**, 1705-1717

28. Christensen-Dalsgaard, M., and Gerdes, K. (2008) Translation affects YoeB and MazF messenger RNA interferase activities by different mechanisms. *Nucleic acids research* **36**, 6472-6481

29. Prysak, M. H., Mozdzierz, C. J., Cook, A. M., Zhu, L., Zhang, Y., Inouye, M., and Woychik, N. A. (2009) Bacterial toxin YafQ is an endoribonuclease that associates with the ribosome and blocks translation elongation through sequence-specific and frame-dependent mRNA cleavage. *Molecular microbiology* **71**, 1071-1087

30. Hurley, J. M., and Woychik, N. A. (2009) Bacterial toxin HigB associates with ribosomes and mediates translation-dependent mRNA cleavage at A-rich sites. *The Journal of biological chemistry* **284**, 18605-18613

31. Takagi, H., Kakuta, Y., Okada, T., Yao, M., Tanaka, I., and Kimura, M. (2005) Crystal structure of archaeal toxin-antitoxin RelE-RelB complex with implications for toxin activity and antitoxin effects. *Nature structural & molecular biology* **12**, 327-331

32. Kamada, K., and Hanaoka, F. (2005) Conformational change in the catalytic site of the ribonuclease YoeB toxin by YefM antitoxin. *Molecular cell* **19**, 497-509

33. Schureck, M. A., Maehigashi, T., Miles, S. J., Marquez, J., Cho, S. E., Erdman, R., and Dunham, C. M. (2014) Structure of the Proteus vulgaris HigB-(HigA)2-HigB toxin-antitoxin complex. *The Journal of biological chemistry* **289**, 1060-1070

34. Ruangprasert, A., Maehigashi, T., Miles, S. J., Giridharan, N., Liu, J. X., and Dunham, C. M. (2014) Mechanisms of toxin inhibition and transcriptional repression by Escherichia coli DinJ-YafQ. *The Journal of biological chemistry* **289**, 20559-20569

35. Williams, J. J., and Hergenrother, P. J. (2008) Exposing plasmids as the Achilles' heel of drug-resistant bacteria. *Current opinion in chemical biology* **12**, 389-399

36. Maisonneuve, E., Shakespeare, L. J., Jorgensen, M. G., and Gerdes, K. (2011) Bacterial persistence by RNA endonucleases. *Proceedings of the National Academy of Sciences of the United States of America* **108**, 13206-13211

37. Li, G. Y., Zhang, Y., Inouye, M., and Ikura, M. (2009) Inhibitory mechanism of Escherichia coli RelE-RelB toxin-antitoxin module involves a helix displacement

near an mRNA interferase active site. *The Journal of biological chemistry* **284**, 14628-14636

38. Boggild, A., Sofos, N., Andersen, K. R., Feddersen, A., Easter, A. D., Passmore, L. A., and Brodersen, D. E. (2012) The crystal structure of the intact E. coli RelBE toxin-antitoxin complex provides the structural basis for conditional cooperativity. *Structure* **20**, 1641-1648

39. Ogle, J. M., Brodersen, D. E., Clemons, W. M., Jr., Tarry, M. J., Carter, A. P., and Ramakrishnan, V. (2001) Recognition of cognate transfer RNA by the 30S ribosomal subunit. *Science* **292**, 897-902

40. Jenner, L., Demeshkina, N., Yusupova, G., and Yusupov, M. Structural rearrangements of the ribosome at the tRNA proofreading step. *Nature structural & molecular biology* **17**, 1072-1078

41. Weixlbaumer, A., Jin, H., Neubauer, C., Voorhees, R. M., Petry, S., Kelley, A. C., and Ramakrishnan, V. (2008) Insights into translational termination from the structure of RF2 bound to the ribosome. *Science* **322**, 953-956

42. Laurberg, M., Asahara, H., Korostelev, A., Zhu, J., Trakhanov, S., and Noller, H. F. (2008) Structural basis for translation termination on the 70S ribosome. *Nature* **454**, 852-857

43. Zegers, I., Haikal, A. F., Palmer, R., and Wyns, L. (1994) Crystal structure of RNase T1 with 3'-guanylic acid and guanosine. *The Journal of biological chemistry* **269**, 127-133

44. Noguchi, S. (2010) Isomerization mechanism of aspartate to isoaspartate implied by structures of Ustilago sphaerogena ribonuclease U2 complexed with adenosine

3'-monophosphate. *Acta crystallographica. Section D, Biological crystallography* **66**, 843-849

45. Datsenko, K. A., and Wanner, B. L. (2000) One-step inactivation of chromosomal genes in Escherichia coli K-12 using PCR products. *Proceedings of the National Academy of Sciences of the United States of America* **97**, 6640-6645

46. Altschul, S. F., Madden, T. L., Schaffer, A. A., Zhang, J., Zhang, Z., Miller, W., and Lipman, D. J. (1997) Gapped BLAST and PSI-BLAST: a new generation of protein database search programs. *Nucleic acids research* **25**, 3389-3402

47. Emsley, P., Lohkamp, B., Scott, W. G., and Cowtan, K. (2010) Features and development of Coot. *Acta crystallographica. Section D, Biological crystallography* **66**, 486-501

48. Kabsch, W. (2010) Xds. *Acta crystallographica. Section D, Biological crystallography* **66**, 125-132

49. Adams, P. D., Afonine, P. V., Bunkoczi, G., Chen, V. B., Davis, I. W., Echols, N., Headd, J. J., Hung, L. W., Kapral, G. J., Grosse-Kunstleve, R. W., McCoy, A. J., Moriarty, N. W., Oeffner, R., Read, R. J., Richardson, D. C., Richardson, J. S., Terwilliger, T. C., and Zwart, P. H. (2010) PHENIX: a comprehensive Python-based system for macromolecular structure solution. *Acta crystallographica. Section D, Biological crystallography* **66**, 213-221

50. Selmer, M., Dunham, C. M., Murphy, F. V. t., Weixlbaumer, A., Petry, S., Kelley, A. C., Weir, J. R., and Ramakrishnan, V. (2006) Structure of the 70S ribosome complexed with mRNA and tRNA. *Science* **313**, 1935-1942

51. Jenner, L., Demeshkina, N., Yusupova, G., and Yusupov, M. (2010) Structural rearrangements of the ribosome at the tRNA proofreading step. *Nature structural & molecular biology* **17**, 1072-1078

52. Powers, T., and Noller, H. F. (1991) A functional pseudoknot in 16S ribosomal RNA. *Embo J* **10**, 2203-2214

Chapter 5

Mechanism of endonuclease cleavage by the HigB toxin

Marc A. Schureck, Adrienne Repack, Stacey J. Miles, Jhomar Marquez and Christine M. Dunham

Towards understanding how HigB cleaves mRNA on the ribosome, I identified several HigB amino acids that are important for mRNA cleavage. Based on the position of these residues in the structure of HigB bound to mRNA on the ribosome, I propose a catalytic mechanism for HigB-catalyzed mRNA cleavage. Comparison across ribosome-dependent toxin family members shows that each family member uses a unique arrangement of catalytic residues suggesting each active site may be tuned for a particular reason, such as compatibility with their corresponding mode of mRNA recognition.

This work has been submitted to Nucleic Acids Research.

Author contributions: M.A.S. and C.M.D. designed research; M.A.S., A.R., S.J.M. and J.M. performed research; M.A.S. and C.M.D. created figures; M.A.S. and C.M.D. analyzed data; and M.A.S. and C.M.D. wrote the paper.

5.1 Abstract

Bacteria encode multiple type II toxin-antitoxin modules that cleave ribosome-bound mRNAs in response to stress. Ribosome-dependent toxin family members have similar microbial RNase architectures despite their low sequence identities. Therefore, predicting functionally important residues in this specialized RNase family is challenging. Structural studies of toxins bound to the 70S have provided significant insights into proposed catalytic residues however only kinetic experiments of the RelE toxin have clearly demonstrated which residues are critical for mRNA cleavage. Here, we solved an X-ray crystal structure of wild-type HigB bound to the 70S ribosome to reveal potential catalytic residues involved in mRNA cleavage and determined important residues using bacterial growth or toxicity assays. Using single turnover kinetics, we found that HigB residues His54, Asp90, Tyr91 and His92 are critical for activity. Furthermore, we propose that HigB residues Tyr91 and His54 likely function as the general acid and base, respectively, in the endonucleolytic reaction based on their orientation around the scissile phosphate and the dramatic effect their substitutions has on the rate of mRNA cleavage. X-ray crystal structures of two HigB variants reveal the importance of His92 in the architecture of the active site required for efficient cleavage.

5.2 Introduction

Toxin-antitoxin complexes regulate bacterial physiology in response to changing environmental conditions. These gene pairs are organized into five classes depending upon the mechanism of inhibition and whether an RNA or protein antitoxin inhibits toxin expression or function (1). During non-stress conditions, type II toxin-antitoxin modules are tightly associated and function as transcription factors by binding at upstream DNA

operator sites where they inhibit transcription. Different types of stress cause antitoxin degradation, which releases the toxin that, in turn, inhibits essential processes including replication, ribosome assembly, protein synthesis, mRNA and tRNA stability, cell wall synthesis and cytoskeletal stability (2-8). Therefore, toxin-antitoxin modules, as part of the stress response, are beneficial and not "toxic" to the bacterial host. For example, type II toxins act as effector molecules that play important roles in an antibiotic-tolerant state known as persistence (9-14). This ability to transition to a persister state represents a possible new pathway to target in the treatment of pathogenic bacteria. However, understanding how toxin-antitoxin complexes function on a molecular level is critical to aid in the rational generation of antimicrobials against these novel effector molecules.

A majority of type II toxins inhibit translation as RNases but some toxins function as protein modification enzymes (*e.g.* HipA or Doc) while others simply inhibit growth by binding components of the cellular replication machinery such as DNA gyrase (*e.g.* CcdB) (2,15-17). The regulation of protein synthesis by toxins predominantly results from mRNA cleavage in the aminoacyl (A) site (4,18-20), the site where tRNAs enter the ribosome to decode mRNA. Other mechanisms by which toxins inhibit translation include cleavage of ribosomal RNA at functionally important sites (21-23), cleavage of tRNAs (5,24), and modification of glutamyl-synthase (13) and elongation factor Tu (15,16). It was initially thought that toxins globally inhibit protein synthesis during stress but rather than a global response, it may be that toxin activation leads to subtle changes in expression that are related to the particular stress encountered by the bacterium.

X-ray crystal structures of *Escherichia coli* RelE and YoeB, and *Proteus vulgaris* HigB toxins bound to the 70S ribosome reveal toxin residues that surround the mRNA

substrate and that may potentially be important for activity (18-20). Despite these significant insights into the structural basis of toxin-mediated mRNA cleavage, the contribution of each potential active site residue in the endonucleolytic activity is still unclear. One reason is the lack of amino acid consensus in toxin active sites. The 70S-RelE structures suggested R81 and Y87 were the general acid and base (18) yet steady-state kinetic analyses of RelE variants implicated Lys52 as the general base (25) and more recently, Lys54 was shown to act as the general base (26). Other ribosome-dependent toxins including YoeB, YafQ and HigB lack analogous basic residues found in RelE suggesting that alternative mechanisms of substrate recognition and cleavage may exist for different toxins.

The ribosome-dependent toxin *P. vulgaris* HigB has a preference for cleaving adenosine-rich codons (27). X-ray crystal structures of HigB bound to the 70S reveal that the concave cleft of HigB interacts with mRNA, implicating a number of HigB residues that could be involved in the cleavage reaction (20). Here, we report the X-ray crystal structure of wild-type HigB bound in a precleavage 70S state. We perform steady-state kinetic analyses to test the importance of HigB toxin residues that surround the mRNA. We demonstrate that HigB residues His54, Asp90, Tyr91 and His92 are important for HigB endonuclease activity. We propose that His54 is the general base that abstracts a proton from the 2' oxygen of the second nucleotide of the A-site codon, Arg73 stabilizes the transition state and Tyr91 donates a proton to the 5' oxygen leaving group. Comparison with other ribosome-dependent toxins RelE, YoeB and YafQ reveals that each toxin interacts with the the third nucleotide of the A-site codon in distinct ways that

is incompatible with the HigB toxin active site. Therefore, the manner in which each toxin engages the third A site nucleotide represents a critical difference among toxins.

5.3 Materials and methods

5.3a Strains and plasmids.

Overexpression experiments with HigB or HigB variants were performed in *E. coli* BW25113 cells (Δ(*araD-araB*)567 Δ(*rhaD-rhaB*)568 Δ*lacZ*4787(::rrnB-3) *lacI*p-400(*lacI*Q)λ- *rpoS*396(Am) *rph*-1 *rrnB*-4 *hsdR*514) (28). The pBAD24-HigB, pBAD-Myc-HisA-HigB$(His)_6$ and pBAD-Myc-HisA-HigBΔHis92$(His)_6$ vectors were a kind gift from Prof. Nancy A. Woychik (Rutgers University). Site-directed mutagenesis followed by DNA sequencing (Genewiz) was used to introduce and confirm HigB variants (**Table 5.1**).

5.3b 70S purification, complex formation and structure determination of the 70S-HigB precleavage state complex.

Thermus thermophilus (Tth) 70S ribosomes were purified and crystallized as previously described (20,29). Wild-type HigB expression and purification was performed as previously described (20). 70S ribosomes were incubated with CC-Puromycin to bind at the 50S A site, mRNA (IDT; 5'-GGCAAGGAGGUAAAAAUGAmAmAmUAGU-3', where the "m" indicates A-site 2'-OCH_3 modifications prevent mRNA cleavage) and P-site $tRNA^{fMet}$ (Chemical Block). Crystals grew to dimensions of 70 x 70 x 400 μM in one week in a final concentration of 0.1 M Tris-HCl, pH 7.0, 0.2 M KSCN, 3.75-4.5% PEG 20K and 3.75-4.5% PEG 550 MME. Both PEG concentrations were raised to 7% (w/v) and crystals were incubated with HigB (100 μM) for 1.5 hrs. Crystals were cryoprotected

in a step-wise manner to a final concentration of 30% PEG 550 MME before plunging in liquid nitrogen. X-ray diffraction data was collected at the Northeast Collaborative Access Team (NE-CAT) ID24C beamline at the Advanced Photon Source (APS; Argonne, IL) and processed with the XDS software (30) (**Table 5.2**). The structure was solved using a 70S-HigB ΔH92 precleavage state model lacking HigB and A-site mRNA as a start model (PDB code 4YZV) (20). HigB residues 1-90 were placed into unbiased electron difference density and manual model building was performed in Coot (31) followed by iterative rounds of refinement in Phenix (32). mRNA was visible for the E-site, P-site and A-site codons and one nucleotide 3' of the A-site AAA codon. The positions of 16S rRNA, 23S rRNA, mRNA and tRNAs were refined using the individual site refinement procedure with base-pair restraints in Phenix, while HigB was refined individually with secondary structure restraints.

5.3c Bacterial growth or toxicity assays.

Bacterial growth assays were performed in *E. coli* BW25113 as previously described (27). Wild-type HigB and HigB variants were expressed from the pBAD24-HigB vector by induction with 0.2% arabinose and growth monitored every hour for six hours after induction. In this assay, growth indicates that the corresponding amino acid substitution has inactivated HigB. The average OD_{600} values and associated standard error of the mean (SEM) were plotted in GraphPad Prism 5. For HigB variants that had robust growth, we performed Western blot analysis to confirm the presence of soluble HigB protein as previously described (27).

5.3d Single-turnover kinetic measurements.

E. coli 70S ribosomes were purified as previously described (33). HigB variants were overexpressed and purified essentially as wild-type HigB with the exception that Ni^{2+} affinity purification of the HigB variants was manually performed with Ni^{2+} Sepharose High Performance Resin (GE Healthcare). 70S (1.2 μM) were programmed with 5'-^{32}P-labeled mRNA (0.6 μM; 5'-GGCAAGGAGGUAAAAAUGAAAUAGU-3-' (IDT)) for 6 mins at 37 °C to ensure all mRNA was ribosome-bound. *E. coli* $tRNA^{fMet}$ (3 μM; Chemical Block) was next added to the P site for 30 mins. Wild-type or variant HigB (10 μM) was added to the 70S mixture and incubated at 37 °C for 120 min. Aliquots were taken at 0.5 (wild-type only), 1, 3, 10, 30, 60, and 120 mins, diluted two fold in formamide dye, heated to 70 °C for two mins to halt the reaction, and stored on ice or at -20 °C. Samples were analyzed on a preheated, 8 M urea, 1X TBE, 18% polyacrylamide sequencing gel and the gel was fixed, dried, and exposed to a phosphor storage screen and imaged on a Typhoon FLA 7000 gel imager (GE Healthcare). The intensity of uncleaved and cleaved bands was determined using Image Quant software and pmols of mRNA cleaved was calculated for each time point using the following formula: 12 pmol x (intensity of cleaved band) / (intensity of cleaved band + intensity of cleaved band). The product progression curves were fit and the K_{cat} determined in GraphPad Prism 5 using the equation Product = P_{max} $(1 - e^{-kt})$, where P_{max} represents the mRNA cleavage product plateau (pmol mRNA cleaved), k is the rate constant (min^{-1}), and t is the time after addition of HigB (min). For HigB and HigB R73A, the calculated plateau was unrestrained and yielded ~11 pmol cleaved. For the remainder of the HigB variants which did not reach 11 pmol cleaved, the maximum plateau was restrained to 11

pmol. The results along with standard deviation were plotted in the program GraphPad Prism 5.

5.3e Structure determination of HigB variants.

Crystals of trypsinized HigB HigB Y91A and HigB ΔH92 were grown in the same condition as wild-type HigB (30-40% w/v PEG 2,000 MME and 0.15 M KBr) (20). Crystals were cryoprotected in a stepwise manner to a final cryoprotectant solution of 10% w/v PEG 2,000 MME and 30% v/v ethylene glycol. All X-ray crystallography data were collected at the Southeast Regional Collaborative Access Team (SER-CAT) 22ID beamline at the APS. X-ray data were processed with the XDS software (30) (Y91A) or HKL2000 (34) (ΔH92) (**Table 5.3**). All structures were solved by molecular replacement using a polyalanine model of HigB (PDB code 4PX8) in the AutoMR program in Phenix (32). Although all HigB variants crystallized in the C2 spacegroup, HigB Y91A crystallized with eight copies per asymmetric unit while the HigB ΔHis92 asymmetric unit only contained one HigB. An initial round of automated model building was performed in Phenix with the autobuild program, followed by iterative rounds of manual model building in Coot (31) and refinement in Phenix (32). In general, during refinement the x,y,z coordinates, occupancies and anisotropic B-factors were refined. For the HigB Y91A structure at 1.55 Å, water B-factors were refined isotropically. All HigB residues (1-92) were built in both the HigB Y91A and ΔHis92 models.

5.4 Results

5.4a Structure determination of the 70S - wild-type HigB complex.

We previously solved the X-ray crystal structure of the *Tth* 70S complex in a precleavage state containing a HigB variant lacking His92 (ΔH92) bound to an optimal A-site AAA lysine codon (20). We selected this HigB variant because previous studies demonstrated the importance of His92 whereby the H92Q substitution inactivated HigB function yet still allowed for association with ribosomes (27). This structure provided significant insights into how HigB interacts with the mRNA substrate in the A site and what HigB residues may be catalytic. However, His92 is clearly important for mRNA cleavage therefore, the deletion of His92 may inactivate HigB by interfering with active site organization thus making the identification of potentially critical residues difficult. Therefore, to understand the arrangement of all critical HigB amino acids, we solved the X-ray crystal structure of wild-type HigB bound to the 70S with a preferred AAA codon in the A site (**Figures 5.1A & 5.1B; Table 5.3).** The complex was trapped in the precleavage state by including 2'-OCH_3 modifications at all three A-site nucleotides. The 70S-HigB structure was determined to 3.6 Å ($I/\sigma = 1.8$) and clear F_o-F_c difference electron density maps allowed unambiguous placement of P-site $tRNA^{fMet}$, mRNA and A-site bound HigB (**Figure 5.2**).

HigB is a small globular protein (10.7 kDa) that adopts a microbial ribonuclease fold similar to RNases Sa, U2 and T1 and contains a distinctive cleft of active site residues that interacts with the A-site mRNA substrate (**Figure 5.1B**)(35-42). HigB has a single β-sheet surrounded by surface-exposed two α-helices that mediate interactions with the negatively charged 16S rRNA backbone. HigB pulls the mRNA ~9 Å from the

normal mRNA path into its concave active site to interact with each of the three nucleotides of the mRNA A-site codon in distinct ways (20). This displacement also causes the mRNA to adopt a distorted conformation likely required to properly orient the mRNA substrate for in-line or S_N2 attack at the scissile phosphate, located between the second and third A-site nucleotides. Adjacent to the peptidyl (P) site, the first adenosine of the A-site codon (A4, where the mRNA numbering begins with the P-site AUG start codon as +1, +2 and +3) is sandwiched between HigB residue Lys57 and the P-site $tRNA^{fMet}$ but its nucleobase makes no direct hydrogen bonding or electrostatic interactions with HigB (**Figure 5.1B**). In contrast, HigB more closely monitors the second A-site adenosine (A5) by forming hydrogen bonds with the backbone carbonyl and amino groups of HigB residue Lys57 with the A5 Hoogsteen face while His92 is proximal to the ribose of the A5 nucleotide. Additionally, the side chain of His54 forms a hydrogen bond with the 2'-OH of A5. The third A-site adenosine is splayed from its normal position allowing the Hoogsteen face of A6 to hydrogen bond with the Watson-Crick face of 16S rRNA nucleotide C1054. This structure provides a number of insights into potentially catalytic HigB residues.

5.4b Effect of HigB variants on growth suppression.

To understand which HigB residues are important for function, we generated HigB variants of proposed active site residues and tested their function in bacterial growth assays (**Figures 5.3A & 5.3B**). Overexpression of wild-type HigB halts bacterial growth (27,43). Therefore, in this assay upon specific amino acid substitution, restoration of growth is interpreted as the loss of HigB activity, implicating the residue as essential for HigB function**.** Aromatic HigB residues Tyr84 and Tyr88 are proximal to the HigB

active site but substitution of either residue to alanine has no effect on growth suppression as compared to wild-type HigB suggesting these residues are not critical for mRNA cleavage (**Figure 5.3C**). Polar and acidic HigB residues Asn47, Asn71, Asn80 and Glu89 may influence the pKa of active site residues similar to the role proposed for Asp61 or Asp67 in YafQ (33). Our bacterial growth assays reveal no change on HigB-mediated growth suppression upon substitution to alanine for any of these residues (**Figure 5.3D**). RelE toxin mediates mRNA cleavage using two basic residues (either Lys52 or Lys54, and Arg81) (25,26). We therefore made substitutions of a number of basic HigB residues close to the mRNA path including Arg48, Lys52, Lys57, Arg60 and Arg73 but again, we found that no single residue was essential, although the HigB R73A variant had a modest impact on HigB toxicity (**Figure 5.3E**). HigB residue His54 is close to the 2'-OH of nucleotide A5, the position that will become deprotonated to initiate the reaction, while Asp90, Tyr91 or His92 are all close to the scissile phosphate (**Figure 5.1B).** Cell growth is completely restored when HigB residues His54, Asp90, Tyr91 or His92 are mutated to alanine demonstrating their functional importance (**Figures 5.3C, 5.3D and 5.3E**). To determine if either Tyr91 or His92 is critical for orienting the mRNA substrate (*e.g.* structural) or if either directly participates in mRNA catalysis, we changed each to phenylalanine. In both cases, HigB Y91F and H92F reverse the HigB toxicity strongly suggesting these residues play critical roles in the catalysis of mRNA cleavage rather than exerting a primarily structural role (**Figure 5.3F)**. Consistent with what we observe in the growth assays, all HigB variants that restore growth are expressed and soluble, and therefore, the reversal in the growth phenotype can be attributed to disruption of HigB function (**Figure 5.3B**).

Collectively, these assays identified four HigB residues (His54, Asp90, Tyr91 and His92) important for activity *in vivo*. Further, these results suggest that basic residues are not critical for HigB-mediated mRNA cleavage, in contrast to RelE (25,26). Instead, HigB functions more similarly to ribosome-dependent toxins that utilize histidine and glutamate residues (YoeB, Glu46 and His83; YafQ, His50 and His87) (19,33).

5.4c HigB residues His54, Asp90, Tyr91 and His92 are critical for mRNA cleavage.

To determine whether each of the four HigB residues identified in the growth assays directly affects mRNA cleavage, we performed *in vitro* single turnover mRNA cleavage assays. We incubated 5'-^{32}P-mRNA containing a Shine-Dalgarno upstream of an AUG start codon positioned in the P site and an AAA lysine codon in the A site with a two-molar excess of *E. coli* 70S. We next programmed with $tRNA^{fMet}$ in the P site and added a saturating 17-fold molar excess of wild-type HigB and monitored mRNA cleavage over 120 min (**Figures 5.4A & 5.4B; Figure 5.5 & Table 5.3**). Wild-type HigB cleaved mRNA at a rate of 0.46 ± 0.026 min^{-1} whereas HigB variants showed between 11- to 215-fold reductions in mRNA cleavage. Consistent with not fully ablating HigB toxicity *in vivo*, HigB R73A shows an 11-fold reduction in the rate of mRNA cleavage and the H54A variant exhibits a 52-fold reduction in the cleavage rate. HigB C-terminal residues Asp90, Tyr91 and His92 are highly conserved among HigB homologs and their substitutions with alanine caused the largest effect on the mRNA cleavage rate. HigB variants D90A, Y91A, H92A and ΔHis92 reduced the cleavage rate by 77, 215, 184 and 190 fold, respectively. These data confirm that HigB residues His54, Asp90, Tyr91 and His92 are critical for mRNA cleavage.

5.4d His92 is critical for optimal organization of the HigB active site.

To understand the impact these variants have on the integrity of the HigB active site, we next solved X-ray crystal structures of the HigB variants Y91A and ΔHis92 to 1.55 Å and 1.1 Å, respectively (**Figure 5.6; Table 5.4**). We attempted to solve structure of HigB H54A and H92A variants but were unable to grow diffracting crystals. Comparison of the HigB Y91A and ΔHis92 structures with the wild-type HigB structure (20) (PDB code 4PX8) reveals a similar Cα backbone trace (root mean square deviations (rmsd) = 0.28 and 0.41 Å, respectively).

The 1.55-Å structure of HigB Y91A reveals a minimal effect on the positions of active site residues His54, Arg73, Asp90 and His92 as compared to wild-type HigB (**Figure 5.6B**). Therefore, it appears the Y91A variant does not alter the overall active site but rather, may be defective in catalysis. In contrast, the 1.1-Å structure of the HigB ΔHis92 reveals a dramatic reorganization of the active site residues (**Figure 5.6B**). Arg73 and Tyr91 move ~6 and 9 Å changes, respectively while Asp90 and Tyr91 exist in alternative conformations. The deletion of His92 causes the backbone and sidechain of Tyr91 to rotate ~65° away from His54 while the sidechain of Arg73 is shifted ~180° towards the new position of Tyr91 (**Figure 5.6C**, bottom). In summary, the Y91A variant has little to no effect on the HigB active site while ΔHis92 severely distorts the active site. Although substitutions of either has a large effect on the rate of cleavage (215 and 190 fold), they each affect the mechanism in distinct manners.

5.5 Discussion

The structure of the HigB toxin in a precleavage state bound to the 70S provided significant insights into the possible catalytic roles of residues surrounding the scissile

phosphate of the mRNA (20). However because a HigB variant was used to trap the toxin on the ribosome, it is unclear if the substitution alters the positions of HigB active site residues. Here, we solved an X-ray crystal structure of wild-type HigB bound to the 70S in a precleavage state trapped instead by mRNA modifications that prevent cleavage. Our structure reveals that HigB residue His54 is within hydrogen bonding distance of the 2'-OH of the second nucleotide of the A-site codon; Arg73 forms a hydrogen bond with the scissile phosphate before and after mRNA cleavage; and Tyr91 is adjacent to the 5'-oxygen of the leaving group at the third A-site nucleotide and is potentially supported in a catalytic role by the proximal Asp90 and His92 (**Figure 5.7A**) (20). Based on the bacterial growth and single turnover kinetic assays presented in this study, we propose that His54 initiates deprotonation of the 2'-OH of A5, a step required for attack at the scissile phosphate (**Figures 5.7A & 5.7B**). The basic nature of Arg73 likely helps stabilize the negative charge of the transition state, an important but clearly not critical role in catalysis. Although aromatic residues such as Y87 in RelE and F91 in YafQ stack with the mRNA nucleobase of A5 to optimally position the substrate (25,33,44), our results indicate that Tyr91 plays a more direct catalytic role in HigB-mediated cleavage as substitution with either alanine or phenylalanine renders the enzyme inactive. Because Tyr91 is proximal to the 5'-oxygen in our structure, we propose that Tyr91 functions as the essential proton donor. Based on the impacts of similar substitutions of HigB residues Asp90 and His92, we propose these residues likely serve supporting roles in promoting the correct orientation of Tyr91 and/or participation in catalysis through donation of a proton to Tyr91. Consistent with this idea, our structure of HigB ΔHis92 reveals a

significant distortion of the active site, in particular the location of Tyr91, suggesting that His92 is critical for optimal positioning of Tyr91.

Ribosome-dependent toxins only cleave mRNA positioned in the ribosomal A site representing a novel mechanism to regulate translation in response to diverse environmental stress (1,45,46). These toxins facilitate mRNA cleavage at the phosphodiester backbone using acid-base catalysis to leave a 2'-3' cyclic phosphate (33,44) or a 3'-phosphate product (19). Bacterial genomes contain multiple toxin-antitoxin genes but identifying new toxin-antitoxin modules is one of the challenges in the field because of their low sequence identities even among proposed active site residues (**Figure 5.8A**). Although these toxins adopt a microbial RNase fold, each is appended with a diverse set of active site residues. RelE lacks a histidine and charged residue pair typical of canonical RNases (47) and instead, contains basic residues that interact directly with the mRNA substrate and are important for catalysis (**Figure 5.8B**) (25,26,44). In contrast, YoeB contains a histidine-glutamate pair (41), YafQ contains a histidine-histidine pair (33) and HigB uses a histidine-tyrosine pair for catalysis (**Figure 5.8B**). These data suggest that RelE is the outlier of ribosome-dependent toxins and the significance of this is unknown.

Although ribosome-dependent toxins contain diverse active site residues, structures of toxins bound to the 70S in combination with steady-state kinetic analyses are beginning to define both some emerging common themes and specific mechanistic differences (20,25,26,33,44). RelE, HigB and YoeB all form a selective pocket around the splayed third A-site nucleotide of the mRNA, however contributions from the ribosome are different (19,20,44). For example, RelE and HigB form this pocket with

help from 16S rRNA nucleotide C1054 while YoeB residues alone forms the nucleotide-binding pocket (19,20,44). HigB binding to the A site flips the third nucleotide from the mRNA path that positions its Hoogsteen edge to interact directly with the Watson-Crick face of 16S rRNA nucleotide C1054 likely contributing significantly to the selection of an adenosine at this third A-site position (**Figure 5.8C**). Superpositioning of RelE- or YoeB-bound mRNA in place of the HigB-bound mRNA reveals that HigB active site residues Asn71 and Tyr91 would significantly clash with either G6 (RelE) or A6 (YoeB) nucleotides located in the selective pocket (**Figure 5.8C**). These data suggest that although the local position of the general acid for each ribosome-dependent toxin (RelE Arg81, YoeB His83 and YafQ His87) is similar, the identity of the residue that functions as the acid significantly influences the nucleotide that can optimally fit into the pocket. Thus we predict the general acid of ribosome-dependent toxins to be the most important determinant in mRNA selectivity. Our and other studies are beginning to decipher the rules that govern toxin selectivity for different mRNA transcripts suggesting that this specificity is not indicative of global translation inhibition but rather, appears to modulate selective translation. The biological consequence for this exquisite mRNA specificity during stress is unknown.

5.6 Acknowledgment

We thank F. M. Murphy IV and staff members of the NE-CAT beamlines for assistance during data collection and Dr. G. L. Conn for critical reading of the manuscript.

5.7 Funding

Research reported in this publication was partially supported by the National Science Foundation [CAREER award MCB 0953714 to CMD], the National Institute of

Health (NIH) [GM093278 to CMD; Biochemistry, Cell and Developmental Biology Graduate Training Grant 5T32GM8367; and F31 Fellowship [GM108351 to MAS] and the Pew Biomedical Sciences Program (to CMD). This work is based upon research conducted at the Northeastern Collaborative Access Team beamlines, which are funded by the National Institute of General Medical Sciences from the National Institutes of Health (P41 GM103403) and at the Southeastern Collaborative Access Team beamlines (SER-CAT). The Pilatus 6M detector on 24-ID-C beam line is funded by a NIH-ORIP HEI grant (S10 RR029205). This research used resources of the Advanced Photon Source, a U.S. Department of Energy (DOE) Office of Science User Facility operated for the DOE Office of Science by Argonne National Laboratory under Contract No. DE-AC02-06CH11357.

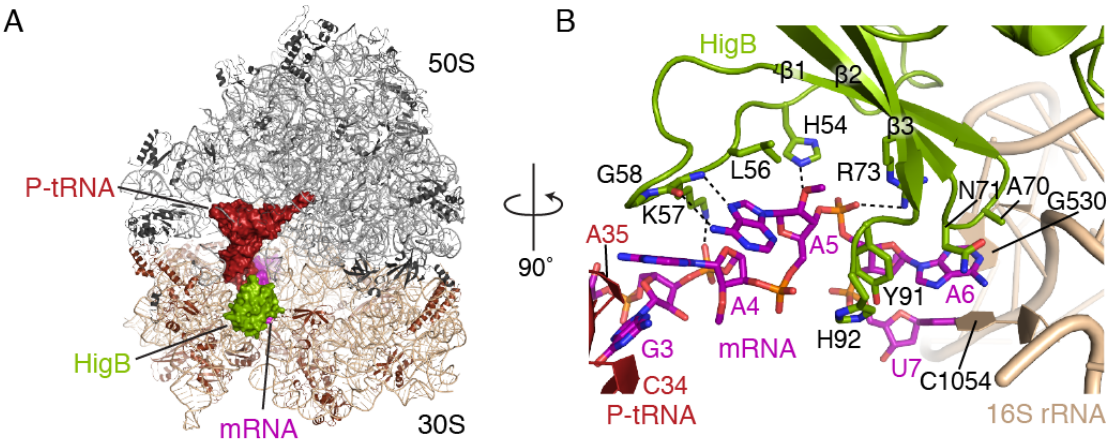

Figure 5.1: Recognition of the ribosomal A site by endonuclease HigB.

A. 3.6-Å X-ray crystal structure of HigB bound to a AAA lysine codon containing 2'-O-methyl modifications to prevent cleavage. The side view shows the A site in the forefront with the P-site tRNA (red) behind. B. A 90° rotation of A) and zoomed view reveal how HigB engages the AAA mRNA substrate. The mRNA is numbered from the P-site AUG codon (start with +1) with A4, A5, and A6 nucleotides residing in the A site. 16S rRNA nucleotides that interact with the mRNA or HigB are shown.

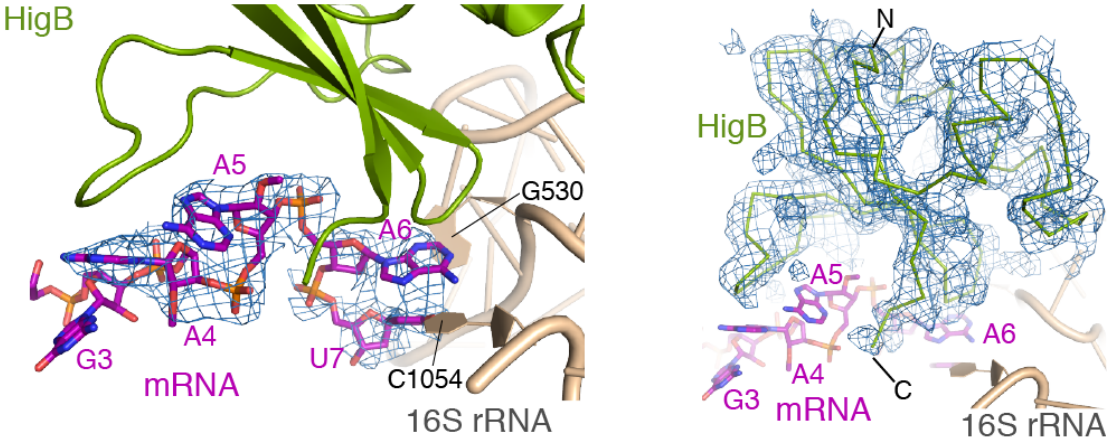

Figure 5.2: Difference electron density for the A-site mRNA and HigB.

F_o-F_c difference electron density contoured to 2σ for A-site mRNA (left panel) and 70S-bound HigB (right panel).

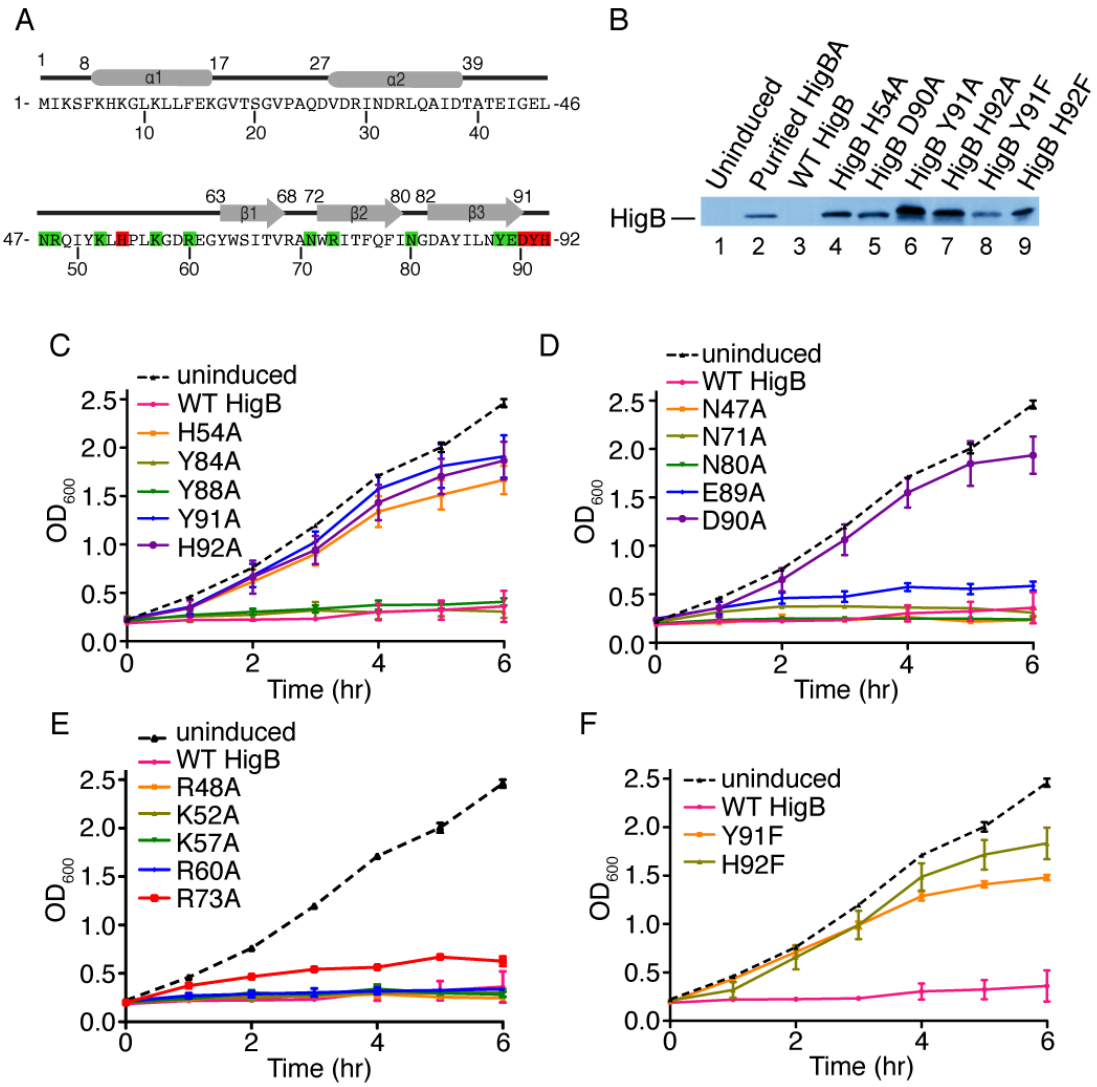

Figure 5.3. Identification of essential HigB residues.

A. *P. vulgaris* HigB sequence labeled with its secondary structure. Residues essential for function in bacterial growth assays are highlighted in red and nonessential residues highlighted in green. B. Western blot analysis of the soluble fraction from the bacterial growth assays that permit growth (panels C-F) at 4 hrs postinduction using polyclonal antibodies against the HigBA toxin-antitoxin complex. Overexpression of wild-type HigB results in an inhibition of protein synthesis with no detectable HigB protein in the immunoblot (lane 3). C. Bacterial growth assays where wild-type HigB and HigB

variants are overexpressed. HigB residues that cluster around the mRNA were substituted with alanine and their effect on *E. coli* growth was monitored at 600 nm for 6 hrs after protein induction. HigB aromatic residues proximal to the scissile phosphate were changed to alanine. HigB charged and acidic residues proximal to the HigB active site (D) and HigB basic residues that interact with or are proximal to the mRNA phosphate backbone (E) were substituted with alanine and their effect on bacterial growth was monitored. F. HigB aromatic residues whose functional side chains were mutated to neutral phenylalanine to retain its aromatic stacking ability. Error bars display standard error of the mean from at least three experiments.

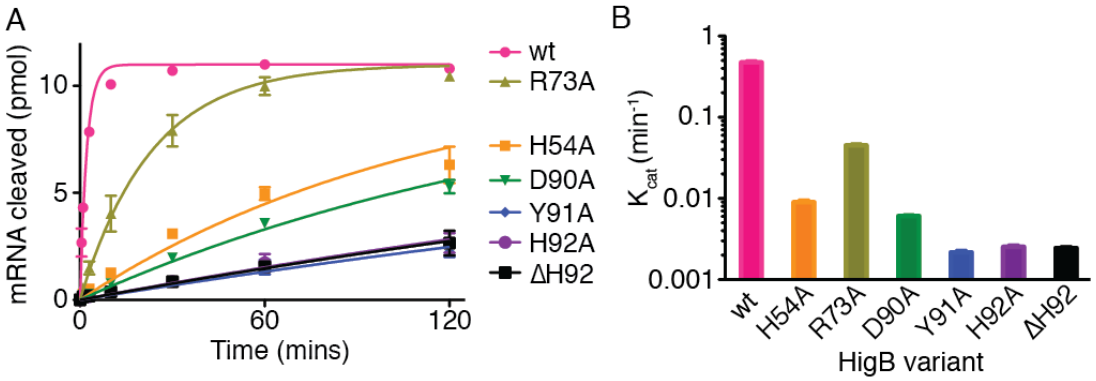

Figure 5.4: Analysis of HigB residues important for mRNA cleavage.

A. Product progression curves of wild-type HigB and HigB variants incubated with programmed *E. coli* 70S - mRNA complexes and the amount of mRNA cleaved was monitored under single-turnover conditions. B. K_{cat} values for wild-type HigB and HigB variants derived from panel A. In both panels, error bars display standard deviations from two replicates.

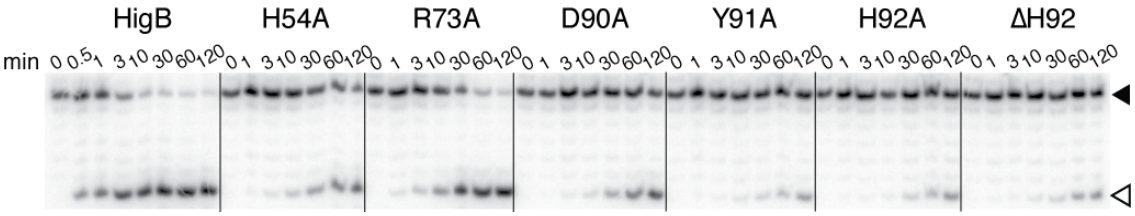

Figure 5.5: Effect HigB variants on the rate of mRNA cleavage.

70S *E. coli* ribosomes were programmed with mRNA and P-site $tRNA^{fMet}$ and the rate of mRNA cleavage by wild-type HigB and variants over 2 hrs was assessed by running the products on a 8M urea/ 18% polyacrylamide gel. Two technical replicates were performed and all reactions were run on a single gel. The vertical lines depicted on the gel are shown to help in interpreting the gel. Uncleaved and cleaved mRNA are indicated by solid and open arrowheads, respectively.

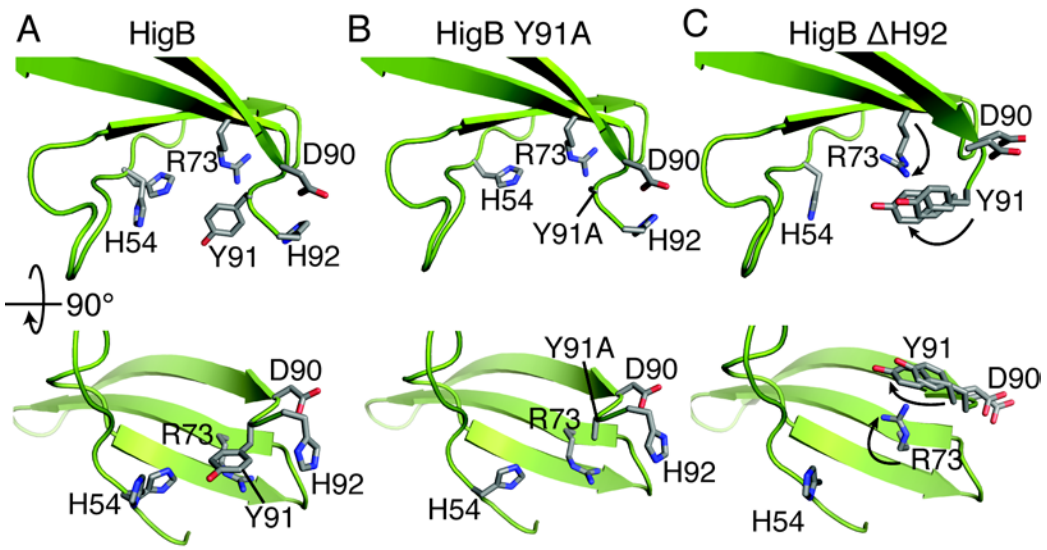

Figure 5.6: HigB His92 is critical for preordering the HigB active site.

A. Wild-type HigB solved to 1.25 Å (PDB code 4PX8) shown with active site residues His54, Arg73, Asp 90, Tyr91 and His92 depicted as sticks. X-ray crystal structures of HigB Y91A (B;1.55 Å) and HigB ΔHis92 (C; 1.1 Å). The bottom panels are 90° rotations of the top panels.

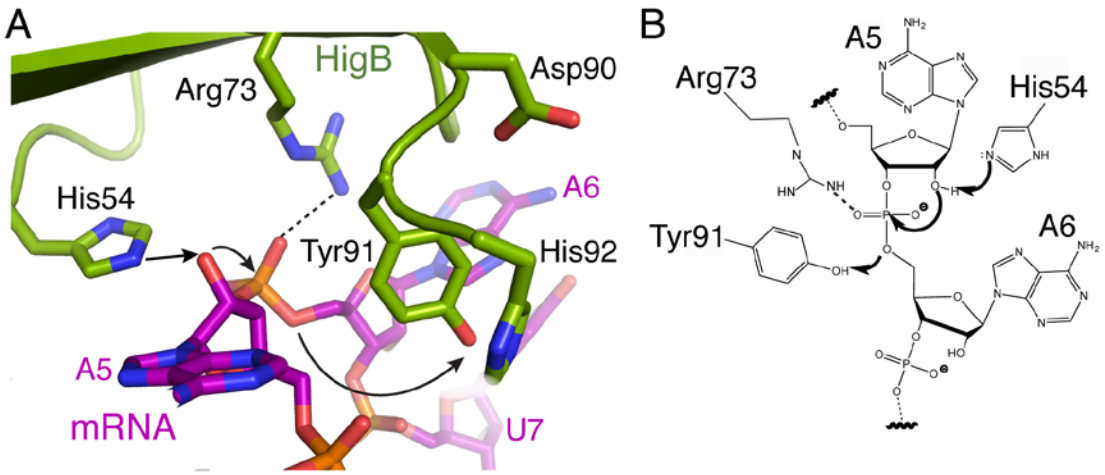

Figure 5.7: Proposed mechanism of HigB-mediated mRNA degradation on the ribosome.

A. View of the HigB active site with proposed catalytic residues His54, Arg73, Asp90, Tyr91 and His92 shown surrounding the mRNA substrate. His54 likely functions as a general base to deprotonate the 2'-proton of the 2'-OH of the A5 nucleotide of the mRNA, Arg73 stabilizes the bipyramidal transition state and Tyr91 stabilizes the 5'-leaving group as a general acid. Asp90 and His92 may play structural roles to properly orient Tyr91 to donate a proton or may aid by donating a proton to the Tyr91 oxyanion form.

B. A schematic of these critical interactions for HigB-mediated mRNA cleavage as inferred from our structures and kinetic analyses.

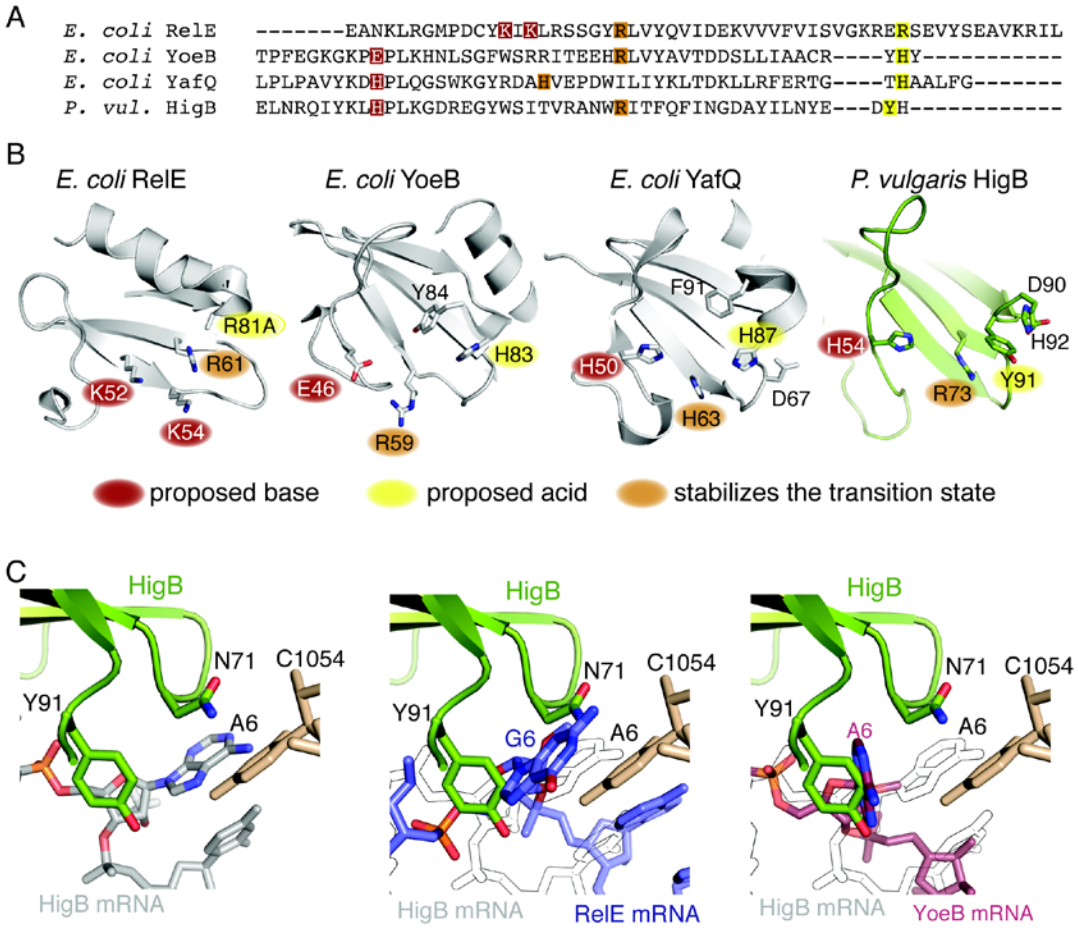

Figure 5.8: Mechanistic differences in how ribosome-dependent toxins recognize the A-site mRNA substrate.

A. Sequence alignments of ribosome-dependent toxins RelE, YoeB, YafQ and HigB with the proposed roles of the active site residues highlighted as indicated in panel B. B. Comparisons of ribosome-dependent active site residues (shown as sticks) and their proposed roles in acid-base catalysis (PDB codes 4V7J (70S-RelE), 4V8X (70S-YoeB), 4ML2 (YafQ), 4ZSN (HigB; this study)). C. HigB residues N71 and Y91 flank the A6 A-site nucleotide positioning A6 to interact directly with 16S rRNA residue C1054 (left). Superpositioning of the mRNA upon RelE interaction on the 70S (purple; middle; PDB code 4V7J) and the mRNA upon YoeB interaction on the 70S (pink; right; PDB code

4V8X) reveals significant clashing of HigB residues N71 and Y91 with G6 (middle; mRNA from the 70S-RelE structure) and A6 (right; mRNA from the 70S-YoeB structure). In the middle and right panels, the path of the mRNA when HigB binds the 70S is shown in white with gray outline.

Table 5.1. DNA primers used.

Primer	Sequence (5'-3')
N47A	CGATACAGCGACAGAGATTGGTGAACTAGCGCGC CAGATTTACAAATTA
N47A-AS	TAATTTGTAAATCTGGCGCGCTAGTTCACCAATCT CTGTCGCTGTATCG
R48A	GCGACAGAGATTGGTGAACTAAACGCGCAGATTT ACAAATTACATCCATTA
R48A-AS	TAATGGATGTAATTTGTAAATCTGCGCGTTTAGTT CACCAATCTCTGTCGC
K52A	GTGAACTAAACCGCCAGATTTACGCGTTACATCC ATTAAAGGGGGATCG
K52A-AS	CGATCCCCCTTTAATGGATGTAACGCGTAAATCTG GCGGTTTAGTTCAC
H54A	AACTAAACCGCCAGATTTACAAATTAGCGCCATT AAAGGGGGATCGGG
H54A-AS	CCCGATCCCCCTTTAATGGCGCTAATTTGTAAATC TGGCGGTTTAGTT
K57A	CGCCAGATTTACAAATTACATCCATTAGCGGGGG ATCGGGAAG
K57A-AS	CTTCCCGATCCCCCGCTAATGGATGTAATTTGTAA ATCTGGCG
R60A	TTACATCCATTAAAGGGGGATGCGGAAGGTTACT GGTCTAT
R60A-AS	ATAGACCAGTAACCTTCCGCATCCCCCTTTAATGG ATGTAA
N71A	GGTCTATCACTGTCCGGGCGGCGTGGCGCATTACT TTTCAGTT
N71A-AS	AACTGAAAAGTAATGCGCCACGCCGCCCGGACAG TGATAGACC
R73A	ATCACTGTCCGGGCGAATTGGGCGATTACTTTTCA GTTCATTAACG

R73A-AS	CGTTAATGAACTGAAAAGTAATCGCCCAATTCGC CCGGACAGTGAT
N80A	GGCGAATTGGCGCATTACTTTTCAGTTCATTGCGG GTGATGCTTACATTT
N80A-AS	AAATGTAAGCATCACCCGCAATGAACTGAAAAGT AATGCGCCAATTCGCC
Y84A	CATTACTTTTCAGTTCATTAACGGTGATGCTGCGA TTTTAAATTATGAGGATTATCACTAACTCG
Y84A-AS	CGAGTTAGTGATAATCCTCATAATTTAAAATCGCA GCATCACCGTTAATGAACTGAAAAGTAATG
Y88A	GTTCATTAACGGTGATGCTTACATTTTAAATGCGG AGGATTATCACTAACTCGAGG
Y88A-AS	CCTCGAGTTAGTGATAATCCTCCGCATTTAAAATG TAAGCATCACCGTTAATGAAC
E89A	CGGTGATGCTTACATTTTAAATTATGCGGATTATC ACTAACTCGAGG
E89A-AS	CCTCGAGTTAGTGATAATCCGCATAATTTAAAATG TAAGCATCACCG
D90A	GTGATGCTTACATTTTAAATTATGAGGCGTATCAC TAACTCGAGGGATCCG
D90A-AS	CGGATCCCTCGAGTTAGTGATACGCCTCATAATTT AAAATGTAAGCATCAC
D90A*	TTCGGGCCCAAGCTTGTGATACGCCTCATAATTTA AAATGTAAGCATC
D90A-AS*	GATGCTTACATTTTAAATTATGAGGCGTATCACAA GCTTGGGCCCGAA
Y91A	CGGTGATGCTTACATTTTAAATTATGAGGATGCGC ACTAACTCGAGGGATCCGAATTC
Y91A-AS	GAATTCGGATCCCTCGAGTTAGTGCGCATCCTCAT AATTTAAAATGTAAGCATCACCG
Y91A*	TTTTGTTCGGGCCCAAGCTTGTGCGCATCCTCATA ATTTAAAATGTAAGCATCAC

Y91A-AS*	GTGATGCTTACATTTTAAATTATGAGGATGCGCAC AAGCTTGGGCCCGAACAAAA
Y91F	GATGCTTACATTTTAAATTATGAGGATTTTCACTA ACTCGAGGGATC
Y91F-AS	GATCCCTCGAGTTAGTGAAAATCCTCATAATTTAA AATGTAAGCATC
H92A	GGTGATGCTTACATTTTAAATTATGAGGATTATGC GTAACTCGAGGGATCCGAA
H92A-AS	TTCGGATCCCTCGAGTTACGCATAATCCTCATAAT TTAAAATGTAAGCATCACC
H92A*	TGTTCGGGCCCAAGCTTCGCATAATCCTCATAATT TAAAATGTAAGCATCAC
H92A-AS*	GTGATGCTTACATTTTAAATTATGAGGATTATGCG AAGCTTGGGCCCGAACA
H92F	ACGGTGATGCTTACATTTTAAATTATGAGGATTAT TTTTAACTCGAGGGATCCGAAT
H92F-AS	ATTCGGATCCCTCGAGTTAAAAATAATCCTCATAA TTTAAAATGTAAGCATCACCGT

* denotes primers used for pBAD-Myc-HisA-HigB$(His)_6$. All other primers were applied to pBAD24-HigB except for H54A and R73A primer sets which were applied to both pBAD24-HigB and pBAD-Myc-HisA-HigB$(His)_6$.

Table 5.2. 70S - HigB precleavage state structure

Data collection	
Space group	P 2_1 2_1 2_1
Cell dimensions	
a, b, c (Å)	213.4, 452.9, 608.9
α, β, γ (°)	90, 90, 90
Resolution (Å)*	50 – 3.6 (3.72 - 3.60)
R_{merge} (%)	21.6 (83)
R_{meas} (%)	23.7 (95)
R_{pim} (%)	10.4 (45)
I / σ	6.6 (1.8)
Completeness (%)	98.7 (99.2)
Redundancy	5.2 (4.2)
Refinement	
Resolution (Å)	50 – 3.6
Total reflections	3,450,846
Unique reflections	675,750
R_{work} / R_{free} (%)	19.8/23.4
No. atoms	294,410
Protein/RNA	293125
Ligand/ion	1,285
Water	0
B-factors	95.8
Protein/RNA	96.0
Ligand/ion	38.00
R.m.s. deviations	
Bond lengths (Å)	0.004
Bond angles (°)	0.87
PDB ID	4ZSN

Two crystals were used for data collection.
*Values in parentheses are for the highest resolution shell.

Table 5.3: Summary of the effects of HigB mutations on the K_{cat} of mRNA cleavage.

HigB	K_{cat} (min^{-1}) ± standard error	Fold change
Wild-type	0.46 ± 0.026	-
H54A	0.0087 ± 0.00057	52
R73A	0.043 ± 0.0022	11
D90A	0.0059 ± 0.00019	77
Y91A	0.0021 ± 0.00013	215
H92A	0.0025 ± 0.0013	184
ΔH92	0.0024 ± 0.00011	190

Table 5.4: Crystallographic table of HigB variants

	HigB Y91A	**HigBΔH92**
Data collection		
Space group	C2	C2
Unit cell dimensions		
a, *b*, *c* (Å)	113.4, 64.0, 94.1	55.8, 33.2, 51.5
α, β, γ (°)	90 , 98.1, 90	90, 115.5, 90
Resolution (Å)*	100 - 1.55 (1.55 - 1.60)	15.0 - 1.10 (1.14 - 1.10)
R_{meas} (%)	5.8 (54.4)	5.0 (13.3)
I / σ	12.0 (2.4)	20.7 (9.3)
Completeness (%)	85.7 (89.9)	94.7 (96.7)
Redundancy	2.6 (2.5)	2.0 (2.0)
Refinement		
Resolution (Å)	100 - 1.55	15.0 - 1.10
Total reflections	213,899	66,552
Unique reflections	82,947	32,761
R_{work} / R_{free} (%)[a]	17.0/22.0	13.8/16.9
No. atoms	6,865	1,020
Protein	6,231	894
Ion	12	2
Water	622	124
Mean B-factors (Å^2)	22.20	13.4
Protein (Å^2)	21.10	11.9
Ion (Å^2)	30.80	14.7
Water (Å^2)	32.10	24.3
R.m.s. deviations		
Bond lengths (Å)	0.012	0.011
Bond angles (°)	1.316	1.48
PDB deposition ID		

One crystal was used for each dataset reported.
*Values in parentheses are for the highest resolution shell.

5.8 References

1. Maisonneuve, E., and Gerdes, K. (2014) Molecular mechanisms underlying bacterial persisters. *Cell* **157**, 539-548
2. Bernard, P., and Couturier, M. (1992) Cell killing by the F plasmid CcdB protein involves poisoning of DNA-topoisomerase II complexes. *Journal of molecular biology* **226**, 735-745
3. Zhang, Y., and Inouye, M. (2011) RatA (YfjG), an Escherichia coli toxin, inhibits 70S ribosome association to block translation initiation. *Molecular microbiology* **79**, 1418-1429
4. Pedersen, K., Zavialov, A. V., Pavlov, M. Y., Elf, J., Gerdes, K., and Ehrenberg, M. (2003) The bacterial toxin RelE displays codon-specific cleavage of mRNAs in the ribosomal A site. *Cell* **112**, 131-140
5. Winther, K. S., and Gerdes, K. (2011) Enteric virulence associated protein VapC inhibits translation by cleavage of initiator tRNA. *Proceedings of the National Academy of Sciences of the United States of America* **108**, 7403-7407
6. Ainelo, A., Tamman, H., Leppik, M., Remme, J., and Horak, R. (2016) The toxin GraT inhibits ribosome biogenesis. *Molecular microbiology*
7. Mutschler, H., Gebhardt, M., Shoeman, R. L., and Meinhart, A. (2011) A novel mechanism of programmed cell death in bacteria by toxin-antitoxin systems corrupts peptidoglycan synthesis. *PLoS Biol* **9**, e1001033
8. Tan, Q., Awano, N., and Inouye, M. (2011) YeeV is an Escherichia coli toxin that inhibits cell division by targeting the cytoskeleton proteins, FtsZ and MreB. *Molecular microbiology* **79**, 109-118

9. Keren, I., Shah, D., Spoering, A., Kaldalu, N., and Lewis, K. (2004) Specialized persister cells and the mechanism of multidrug tolerance in Escherichia coli. *Journal of bacteriology* **186**, 8172-8180

10. Maisonneuve, E., Shakespeare, L. J., Jorgensen, M. G., and Gerdes, K. (2011) Bacterial persistence by RNA endonucleases. *Proceedings of the National Academy of Sciences of the United States of America* **108**, 13206-13211

11. Maisonneuve, E., Castro-Camargo, M., and Gerdes, K. (2013) (p)ppGpp controls bacterial persistence by stochastic induction of toxin-antitoxin activity. *Cell* **154**, 1140-1150

12. Hu, Y., Kwan, B. W., Osbourne, D. O., Benedik, M. J., and Wood, T. K. (2015) Toxin YafQ increases persister cell formation by reducing indole signalling. *Environ Microbiol* **17**, 1275-1285

13. Germain, E., Roghanian, M., Gerdes, K., and Maisonneuve, E. (2015) Stochastic induction of persister cells by HipA through (p)ppGpp-mediated activation of mRNA endonucleases. *Proceedings of the National Academy of Sciences of the United States of America* **112**, 5171-5176

14. Helaine, S., Cheverton, A. M., Watson, K. G., Faure, L. M., Matthews, S. A., and Holden, D. W. (2014) Internalization of Salmonella by macrophages induces formation of nonreplicating persisters. *Science* **343**, 204-208

15. Castro-Roa, D., Garcia-Pino, A., De Gieter, S., van Nuland, N. A., Loris, R., and Zenkin, N. (2013) The Fic protein Doc uses an inverted substrate to phosphorylate and inactivate EF-Tu. *Nat Chem Biol* **9**, 811-817

16. Cruz, J. W., Rothenbacher, F. P., Maehigashi, T., Lane, W. S., Dunham, C. M., and Woychik, N. A. (2014) Doc toxin is a kinase that inactivates elongation factor Tu. *J Biol Chem* **289**, 19276

17. Germain, E., Castro-Roa, D., Zenkin, N., and Gerdes, K. (2013) Molecular mechanism of bacterial persistence by HipA. *Molecular cell* **52**, 248-254

18. Neubauer, C., Gillet, R., Kelley, A. C., and Ramakrishnan, V. (2012) Decoding in the absence of a codon by tmRNA and SmpB in the ribosome. *Science* **335**, 1366-1369

19. Feng, S., Chen, Y., Kamada, K., Wang, H., Tang, K., Wang, M., and Gao, Y. G. (2013) YoeB-ribosome structure: a canonical RNase that requires the ribosome for its specific activity. *Nucleic acids research* **41**, 9549-9556

20. Schureck, M. A., Dunkle, J. A., Maehigashi, T., Miles, S. J., and Dunham, C. M. (2015) Defining the mRNA recognition signature of a bacterial toxin protein. *Proc Natl Acad Sci U S A*

21. Winther, K. S., Brodersen, D. E., Brown, A. K., and Gerdes, K. (2013) VapC20 of Mycobacterium tuberculosis cleaves the sarcin-ricin loop of 23S rRNA. *Nature communications* **4**, 2796

22. Schifano, J. M., Edifor, R., Sharp, J. D., Ouyang, M., Konkimalla, A., Husson, R. N., and Woychik, N. A. (2013) Mycobacterial toxin MazF-mt6 inhibits translation through cleavage of 23S rRNA at the ribosomal A site. *Proceedings of the National Academy of Sciences of the United States of America* **110**, 8501-8506

23. Schifano, J. M., Vvedenskaya, I. O., Knoblauch, J. G., Ouyang, M., Nickels, B. E., and Woychik, N. A. (2014) An RNA-seq method for defining endoribonuclease

cleavage specificity identifies dual rRNA substrates for toxin MazF-mt3. *Nature communications* **5**, 3538

24. Cruz, J. W., Sharp, J. D., Hoffer, E. D., Maehigashi, T., Vvedenskaya, I. O., Konkimalla, A., Husson, R. N., Nickels, B. E., Dunham, C. M., and Woychik, N. A. (2015) Growth-regulating Mycobacterium tuberculosis VapC-mt4 toxin is an isoacceptor-specific tRNase. *Nature communications* **6**, 7480

25. Griffin, M. A., Davis, J. H., and Strobel, S. A. (2013) Bacterial toxin RelE: a highly efficient ribonuclease with exquisite substrate specificity using atypical catalytic residues. *Biochemistry* **52**, 8633-8642

26. Dunican, B. F., Hiller, D. A., and Strobel, S. A. (2015) Transition State Charge Stabilization and Acid-Base Catalysis of mRNA Cleavage by the Endoribonuclease RelE. *Biochemistry* **54**, 7048-7057

27. Hurley, J. M., and Woychik, N. A. (2009) Bacterial toxin HigB associates with ribosomes and mediates translation-dependent mRNA cleavage at A-rich sites. *The Journal of biological chemistry* **284**, 18605-18613

28. Datsenko, K. A., and Wanner, B. L. (2000) One-step inactivation of chromosomal genes in Escherichia coli K-12 using PCR products. *Proceedings of the National Academy of Sciences of the United States of America* **97**, 6640-6645

29. Selmer, M., Dunham, C. M., Murphy, F. V. t., Weixlbaumer, A., Petry, S., Kelley, A. C., Weir, J. R., and Ramakrishnan, V. (2006) Structure of the 70S ribosome complexed with mRNA and tRNA. *Science* **313**, 1935-1942

30. Kabsch, W. (2010) Xds. *Acta crystallographica. Section D, Biological crystallography* **66**, 125-132

31. Emsley, P., Lohkamp, B., Scott, W. G., and Cowtan, K. (2010) Features and development of Coot. *Acta crystallographica. Section D, Biological crystallography* **66**, 486-501

32. Adams, P. D., Afonine, P. V., Bunkoczi, G., Chen, V. B., Davis, I. W., Echols, N., Headd, J. J., Hung, L. W., Kapral, G. J., Grosse-Kunstleve, R. W., McCoy, A. J., Moriarty, N. W., Oeffner, R., Read, R. J., Richardson, D. C., Richardson, J. S., Terwilliger, T. C., and Zwart, P. H. (2010) PHENIX: a comprehensive Python-based system for macromolecular structure solution. *Acta crystallographica. Section D, Biological crystallography* **66**, 213-221

33. Maehigashi, T., Ruangprasert, A., Miles, S. J., and Dunham, C. M. (2015) Molecular basis of ribosome recognition and mRNA hydrolysis by the E. coli YafQ toxin. *Nucleic acids research* **43**, 8002-8012

34. Otwinowski, Z., and Minor, W. (1997) Processing of X-ray Diffraction Data Colleceted in Oscillation Mode. in *Methods in Enzymology* (Carter, J., C.W., and Sweet, R. M. eds.), Academic Press, New York. pp 307-326

35. Sevcik, J., Dodson, E. J., and Dodson, G. G. (1991) Determination and restrained least-squares refinement of the structures of ribonuclease Sa and its complex with 3'-guanylic acid at 1.8 A resolution. *Acta crystallographica. B* **47 (Pt 2)**, 240-253

36. Heinemann, U., and Saenger, W. (1983) Crystallographic study of mechanism of ribonuclease T1-catalysed specific RNA hydrolysis. *J Biomol Struct Dyn* **1**, 523-538

37. Noguchi, S., Satow, Y., Uchida, T., Sasaki, C., and Matsuzaki, T. (1995) Crystal structure of Ustilago sphaerogena ribonuclease U2 at 1.8 A resolution. *Biochemistry* **34**, 15583-15591

38. Li, G. Y., Zhang, Y., Inouye, M., and Ikura, M. (2009) Inhibitory mechanism of Escherichia coli RelE-RelB toxin-antitoxin module involves a helix displacement near an mRNA interferase active site. *The Journal of biological chemistry* **284**, 14628-14636

39. Ruangprasert, A., Maehigashi, T., Miles, S. J., Giridharan, N., Liu, J. X., and Dunham, C. M. (2014) Mechanisms of toxin inhibition and transcriptional repression by Escherichia coli DinJ-YafQ. *The Journal of biological chemistry* **289**, 20559-20569

40. Liang, Y., Gao, Z., Wang, F., Zhang, Y., Dong, Y., and Liu, Q. (2014) Structural and functional characterization of Escherichia coli toxin-antitoxin complex DinJ-YafQ. *The Journal of biological chemistry* **289**, 21191-21202

41. Kamada, K., and Hanaoka, F. (2005) Conformational change in the catalytic site of the ribonuclease YoeB toxin by YefM antitoxin. *Molecular cell* **19**, 497-509

42. Schureck, M. A., Maehigashi, T., Miles, S. J., Marquez, J., Cho, S. E., Erdman, R., and Dunham, C. M. (2014) Structure of the Proteus vulgaris HigB-(HigA)2-HigB toxin-antitoxin complex. *The Journal of biological chemistry* **289**, 1060-1070

43. Tian, Q. B., Ohnishi, M., Murata, T., Nakayama, K., Terawaki, Y., and Hayashi, T. (2001) Specific protein-DNA and protein-protein interaction in the hig gene system, a plasmid-borne proteic killer gene system of plasmid Rts1. *Plasmid* **45**, 63-74

44. Neubauer, C., Gao, Y. G., Andersen, K. R., Dunham, C. M., Kelley, A. C., Hentschel, J., Gerdes, K., Ramakrishnan, V., and Brodersen, D. E. (2009) The structural basis for mRNA recognition and cleavage by the ribosome-dependent endonuclease RelE. *Cell* **139**, 1084-1095

45. Yamaguchi, Y., Park, J. H., and Inouye, M. (2011) Toxin-antitoxin systems in bacteria and archaea. *Annual review of genetics* **45**, 61-79

46. Sofos, N., Xu, K., Dedic, E., and Brodersen, D. E. (2015) Cut to the chase--Regulating translation through RNA cleavage. *Biochimie* **114**, 10-17

47. Zegers, I., Haikal, A. F., Palmer, R., and Wyns, L. (1994) Crystal structure of RNase T1 with 3'-guanylic acid and guanosine. *J Biol Chem* **269**, 127-133

Chapter 6

Conclusion

6.1 Abstract

Bacteria contain numerous factors that directly inhibit protein synthesis in response to changes in the environment. Some factors block mRNA and tRNA access to the ribosome, while others cleave mRNA as it is translated by the ribosome. Although these proteins all inhibit translation, whether each of these uniquely alters the spectrum of proteins translated during stress is unknown. For example, do these translational inhibitors lead to translation of specific transcripts? In this conclusion, I discuss how ribosome-dependent toxins cleave mRNA on the ribosome and argue that each toxin likely plays a unique role in translational regulation. I further describe distinguishing features of each ribosome-dependent toxin family member that could be useful in future studies aimed at identifying orthologues. A model to describe how each ribosome-dependent toxin selects mRNA targets will shed light on an important bacterial survival mechanism and provide critical insights into different modes of translational regulation.

6.2 Introduction

Bacteria often have multiple ribosome-dependent toxins that differ in the mRNA they cleave, but how these unique cleavage patterns affect the spectrum of proteins translated during stress is unknown. Ribosome-dependent toxins can serve to downregulate all translation, but in some circumstances, the activity of these toxins only affects a subset of mRNAs, allowing for considerable translation to occur during stress. Here, I discuss potential ways that ribosome-dependent toxins can regulate protein synthesis, examine the mechanisms of regulation of toxin activity and transcriptional regulation from toxin-antitoxin operons and show that motifs that confer mRNA cleavage specificity are highly conserved among individual ribosome-dependent family members. The conserved attributes of mRNA cleavage within individual family members suggests that the activity of each toxin is tuned to degrade a specific set of mRNA transcripts across many bacterial species to regulate translation during stress.

My graduate work identified the molecular basis for ribosome-dependent mRNA cleavage by the *Proteus vulgaris* HigB toxin and regulation of its activity. I first examined how HigB activity is inhibited through interactions with the HigA antitoxin (**Chapter 2**). I next investigated how HigB interacts with the ribosome, recognizes mRNA and catalyzes mRNA cleavage (**Chapters 3-5**). These studies have shown how HigB attains the unique specificity of cleaving several adenosine-containing codons. My investigations have also uncovered several previously unappreciated commonalities and differences between ribosome-dependent toxin family members. These differences likely underlie key functional distinctions in how each toxin regulates protein synthesis during stress.

6.3 Toxin activity can have varying effects on translation

Ribosome-dependent toxins appear to have two modes in which they regulate translation. The first is an almost complete halting of protein synthesis resulting in cessation of growth. The second has a much milder effect on protein synthesis causing a small reduction in translation and causing little reduction in cell growth. In the situation where some translation occurs during toxin activity, the mRNA cleavage specificities of toxins (**Chapter 4**) have opportunity to tune which proteins are translated during stress. The difference between these two modes of toxin-mediated translation repression appears to be caused by the ability of a bacterial cell to replenish degraded antitoxin.

When antitoxin protein is not replenished after toxin activation, toxin activity suppresses all translation and limits growth. Overexpression experiments clearly show that most, if not all, ribosome-dependent toxins can stop cell growth and almost completely inhibit protein synthesis (1-3). However, the levels of toxin proteins in these overexpression experiments are likely several orders of magnitude higher than during physiological conditions (4,5). One potent feature of toxin-antitoxin systems is their ability to stabilize plasmids they are encoded in. There are no inherent differences between plasmid and chromosomally-encoded toxin-antitoxin systems at the amino acid level. The main difference appears to be that plasmid-encoded toxin-antitoxin systems have the possibility of not replenishing antitoxin protein because plasmids can be lost. If a toxin-antitoxin system is encoded on a plasmid, loss of plasmid will result in cell death because the bacterial cell cannot synthesize more antitoxin to replace the rapidly degraded antitoxin, freeing the toxin to continuously inhibit cell growth (6). Failure to replenish antitoxin protein, leading to unchecked toxin activation, can also be observed

using toxin-antitoxin overexpression. In this experiment, the RelE-RelB (RelEB) toxin-antitoxin complex was overexpressed prior to treatment with serine hydroxamate, a competitive inhibitor of seryl-tRNA synthetase that mimics amino acid deprivation and activates RelE toxin (7). If RelEB complex was continuously overexpressed throughout serine hydroxamate treatment, cells experienced a slight loss in viability. If the RelEB complex overexpression was halted just prior to serine hydroxamate treatment, creating a large amount of RelE and RelB with no means of replenishing degraded antitoxin, serine hydroxamate treatment drastically reduced cellular viability. These observations show that continued synthesis of the antitoxin protein during stress is an important aspect of limiting ribosome-dependent toxin activity. In situations where cells fail to synthesize more antitoxin, toxin activity can severely inhibit translation and stop cell growth.

When antitoxin protein can be replenished, such as in chromosomally encoded toxin-antitoxin systems, toxin activity has a mild effect on the translational inhibition. Chromosomally-encoded RelE is activated by RelB antitoxin degradation in response to nutritional starvation by serine hydroxamate treatment (7). In wild-type *E. coli* cells, treatment with serine hydroxamate downregulates translation to about 95% of pre-starvation levels (7). When the same strain of *E. coli* lacking *the relEB* locus is treated with serine hydroxamate, protein synthesis is only decreased to 90% of prestarvation levels. Thus, endogenous activation of RelE contributes somewhat to inhibition of translation but does not completely halt it. Likewise, the *E. coli* YoeB toxin is activated by elevated temperatures but does not globally decrease translation or growth rates when activated by heat (8). Thus, when the toxin-antitoxin locus is intact and able to replenish degraded antitoxin, it appears that ribosome-dependent toxin activity mildly affects

translation but does not completely shut it down.

The initial observation that toxins downregulated protein synthesis during stress suggested a global translation inhibition. However, the recent studies mentioned suggest ribosome-dependent toxins do not globally inhibit translation, but target different mRNAs and have different activation profiles (**Chapter 1**). Considering that bacterial genomes often encode several members of the ribosome-dependent family of toxins (9), one ribosome-dependent toxin per genome should be sufficient if their role was simply to downregulate translation. These different specificities and activation profiles of toxins suggest ribosome-dependent toxins have more specialized yet unknown roles in translational regulation.

6.4 Potential ways in which toxins reshape the translational landscape

The identification of how toxin-antitoxin systems affect protein synthesis will provide biological insight into how bacteria survive environmental stress. Given that they are beneficial host genes, a complete inhibition of translation over long periods of time would in fact be detrimental to any cell and ultimately cause death. Therefore, one model for how toxin-antitoxin systems work is the following: ribosome-dependent toxins could cause selective inhibition of translation rather than having a global inhibitory effect (**Figure 6.1A**). In this scenario, a toxin could cleave a particular subset of mRNA transcripts (sensitive transcripts) while not degrading others (resistant transcripts) to lead to translation of specific proteins potentially required to sustain viability during stress. This hypothesis suggests that the mRNA cleavage specificity of a toxin is tuned to a particular stress.

Another model in which toxins lead to translation of specific transcripts hypothesizes that toxin proteins clear the way for translation of stress-related proteins (**Figure 6.1B**). Activation of a toxin may rapidly halt all translation. The reduction in translation may allow remaining resources to be used for synthesizing stress-related proteins. Toxin activity would have to be quenched after global shutdown of protein synthesis to allow for translation of newly transcribed mRNA. This hypothesis has been referred to as the translational reset model (10). During normal growth, a large number of ribosomes are actively translating ribosomal proteins (5). During the stringent response, guanosine tetra/penta phosphate signaling halts transcription of ribosomal proteins and increases transcription of stress-related genes (11). Thus, toxins may clear the ribosomes, perhaps of ribosomal protein transcripts, to translate these newly needed transcripts, and the diverse mRNA-cleavage specificities of ribosome-dependent toxins may simply serve to target the majority of transcripts.

A third model to explain why cells have several ribosome-dependent toxin-antitoxin systems is that the multiplicity of antitoxins allows for translational inhibition in response to a variety of stresses. If the inhibition of protein synthesis is the only important feature of toxins, then by utilizing antitoxins that are each degraded by a subset of stresses, bacteria can downregulate translation in response to a multitude of environmental cues (**Figure 6.1C**). Here, the transcripts targeted by the toxin may or may not matter, but the ability to repress translation in response to several environmental stresses is important. Toxin and antitoxin-centric views are not mutually exclusive and understanding the molecular basis of action will provide insights into the physiological role of toxin-antitoxin systems.

6.5 Towards an understanding of the roles of ribosome-dependent toxins

There are several unknowns about the impact ribosome-dependent toxins have on translation during stress. Ideally, toxin activity will be studied *in vivo* with extremely low levels of expression to mimic their levels during stress. The first question is which mRNA transcripts are targeted by each ribosome-dependent toxin? Knowledge of mRNA transcripts that are sensitive and resistant to cleavage by particular toxins will help uncover overlapping and distinct specificities. The location of cleavage sites will help determine if particular stages of translation (initiation, elongation or termination) are more susceptible to cleavage by certain toxins. If toxins serve to reset translation, identification of the transcripts targeted by ribosome-dependent toxins will not be as important as identification of the transcripts translated after ribosome-dependent cleavage. Ribosomal profiling, a technique that uses sequencing of ribosome-bound mRNA to approximate translation rates, should be able to identify which mRNAs are translated during or after toxin activity (12). Mapping by overexpression of an RNase in Escherichia coli RNA-sequencing, which selectively ligates an adaptor to mRNA at the site it was cleaved before sequencing is performed, should help identify cleavage sites in mRNA (13).

The second question is when is each ribosome-dependent toxin active? Some antitoxin degradation appears to be stress sensitive (10,14). Identification of the stresses that degrade each antitoxin will provide a context to analyze the alteration in translation that occurs. For instance, do toxins that are activated during nitrogen starvation facilitate translation of proteins that help scavenge nitrogen? Reporters, such as Spinach, an RNA

mimic of green fluorescent protein (15), inserted behind toxin-antitoxin systems should allow for rapid screening of stresses that activate toxin-antitoxin systems.

A third question is how many ribosome-dependent toxins are there? I have presented five ribosome-dependent toxins but more ribosome-dependent toxins may exist. Toxins with very low sequence identity relative to established toxins could very well make up a new family member of ribosome-dependent toxins. Bioinformatic classification of toxin sequences along with knowledge of the molecular features of cleavage specificity should help identify toxins that have novel specificities.

6.6 Molecular studies will aid the accurate annotation of ribosome-dependent toxins

I hypothesize the toxin-antitoxin field will attain an understanding of the molecular basis for mRNA recognition that enables prediction of distantly-related ribosome-dependent toxin specificity from sequence alone. Molecular studies of toxins are improving and we are beginning to understand how specific amino acid sequences confer cleavage preferences. With this knowledge in hand, one can look at distantly related toxin proteins and predict their mRNA cleavage specificity. Analysis of the wealth of bacterial genomic data should allow identification of the characteristics of each toxin in a genome and prediction of these toxins' cumulative effect on shaping translation during stress.

One problem in the field is that toxin-antitoxin systems are sometimes misannotated. Toxin-antitoxin systems with low sequence identity to known toxin-antitoxin systems are present in hundreds of bacteria. In annotation of a new protein, one must decide which ribosome-dependent family member the toxin protein is most similar to. The typical gene organization in a toxin-antitoxin loci is the antitoxin followed by the

toxin (6). The *hig* operon is unique in that the *higB* toxin precedes the *higA* antitoxin (16). The significance of this is unknown with only nonribosome-dependent toxin-antitoxin systems HipA-HipB (HipAB) and MqsR-MqsA (MqsRA) sharing this reversal of the gene organization. The reversed gene order and homology to the RelE ribosome-dependent toxin was used for identification of several Hig-like toxin-antitoxin systems (9,10). However, as our molecular understanding of toxin-antitoxin systems grow, it is clear that many of the ribosome-dependent toxins classified as "HigB" lack several distinguishing features of *P. vulgaris* HigB and likely do not function as does *P. vulgaris* HigB. For example, sequence alignments of *P. vulgaris* HigB with "HigB" studied in *Vibrio cholerae* HigB-1 & HigB-2, and *E. coli* K12 HigB (10,17) show they share sequence identities of 18, 26 and 21%, respectively, and more importantly, these "HigB" proteins lack several residues required for 16S rRNA recognition, mRNA recognition and mRNA cleavage that I have demonstrated are important for *P. vulgaris* HigB function (18) (**Figure 6.3**). In some instances, the ribosome-dependent toxin more closely resembles another family member. For example, *M. tuberculosis* RelE-3 toxin has 45% sequence identity with *E. coli* YoeB and contains the same catalytic residues as YoeB (19). *M. tuberculosis* RelE-3 was subsequently renamed YoeB (20). Accurate annotation of ribosome-dependent toxins will allow the findings from one species to be applied to a ribosome-dependent toxin from many other species, a necessary step for the advancement of the toxin-antitoxin field.

Biochemical and structural studies have revealed how ribosome-dependent toxins are inactivated by antitoxins and how they cleave mRNA on the ribosome. Here, I will focus on the *E. coli* RelEB, YoeB-YefM and YafQ-DinJ and *P. vulgaris* HigBA toxin-

antitoxin systems. Structures of each toxin-antitoxin complex exist allowing for mechanistic understanding of how each antitoxin inhibits toxin and presents a DNA-binding motif to interact with DNA. Structures of the RelE, YoeB and HigB toxins bound to the 70S ribosome and functional analyses thereof have illuminated several common as well as several distinct features among ribosome-dependent toxin-mediated mRNA cleavage (18,21-23). Continued mechanistic studies of ribosome-dependent toxin family members will aid our understanding of how these toxins function and the identification of which residues are involved in critical aspects of mRNA cleavage.

6.7 Mechanism of antitoxin inhibition of toxin function

X-ray crystal structures of toxin-antitoxin complexes have highlighted two different modes of antitoxin-mediated toxin inhibition. All ribosome-dependent toxins that cleave mRNA in the A site of the ribosome have distinct concave active sites (indicated by red stars in **Figure 6.4**) (24-29). *E. coli* antitoxins RelB, YefM and DinJ bind their cognate toxin through their extended C termini that wraps around the toxin protein and is proximal to the toxin active site (**Figure 6.4A-C**) (24-28). Mechanistically, mRNA is blocked from entering the toxin active site when antitoxin is bound. Additionally, the large nature of the toxin-antitoxin complex likely prevents binding the A site of the ribosome by steric inhibition. Prior to my structural studies of the HigBA complex, an X-ray crystal structure of the *E. coli* CFT073 HigA was solved and the authors hypothesized that HigA interacts with HigB through the extended C-terminus of HigA, similar to RelB, YefM and DinJ (30). However, my structure of the *P. vulgaris* HigBA complex reveals the HigA antitoxin interacts with its cognate toxin differently than RelB, YefM and DinJ antitoxins do (**Chapter 2**) (29). HigA does not wrap around

HigB and in fact, the HigB active site is solvent exposed. When modeled onto the ribosome, HigA sterically clashes with components of the small ribosomal subunit suggesting HigA-bound HigB cannot bind the ribosome. I hypothesize that HigA binding inhibits HigB activity by preventing interaction between HigB and the ribosome. These studies illustrate the diversity of antitoxin-mediated inhibition of toxin.

Antitoxins appear to have degradation tags (protein sequence important for degradation). The last 16 residues of the HipB antitoxin are disordered in X-ray crystal structures, implying significant flexibility, and this region is proposed to be the HipA degradation tag (31). Deletion of the C terminus stabilizes HipA and appending the 16 HipB C-terminal residues to GFP causes GFP degradation by Lon protease (31). Although HipB regulates a toxin that phosphorylates glutamyl-tRNA synthetase and does not cleave ribosome-bound mRNA, its C terminus is very similar to that of the disordered C-terminus of the HigA antitoxin suggesting their proteolysis may be similarly regulated (**Figure 6.2**). Degradation tags for each antitoxin should be identified and linked to the particular stress that activates them. Knowledge of which degradation tags are targeted for degradation by particular stresses will enable identification of which stresses activate each toxin by antitoxin sequence alone.

To date, all antitoxins are obligate dimers and usually contain a N-terminal DNA-binding domain to allow for interaction with upstream operator regions to prevent transcription. The N-terminal DNA-binding domains each bind the major groove of DNA. *E. coli* RelB, YefM and DinJ antitoxin dimers form one DNA-binding domain and full occupation of one operator sequence, which is ~20 nucleotides in length, requires two antitoxin dimers (4 total antitoxins) (**Figure 6.4 A-C**) (24-28). In the case of RelB and

DinJ, the homodimer forms a ribbon-helix-helix DNA binding motif while the YefM dimer forms a DNA binding domain similar to that of the Phd antitoxin, which inhibits a toxin that modifies EF-Tu (32-34). In contrast, a *P. vulgaris* HigA antitoxin homodimer creates two DNA-binding domains as each HigA protein contains an entire helix-turn-helix DNA binding motif and thus requires only two HigA proteins to bind one *hig* operator (**Figure 6.4 A-C**) (**Chapter 2**) (18). Thus, the DNA-binding motif of antitoxins influences the stoichiometry of the complex bound to DNA.

Changing the ratio of toxin to antitoxin affects transcription from certain toxin-antitoxin loci (4,32,35). *In vivo* experiments demonstrate that overexpression of toxin protein actually increases transcription from the toxin-antitoxin operon (4). Analysis by electrophoretic mobility shift assay shows that antitoxin by itself has a weak affinity for DNA. Addition of a small amount of toxin enhances the affinity of the toxin-antitoxin complex for DNA and the presence of a larger amount of toxin ablates the interactions between antitoxin and DNA (4,32,35). Taken together, these data support a model termed conditional cooperativity where low ratios of toxin to antitoxin facilitate tight cooperative binding of the antitoxin to DNA while high ratios of toxin to antitoxin destabilize interactions between the antitoxin and DNA (4). This model may explain why transcription from toxin-antitoxin operons is upregulated during environmental stress, a condition in which toxin levels exceed antitoxin levels.

RelEB complexes of differing stoichiometry bind their operator DNA with varying affinities. Transcription from the RelEB TA operon is regulated by conditional cooperativity and it is thought that two trimeric $RelE_1RelB_2$ complexes bind DNA with high affinity while tetrameric $RelE_2RelB_2$ complexes bind DNA with low affinity (**Figure**

6.5) (4,25). The current model explaining why tetrameric RelEB complex binds DNA poorly is based on a model of the X-ray crystal structure of tetrameric RelEB complex onto DNA (25). From this alignment, the authors hypothesize that two trimeric $RelE_1RelB_2$ complexes can stably bind DNA at the same time while binding of two tetrameric $RelE_2RelB_2$ complexes would cause a steric clash because of the additional two RelE proteins and result in decreased affinity for DNA. A fundamental property of this model is that four RelB antitoxins bind DNA and not all of these antitoxins must be bound by toxin for high-affinity DNA interactions to occur. Because one RelB is not bound to RelE when the RelEB complex is bound to DNA, a high-affinity RelE-binding site is present on the RelBE complex, allowing for an additional RelE to bind and alter the affinity of the complex for DNA.

The *yafQ-dinJ* operon does not appear to be regulated by conditional cooperativity. Recent biochemical studies from our lab have found that in contrast to RelE, excess YafQ does not destabilize interactions between DinJ and DNA (27). DinJ in the absence of YafQ was still able to bind DNA efficiently whereas RelB exhibits a sharp decrease in affinity for DNA in the absence of RelE. Lastly, just one DinJ dimer bound to one half of an operator was sufficient to repress transcription from the *yafQ-dinJ* operon. Thus, interactions between DinJ and DNA do not appear to be regulated by YafQ even though the structures of YafQ-DinJ and RelE-RelB are very similar (**Figure 6.4 A and C**). These findings highlight that not all toxin-antitoxin systems are regulated by conditional cooperativity and that a more refined mechanistic understanding, based not solely on structure, is needed to predict which toxin-antitoxin systems are regulated by conditional cooperativity.

My studies of the HigBA complex initially suggested that transcription from the *HigBA* operon may not be regulated by toxin to antitoxin ratio. I solved two structures of HigBA that revealed both form hetereotetrameric complexes. Furthermore, the structures show that two HigA proteins bind each *hig* operator in contrast to several toxin-antitoxin systems that are transcriptionally regulated by toxin to antitoxin ratios which require four total antitoxins to bind to one operator (29). In unpublished work, I biochemically tested whether an increased ratio of HigB to HigA affects interaction between HigA and DNA and found that high ratios of HigB to HigA destabilize interactions between HigA and DNA. I am actively pursuing the mechanism by which HigB alters the affinity of HigA for DNA and hypothesize that it occurs by a novel mechanism.

A fundamental unanswered question in the toxin-antitoxin field is: what limits toxin activity once antitoxin is degraded? At some point, antitoxin has to be replenished for uninhibited translation to continue. If toxin activity was left completely unregulated, the cell could never recover from toxin activation. One example of unchecked toxin activity is when a plasmid encoding a toxin-antitoxin system is lost. Cell growth is halted because antitoxin protein is degraded faster than toxin, leading to free toxin and antitoxin cannot be replenished when the plasmid encoding the toxin antitoxin system was lost (6). With toxin to antitoxin ratios regulating transcription, free toxin can cleave mRNA on the ribosome but it also activates transcription from its operon. Ribosome profiling shows that antitoxins are translated at higher levels than toxins even though both genes are transcribed together from a single operon (5). Thus, increased transcription from the toxin-antitoxin loci during stress is not likely meant to create more free toxin. Toxin-mediated translational repression is likely not complete and allows for higher levels of

antitoxin to be translated than toxin. The transcriptional derepression would continue until higher ratios of antitoxin to toxin have been reestablished and toxin activity is quenched. Transcriptional derepression seems to be so important that the toxin protein plays an active role in it. Simply waiting for antitoxin to be degraded to increase transcription would not be as rapid and would not facilitate reestablishment of a low toxin to antitoxin ratio. Additionally, if antitoxin degradation is stopped and there was not conditional cooperativity, only a few antitoxins would be required to repress transcription from the toxin-antitoxin operon while free toxin was still present. I hypothesize that conditional cooperativity is an auto-feedback loop that limits toxin activity to short bursts (**Figure 6.6**).

There are other examples where toxin to antitoxin ratios do not appear to regulate the transcription from the toxin-antitoxin system operon. As assessed using EMSA, DinJ antitoxin binding to its operator DNA was not affected by elevated levels of the YafQ toxin (27,28). The DinJ-YafQ and the YafNO TA system are also regulated by LexA and DNA damage (2,10). DNA damage induces the SOS response, which induces expression of several proteins involved in DNA repair. These genes are regulated by LexA, a protein that during non-stress conditions is a transcriptional repressor but during DNA damage cleaves itself relieving transcriptional repression. LexA represses transcription from both the *yafNO* and *dinJ-yafQ* operons suggesting a more complex transcriptional regulation occurs at these loci and may rationalize why the DinJ-YafQ and potentially YafNO toxin-antitoxin systems are not transcriptionally regulated by toxin to antitoxin ratios.

My argument that transcriptional regulation permits only short bursts of toxin activity also argues that ribosome-dependent toxins only target a subpopulation of mRNA.

Toxin proteins are present at low levels in the cell and a conditional cooperativity autofeedback loop would likely limit the time they are active to a short period. Thus, toxins probably only have the opportunity to cleave select mRNA targets before they are inhibited. Although we do not know the mRNA targets of most ribosome-dependent toxins yet, I hypothesize that toxins reshape the translational landscape to promote translation of a particular set of transcripts that are important for cellular survival.

6.8 Molecular mechanisms of cleavage of mRNA by ribosome-dependent toxins

I mapped sequence conservation within individual ribosome-dependent toxin family members. Important portions of each ribosome-dependent toxin are often conserved within their homologs but not across ribosome-dependent toxin family members. I identified sequences of 1000 homologs for RelE, YafQ, YoeB and HigB (36), aligned homologous sequences in Clustal Omega (37) and then plotted sequence conservation using the WebLogo format (38) (**Figure 6.7**). WebLogo plots amino acid sequence as a function of relative amino acid conservation, where the vertical size of the single letter represents its conservation. I have mapped highly-conserved critical residues for the four toxins in WebLogo format (**Figure 6.7**) and on their structure bound to mRNA (**Figure 6.8**). Throughout my analysis of toxin function, I refer to the conservation and function of residues and suggest that this information be used in future annotation of ribosome-dependent toxins.

The structures of RelE, YoeB and HigB bound to mRNA on the ribosome have uncovered several important aspects of how these toxins target the A site (18,21,39). First, each toxin binds the A site of the 30S ribosomal subunit where mRNA is decoded by the anticodon stem loop of tRNA. tRNAs decode mRNA by Watson-Crick base pairing with

the three nucleotides of the A-site codon. When free or bound to tRNA, the path of A-site mRNA is a relatively straight line. In contrast to how tRNAs decode mRNA, each toxin drastically reorients the A-site mRNA path pulling the mRNA into its concave active site. Each toxin makes extensive interactions with 16S rRNA and contacts ribosomal protein S12. The RelE and HigB proteins bind the ribosome as monomers while YoeB binds the ribosome as a dimer. The dimerization interface of YoeB contains three highly-conserved hydrophobic residues (Trp5, Trp10 and Tyr13) surrounded by several hydrophilic residues. The presence of these highly-conserved aromatic residues should help distinguish YoeB from other ribosome-dependent toxins (**Figure 6.7B and 6.8B**). These observations show that overall, the toxins recognize mRNA on the ribosome in a similar fashion but several molecular differences exist causing distinctions in how these toxins cleave specific mRNA sequences.

Each ribosome-dependent toxin contains two clusters of basic residues that contact 16S rRNA. Deletion of these residues in combination results in toxin inactivation illustrating their importance in ribosome binding (**Chapter 3**) (40). Sequence conservation analysis shows variable conservation of these residues. The only conserved HigB basic residue used to contact 16S rRNA is Lys8 while other basic residues HigB uses to contact the ribosome are not highly conserved (**Figure 6.7D and 6.8D**). In contrast, RelE residues Lys13, Lys17, Lys28 and Lys29, YoeB residues Lys21, Arg22, Lys25, Lys26 and Arg36 and YafQ residues Lys14, Lys17, Lys21 and Arg22 are conserved in sequence (**Figure 6.7A-C and 6.8A-C**). The N termini of these toxins are enriched in basic residues used to contact the ribosome.

Ribosome-dependent toxins all use acid-base catalysis to catalyze mRNA cleavage between the second and third A-site nucleotides via a S_N2 reaction. The reaction is initiated by abstraction of the 2'-proton of the 2'-OH of the second A-site nucleotide by a toxin residue. The activated 2'-oxyanion attacks the scissile phosphate creating a trigonal bipyramidal transition state with two negative charges that are stabilized by a positively charged toxin residue. Then, the bond between the phosphorus atom and 5'-oxygen of the third A-site nucleotide is broken and a toxin residue acting as the general acid donates a proton to 5'-oxyanion leaving group. This reaction is similar to how general RNases such as RNase U2 and RNase T1 cleave mRNA in the absence of the ribosome (41,42).

Ribosome-dependent toxins cleave between the second and third nucleotide of the A-site codon and recognize the first two nucleotides of the A-site codon in similar manners, however differentially recognize the third nucleotide (18,21,39). The first A-site nucleotide is positioned between the P-site tRNA and a loop of the ribosome-dependent toxin (**Figure 6.8**). Few nucleotide-specific interactions are made with the first nucleotide suggesting A-site codons are not strictly monitored at this position. The second A-site nucleotide interacts solely with the toxin (**Figure 6.8**). The RelE toxin recognizes an adenosine in the *trans* configuration in part through base stacking with highly conserved residues Leu44 and Tyr87 (**Figure 6.7A and 6.8A**). In contrast, YoeB, HigB and likely YafQ appear to recognize the second nucleotide in the *syn* conformation (**Figure 6.7B-D and 6.8B-D**). For these toxins, the Hoogsteen face of the second A-site adenosine hydrogen bonds with the backbone amine and carbonyl of a nonconserved residue. Also, a leucine residue is positioned above the face of the second position adenosine and the

general base interacts with the 2' hydroxyl. The general base-leucine signature of YoeB is Glu46-Leu48, YafQ is His50-Leu52 and HigB is His54-Leu56 (**Figure 6.8B-D**). As these residues are similar, I propose that the backbone-leucine-general base motif is a common feature YoeB, YafQ and HigB use to recognize the second nucleotide (**Chapter 4**). In Chapter 4, I showed that the same interactions that HigB makes with the Hoogsteen face of the second A-site adenosine allow for HigB to interact with the second position cytosine. YoeB and YafQ share the second nucleotide position-binding motif with HigB and may also be able to recognize a second position cytosine in a similar fashion. Thus, the functional differences between toxins likely do not stem from their interactions with the first two A-site nucleotides.

The recognition of the third A-site nucleobase is the most divergent among ribosome-dependent toxins. All toxins contain a highly conserved residue that coordinates the oxygen of the scissile phosphate (Arg61 for RelE, Arg65 for YoeB, His63 for YafQ and Arg73 for HigB) (**Figure 6.7 and 6.8**). The three 70S ribosome structures with RelE, YoeB and HigB bound show distinct binding pockets for the third nucleobase. RelE re-positions a third position guanosine so that it forms stacking interactions with 16S rRNA nucleotide C1054 and RelE Glu82. YoeB binding causes the third adenosine to stack with a highly conserved His83 but not with 16S rRNA (**Figure 6.7B and 6.8B**). HigB binding causes the Hoogsteen face of the third adenosine to hydrogen bond with the Watson-Crick face of C1054. HigB is the only toxin for which the molecular basis for its specificity for the third nucleotide was investigated. A highly conserved Asn71, sometimes a Gln, is positioned to stack with C1054 potentially orienting C1054 for interactions with the third A-site adenosine and position 70 is an

amino acid with a small side chain (Ala or Gly). Mutation of Asn71 drastically reduces the preference of HigB for a third position adenosine implicating Asn71 in playing a role in third nucleotide specificity. As there are no 70S ribosome structures with YafQ bound, it is currently unclear how YafQ binding affects the position of the third A-site nucleotide. In summary, three mRNA recognition signatures have been found thus far. The RelE tyrosine stacking with the second A-site nucleotide, the YoeB, YafQ and HigB backbone-leucine-general base motif for recognizing the second A-site adenosine and the HigB small residue (Ala or Gly) followed by asparagine or glutamine for recognition of the third position adenosine are amino acid signatures for mRNA recognition. Mutagenesis of ribosome-dependent toxins RelE, YoeB, YafQ and HigB has identified several critical residues for activity in two ways (1,21-24,40,43). The first method examined the ability of toxin mutants to suppress bacterial growth upon toxin overexpression (2,40,43,44). Overexpression of wild-type toxin stops cell growth and mutation of an essential residue reverses the growth phenotype. The other method used is single turnover kinetics, which examines the *in vitro* cleavage rates by toxins. Both of these approaches have led to the identification of RelE Lys52 or Lys54 as the general base, Arg61 functions in transition state stabilization, and Arg81 as the general acid (21-23) (**Figure 6.7A and 6.8A**). A distinguishing feature of RelE is the high density of conserved-basic residues used to catalyze mRNA cleavage. YoeB toxin uses highly conserved Glu46 as a general base, Arg59 to stabilize the transition state and His83 as the general acid (24,39) (**Figure 6.7B and 6.8B**). YafQ likely uses histidines at each step with His50, His63, and His87 acting as the general base, transition state stabilizer and general acid, respectively (40,43) (**Figure 6.7C and 6.8C**). Lastly, I determined that HigB uses highly conserved His54 as

a general base, Arg73 to stabilize the transition state and Tyr91 as the general acid (**Chapter 5**) (**Figure 6.7D and 6.8D**). Together, these studies reaffirmed the diversity in how ribosome-dependent toxins inspect and degrade the mRNA transcripts. Thus, the presence of one of these unique sets of residues should help in identifying which ribosome-dependent toxin the uncharacterized toxin is most similar to.

6.9 Concluding remarks

In the past 5 years, a number of new insights into the roles ribosome-dependent toxins play in bacterial physiology have been examined. Despite this, the role of each ribosome-dependent toxin in reshaping the translational landscape is unknown. As the molecular signatures of toxins become known, we will gain important insights into how toxins alter the translational landscape in the face of multiple of stress to ensure bacterial survival.

The identification of how toxins alter the translational landscape will answer several questions about toxin function but also generate new hypotheses about bacterial survival. Ribosome-dependent toxins have the potential to reshape translation during stress in several ways. Once it is known how translation is affected, we can begin to analyze the roles of the proteins translated during stress. These findings should validate established proteins involved in survival but also identify several novel factors important for survival during stress. The novel factors will likely be responsible for increased survival to particular stresses and this knowledge will aid the identification of the biological function of these proteins. Understanding the biological significance of these proteins will benefit the toxin-antitoxin field as well as other microbial fields.

The conservation of important residues for mRNA specificity within individual family members of ribosome-dependent toxins suggests that toxins have universal rather host-specific cleavage properties. When the HigB toxin was originally discovered to cleave several adenosine-rich codons, the authors hypothesized that this activity was advantageous to *P. vulgaris* because HigB could cleave mRNA from the adenosine-rich *P. vulgaris* genome and an adenosine-rich plasmid that HigB was not located on (1). These views were based on the assumption that the HigB toxin has a specificity that is tuned for its host genome. However, components of HigB that are important for specificity are conserved across several hundred orthologues. Thus, toxin specificity is likely not tuned for the host but is predetermined and functions in a similar, but unknown, manner across many bacterial species.

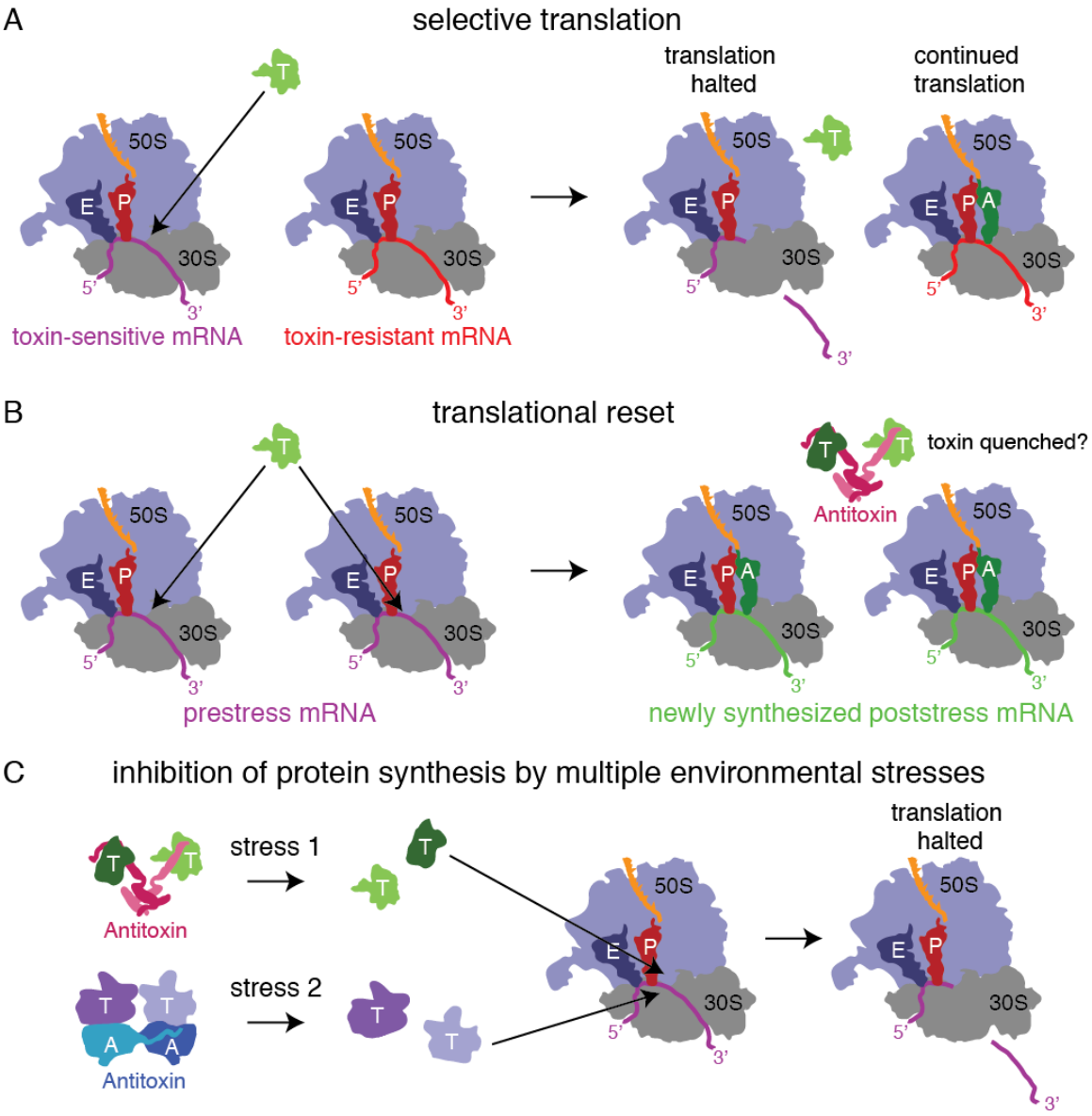

Figure 6.1: Ribosome-dependent toxins have several potential roles in translational regulation.

(A) One potential way in which ribosome-dependent toxins can cause selective translation. mRNA that contains ribosome-dependent cleavage sites will be sensitive to toxin cleavage while mRNA lacking ribosome-dependent toxin cleavage sites will not be cleaved and continue to be translated. (B) The translational reset hypothesis of toxins. Here, ribosome-dependent toxins shut down translation of mRNA transcripts translated

during non-stress conditions to make way for translation of stress-related mRNA. In this hypothesis, the toxin protein would likely need to have its activity quenched by antitoxin protein before translation of newly transcribed mRNA can occur. (C) An antitoxin-centric view of why cells often encode multiple toxin-antitoxin systems. Different antitoxins may be targeted by different environmental stress. Here, codon-preference of toxin matters little and having multiple toxin-antitoxin systems allows bacteria to downregulate translation in response to more environmental stress than if only one toxin-antitoxin system was present.

E. coli HipA 73-AKNASPESTEQQ-NL-EW-88

P. vulgaris HigA 88---VLYGESNEQQQNAQEH-104

Figure 6.2: The HipB and HigA antitoxins may share a degradation tag.

The last 16 residues of each antitoxin are aligned and identical residues and residues with similar physical properties are colored red.

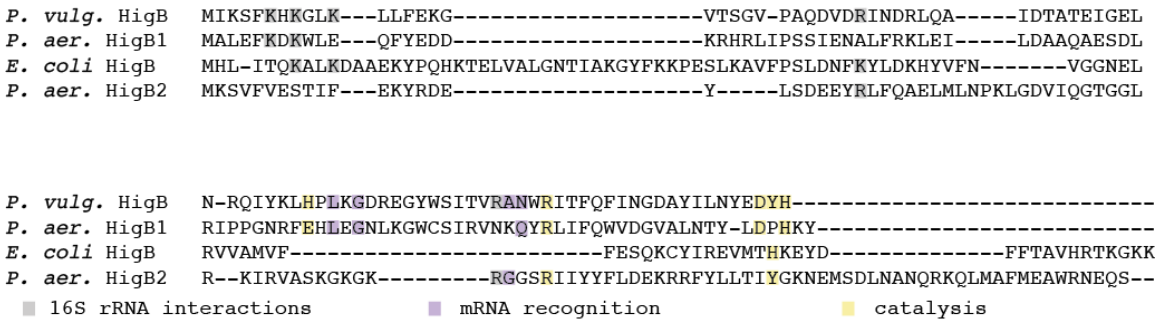

Figure 6.3: Toxins named HigB lack several key residues that define *Proteus vulgaris* HigB.

Alignment of *Proteus vulgaris* HigB, *Vibrio cholerae* HigB-1, *Escherichia coli* HigB and *Vibrio cholerae* HigB-2. *P. vulgaris* HigB residues that are important for 16S rRNA recognition, mRNA recognition or mRNA cleavage (catalysis) are indicated and residues with similar putative functions are highlighted in other bacterial species.

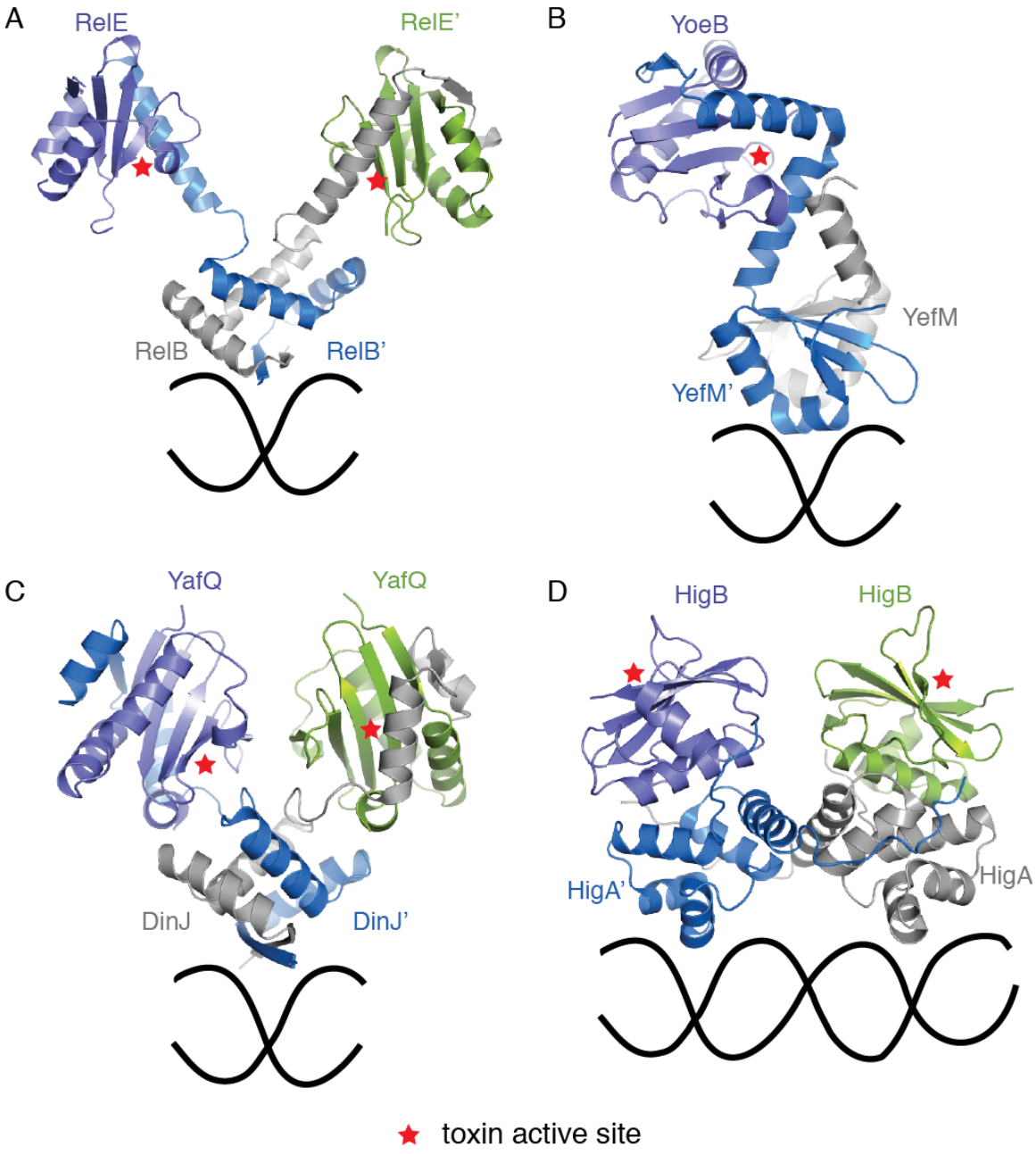

Figure 6.4: Antitoxin proteins interact with toxin proteins through diverse mechanisms.

X-ray crystal structures of the RelEB toxin-antitoxin complex (PDB ID 4FXE) (A), the YoeB-YefM toxin-antitoxin complex (PDB ID 2A6Q) (B), DinJ-YafQ (PDB ID 4Q2U)

(C) and HigBA toxin-antitoxin complex (PDB ID 4MCT) (D). Antitoxins are colored gray or blue and toxins are colored purple or green. The location of toxin active sites are denoted by a red star and a schematic of double-stranded DNA is shown near the DNA-binding motif to illustrate how each antitoxin likely interacts with DNA.

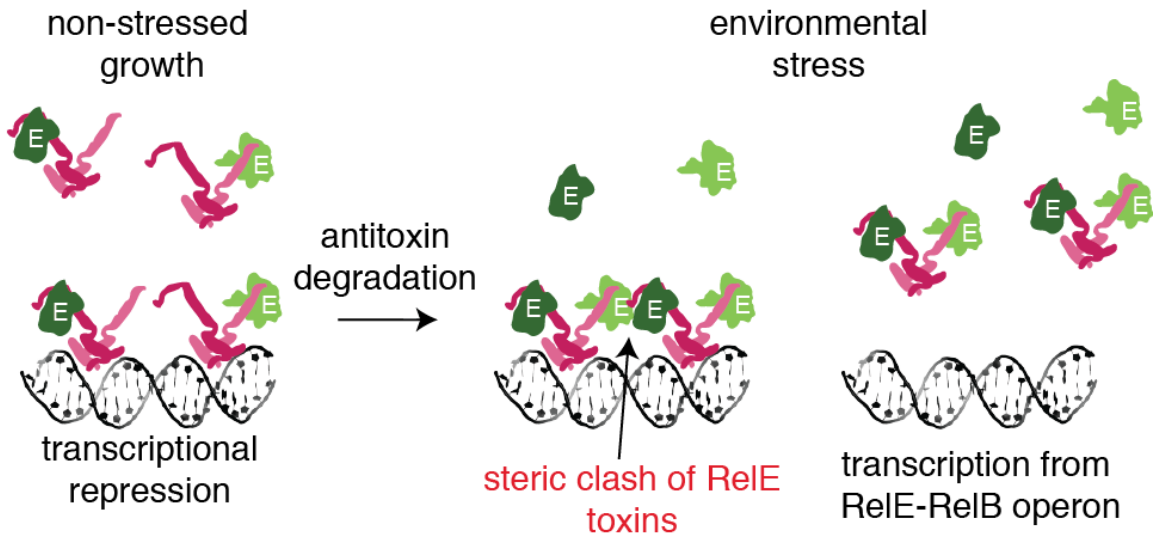

Figure 6.5: The RelEB toxin-antitoxin systems is transcriptionally regulated by toxin to antitoxin ratios.

Schematic of transcriptional regulation of the RelEB operon with RelE colored green and RelB colored pink. Low ratios of toxin to antitoxin lead to transcriptional repression while stress-induced antitoxin degradation results in higher ratios of RelE to RelB, destabilization of the tetrameric RelEB complex from DNA due to steric clash and transcriptional derepression.

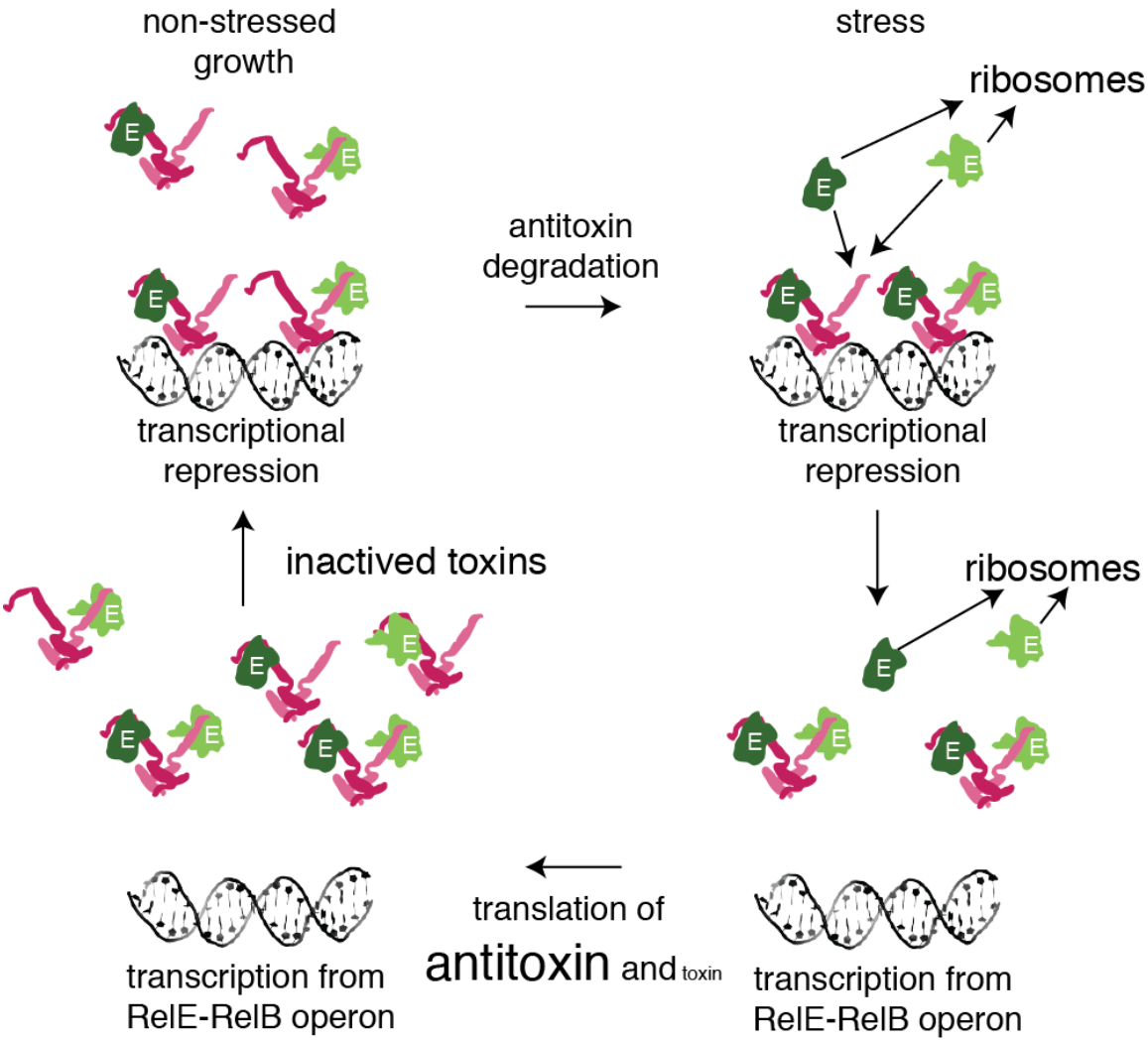

Figure 6.6: Working model for how transcriptional regulation by toxin to antitoxin ratios limit active toxin to short periods.

It is unknown why toxin to antitoxin ratios regulate transcription from toxin-antitoxin systems. I hypothesize that this mechanism serves to rapidly quench toxin activity. Antitoxin degradation leads to free toxin, which can cleave mRNA on the ribosome or bind antitoxin bound to DNA. Eventually, enough toxin will bind DNA-bound antitoxin to cause transcriptional derepression of the toxin-antitoxin loci. This leads to mRNAs encoding toxin and antitoxin. Antitoxins are translated at much higher levels than toxins creating much more antitoxin than toxin. The newly synthesized antitoxins bind and

inactivate toxins and would repress transcription if antitoxin degradation has stopped. This autofeedback loop would keep the time period in which toxins are active short.

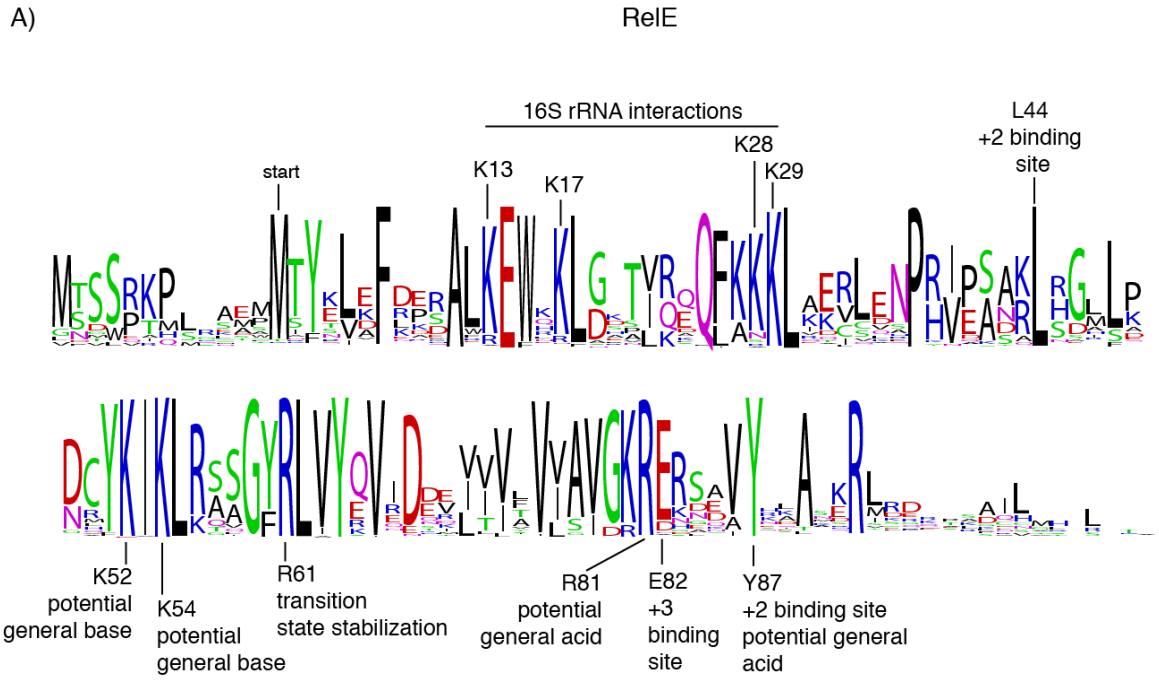

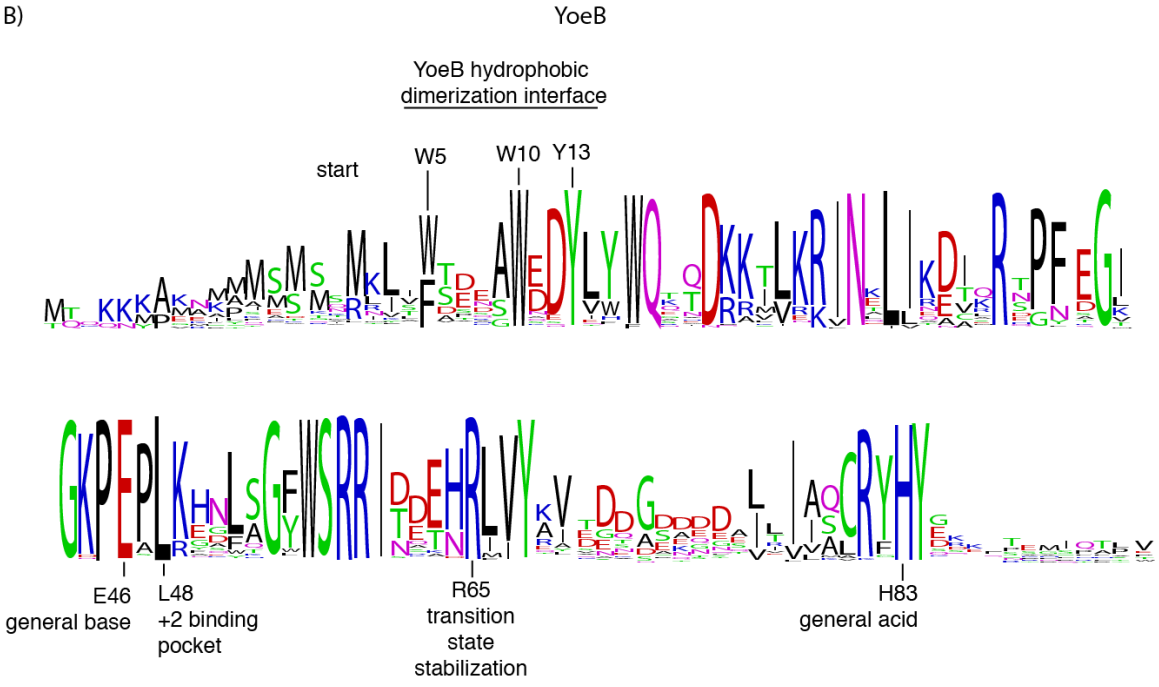

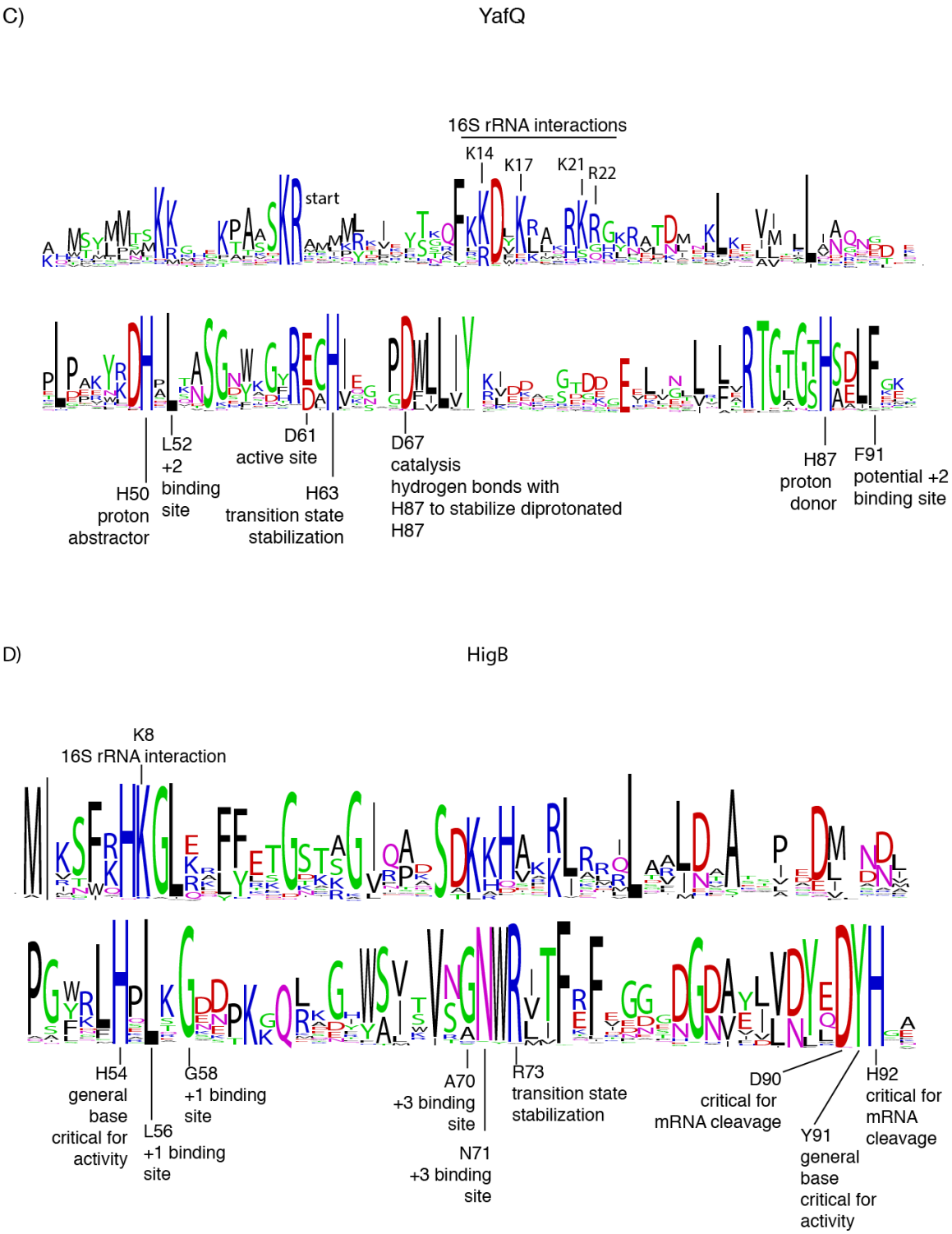

Figure 6.7: Sequence conservation of ribosome-dependent toxins.

The amino acid sequence conservation of *Escherchia coli* RelE (A), YoeB (B) and YafQ (C) and *Proteus vulgaris* HigB (D) from 1,000 homologs is shown in WebLogo format. Highly conserved amino acids with roles in 16S rRNA interactions, mRNA recognition, mRNA cleavage and in the case of YoeB, dimerization, are indicated. Gaps in the alignment extend the toxin sequences. For example, the search and alignment process with the 92 amino acid HigB sequence yields a WebLogo that is 131 amino acids long. The additional residues are poorly conserved and should not influence interpretation.

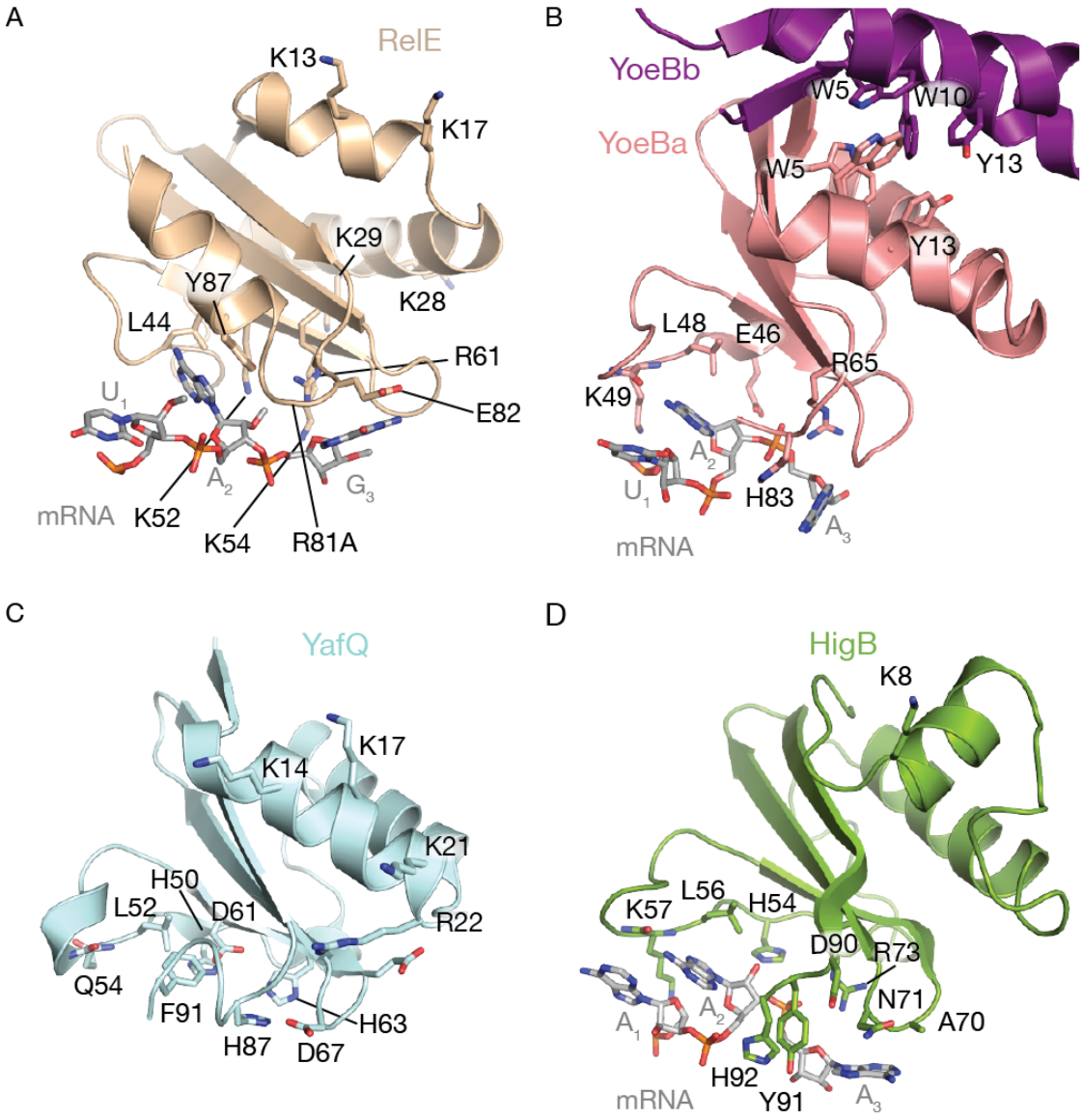

Figure 6.8: Highly conserved residues of individual toxin family members mainly cluster around mRNA path.

View of the *Escherichia coli* RelE (A), *Escherchia coi* YoeB (B) and *Proteus vulgaris* HigB (D) toxins bound to A-site mRNA. In panel C is a view of *Escherchia coli* YafQ in a similar orientation as YoeB and HigB. Highly conserved functional amino acids for each toxin from figure 6.7 are shown. All ribosomal components and nonA-site mRNA have been stripped away for clarity.

6.10 References

1. Hurley, J. M., and Woychik, N. A. (2009) Bacterial toxin HigB associates with ribosomes and mediates translation-dependent mRNA cleavage at A-rich sites. *The Journal of biological chemistry* **284**, 18605-18613
2. Prysak, M. H., Mozdzierz, C. J., Cook, A. M., Zhu, L., Zhang, Y., Inouye, M., and Woychik, N. A. (2009) Bacterial toxin YafQ is an endoribonuclease that associates with the ribosome and blocks translation elongation through sequence-specific and frame-dependent mRNA cleavage. *Molecular microbiology* **71**, 1071-1087
3. Zhang, Y., and Inouye, M. (2009) The inhibitory mechanism of protein synthesis by YoeB, an Escherichia coli toxin. *The Journal of biological chemistry* **284**, 6627-6638
4. Overgaard, M., Borch, J., Jorgensen, M. G., and Gerdes, K. (2008) Messenger RNA interferase RelE controls relBE transcription by conditional cooperativity. *Molecular microbiology* **69**, 841-857
5. Li, G. W., Burkhardt, D., Gross, C., and Weissman, J. S. (2014) Quantifying absolute protein synthesis rates reveals principles underlying allocation of cellular resources. *Cell* **157**, 624-635
6. Gerdes, K., Christensen, S. K., and Lobner-Olesen, A. (2005) Prokaryotic toxin-antitoxin stress response loci. *Nature reviews. Microbiology* **3**, 371-382
7. Christensen, S. K., Mikkelsen, M., Pedersen, K., and Gerdes, K. (2001) RelE, a global inhibitor of translation, is activated during nutritional stress. *Proceedings*

of the National Academy of Sciences of the United States of America **98**, 14328-14333

8. Janssen, B. D., Garza-Sanchez, F., and Hayes, C. S. (2015) YoeB toxin is activated during thermal stress. *MicrobiologyOpen* **4**, 682-697

9. Pandey, D. P., and Gerdes, K. (2005) Toxin-antitoxin loci are highly abundant in free-living but lost from host-associated prokaryotes. *Nucleic acids research* **33**, 966-976

10. Christensen-Dalsgaard, M., Jorgensen, M. G., and Gerdes, K. (2010) Three new RelE-homologous mRNA interferases of Escherichia coli differentially induced by environmental stresses. *Molecular microbiology* **75**, 333-348

11. Boutte, C. C., and Crosson, S. (2013) Bacterial lifestyle shapes stringent response activation. *Trends in microbiology* **21**, 174-180

12. Oh, E., Becker, A. H., Sandikci, A., Huber, D., Chaba, R., Gloge, F., Nichols, R. J., Typas, A., Gross, C. A., Kramer, G., Weissman, J. S., and Bukau, B. (2011) Selective ribosome profiling reveals the cotranslational chaperone action of trigger factor in vivo. *Cell* **147**, 1295-1308

13. Schifano, J. M., Vvedenskaya, I. O., Knoblauch, J. G., Ouyang, M., Nickels, B. E., and Woychik, N. A. (2014) An RNA-seq method for defining endoribonuclease cleavage specificity identifies dual rRNA substrates for toxin MazF-mt3. *Nature communications* **5**, 3538

14. Singh, R., Barry, C. E., 3rd, and Boshoff, H. I. (2010) The three RelE homologs of Mycobacterium tuberculosis have individual, drug-specific effects on bacterial antibiotic tolerance. *Journal of bacteriology* **192**, 1279-1291

15. Paige, J. S., Wu, K. Y., and Jaffrey, S. R. (2011) RNA mimics of green fluorescent protein. *Science* **333**, 642-646

16. Tian, Q. B., Ohnishi, M., Tabuchi, A., and Terawaki, Y. (1996) A new plasmid-encoded proteic killer gene system: cloning, sequencing, and analyzing hig locus of plasmid Rts1. *Biochemical and biophysical research communications* **220**, 280-284

17. Christensen-Dalsgaard, M., and Gerdes, K. (2006) Two higBA loci in the Vibrio cholerae superintegron encode mRNA cleaving enzymes and can stabilize plasmids. *Molecular microbiology* **62**, 397-411

18. Schureck, M. A., Dunkle, J. A., Maehigashi, T., Miles, S. J., and Dunham, C. M. (2015) Defining the mRNA recognition signature of a bacterial toxin protein. *Proceedings of the National Academy of Sciences of the United States of America* **112**, 13862-13867

19. Miallau, L., Jain, P., Arbing, M. A., Cascio, D., Phan, T., Ahn, C. J., Chan, S., Chernishof, I., Maxson, M., Chiang, J., Jacobs, W. R., Jr., and Eisenberg, D. S. (2013) Comparative proteomics identifies the cell-associated lethality of M. tuberculosis RelBE-like toxin-antitoxin complexes. *Structure* **21**, 627-637

20. Sala, A., Bordes, P., and Genevaux, P. (2014) Multiple toxin-antitoxin systems in Mycobacterium tuberculosis. *Toxins* **6**, 1002-1020

21. Neubauer, C., Gao, Y. G., Andersen, K. R., Dunham, C. M., Kelley, A. C., Hentschel, J., Gerdes, K., Ramakrishnan, V., and Brodersen, D. E. (2009) The structural basis for mRNA recognition and cleavage by the ribosome-dependent endonuclease RelE. *Cell* **139**, 1084-1095

22. Griffin, M. A., Davis, J. H., and Strobel, S. A. (2013) Bacterial toxin RelE: a highly efficient ribonuclease with exquisite substrate specificity using atypical catalytic residues. *Biochemistry* **52**, 8633-8642

23. Dunican, B. F., Hiller, D. A., and Strobel, S. A. (2015) Transition State Charge Stabilization and Acid-Base Catalysis of mRNA Cleavage by the Endoribonuclease RelE. *Biochemistry* **54**, 7048-7057

24. Kamada, K., and Hanaoka, F. (2005) Conformational change in the catalytic site of the ribonuclease YoeB toxin by YefM antitoxin. *Molecular cell* **19**, 497-509

25. Boggild, A., Sofos, N., Andersen, K. R., Feddersen, A., Easter, A. D., Passmore, L. A., and Brodersen, D. E. (2012) The crystal structure of the intact E. coli RelBE toxin-antitoxin complex provides the structural basis for conditional cooperativity. *Structure* **20**, 1641-1648

26. Li, G. Y., Zhang, Y., Inouye, M., and Ikura, M. (2009) Inhibitory mechanism of Escherichia coli RelE-RelB toxin-antitoxin module involves a helix displacement near an mRNA interferase active site. *The Journal of biological chemistry* **284**, 14628-14636

27. Ruangprasert, A., Maehigashi, T., Miles, S. J., Giridharan, N., Liu, J. X., and Dunham, C. M. (2014) Mechanisms of toxin inhibition and transcriptional repression by Escherichia coli DinJ-YafQ. *The Journal of biological chemistry* **289**, 20559-20569

28. Liang, Y., Gao, Z., Wang, F., Zhang, Y., Dong, Y., and Liu, Q. (2014) Structural and functional characterization of Escherichia coli toxin-antitoxin complex DinJ-YafQ. *The Journal of biological chemistry* **289**, 21191-21202

29. Schureck, M. A., Maehigashi, T., Miles, S. J., Marquez, J., Cho, S. E., Erdman, R., and Dunham, C. M. (2014) Structure of the Proteus vulgaris HigB-(HigA)2-HigB toxin-antitoxin complex. *The Journal of biological chemistry* **289**, 1060-1070

30. Arbing, M. A., Handelman, S. K., Kuzin, A. P., Verdon, G., Wang, C., Su, M., Rothenbacher, F. P., Abashidze, M., Liu, M., Hurley, J. M., Xiao, R., Acton, T., Inouye, M., Montelione, G. T., Woychik, N. A., and Hunt, J. F. (2010) Crystal structures of Phd-Doc, HigA, and YeeU establish multiple evolutionary links between microbial growth-regulating toxin-antitoxin systems. *Structure* **18**, 996-1010

31. Hansen, S., Vulic, M., Min, J., Yen, T. J., Schumacher, M. A., Brennan, R. G., and Lewis, K. (2012) Regulation of the Escherichia coli HipBA toxin-antitoxin system by proteolysis. *PloS one* **7**, e39185

32. Garcia-Pino, A., Balasubramanian, S., Wyns, L., Gazit, E., De Greve, H., Magnuson, R. D., Charlier, D., van Nuland, N. A., and Loris, R. (2010) Allostery and intrinsic disorder mediate transcription regulation by conditional cooperativity. *Cell* **142**, 101-111

33. Cruz, J. W., Rothenbacher, F. P., Maehigashi, T., Lane, W. S., Dunham, C. M., and Woychik, N. A. (2014) Doc toxin is a kinase that inactivates elongation factor Tu. *The Journal of biological chemistry* **289**, 7788-7798

34. Castro-Roa, D., Garcia-Pino, A., De Gieter, S., van Nuland, N. A., Loris, R., and Zenkin, N. (2013) The Fic protein Doc uses an inverted substrate to phosphorylate and inactivate EF-Tu. *Nature chemical biology* **9**, 811-817

35. Afif, H., Allali, N., Couturier, M., and Van Melderen, L. (2001) The ratio between CcdA and CcdB modulates the transcriptional repression of the ccd poison-antidote system. *Molecular microbiology* **41**, 73-82

36. Altschul, S. F., Madden, T. L., Schaffer, A. A., Zhang, J., Zhang, Z., Miller, W., and Lipman, D. J. (1997) Gapped BLAST and PSI-BLAST: a new generation of protein database search programs. *Nucleic acids research* **25**, 3389-3402

37. Sievers, F., Wilm, A., Dineen, D., Gibson, T. J., Karplus, K., Li, W., Lopez, R., McWilliam, H., Remmert, M., Soding, J., Thompson, J. D., and Higgins, D. G. (2011) Fast, scalable generation of high-quality protein multiple sequence alignments using Clustal Omega. *Molecular systems biology* **7**, 539

38. Crooks, G. E., Hon, G., Chandonia, J. M., and Brenner, S. E. (2004) WebLogo: a sequence logo generator. *Genome research* **14**, 1188-1190

39. Feng, S., Chen, Y., Kamada, K., Wang, H., Tang, K., Wang, M., and Gao, Y. G. (2013) YoeB-ribosome structure: a canonical RNase that requires the ribosome for its specific activity. *Nucleic acids research* **41**, 9549-9556

40. Maehigashi, T., Ruangprasert, A., Miles, S. J., and Dunham, C. M. (2015) Molecular basis of ribosome recognition and mRNA hydrolysis by the E. coli YafQ toxin. *Nucleic acids research* **43**, 8002-8012

41. Zegers, I., Haikal, A. F., Palmer, R., and Wyns, L. (1994) Crystal structure of RNase T1 with 3'-guanylic acid and guanosine. *The Journal of biological chemistry* **269**, 127-133

42. Noguchi, S. (2010) Isomerization mechanism of aspartate to isoaspartate implied by structures of Ustilago sphaerogena ribonuclease U2 complexed with adenosine

3'-monophosphate. *Acta crystallographica. Section D, Biological crystallography* **66**, 843-849

43. Armalyte, J., Jurenaite, M., Beinoraviciute, G., Teiserskas, J., and Suziedeliene, E. (2012) Characterization of Escherichia coli dinJ-yafQ toxin-antitoxin system using insights from mutagenesis data. *Journal of bacteriology* **194**, 1523-1532

44. Takagi, H., Kakuta, Y., Okada, T., Yao, M., Tanaka, I., and Kimura, M. (2005) Crystal structure of archaeal toxin-antitoxin RelE-RelB complex with implications for toxin activity and antitoxin effects. *Nature structural & molecular biology* **12**, 327-331